RESEARCH

UDOT

Keeping Utah Moving

Utah Department of Transportation - Research Division
4501 South 2700 West - P.O. Box 148410 - SLC,UT 84114-8410

Report No. UT-18.12

LATERAL RESISTANCE OF PIPE PILES ADJACENT TO A 15-FT HIGH MSE WALL

Prepared For:

Utah Department of Transportation
Research Division

Submitted By:

Brigham Young University
Department of Civil and Environmental Engineering

Authored By:

Kyle M. Rollins
Cody K. Hatch
Jarell J.C. Han

Final Report
August 2018

DISCLAIMER

The authors alone are responsible for the preparation and accuracy of the information, data, analysis, discussions, recommendations, and conclusions presented herein. The contents do not necessarily reflect the views, opinions, endorsements, or policies of the Utah Department of Transportation, the U.S. Department of Transportation, or other agencies that provided funding for the project. The Utah Department of Transportation makes no representation or warranty of any kind, and assumes no liability therefore.

ACKNOWLEDGMENTS

Funding for this study was provided by FHWA pooled fund study TPF-5(272) "Evaluation of Lateral Pile Resistance Near MSE Walls at a Dedicated Wall Site," supported by Departments of Transportation from the states of Florida, Iowa, Kansas, Massachusetts, Minnesota, Montana, New York, Oregon, Texas, Utah, and Wisconsin. Utah DOT served as the lead agency with Jason Richins and David Stevens as the research project managers and Jon Bischoff as the geotechnical champion. This support is gratefully acknowledged; however, the opinions, conclusions and recommendations in this paper do not necessarily represent those of the sponsoring organizations.

In addition, significant in-kind contributions from a number of entities made it possible for this project to be undertaken with a scope sufficient to accomplish the project objectives. We gratefully acknowledge the assistance of Chris Ragan at Atlas Tube in donating the circular and square steel piles along with Price Bethel at Spartan Steel in donating the H piles used in this study. Eric Hendricksen at Desert Deep Foundations, Inc. provided pile driving services at cost, and Carl Clyde at Geneva Rock, Inc. donated site grading services and the use of their land for the MSE abutment test site. Lastly, the Reinforced Earth Company and SSL, Inc. donated wall panels and reinforcing elements necessary to construct the abutment wall.

TECHNICAL REPORT ABSTRACT

1. Report No. UT-18.12	2. Government Accession No. N/A	3. Recipient's Catalog No. N/A
4. Title and Subtitle LATERAL RESISTANCE OF PIPE PILES ADJACENT TO A 15-FT HIGH MSE WALL		5. Report Date August 2018 6. Performing Organization Code N/A
7. Author(s) Kyle M. Rollins, Cody K. Hatch, Jarell J.C. Han		8. Performing Organization Report No. N/A
9. Performing Organization Name and Address Brigham Young University Department of Civil and Environmental Engineering 368 CB Provo, UT 84602		10. Work Unit No. 4205315D 11. Contract or Grant No. 14-8434
12. Sponsoring Agency Name and Address Utah Department of Transportation 4501 South 2700 West P.O. Box 148410 Salt Lake City, UT 84114-8410		13. Type of Report & Period Covered Final Report May 2014 – Aug. 2018 14. Sponsoring Agency Code PIC No. UT11.404

15. Supplementary Notes

Prepared in cooperation with the Utah Department of Transportation, the U.S. Department of Transportation, Federal Highway Administration, and other state DOTs on pooled fund study TPF-5(272)

16. Abstract

A 15-foot tall Mechanically Stabilized Earth (MSE) retaining wall was constructed, and piles were driven at various distances behind the wall. Lateral pile load tests were conducted in the direction of the wall, and the performance of the pile, wall, and reinforcement were measured. The piles were 12.75-inch diameter pipe piles, and one half of the wall was reinforced with welded wire grid reinforcement while the other half had ribbed strip reinforcements. For each reinforcement type, tests were performed on four piles located at nominal distances of 5, 4, 3 and 2 pile diameters from the back of the wall to the center of the pile. The objective of the testing was to characterize the relationship between the lateral pile resistance and the distance of the pile behind the back face of the MSE wall.

Based on the measured load-displacement curves from the tests, the lateral resistance of the piles decreased as the spacing behind the wall decreased. The results of the tests have been matched with the computer program LPILE using p-multipliers to reduce the lateral resistance for piles closer to the wall. A best-fit line was developed showing the variation of p-multiplier with normalized pile spacing behind the wall, including data from previous studies. The best-fit curve suggests that a p-multiplier of 1 (no reduction in lateral resistance) can be used when the normalized distance from the back face of the wall to the center of the pile is at least 4 pile diameters and the p-multiplier decreases relatively linearly for smaller spacings.

17. Key Words Laterally loaded piles, MSE wall, p-multiplier, welded wire reinforcement, ribbed strip reinforcement, p-y curve, tensile force, reinforcement load, bridge abutments		18. Distribution Statement Not restricted. Available through: UDOT Research Division 4501 South 2700 West P.O. Box 148410 Salt Lake City, UT 84114-8410 www.udot.utah.gov/go/research		23. Registrant's Seal N/A
19. Security Classification (of this report) Unclassified	20. Security Classification (of this page) Unclassified	21. No. of Pages 178	22. Price N/A	

TABLE OF CONTENTS

LIST OF TABLES

LIST OF FIGURES

UNIT CONVERSION FACTORS

SI* (MODERN METRIC) CONVERSION FACTORS

APPROXIMATE CONVERSIONS TO SI UNITS

Symbol	When You Know	Multiply By	To Find	Symbol
		LENGTH		
in	inches	25.4	millimeters	mm
ft	feet	0.305	meters	m
yd	yards	0.914	meters	m
mi	miles	1.61	kilometers	km
		AREA		
in^2	square inches	645.2	square millimeters	mm^2
ft^2	square feet	0.093	square meters	m^2
yd^2	square yard	0.836	square meters	m^2
ac	acres	0.405	hectares	ha
mi^2	square miles	2.59	square kilometers	km^2
		VOLUME		
fl oz	fluid ounces	29.57	milliliters	mL
gal	gallons	3.785	liters	L
ft^3	cubic feet	0.028	cubic meters	m^3
yd^3	cubic yards	0.765	cubic meters	m^3
		NOTE: volumes greater than 1000 L shall be shown in m^3		
		MASS		
oz	ounces	28.35	grams	g
lb	pounds	0.454	kilograms	kg
T	short tons (2000 lb)	0.907	megagrams (or "metric ton")	Mg (or "t")
		TEMPERATURE (exact degrees)		
°F	Fahrenheit	5 (F-32)/9 or (F-32)/1.8	Celsius	°C
		ILLUMINATION		
fc	foot-candles	10.76	lux	lx
fl	foot-Lamberts	3.426	candela/m^2	cd/m^2
		FORCE and PRESSURE or STRESS		
lbf	poundforce	4.45	newtons	N
lbf/in^2	poundforce per square inch	6.89	kilopascals	kPa

APPROXIMATE CONVERSIONS FROM SI UNITS

Symbol	When You Know	Multiply By	To Find	Symbol
		LENGTH		
mm	millimeters	0.039	inches	in
m	meters	3.28	feet	ft
m	meters	1.09	yards	yd
km	kilometers	0.621	miles	mi
		AREA		
mm^2	square millimeters	0.0016	square inches	in^2
m^2	square meters	10.764	square feet	ft^2
m^2	square meters	1.195	square yards	yd^2
ha	hectares	2.47	acres	ac
km^2	square kilometers	0.386	square miles	mi^2
		VOLUME		
mL	milliliters	0.034	fluid ounces	fl oz
L	liters	0.264	gallons	gal
m^3	cubic meters	35.314	cubic feet	ft^3
m^3	cubic meters	1.307	cubic yards	yd^3
		MASS		
g	grams	0.035	ounces	oz
kg	kilograms	2.202	pounds	lb
Mg (or "t")	megagrams (or "metric ton")	1.103	short tons (2000 lb)	T
		TEMPERATURE (exact degrees)		
°C	Celsius	1.8C+32	Fahrenheit	°F
		ILLUMINATION		
lx	lux	0.0929	foot-candles	fc
cd/m^2	candela/m^2	0.2919	foot-Lamberts	fl
		FORCE and PRESSURE or STRESS		
N	newtons	0.225	poundforce	lbf
kPa	kilopascals	0.145	poundforce per square inch	lbf/in^2

*SI is the symbol for the International System of Units. (Adapted from FHWA report template, Revised March 2003)

EXECUTIVE SUMMARY

A 15-foot tall Mechanically Stabilized Earth (MSE) retaining wall was constructed, and piles were driven at various distances behind the wall. Lateral pile load tests were conducted in the direction of the wall, and the performance of the pile, wall, and reinforcement were measured. The piles were 12.75-inch diameter pipe piles, and one half of the wall was reinforced with welded wire grid reinforcement while the other half had ribbed strip reinforcements. For each reinforcement type tests were performed on four tests located at nominal distances of 5, 4, 3 and 2 pile diameters from the back of the wall to the center of the pile. The objective of the testing was to characterize the relationship between the lateral pile resistance and the distance of the pile behind the back face of the MSE wall.

Based on the measured load-displacement curves from the tests, the lateral resistance of the piles decreased as the spacing behind the wall decreased. The results of the tests have been matched with the computer program LPILE using p-multipliers to reduce the lateral resistance for piles closer to the wall. A best-fit line was developed showing the variation of p-multiplier with normalized pile spacing behind the wall, including data from previous studies. The best-fit curve suggests that a p-multiplier of 1 (no reduction in lateral resistance) can be used when the normalized distance from the back face of the wall to the center of the pile is at least 4 pile diameters and the p-multiplier decreases relatively linearly for smaller spacings.

1 INTRODUCTION

The use of integral-abutment bridges (IAB) has become more common in the United States over the last decade. Compared to traditional full-height abutment bridges, IAB is more efficient in design and has better capacity and redundancy for catastrophic events such as earthquakes (Maruri and Petro 2005). Moreover, right-of-way constraints have favored a transition from embankments to retaining walls in recent years. Research indicates that Mechanically Stabilized Earth (MSE) retaining wall systems perform better than conventional type retaining walls during earthquakes. In the 1995 Hyogoken-nanbu earthquake in Kobe Japan, conventional retaining walls such as cantilever and gravity walls suffered significant tilting with failure in some systems. In contrast, a geosynthetic MSE wall survived the earthquake with minor displacements of about 4 – 8 in. (Koseki 2012). Although the use of IAB with MSE walls at abutment faces is growing rapidly, there are currently insufficient guidelines for engineers on the lateral resistance of piles located near MSE wall faces. Some designers assume that the soil provides no resistance to lateral forces on the pile, which lead to larger pile dimensions or more piles at higher costs. Other designers place abutment piles at six to eight pile diameters behind the wall to minimize the effects of soil-structure interaction, which result in a larger bridge span at higher cost. Most engineers agree that the soil provides some resistance but that there is reduction in lateral resistance as the piles are located closer to the wall, but the appropriate reduction factor is not well defined. The Federal Highway Administration (FHWA) recommends a clear horizontal distance of 18 in. between the back of the wall and the front edge of the pile (Elias and Christopher, 1997). The Utah Department of Transportation (UDOT) specifies a minimum spacing of 3 ft. from the back of the

wall to the front face of the pile (UDOT Standard Drawing DD8). However, a reduction in lateral resistance is not addressed.

Not many lateral load tests have been conducted to determine pile lateral resistance near MSE walls. Pierson et al. (2009) conducted a series of full-scale lateral load tests on 36 in. diameter drilled shafts located at four distances behind a 20 ft. high masonry wall reinforced with extensible geogrids. Test results showed that the lateral resistance of the shaft spaced two diameters behind the wall was about 50 percent of the resistance provided by the shaft spaced four diameters behind the wall. The lateral resistance of the shaft spaced one diameter behind the wall was even lower, clearly indicating that lateral resistance of piles decreases significantly as the piles are located closer to the MSE wall face.

Recently two other full-scale studies were conducted to further understand the relationship between pile location from the wall and lateral resistance of piles. One study was done by Nelson (2013) on 12.75 in. diameter pipe piles at three locations behind wire mesh wall panels reinforced with strip reinforcements. Similar to Pierson, test results showed that piles closer to MSE wall have less lateral resistance. However, in contrast to Pierson the lateral resistance of the pile spaced 2.7 diameters from the wall was more than 50 percent of the resistance of the pile spaced 6.3 diameters behind the wall. In another full-scale study done by Price (2012), two 12.75 in. pipe piles and three 16 in. pipe piles were laterally loaded against soil reinforced with welded wire grids supported by concrete wall panels. In general, test results on pile lateral resistance agree with those obtained from the previous two full-scaled tests. Nevertheless, the results could not be compared directly because the reinforcement lengths to wall height ratios were different, suggesting that reinforcement lengths may have an impact on pile lateral resistance.

Due to the limited number of tests previously performed, correlations between pile location and lateral resistance are tentative and relationships between pile load and tensile force on the reinforcements are uncertain. To improve our understanding of pile-MSE interaction and develop accurate correlations as guidelines for engineers, additional lateral load tests were performed on sixteen piles located behind an MSE wall. Twelve steel pipe piles, seven square steel piles and five steel H piles were used in the test. Inextensible strip and grid steel were used as the reinforcement. The pile test was conducted at Geneva Rock Mt. Jordan gravel pit in Draper, Utah.

The objectives of the lateral load tests are to determine the effect of spacing from the wall on the lateral resistance of the pile and on the force developed by the MSE reinforcement. Additionally, the three pile types were tested to compare the reaction of different piles to lateral forces while the two reinforcement types were used to compare the forces on different reinforcements. Due to the large overall scope of the project, this report will only focus on the behavior of eight steel pipe piles behind the 15-ft high MSE wall with reinforcement consisting of inextensible ribbed steel strips and welded wire reinforcements. The test procedures, results and analysis are described herein.

2 LITERATURE REVIEW

The literature review in this section includes MSE wall design and recent findings on subjects related to lateral capacity of IAB.

2.1 MSE Walls

Mechanically Stabilized Earth (MSE) walls are cost-effective soil-retaining structures that can tolerate much larger distortion than reinforced concrete walls. By placing tensile reinforcing elements in the soil, the strength of the soil can be improved significantly such that the vertical face of the wall system is essentially self-supporting (Berg et al. 2009). In the early 1960s, French architect and engineer Henri Vidal developed Reinforced Earth®, a MSE wall system using steel strip reinforcement. This technology has been used in the United States since the early 1970s.

Reinforcements used today are categorized into two types of extensibility, i.e. extensible or inextensible reinforcement. Extensible reinforcements are generally made from nonmetallic material and the deformation of the reinforcement at failure is comparable or greater than the deformability of the surrounding soil. Inextensible reinforcements are made of metallic material and the deformation of the reinforcement at failure is much less than the deformability of the soil.

External and internal stability need to be considered in the analysis of MSE walls. The guidelines for MSE wall external stability analysis are the same as for gravity retaining walls which include resistance against sliding, overturning, bearing failure and global shear failure. Analysis for internal stability requires evaluating tensile strength of reinforcement against failure by

elongation or breakage, and determining the pullout resistance which is the resistance against the force required to pull the reinforcement out of the soil mass. The steps for internal design are as follows:

- Select a reinforcement type (inextensible or extensible).
- Define the critical failure surface.
- Define unfactored loads.
- Select reinforcement spacing compatible with the facing.
- Calculate the factored tensile force at each reinforcement level.
- Calculate soil reinforcement resistance.
- Select number of soil reinforcement elements at each level.
- Calculate the pullout capacity at each reinforcement level.

For inextensible reinforcements, the surface defining maximum tensile forces is assumed to be approximately bilinear as shown in Figure 2.1 and defines the boundary between active and passive zones within the MSE wall. The maximum tensile force per unit length, T_{max}, for a given reinforcement is given by the following Equation:

$$T_{max} = \sigma_H S_V \tag{2-1}$$

where

σ_H is the horizontal stress along the potential failure line per Equation 2-2, and

S_v is the vertical spacing between reinforcement levels.

$$\sigma_H = K_r \sigma_v + \Delta\sigma_H \tag{2-2}$$

where

K_r is the lateral earth pressure coefficient from Figure 2.2,

σ_v is the factored vertical stress as calculated by Equation 2-3, and

$\Delta\sigma_H$ is the supplemental factored horizontal stress due to external surcharges.

$$\sigma_v = (\gamma_r Z + q + \Delta\sigma_v)\gamma_{P\_EV} \quad (2\text{-}3)$$

where

γ_r is the moist unit weight of the retained soil,

Z is the depth below the top of the wall to the reinforcement,

q is the uniform surcharge load,

$\Delta\sigma_v$ is the concentrated vertical surcharge load, and

γ_{P_EV} is the load factor equal to 1.35 for vertical earth loads.

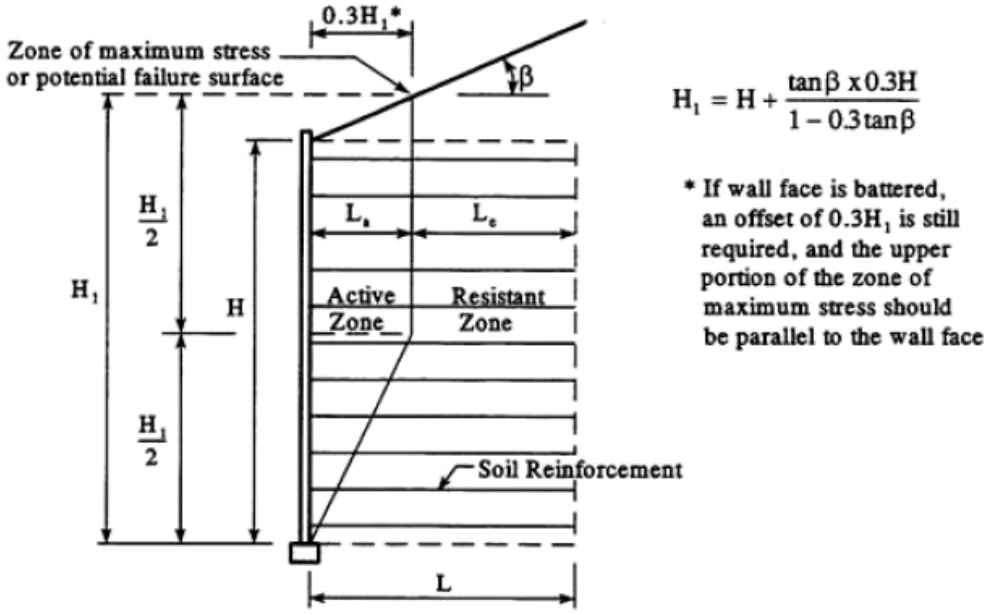

Figure 2.1: Location of potential failure surface for MSE wall with inextensible reinforcement (Berg et al. 2009).

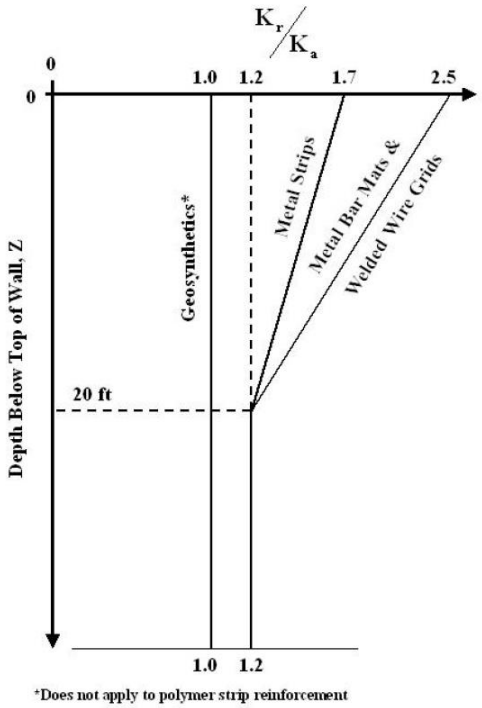

Figure 2.2: Variation of coefficient of lateral stress ratio (K_r/K_a) with depth of MSE wall (Berg et al. 2009).

Once the maximum tensile force is calculated, stability with respect to breakage of the reinforcement requires that:

$$T_{max} \leq \varphi T_{al} \tag{2-4}$$

where

φ is the resistance factor for static loading of steel strips, 0.75, and

T_{al} is the factored reinforcement resistance as defined in Equation 2-5.

$$T_{al} = \frac{F_y A_c}{b} \tag{2-5}$$

where

b is the gross width of the steel strip,

F_y is the yield stress of steel, and

A_c is the design cross section area of the steel as shown in Figure 2.3.

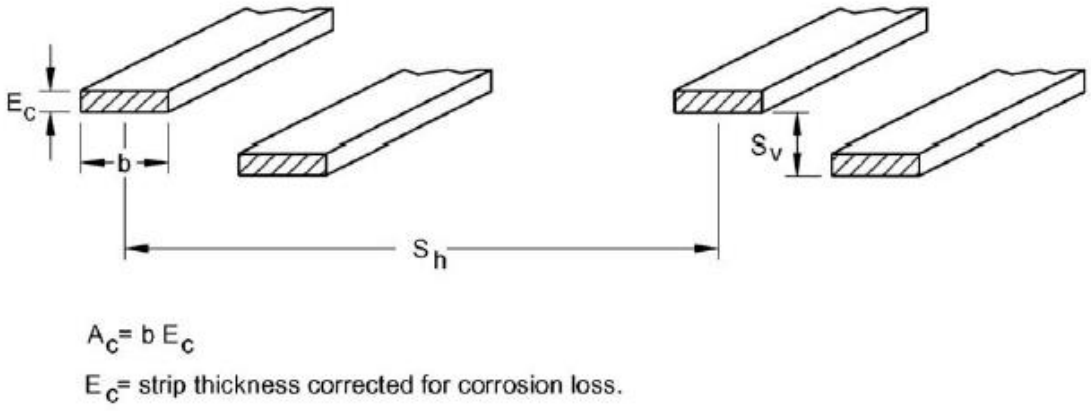

Figure 2.3: Parameters for Ac.

The pullout capacity requires the following criteria to be satisfied:

$$T_{max} \leq \varphi F^{*}(\sigma_v)(L_e)C(R_c)\alpha \tag{2-6}$$

where

φ is the resistance factor for static loading of steel strips, 0.75,

F^{*} is the pullout resistance factor as defined by Equation 2-7 for steel strips,

σ_v is the nominal (unfactored) vertical stress at the reinforcement level in the resistance zone, including distributed dead load surcharges,

L_e is the length of embedment in the resisting zone,

C is the surface area factor, equal to 2 for strip and grids reinforcement,

R_c is the reinforcement coverage ratio as defined in Equation 2-8, and

α is the scale correction factor, equal to 1 for inextensible reinforcement.

$$F^{*} = \begin{cases} 1.2 + \log C_u = 2.0 \; maximum, & Z = 0 \\ tan\,\phi\,, & Z \geq 20ft \end{cases} \tag{2-7}$$

where

C_u is the uniformity coefficient of the backfill (D_{60}/D_{10}), and

ϕ is the friction angle of the backfill.

$$R_c = \frac{b}{S_h} \tag{2-8}$$

where

B is the unit width of the reinforcement, and

S_h is the horizontal center to center spacing of grids.

2.2 Lateral Load Analysis of Piles

The p-y method is a common approach to analyze laterally loaded piles where a pile is modeled as a beam and the soil is modeled as a series of discrete non-linear springs. Figure 2.4(a) shows a model of a pile with a lateral load P_t, an axial load P_x, and a moment M_t, applied at the pile head. Figure 2.4(b) shows the non-linear springs of the soil which are described by the p-y curves in Figure 2.4(c), where p is the resistance of the soil and y is the horizontal deflection of the pile (Reese et al. 2004).

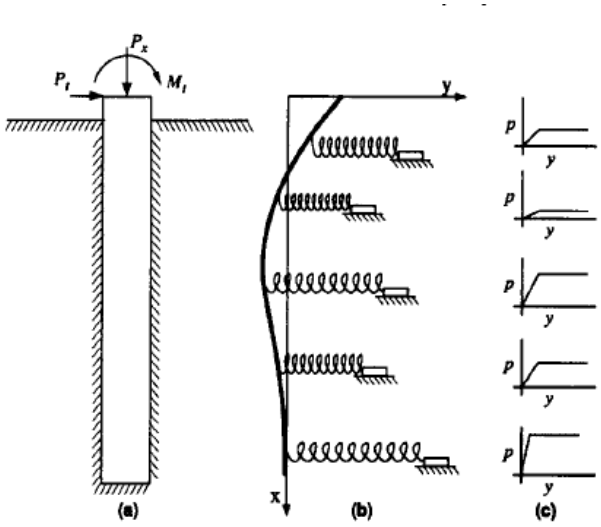

Figure 2.4: Model of laterally loaded pile: (a) Elevation view; (b) non-linear springs of soil; (c) p-y curves (Reese et al. 2004).

The computer program LPILE uses a finite difference method to analyze lateral loads with the p-y method. By using an iterative process, the program solves for the forces and displacements along the length of the pile and provides both numerical and graphical outputs (Reese et. al, 2004).

The soil properties used for LPILE input was obtained from the American Petroleum Institute (API, 1982). These properties include the unit weight γ, modulus of subgrade reaction k and friction angle φ. The friction angle has the greatest effect at large displacements where the soil failure occurs, while the subgrade reaction has the greatest effect at small displacements.

2.3 Seismic Performance of MSE Walls

Koseki (2012) did a seismic performance review on case histories in Japan and discovered that geosynthetic reinforced retaining structures outperformed conventional type retaining walls during earthquakes. After the 1995 Hyogoken-nanbu (Kobe) earthquake, retaining walls without a deep foundation suffered significant tilting or failure of the wall. In contrast, a geosynthetic-reinforced wall that was severely shaken displaced only about 4-8 in. During the 2011 Tohoku earthquake, an unreinforced embankment for newly-developed housing estates collapsed whereas an MSE wall at an adjacent site survived the earthquake (Figure 2.5).

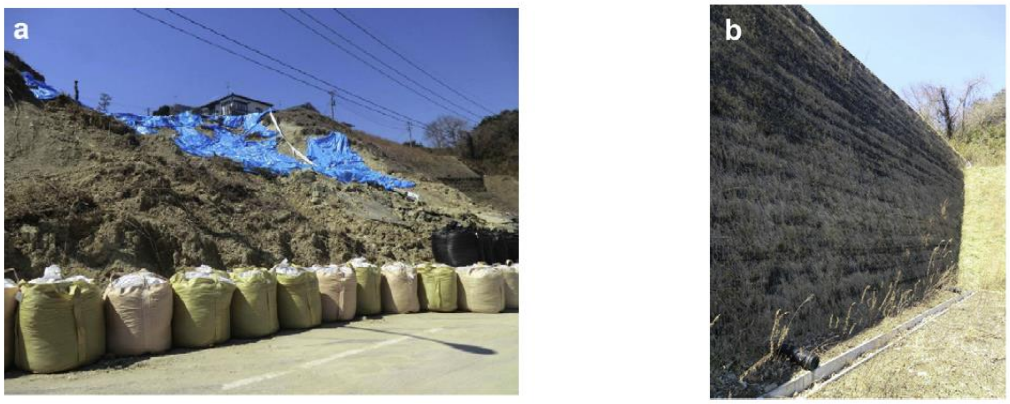

Figure 2.5: (a) Collapse of unreinforced embankment and (b) undamaged GRS RW at Yamamoto town, Miyagi (Koseki 2012).

Additionally, a series of small-scale 1 –g model tests was conducted on six different types of retaining walls. Test results indicate that up to seismic coefficient of about 0.35, there was no significant difference as far as horizontal displacements observed among the different wall types. However, under higher seismic loads, the wall displacements of conventional retaining walls increased rapidly while geosynthetic-reinforced walls exhibited more ductile behavior. Further observations showed that the uppermost reinforcement could effectively resist against overturning of the facing because the mobilization of tensile force was concentrated on that part of the reinforcement. Koseki suggests that partial extension of upper reinforcement layers improves the seismic stability of geosynthetic reinforced walls significantly.

An extension of the model tests was conducted using two different reinforcement materials: phosphor bronze and polyester reinforcements (Figure 2.6). The phosphor bronze (PB) reinforcement has higher tensile stiffness per single strip in direct tension and larger pull-out resistance per unit width at small levels of pull-out displacement. On the other hand, the polyester (PE) reinforcement has higher tensile stiffness per unit width and higher ultimate pull-out resistance per unit width (Table 2.1). Despite the reinforcement differences, the cumulative tilting angles and base sliding of the wall models were observed to be similar. Therefore, the results show that there was no significant difference between the two reinforcements.

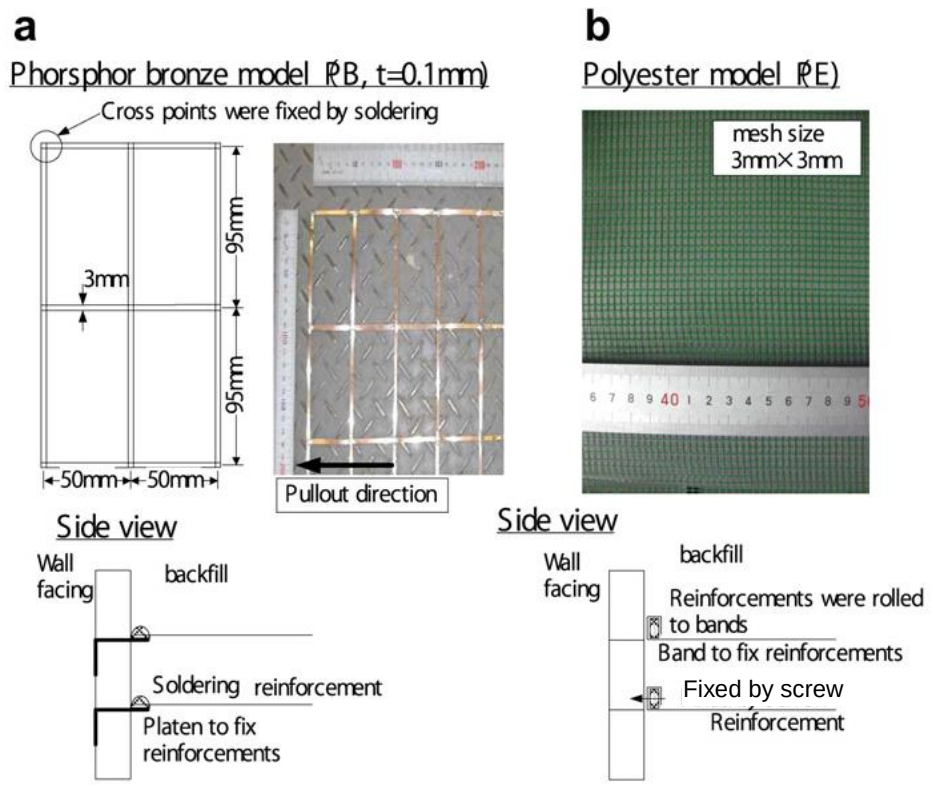

Figure 2.6: Model of reinforcement layer: (a) phosphor bronze model and (b) polyester model (Koseki 2012).

Table 2.1: Properties of model reinforcements (Koseki 2012).

Property	Secant tensile stiffness at $T = T_{max}/2$		Ultimate pull-out resistance, T_{max} at $\sigma_v = 5$ kPa
Unit	per single strip (kN/ε/strip)	per unit width (kN/ε/m)	per unit width for buried length of 0.5 m (kN/m)
PB	3.5–5.7	41–66	2.96[a]
PE	0.31–0.36	105–121	4.48

[a] Strips in the air ruptured under this tensile force.

2.4 Foundations for Integral Abutments

Dunker (2007) conducted research on foundation types used for integral abutment bridges. Steel H piles are the most common foundation for IAB in the United States but some soils require

the use of displacement piles. Therefore, some states permit the use of other foundations including precast pre-stressed concrete piles, pipe piles, and timber piles.

Currently many researchers analyze integral-abutment bridges using complex finite element methods but in practice such detailed analysis is seldom warranted. Most states use relatively simple length and skew rules for bridge design with typical state-designed details.

A recent survey shows that nearly half of the states preferred steel H piles oriented for weak axis bending while one-third preferred the piles oriented for strong axis bending (Maruri and Petro 2005). The weak-axis orientation preference was based on the argument that only the tips of flanges will yield under large-bending stresses allowing the basic core of the pile to carry vertical load, although some states claim that H piles oriented for strong-axis bending are better able to resist flange buckling. Some states permit the use of pipe piles for integral abutments, but since the piles are not as flexible as H piles there are shorter maximum bridge length requirements. Table 2.2 shows a summary of the different foundation types.

Table 2.2: Summary of foundation types (Dunker 2007).

Type	Comments	State policies and examples	References
Steel H pile, weak axis	Potential for yield and low-cycle fatigue, need for relatively compact shape	Iowa, N.Y., and W.Va. policies	Iowa DOT (2006), New York DOT (2002), West Virginia DOT (2004)
Steel H pile, strong axis	Less flexible than weak axis orientation, may be less subject to flange buckling	Tenn., Colo., and Ill. policies	Burdette et al. (2002), Colorado DOT (2002), Illinois DOT (2003)
Prestressed concrete pile	Less flexible than H pile, may require padding	Tenn. policy, Iowa example	Burdette et al. (2004), Abendroth et al., unpublished manuscript, (2006)
Pipe pile	Less flexible than H pile	Ill., N.Y., and N.J. policies	Illinois DOT (2003), New York DOT (2002), New Jersey DOT (2004)
Timber pile	Less flexible than H pile, may require padding	Iowa policy	Iowa DOT (2006)
Combined pile and drilled shaft	Accommodates sensitive adjacent structures	Iowa example, Colo. examples	Liu et al. (2005)
Drilled shaft	Minimal flexibility	Colo. example	Liu et al. (2005)
Sheet pile	Limited to relatively short bridges	N.Y. examples	Carle and Whitaker (1989)
Spread footing	Minimal flexibility	Tenn. and Me. policies	PCI (2001), Maine DOT (2003)

2.5 Full Scale Testing of Piles behind MSE Walls

2.5.1. Full Scale Testing by Pierson.

Relatively few full-scale tests have been performed to evaluate the lateral resistance of piles near MSE walls. Pierson et al. (2009) conducted a series of full-scale lateral load tests on 36 in. diameter drilled shafts located at four distances behind a 20 ft. high block masonry wall reinforced with extensible geogrids. The reinforcement layers consisted of uniaxial high density polyethylene punched-drawn geogrid that were spaced vertically every 2 ft. of elevation. The lowest four reinforcement layers had an ultimate tensile strength of 7810 lb/ft while the upper six layers had an ultimate tensile strength of 4800 lb/ft. The geogrid length was 14 ft. or 0.7 times the height of the wall. The shafts were embedded 15 and 20 ft. into the reinforced soil to compare the capacity of shorter shafts with their full depth counterparts. Additionally, vertical slip joints were used to isolate the test sections from each other.

The shafts were instrumented with five LVDTs, a hydraulic pressure gage, and a load cell attached to a data acquisition system to monitor pile head load and deflection. The hydraulic pressure gauge was used to check the accuracy of the load cell. Each test shaft and reaction shaft had two LVDTs attached while the hydraulic ram had a LVDT to check the accuracy of the shaft LVDTs. Inclinometers were used to determine shaft deflection versus depth and to determine shaft bending. A second data acquisition system was used to measure the performance of the MSE wall using pressure cells and strain gauges. The pressure cells were placed against the back face of the wall in line with each test pile at three different elevations. The strain gauges were placed along the geogrid reinforcement at varying distances from the wall. Figure 2.7 shows the instrumentation layout for one shaft. Photogrammetry was used to monitor the displacement of the MSE wall during testing. This process involved using PVC targets attached to the wall with a 6 in. scale on

each target. Images of the wall and targets were taken using a high-quality digital SLR camera before and during testing. The images were rastered into AutoCAD to determine the wall displacements at different locations.

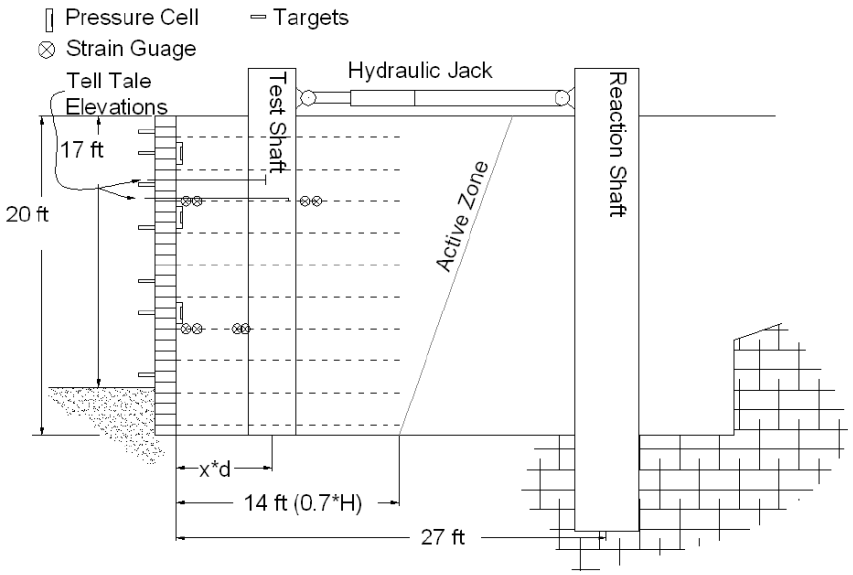

Figure 2.7: Elevation view of shaft and instrumentation locations (Pierson et al. 2009).

Test results showed that the lateral resistance of the shaft spaced two diameters behind the wall (Shaft B) was about 50 percent of the resistance provided by the shaft spaced four diameters behind the wall (Shaft D) as shown in Figure 2.8. The lateral resistance of the shaft spaced one diameter behind the wall (Shaft A) was even lower, clearly indicating that lateral resistance of piles decreases significantly as the piles are located closer to the MSE wall face. Cracks behind the reinforced zone were observed after testing which showed that longer reinforcements may provide additional capacity.

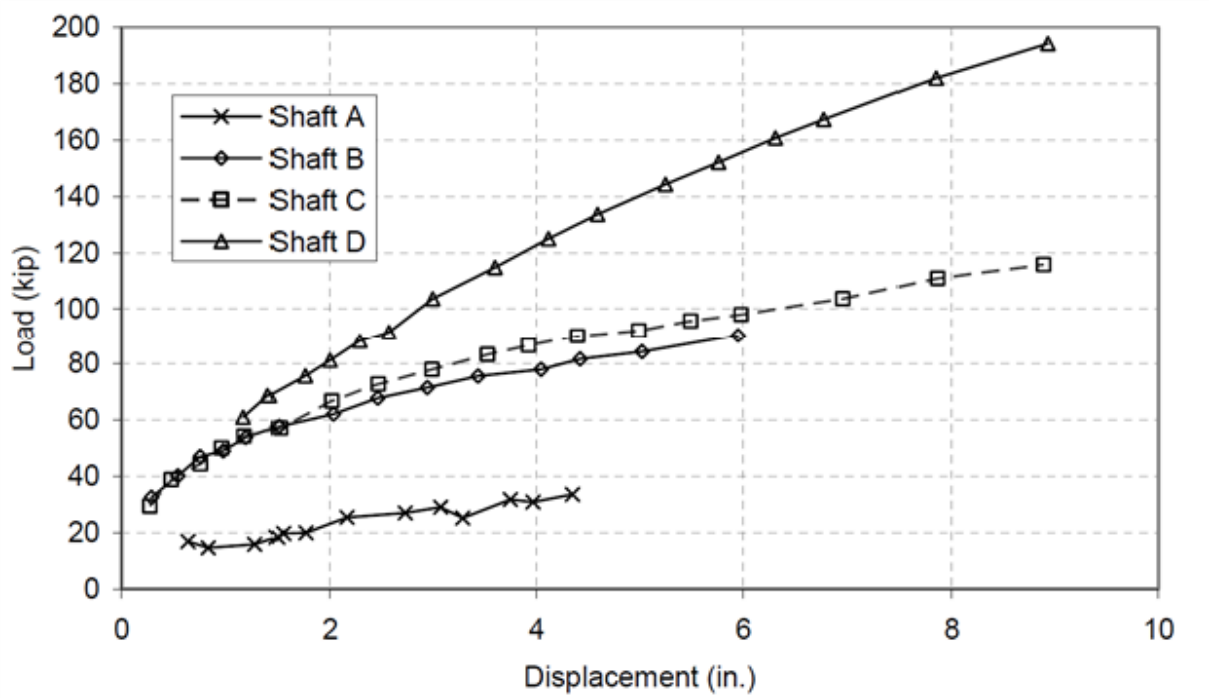

Figure 2.8: Load vs. deflection curve modified from Piersons et al. (2009).

2.5.2. Full Scale Testing by Nelson

In another full-scale test conducted by Nelson (2013), 12.75 in. diameter piles were tested at three locations behind wire mesh wall panels reinforced with steel strip reinforcements. Test piles were spaced at 6.3, 2.7 and 1.3 pile diameters behind the wall face. The reinforcement layers consisted of galvanized ribbed steel strips manufactured by Reinforced Earth Co. that were 2 in. wide and 1/8 in. thick spaced vertically every 2 ft. At the time of testing, the strip length to wall ratio was 1.1 and the static factor of safety against pull-out of the reinforcement was approximately 2.6. The piles extended 20 ft. below the base of the wall and were hollow during testing so that the section would behave elastically to facilitate interpretation of the results.

The pile load was monitored by a load cell placed between the hydraulic jack and the pile. Hemispherical end platens were placed between the load cell and the pile to minimize eccentric

loading on the load cell. A pressure gauge attached to the hydraulic jack was used as a check on the load cell by comparing the measured hydraulic pressure to readings obtained from the load cell during testing. Strain gauges were installed in pairs at varying distances along the steel strips to determine the load in the reinforcement. Strain gauges were also mounted on the piles at different depths to measure the pile bending moment. String potentiometers (linear motion transducers) were used to measure the displacement and rotation of the piles along with the displacement of the ground and top of the wall in line with the pile. LVDTs were placed against the front face of the MSE wall to measure the displacement of the top wall panel.

Test results showed that the piles at a distance of 1.3 diameter (1.3D) and 2.7D from the wall provided 40 percent and 70 percent of the resistance of the pile at 6.3D from the wall, respectively (Figure 2.9). Although evidently there was decrease in resistance with decreasing distance from the wall as determined by Pierson et al. (2009), the amount of resistance which was not consistent with Pierson suggests that further studies would be required to determine a better relationship between pile resistance and distance from wall. Results from the analysis was also used to develop a plot of the p-multiplier vs. normalized distance from the wall, taken as the distance from the back face of the wall to the center of the pile (S) divided by the diameter of the pile (D) as shown in Figure 2.10. According to Figure 2.10, when a pile is spaced at least 4.5 pile diameters behind the wall with a reinforcement length to wall height ratio of 1.1, a p-multiplier of 1 can be used which means that there is no influence of the wall on the lateral resistance of the pile.

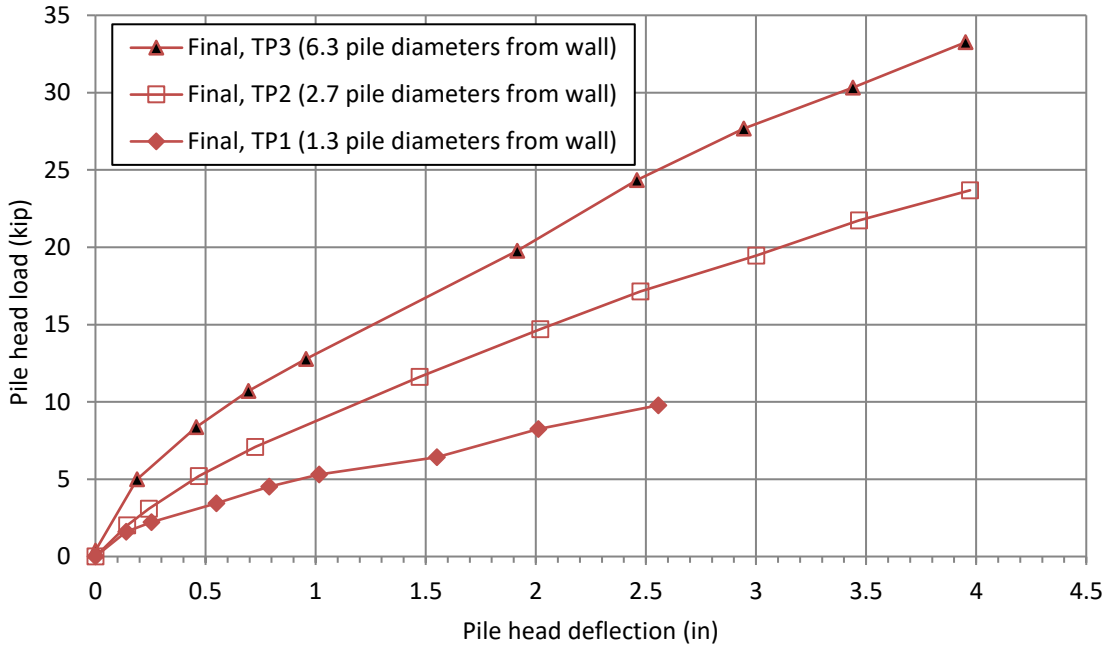

Figure 2.9: Load vs. deflection curve for final data points (Nelson 2013).

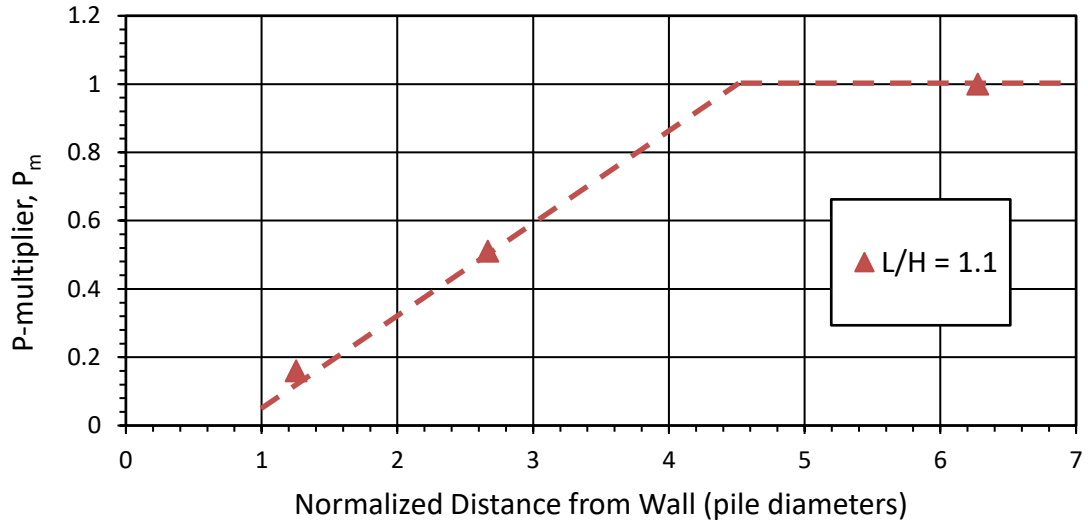

Figure 2.10: Tentative p-multiplier curve as a function of normalized distance. Note: L is the length of the MSE reinforcement and H is the wall height (Nelson 2013).

Induced loads in reinforcement obtained from the strain gauges were used to develop a normalized induced force vs. normalized transverse distance plot as shown in Figure 2.11. The

normalized force is taken as the maximum measured load in the reinforcement divided by the maximum lateral load while the normalized transverse distance is taken as the transverse spacing from the center of the strip reinforcement to the center of the pile divided by the spacing from the back face of the wall to the center of the pile. Due to a significant scatter of the points (R^2=0.33), a design envelope was developed as a guideline for maximum force in reinforcement with L/H of 1.1.

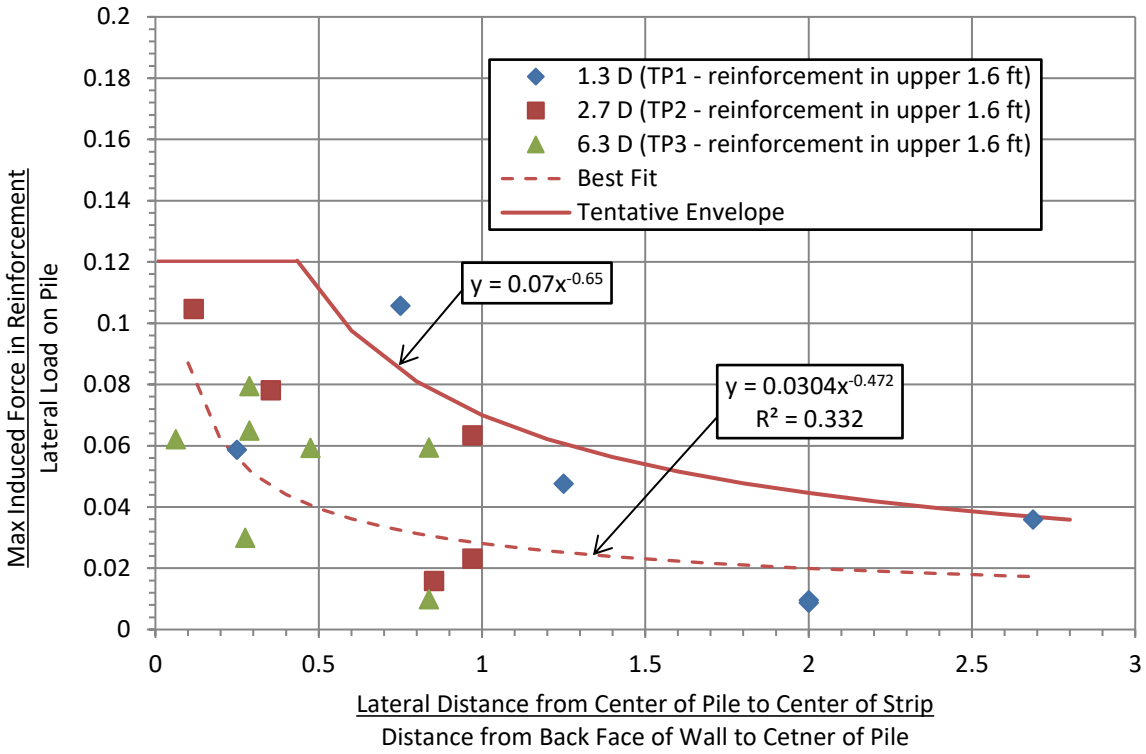

Figure 2.11: Plot of normalized induced force in strap reinforcement vs. normalized transverse distance from pile (Nelson 2013).

2.5.3. Full Scale Testing by Price

Price (2012) conducted a series of full-scale lateral load tests on five piles located at various distances behind MSE walls. The first two pile tests were performed on 12.75 in. diameter steel pipe piles behind a 20 ft. high wall. The wall consisted of 6 in. thick concrete wall panels and the

soil was reinforced with welded wire grids manufactured by SSL, Inc. The welded wire grids consisted of three to six longitudinal wires with a center to center spacing of 8 in. The longitudinal wires were size 20 wires (0.504 in. diameter) for the bottom three to four layers of reinforcement and size 11 wires (0.374 in. diameters) for the upper four to eight layers. The cross wires were size 11 wires spaced every 1.0 to 2.5 ft. The grids were placed horizontally every 6 ft. and spaced vertically every 2.5 ft. The reinforcement length to wall height ratio (L/H) during testing was 1.6. The next three pile tests were performed at a different location on 16 in. diameter steel pipe piles behind a 6 in. thick concrete wall panel and the soil was reinforced with welded wire grids. The layout of the reinforcement was similar to the first two tests. The L/H ratio during testing was 1.7 for one pile and 1.1 for the other two piles.

Instrumentation for this series of tests was essentially the same as the ones used by Nelson (2013) and included a load cell to monitor load, strain gauges to determine load in soil reinforcement and bending moment in piles, string potentiometer to measure the displacement and rotation of the pile, and LVDT to measure the displacement of the top wall panel. In addition to this instrumentation, Price (2012) also used a Measurand ShapeAccelArray (SAA), i.e. Shape Array that was placed vertically along the back face of the wall to measure the deformation of the wall.

The first two test results showed that the lateral resistance of the pile located 7.5D from the wall was only slightly higher than that of the pile located 3.8D from the wall as shown in Figure 2.12. These results suggest that the reinforcement length was sufficient to prevent a reduction in lateral pile resistance or that both piles were far enough back from the wall that the wall had negligible influence on the lateral resistance. Results for the following three tests showed that the piles at a distance of 2.9D and 1.6D from the wall provided about 80 percent and 50 percent of the

resistance of the pile at 5.2D from the wall, respectively, as shown in Figure 2.13. Results from the analysis were used to develop a plot of p-multiplier vs. normalized distance from the wall as shown in Figure 2.14. According to Figure 2.14, when a pile is spaced at least 3.8 pile diameters behind the wall with a reinforcement length to wall height (L/H) ratio of 1.6, a p-multiplier of 1 can be used whereas when a pile is spaced at least 5.2 pile diameters behind the wall with a L/H ratio of 1.1, a p-multiplier of 1 can be used. A normalized induced force vs. normalized transverse distance plot was developed and a design envelope was proposed as a guideline for maximum force in reinforcement with L/H values ranging from 1.1 to 1.6 (Figure 2.15).

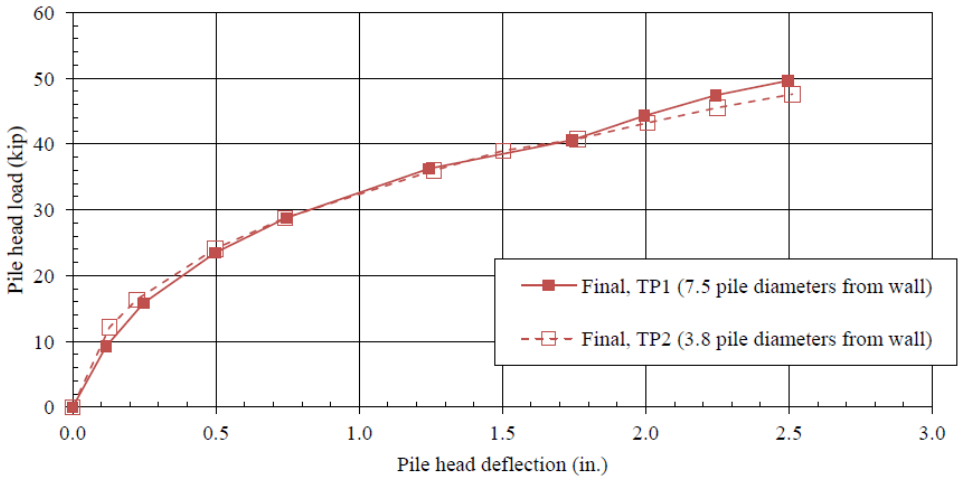

Figure 2.12: Load vs. deflection curve for TP1 and TP2 final points (Price 2012).

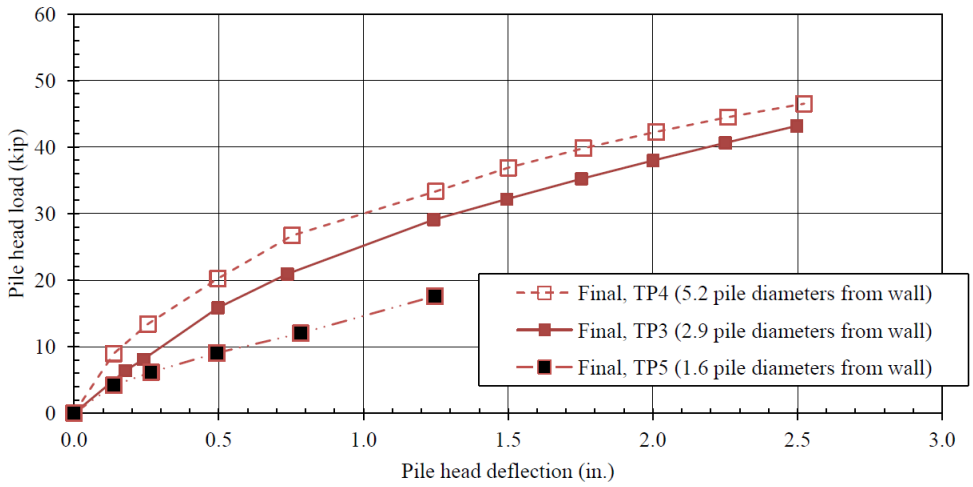

Figure 2.13: Load vs. deflection curve for TP3 to TP5 final points (Price 2012).

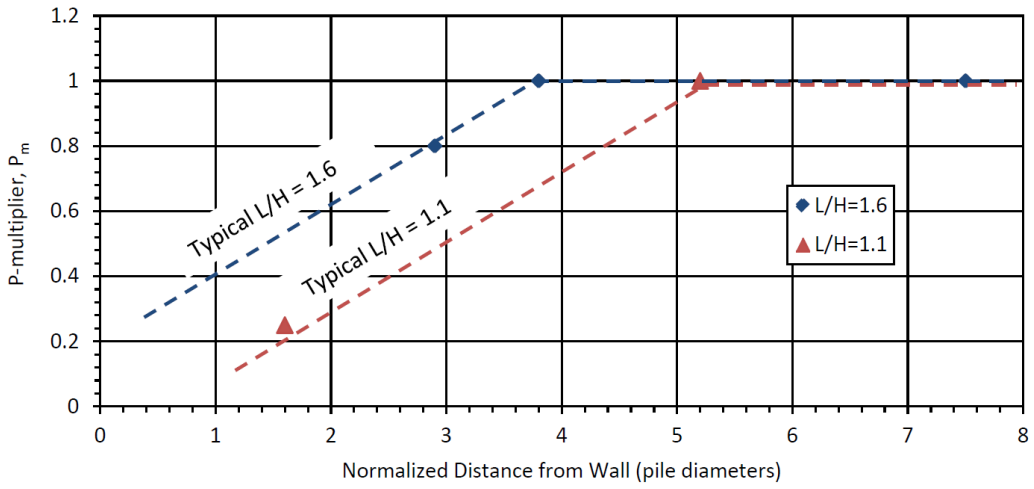

Figure 2.14: Tentative p-multiplier curve as a function of normalized distance. Note: L is the length of the MSE reinforcement and H is the wall height (Price 2012).

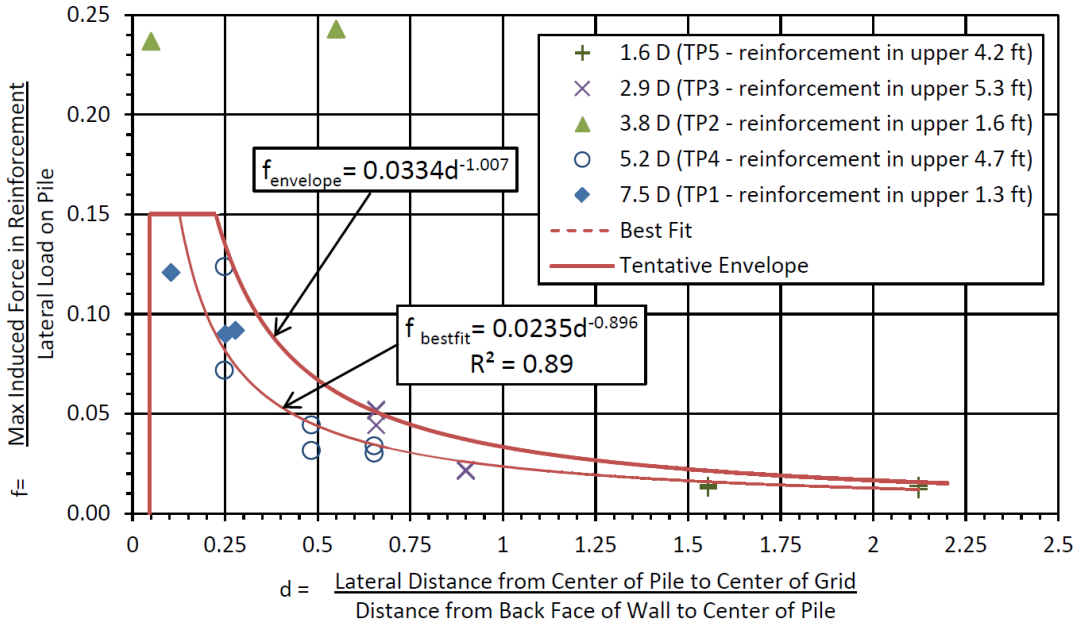

Figure 2.15: Plot of normalized induced force in grid reinforcement vs. normalized transverse distance from pile (Price 2012).

2.6 Numerical Analysis of Piles behind MSE Walls

Daily and seasonal thermal expansions and contractions of bridges have a major influence on the lateral loading of integral bridges. Khodair and Hassiotis (2005) conducted a study on the effect of thermal loading on the soil/pile system. Experimental data was obtained from the Scotch Road I-95 integral bridge that was supported by H-piles with compact flanges. The piles were oriented for weak axes bending to increase flexibility and placed inside a corrugated steel sleeve before being filled with sand. A Finite Element (FE) model was built to simulate the pile by comparing with the measured experimental data and Finite Difference (FD) solutions obtained from LPILE. Their findings showed that the stresses in the piles did not induce significant pressures on the reinforced soil, suggesting that lateral load transfer from the pile to the MSE wall due to thermal loading is inconsequential. The results also showed that the magnitude of the axial

stresses in the pile decreases as the diameter of the sleeve and the amount of sand increases, suggesting that the sand acts as a malleable media that absorbs the energy in the steel pile.

Another study on integral abutment bridge (IAB) response under thermal loading was conducted by Kim and Laman (2010). Two dimensional (2D) numerical models simulating the AASHTO prescribed 75-year bridge life were used to investigate IAB responses of (1) the girder axial force, (2) the girder bending moment, (3) the pile lateral force, (4) the pile bending moment, and (5) the pile head/abutment displacement. The parameter selection was based on a previously conducted study and observed IAB behavior, which were:

- The thermal expansion coefficient, α.
- The span length, L.
- The backfill height, H.
- The backfill stiffness, B.
- The pile soil stiffness, P.

Results showed that both the pile lateral force and moment were significantly influenced by the thermal expansion coefficient, bridge length, and pile soil stiffness. An increase in bridge length and pile soil stiffness increases pile lateral force and pile moment (Figure 2.16). The study case with thermal coefficient, $\alpha = 14.4 \times 10^{-6}/℃$ (8.0×10^{-6}°F), $L = 121.9\,m$ ($400\,ft$), $H = 3.0\,m$ ($10\,ft$), $B = low\ value$, $P = high\ value$ produced the largest pile shear force of 425 kN (96 kips). The pile head/abutment displacement is primarily influenced by the magnitude of the thermal coefficient, bridge length and pile soil stiffness. An increase in bridge length increases pile head displacement but an increase in pile soil stiffness reduces pile head displacement (Figure 2.17). The study case with thermal coefficient, $\alpha = 14.4 \times 10^{-6}/℃$ (8.0×10^{-6}°F), $L =$

$121.9\,m\,(400\,ft)$, $H = 6.1\,m\,(20\,ft)$, $B = low\ value$, $P = low\ value$ produced the extreme displacement of 37 mm (1.45in). The backfill height and backfill stiffness have relatively insignificant influences on the bridge response.

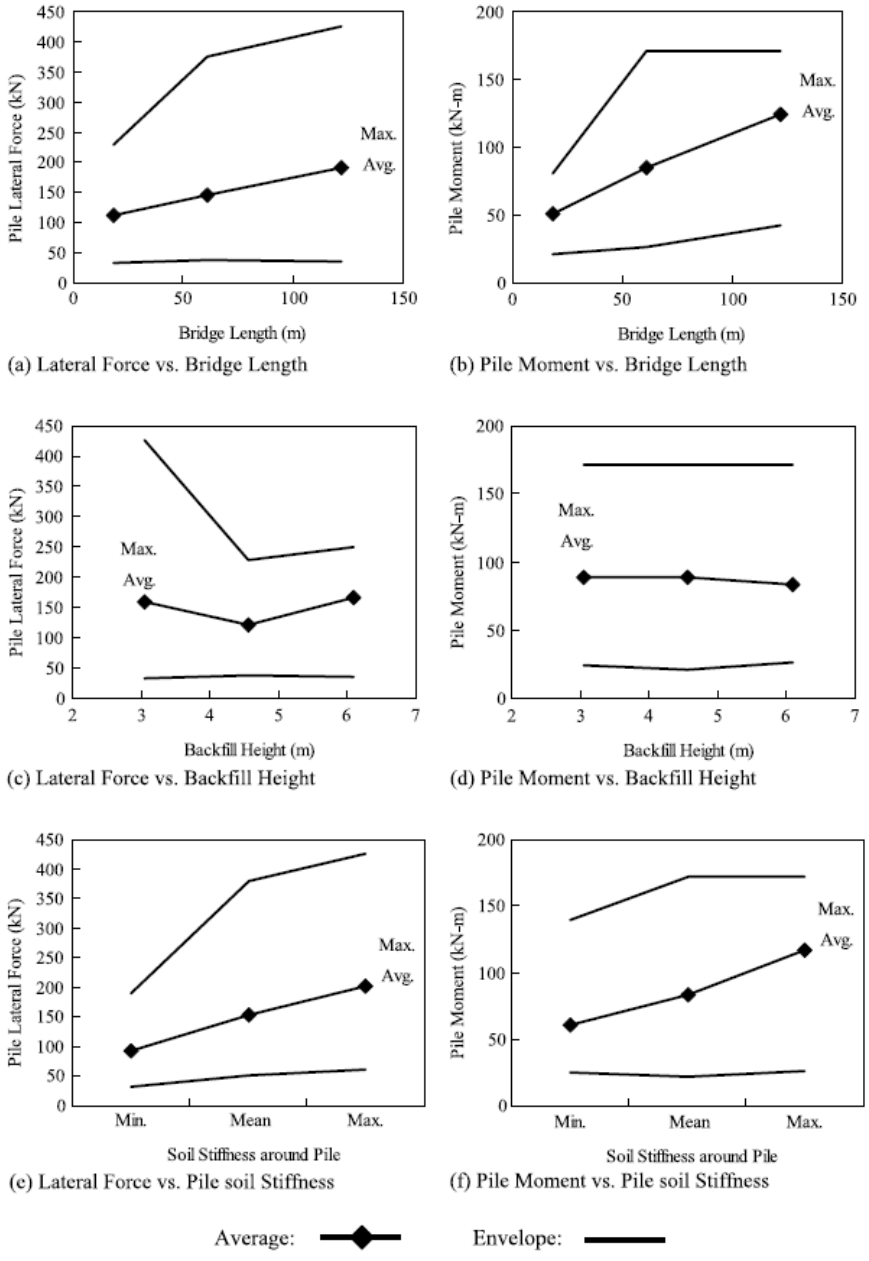

Figure 2.16: Pile responses (Kim and Laman, 2010).

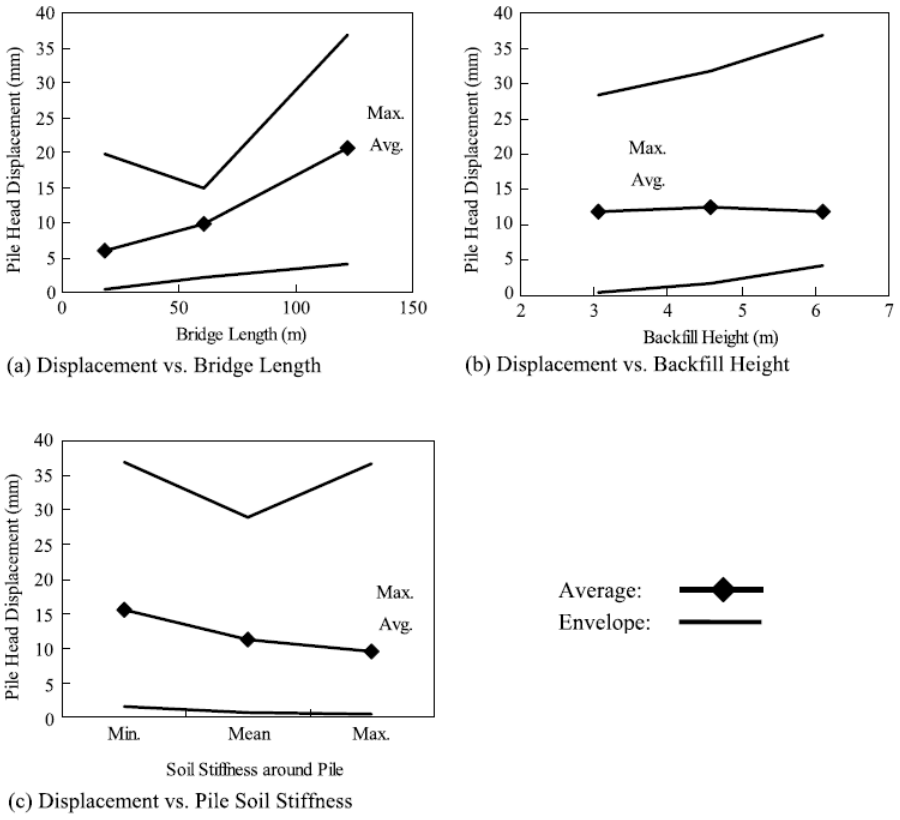

Figure 2.17: Pile head displacements (Kim and Laman, 2010).

2.7 Conclusions and Limitations

Based on previous studies, it can be concluded that the lateral resistance of pile decreases as the distance of the pile behind an MSE wall decreases. However, due to the limited number of test previously performed it is unclear if any of the suggested guidelines can be used with confidence. It is also still uncertain whether the reinforcement length influences the results. Other factors including soil compaction and plastic sheet wrapping may also affect the lateral resistance of piles behind an MSE wall.

This study involves pipe pile behind an MSE wall reinforced with ribbed steel strips and is similar to tests previously performed by Nelson (2013). The data from this study will clarify results and guidelines presented by Nelson.

3 TEST LAYOUT

Lateral load tests were performed at Geneva Rock Mt. Jordan gravel pit in Draper, Utah as shown in Figure 3.1. A full-scale MSE wall was built at the gravel pit with sixteen steel piles placed at various distances behind the wall along with an extra nine piles placed further behind the wall as reaction piles. The plan view, elevation view, and profile view of the load tests are shown in Figures 3.2 through 3.4. The overall scope of the project involved tests on twelve steel pipe piles and seven square steel piles donated by Atlas Steel and five steel H piles donated by Skyline Steel and Spartan Steel. Soil reinforcement consisted of ribbed steel strip reinforcement as well as welded wire grid reinforcement. This thesis will focus exclusively on the lateral load tests involving steel pipe piles behind the MSE wall reinforced with ribbed strip reinforcements.

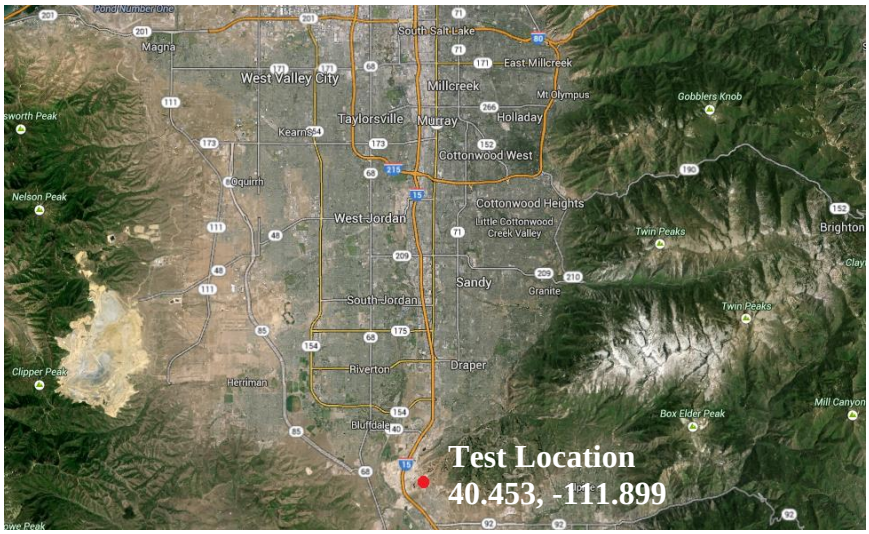

Figure 3.1: Test location shown in red.

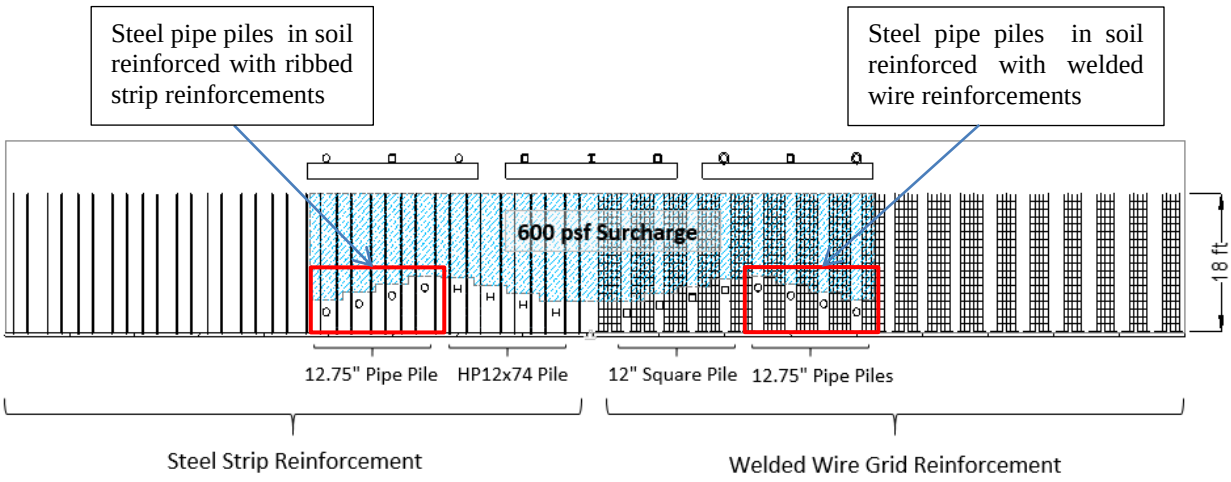

Figure 3.2: Plan view of test wall.

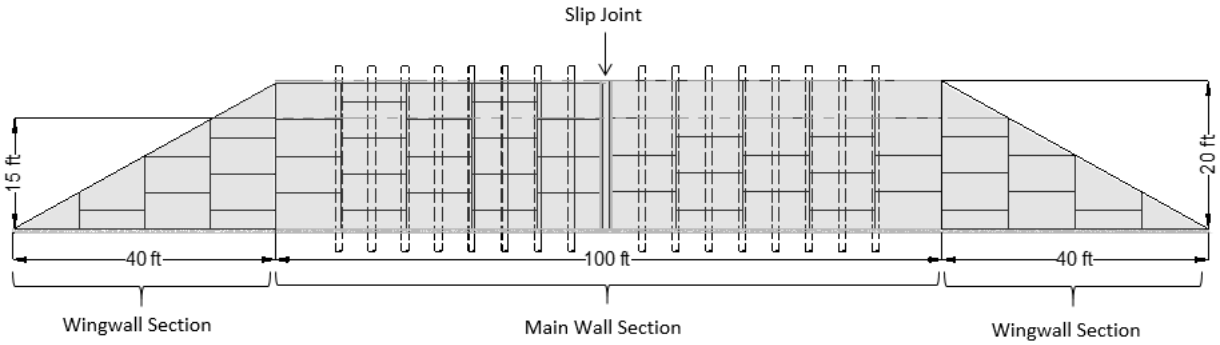

Figure 3.3: Elevation view of test wall.

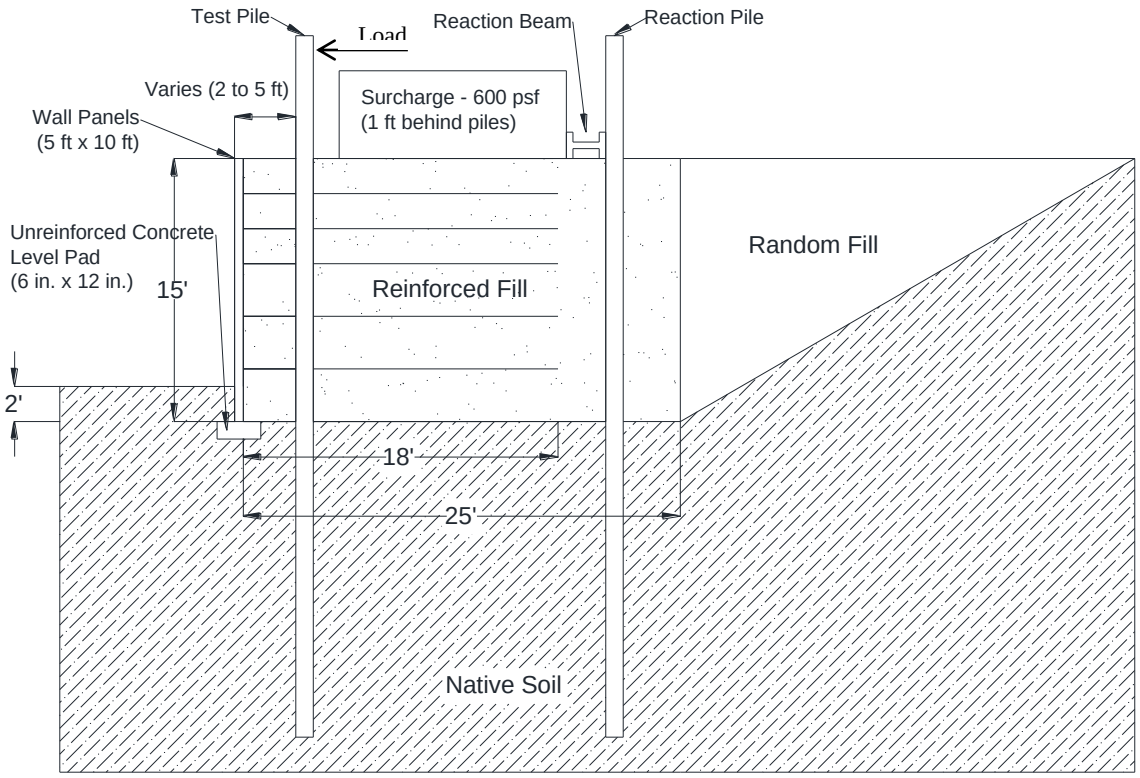

Figure 3.4: Profile view of test wall.

3.1 MSE Wall

The main section of the wall consisted of an MSE wall with concrete facing panels that are 6 in. thick and nominally 5 ft. high by 10 ft. long. The wall panels were embedded 2 ft. below the ground surface and supported on an unreinforced concrete footing as shown in figure 3.4. The first stage of testing involved having the wall constructed to a height of 15 ft. followed by a series of lateral load tests. After the completion of the tests, the wall was constructed to a height of 20 ft. for the next set of lateral load tests. A triangular wall face was constructed at either side of the main section using concrete wall panels to bring the wall down to the native ground surface at a slope of about 2H to 1V. Concrete blocks were placed behind the wall approximately 1 ft. behind

each test pile to simulate a uniform surcharge load of 600 psf as shown in Figure 3.5. The surcharge weight of 600 psf was equivalent to an additional fill height of about 5 ft. which brought the reinforcement length to total height ratio to about 0.90 for the 15 ft. high wall.

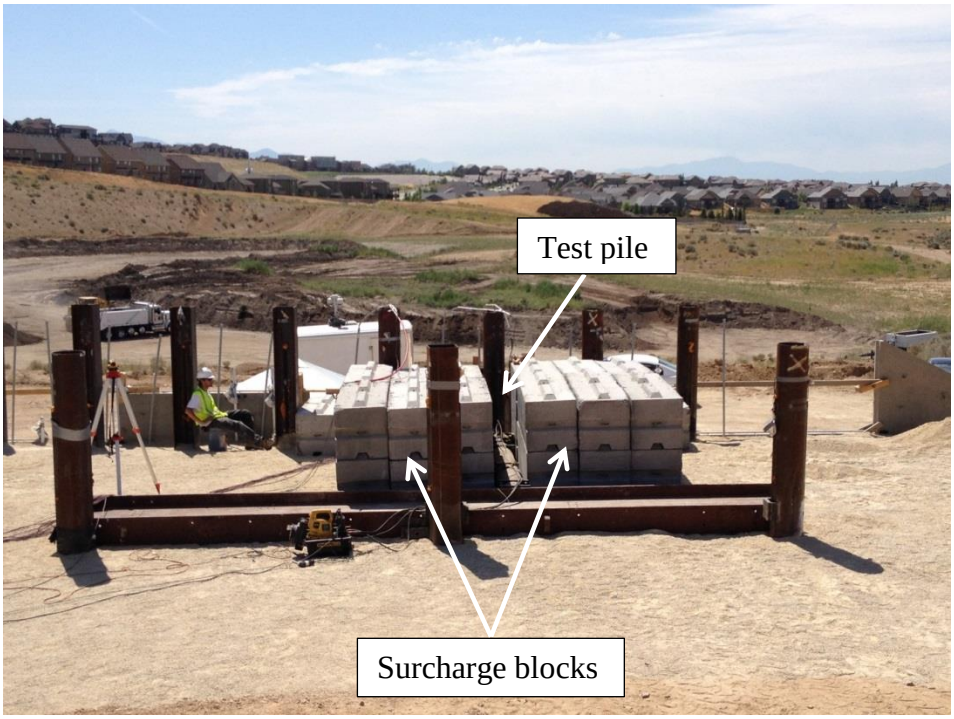

Figure 3.5: Surcharge blocks placed behind pile with gap for load system.

Half of the main wall was reinforced using steel strip type reinforcements designed and donated by Reinforced Earth Company. The other half of the wall was reinforced using steel grid type reinforcements designed and donated by SSL, Inc. for a total wall length of 100 ft. Photographs of the steel strip type and steel grid type reinforcements are shown in Figures 3.6 and 3.7. The strip reinforcements consist of galvanized steel ribbed strips that are 50 mm (1.97 in.) wide and 4 mm (0.16 in.) thick. The welded wire grid reinforcements consist of five or six longitudinal wires with a center to center spacing of 8 in. The center to center spacing of the cross wires for the upper first layer is 6 in. while the rest of the layers have a center to center cross wire

spacing of 12 in. Both longitudinal and cross wires are all size 11 wires (0.374 in. diameter). The horizontal spacing of the steel grids at the same elevation from center to center is typically 5 ft. while the horizontal spacing of the steel strips is typically 2.25 ft. The vertical spacing for both the steel strips and steel grids is typically 2.5 ft. The reinforcement length for both steel strips and steel grids is 18 ft. The design parameters of the MSE wall are shown in Table 3.1.

Figure 3.6: Ribbed strip reinforcements and welded wire grid reinforcements.

Figure 3.7: Welded wire grid reinforcements.

Table 3.1: MSE wall parameters.

MSE wall	Stage 1	Stage 2
Wall height (ft)	15	20
Wall height including surcharge (ft)	20	25
Reinforcement length (ft)	18	18
Reinforcement length to wall height ratio	0.9	0.72

The static factor of safety against pull-out of the steel strip reinforcements for the MSE wall geometry at the time of testing was approximately 2.7 as calculated in Appendix A using procedures specified by FHWA (Berg et al., 2009). The actual locations of the pipe piles in soil reinforced with steel strips are 1.7 (22.4 in.), 2.8 (35.4 in.), 3.1 (39.4 in.) and 3.9 (49.9 in) pile diameters behind the back face of the MSE wall and the test piles will herein be referred to as

1.7D, 2.8D, 3.1D and 3.9D respectively. The piles were laterally loaded normal to the MSE wall on planes shown in the profile view in Figure 3.4.

3.2 Backfill

The reinforced soil consisted of gravelly sand corresponding to AASHTO classification A-1-a provided by Geneva Rock. The laboratory test report by Geneva Rock is found in Appendix B and shows that the standard Proctor maximum density was 128.0 pcf with an optimum moisture content of 7.8 percent. Reinforced soil samples were taken back to the laboratory at Brigham Young University for test comparisons and show that the mean grain size (D_{50}) was 2.3 mm, the coefficient of gradation (C_c) was 2.4, the coefficient of uniformity (C_u) was 40 and the fines content was 14%. The gradation curve is shown in Figure 3.8 below and is comparable with test results provided by Geneva Rock.

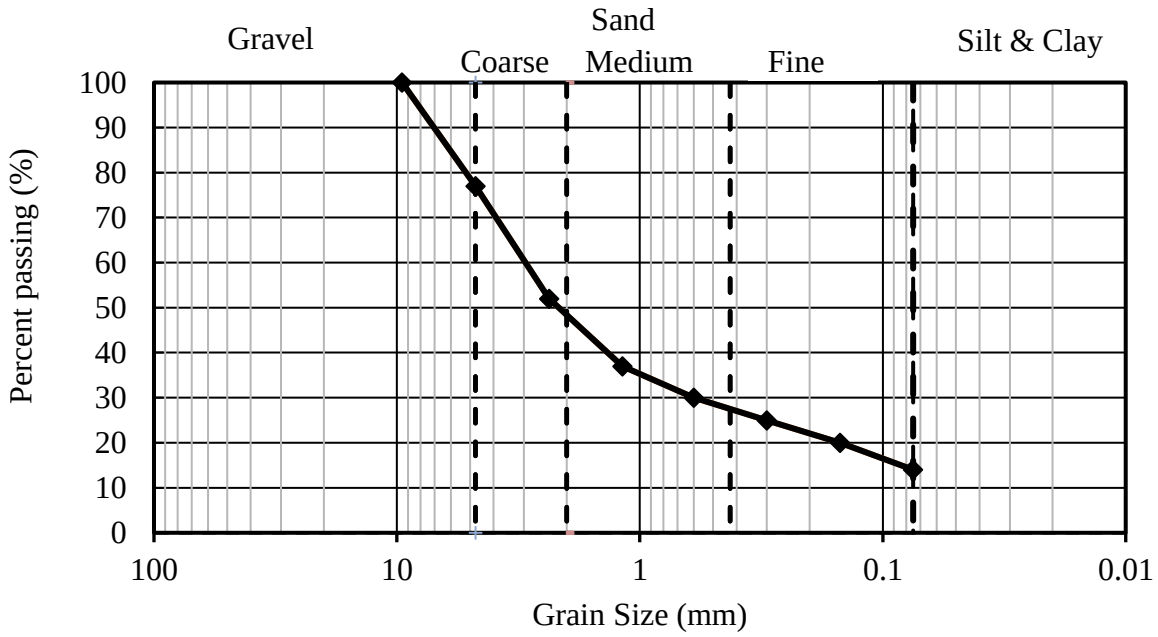

Figure 3.8: Gradation for reinforced soil.

The fill was compacted to 95 percent of the standard Proctor maximum density in accordance with typical AASHTO specifications using roller compactors along with jumping jack compactors around the piles and vibratory plate compactors within 3 ft. of the MSE wall face where roller compactors were not accessible. Photographs of compaction using roller compaction, jumping jack and plate compaction is shown in Figures 3.9 and Figure 3.10. In-place nuclear density tests were typically done for each 12 inch lift thickness with the exception of locations within 3 ft. of the wall where 6 inch lift thickness was required when using the plate compactor. A photo of nuclear density test along with profiles of relative density and moisture content can be found in Figures 3.11, 3.12 and 3.13 respectively.

Figure 3.9: Roller compaction between test and reaction piles.

Figure 3.10: Jumping jacks for compaction around test piles and vibratory plate for compaction within 3 ft. of wall.

Figure 3.11: In-place nuclear density gauge test.

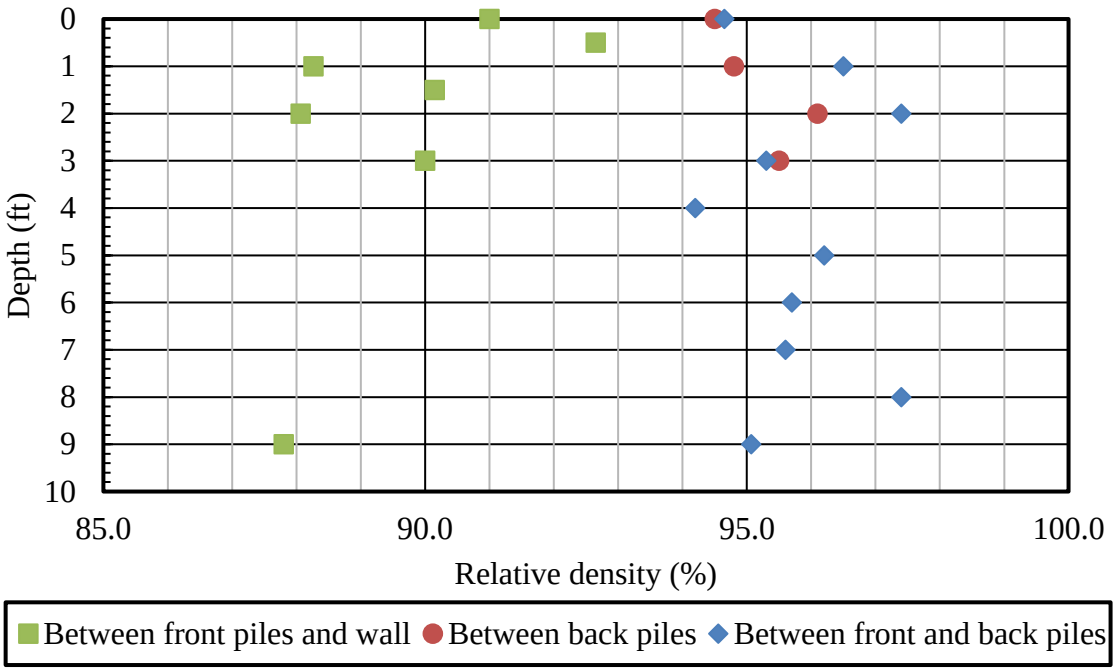

Figure 3.12: Relative density profile of reinforced fill with depth.

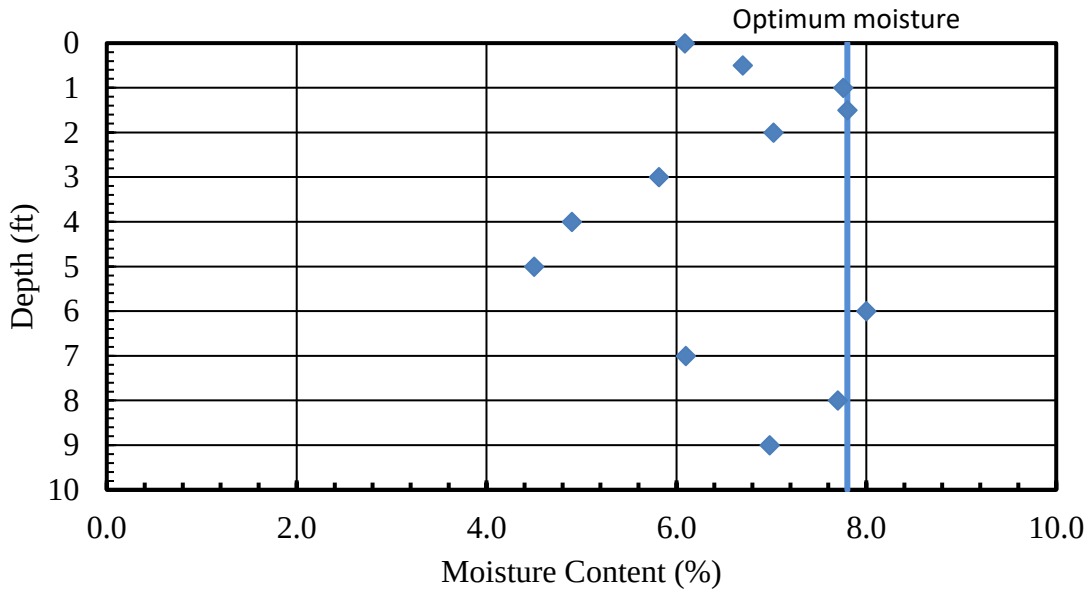

Figure 3.13: Moisture content profile of reinforced fill with depth.

According to Figure 3.12, compaction between test piles and the wall was generally less than the specified 95 percent density. This is because the vibratory plate compactor was not adequate to provide the compaction needed even when 6 inch lift thickness was applied within 3 ft. of the wall. This presents a realistic situation where generally reinforced soil close to the wall might not have proper compaction due to the presence of the piles that prevent access for roller compactors.

3.3 Test Piles

The pipe piles are 12.75 in. in diameter with a wall thickness of 0.375 in, the H piles are HP 12x74, and the square piles have 12 in. dimensions with a wall thickness of 0.233 in. The steel of the pipe pile was fabricated in accordance to ASTM A252-10 Grade 3 specifications and has a minimum yield strength of 45 ksi. The steel of the H pile conforms to ASTM A572-50 specifications and has a minimum yield strength of 50 ksi while the steel of the square pile conforms to ASTM A500-10A Grade B&C specifications and has a minimum yield strength of 46 ksi. Material test report shows that the piles have a yield strength of about 57 ksi. Pile properties are summarized in Table 3.2 below.

Table 3.2: Pile properties.

Pile Type	Diameter/Depth/ Flange Width (in)	Wall/Web/Flange Thickness (in)	Moment of Inertia [with angle iron] (in4)	Yield Strength (ksi)
Round	12.75	0.375	279 [314]	57
Square	12	0.233	248 [335]	57
HP12x74	12.1	0.61	185 [186]	57

The piles were driven open ended prior to the construction of the MSE wall and extend approximately 18 ft. into the underlying sand at the test site. Typically, the test piles were positioned at distances of two, three, four, and five pile diameters/width from the center of the pile to the back of the MSE wall as shown in Figure 3.1. Pile driving was performed by Desert Deep Foundation, Inc. using an ICE I30 v2 diesel hammer. Although pipe piles are often filled with concrete in practice, the test piles were left hollow during testing to eliminate any non-linear behavior from the cracking of concrete. Square steel piles were used rather than square concrete piles for that same reason and to allow direct comparisons without concerns about different interface friction coefficients. A picture of pile driving is shown in Figure 3.14 and pile driving blow counts can be found in Table 3.3.

Figure 3.14: Pile driving using a diesel hammer.

Table 3.3: Pile driving blow counts.

Depth (ft)	N (blowcounts) Strip Reinforcement				N (blowcounts) Welded Wire Reinforcement			
	1.7D	2.8D	3.1D	3.9D	1.9D	3.2D	4.3D	5.3D
1	-	-	-	-	-	-	-	-
2	-	-	-	-	1	1	-	-
3	-	-	2	-	1	1	-	-
4	-	1	-	-	1		2	1
5	1	-	-	-	1	1	-	-
6	-	-	1	2	1	1	-	-
7	-	-	-	-	3	1	2	2
8	-	2	1	-	3	-	-	-
9	2	-	1	2	3	-	-	2
10	1	2	1	1	5	-	7	2
11	1	1	2	3	5	-	6	6
12	1	2	5	3	5	-	7	6
13	3	6	5	5	3	-	5	5
14	5	5	5	5	3	25	4	3
15	6	4	5	4	3	-	-	2
16	4	4	4	2	3	-	3	2
17	4	1	1	2	3	-	4	3
18	2	2	3	3	3	5	3	4
Total	30	30	36	32	47	38	47	33

4 INSTRUMENTATION

4.1 Load Cell and Pressure Gauge

A load cell and a pressure transducer were used to monitor the load applied to each pile. Both the load cell and pressure transducer were connected to a data logger and then placed between the hydraulic jack and the pile. The load cell was pin connected securely to a steel channel that was welded onto the pile. This prevented the whole loading system from slipping when the pile rotated during loading. Hemispherical end platens were placed at the back between the reaction pile and loading system to minimize eccentric loading on the load cell. The typical configuration is shown in the photograph presented in Figure 4.1. The figure shows a typical configuration just prior to testing on a pile.

4.2 Strain Gauges with Strip Reinforcement

Strain gauges were used to determine the load in the soil reinforcements. The gauges were attached to the reinforcements in accordance to the manufacturer's recommended installation procedures. Details on the strain gauge installation are discussed in the following sections.

General purpose Texas Measurements Group standard electrical resistance strain gauges were placed on eight steel ribbed strip reinforcements. WFLA-6-11 series gauges were used with lead wire lengths varying from 10 to 26 ft. The strain gauges were mounted in pairs with one located on the top and one on the bottom of the reinforcement to provide redundancy in case of damage during wall construction. They also allow corrections for bending in the reinforcements.

The strain gauges were placed on two strip reinforcements between selected test piles and only on the top two reinforcement layers (15 in. and 45 in. depth) of the wall where load transfer from the test piles was considered to be greatest. For each test pile, tensile force was measured for the top two reinforcement layers of the wall and at two transverse distances from the test pile. Figure 4.3 shows the plan view for piles 1.7D and 2.8D while Figure 4.4 shows the plan view for piles 3.1D and 3.9D.Figure 4.5 shows the typical profile view for the test piles.

The gauges were placed at varying distances from the face of the MSE wall as shown in Table 4.2 to monitor tensile force development versus distance from the wall and test pile. Some of the ribs on the strip reinforcement were situated at the location where the gauge was supposed to be placed. Whenever there was a rib interfering with the placement of a gauge, the gauge was placed on a smooth surface next to the rib and the exact distance was recorded in Appendix C. The distance from the center line of the pile facing the wall to the location of the strain gauge is shown as R for right or L for left. The lead wires for the gauges were taped to the side of the steel strips and brought to the back face of the MSE wall. Slack was left in the lead wires to prevent the strain gauges from being detached during load testing. At the back face of the wall, the lead wires were placed into a PVC pipe bringing them up along the back face of the wall to the ground surface. Photographs of the reinforcement installation are shown in Figure 4.2.

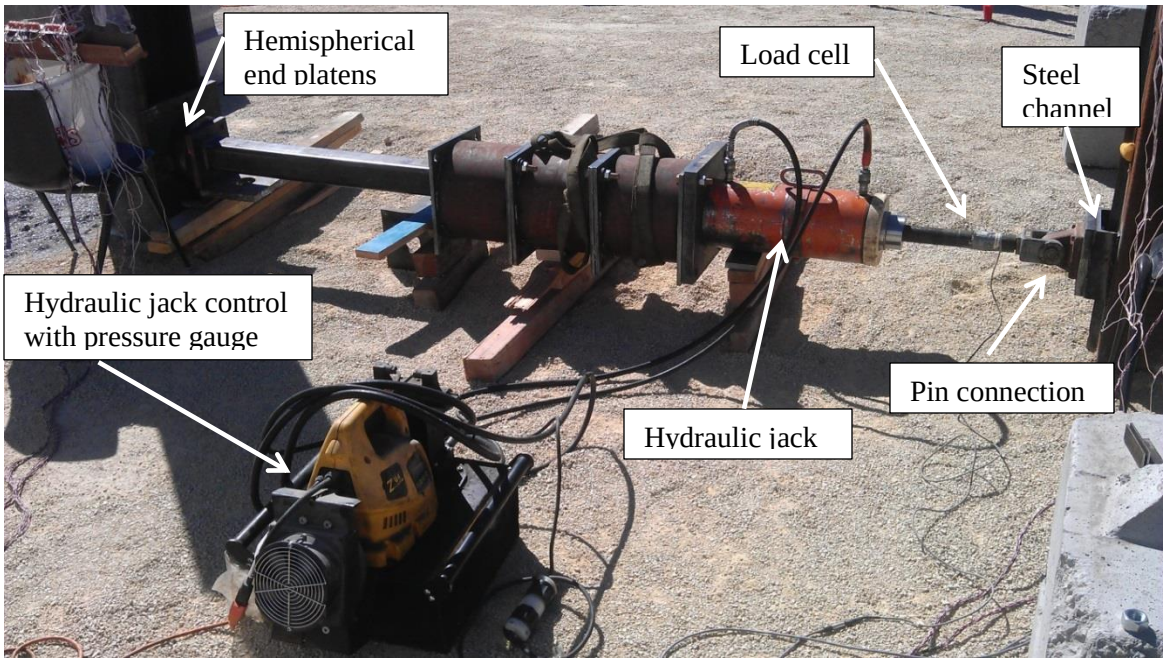

Figure 4.1: Typical load cell and pressure gauge configuration.

Figure 4.2: Photographs of reinforcement installation.

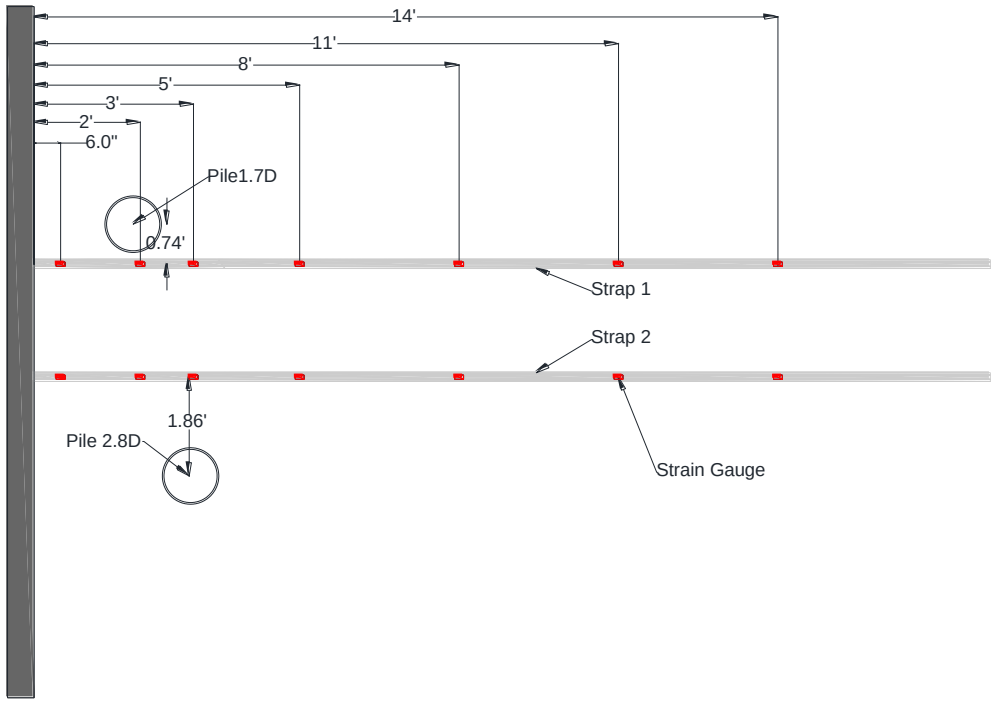

Figure 4.3: Plan view of the top layer of reinforcement for piles at 1.7D and 2.8D.

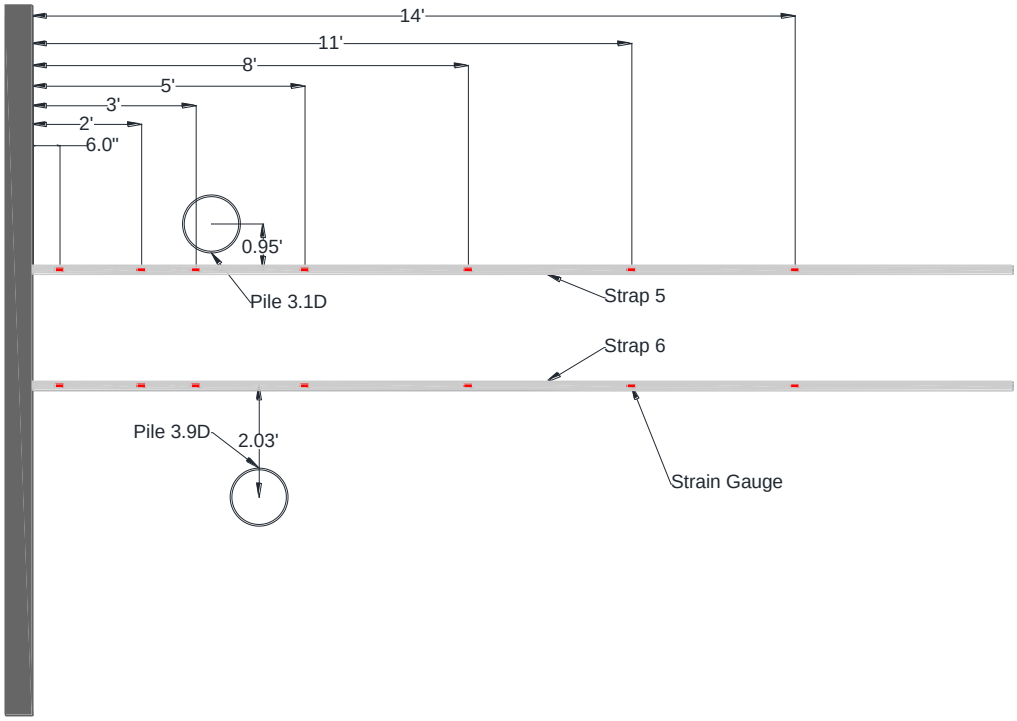

Figure 4.4: Plan view of the top layer of reinforcement for piles at 3.1D and 3.9D.

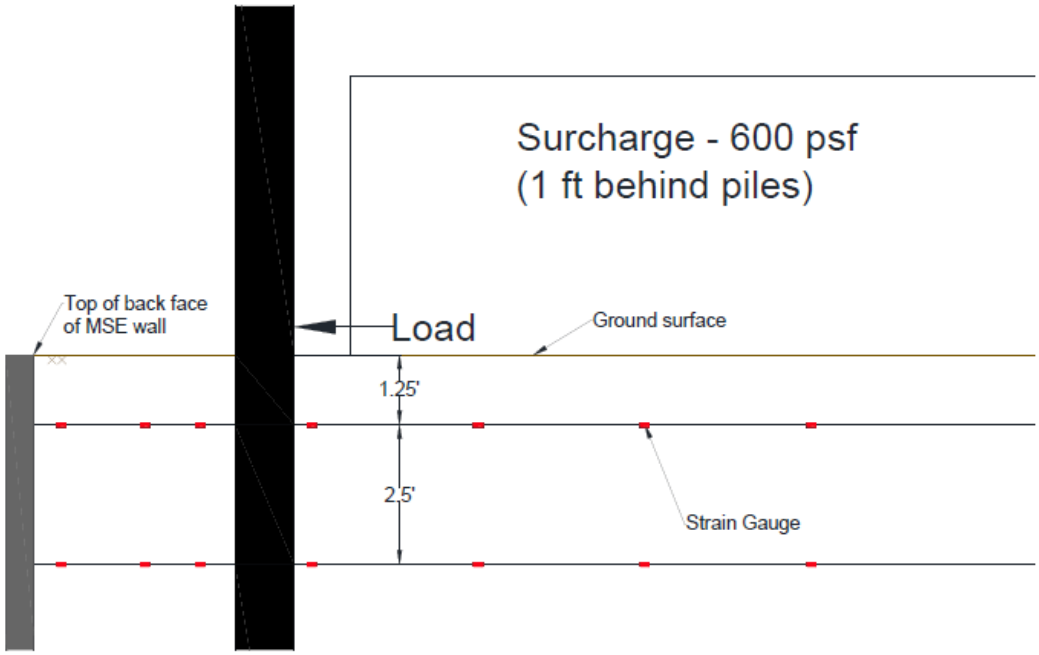

Figure 4.5: Typical profile view of the top two layers of reinforcement

Table 4.1: Location of strain gauge pairs for welded wire reinforcements.

Test Pile	Actual pile distance from wall (diameter)	Strip Name	Distance from center line of pile (ft)	Distance from top of wall (ft)	Strain gauge distances from back face of wall (ft)
3.9D	3.9D [49.9 in.]	6	2.03 R	1.25	0.5, 2, 3, 5, 8, 11, 14
		5	4.16 R		
		12	2.03 R	3.75	0.5, 2, 3, 5, 8, 11, 14
		13	4.28 R		
3.1D	3.1D [39.4 in.]	5	0.95 L	1.25	0.5, 2, 3, 5, 8, 11, 14
		6	3.07 L		
		13	0.87 L	3.75	0.5, 2, 3, 5, 8, 11, 14
		12	3.16 L		
2.8D	2.8D [35.4 in.]	2	1.87 R	1.25	0.5, 2, 3, 5, 8, 11, 14
		1	4.12 R		
		9	1.95 R	3.75	0.5, 2, 3, 5, 8, 11, 14
		10	4.16 R		
1.7D	1.7D [22.4 in.]	1	0.74 L	1.25	0.5, 2, 3, 5, 8, 11, 14
		2	2.99 L		
		10	0.74 L	3.75	0.5, 2, 3, 5, 8, 11, 14
		9	2.91 L		

4.3 Gauges with Welded Wire Reinforcement

Strain gauges were attached to the second longitudinal wire from the right of each welded wire grid at distances of 0.5, 2, 3, 5, 8, 11, and 14 ft from the back face of the MSE wall. Strain gauges were placed on opposing sides of the reinforcement to provide redundancy in case a strain gauge failed and to eliminate bending effects. For a given test, grids on either side of the test pile were monitored at depth of 15 inches and 45 inches below the ground surface. The purpose of instrumenting the reinforcement in this configuration ensured that the load in the reinforcement would be known as a function of depth, distance behind the face of the wall and lateral distance away from the pile. Table 4.2 and Table 4.3 show the distance of the instrumented wires from the center of the pile at each reinforcement level. A photo of the instrumented grids being placed in the fill is shown in Figure 4.6.

Figure 4.6 Instrumented grids being placed in the fill.

At the back face of the wall, a PVC pipe was used to conduct the strain gauge wires from the reinforcement to the top of the wall. During testing, the wires were attached to a computer data acquisition system to monitor and record the strain in the reinforcement.

Table 4.2 Distance from Strain Gauge Wire to Pile Center (in), 1.2 ft Below Ground Surface

	Welded Wire Grid Number				
Test	20	19	18	22	21
5.3D				21.5	46
4.3D			17.5	34.5	
3.2D		23	38		
1.9D	22	43			

Table 4.3 Distance from Strain Gauge Wire to Pile Center (in), 3.7 ft Below Ground Surface

	Welded Wire Grid Number				
Test	13	14	15	16	17
5.3D				23	39
4.3D			19	34	
3.2D		31	38		
1.9D	17	35			

4.4 String Potentiometers

AMETEK RAYELCO model P-20A and Firstmark Controls Position Transducer string potentiometers (also known as linear motion transducers) were installed to measure the displacement and rotation of the pile along with the displacement of the ground and the top of the wall directly in front of the pile. The string potentiometers were attached to an independent reference frame located between the pile and the wall face.

A sturdy 16-ft. long 4x4 timber beam was used as the independent reference frame for all the tests. The independent reference frame was securely strapped to a pre-cast concrete block located about 7 ft. on either side of the test pile. The string potentiometers were attached to a 2x4 piece of lumber that was clamped onto the independent reference as shown in Figure 4.7.

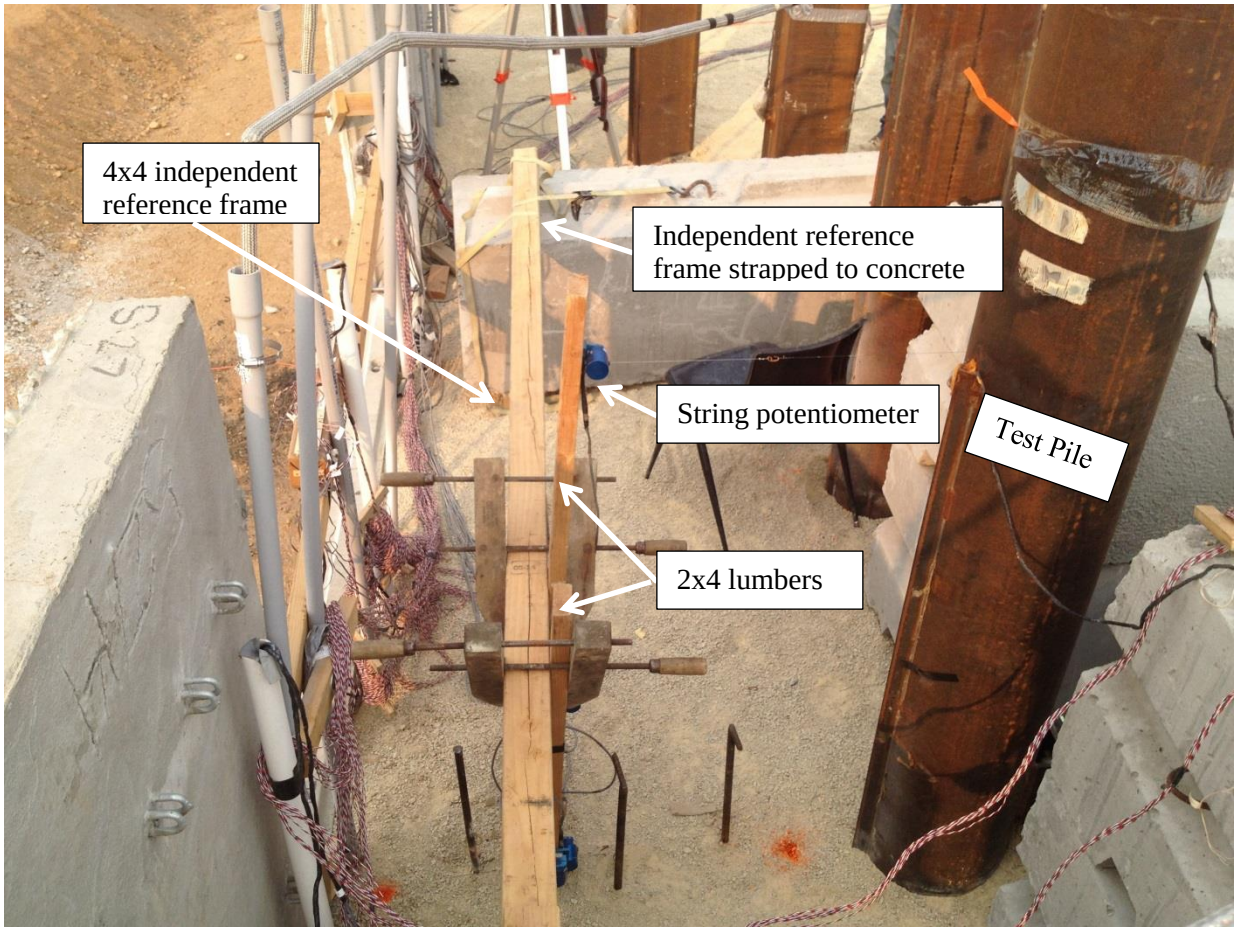

Figure 4.7: Typical setup for string potentiometers.

4.4.1 Pile Head Displacement and Rotation

Pile head displacement and rotation were measured using string potentiometers with one end mounted to the pile and the other end mounted to an independent reference frame. A string potentiometer was mounted on the side of the pile at the elevation of the applied load (12 in. above the ground surface) to measure the pile head displacement. Another string potentiometer was mounted 3 ft. above the load level to determine the rotation of the pile as shown in Figure 4.8. The rotation was obtained from the difference in deflection between the upper and lower string potentiometers.

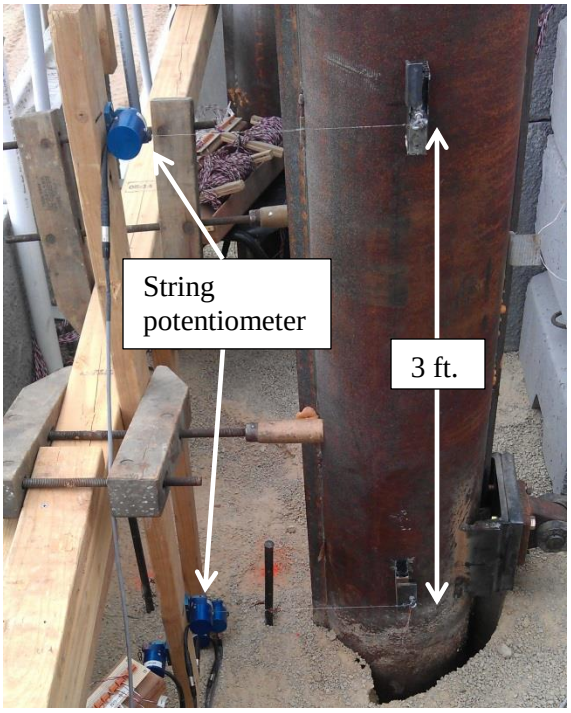

Figure 4.8: Typical string potentiometer setup for measuring pile displacement.

4.4.2 Ground and Wall Displacement

The ground displacement between the pile and the wall face was measured by connecting the wire from the string potentiometer to a metal stake driven into the ground as shown in Figure 4.9. The wall displacement was measured by connecting the string potentiometer to an eyelet pin that was securely placed using epoxy into a drilled hole on the wall panel directly in front of the test pile. Typically, ground displacement was measured at 1 ft. intervals in front of the pile face. Table 4.3 shows the exact location of the stakes where ground displacement was measured for each pile load test.

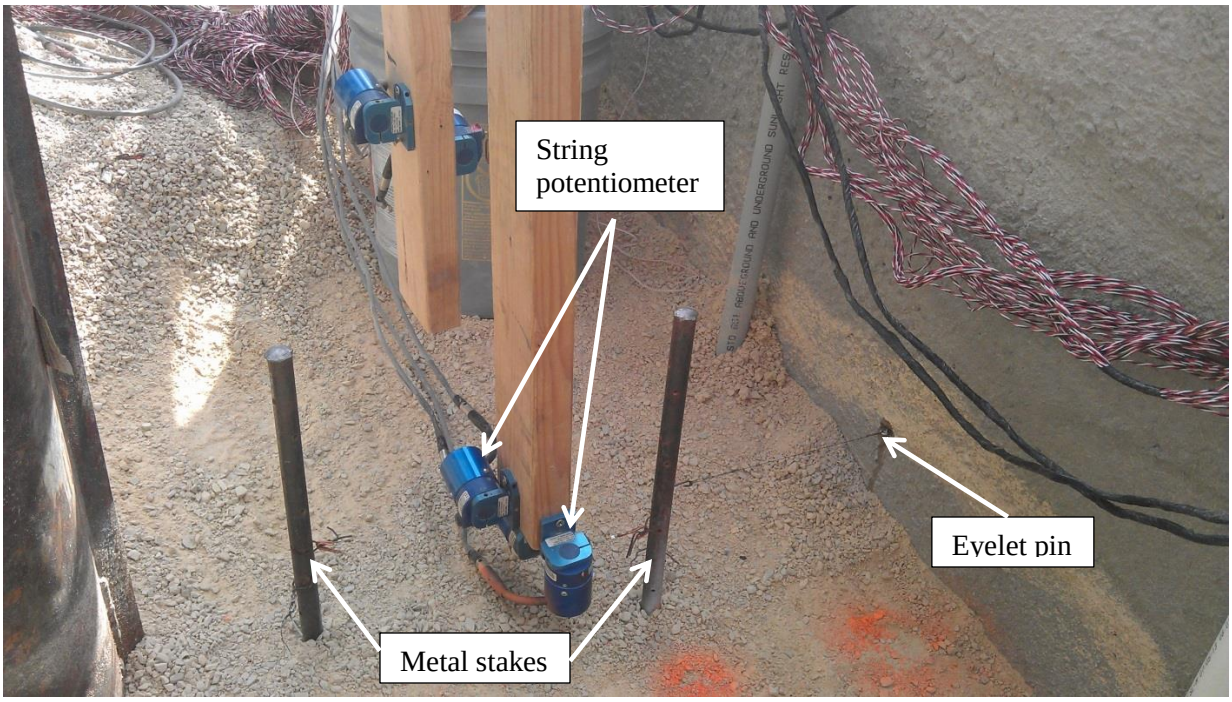

Figure 4.9: Typical string potentiometer setup for measuring ground and wall displacement.

Table 4.4: Location of string potentiometers for measuring ground displacement.

Test Pile	Actual pile distance from wall (diameter)	Distance from back face of wall to string potentiometer (ft)	Distance from back face of wall to center of test pile (ft)
3.9D	3.9D	0.00, 0.63, 1.63, 2.63	4.16
3.1D	3.1D	0.00, 0.75, 1.75	3.28
2.8D	2.8D	0.00, 0.92, 1.92	2.95
1.7D	1.7D	0.00, 0.83	1.86

4.5 Photogrammetry for Wall Panel Displacement

Digital Imaging Correlation (DIC) also known as photogrammetry was used as a state of the art optical measurement method to determine the displacement of the MSE wall. Using two cameras to take images of the same object, the position of an object point in the two images can be identified by applying a correlation algorithm.

A typical setup for the DIC cameras is shown in Figure 4.10 below. For each test, an image of the wall was taken by the two cameras simultaneously before pile loading. Another image was taken immediately after each pile loading increment and again after holding the pile displacement for five minutes. A high contrast grid was used on the wall to aid in the location of identical object points. Grey values from the images are tracked in small local facets which are shown as green squares in Figure 4.11 below. Computer algorithms allow the program to track point movement at the sub-pixel level from camera images. Once the position of the cameras with respect to each other is determined using a calibration target, a correlation algorithm can be used to calculate the three dimensional position of each point which then allows for contours of displacement, deformation and strain on the wall to be determined. The DIC was capable of tracking the movement of thousands of points with accuracy of hundredths of an inch within a 10 ft. by 10 ft. area center on the wall panels in front of the test pile.

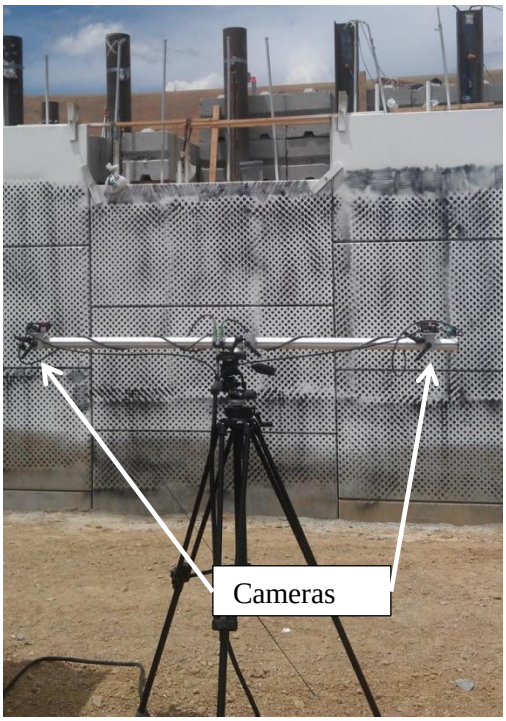

Figure 4.10: Photograph of DIC camera setup.

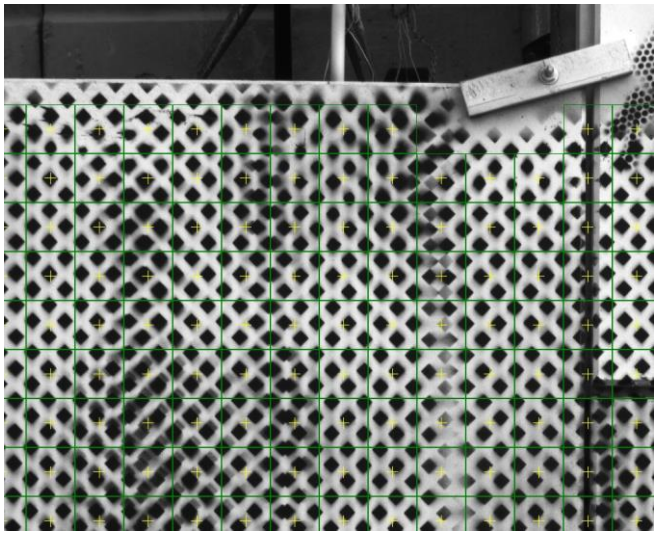

Figure 4.11: Photograph of DIC procedure.

4.6 Shape Arrays

Trade size 1 in. schedule 40 PVC pipes (inside diameter of 1.049 in.) were placed vertically along the back face of the wall during construction at approximately 2.5 ft. intervals. A Measurand ShapeAccelArray (SAA), referred to herein as a Shape Array, was placed in each pipe during testing to measure the deformation of the wall face. The Shape Array consists of 12 in. segments connected by a flexible joint with each segment containing three MEMS accelerometers. Deformation parallel and perpendicular to the wall face were measured at one foot depth intervals. The digital signal sent from each accelerometer was collected by the data logger and analyzed using SAARecorder software. A photograph of the shape arrays in place during a test is shown in Figure 4.12.

Figure 4.12: Photograph of shape arrays in place behind the face of the wall.

5 LATERAL LOAD TESTING WITH WELDED WIRE REIFNORCEMENT

The lateral load test was performed between July 2, 2014 and July 17, 2014. A photo of the wall at the time of testing is shown in Figure 5.1. The test was performed incrementally with a displacement control approach. Load was applied using a free-head boundary condition at a distance of 1 foot above the ground surface to allow for pile rotation rather than restrained conditions. Load was applied to reach pile head displacement increments of 0.25 in. up to a total displacement of 3.0 in. to 3.25 in. Thermal expansions and contractions usually produce displacements of 0.5 in. to 0.75 in. while seismic loads typically produce displacements of up to 3 in. This approach was adopted to define the load-displacement curve in a reasonable manner. After reaching each displacement increment, the load required to reach that increment was held constant for a period of at least five minutes before moving to the next displacement increment. This hold period allowed the deflection to come to equilibrium with the applied load. Typically, the deflection stabilized within about one minute after peak load was reached.

Figure 5.1: Photograph of the MSE wall at the time of testing.

Nine piles were placed 25 ft. behind the back face of the MSE wall as the reaction for the lateral load tests. A 23-ft. long W36x150 beam was placed in front of the reaction piles to transfer the load whenever a test pile did not align with a reaction pile as shown in Figure 5.2. Hemispherical end platens were placed at the back between the reaction beam and loading system to minimize eccentric loading on the load cell (Figure 5.3).

Results for the lateral load tests are discussed in the following sections. The data for each test was collected by the Megadac data logger at a rate of two readings per second. The data was analyzed by looking at the peak values, one minute values and final values for each displacement increment. The peak values are taken as the average of the first two or three data points when the desired displacement interval was reached. The one minute and final values are taken as the average of the data points 30 seconds into the one minute hold and five minutes hold time at the desired displacement. Due to the size of the project, the following sections will only discuss the results for the four load tests on pipe piles reinforced with steel strips.

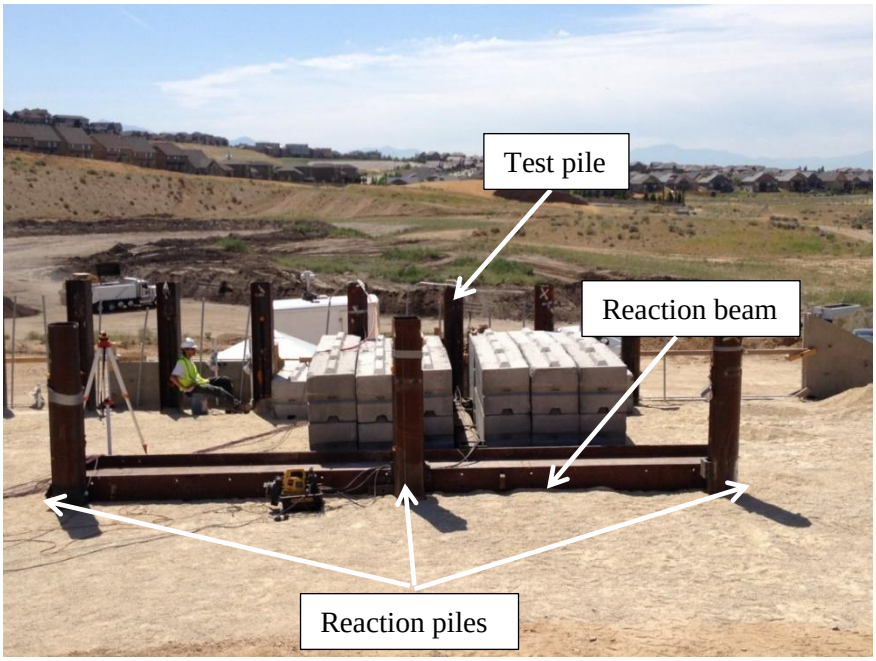

Figure 5.2: Reaction piles and reaction beam for lateral load tests.

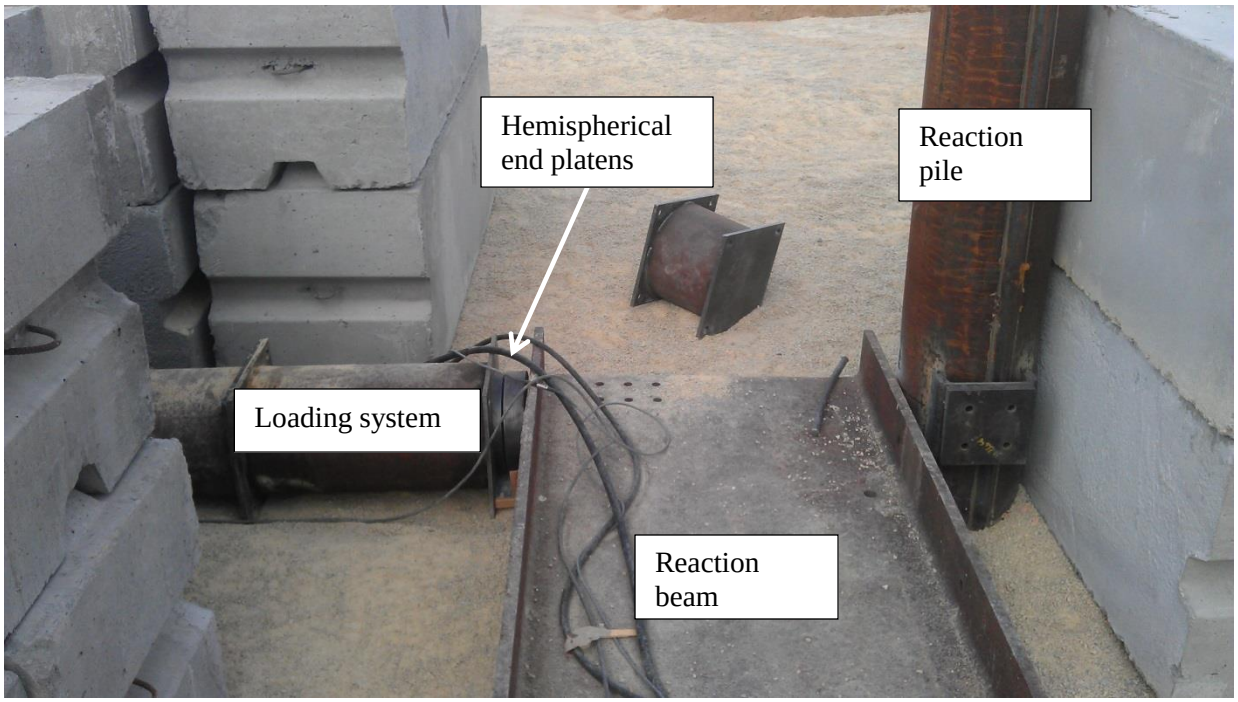

Figure 5.3: Hemispherical end platens to minimize eccentric loading

5.1 Load Displacement Curves

The peak pile head load versus deflection curves for all four pipe pile lateral load tests are shown in Figure 5.4. Appendix D contains load-displacement curves for each individual test pile. Figures 5.5 and 5.6 show the load-displacement curves for lateral load tests at one minute hold and five minute hold respectively. These curves typically have a relatively linear initial section due to the stiffness of the soil followed by an increasingly non-linear segment as the soil resistance is mobilized progressively from the top of the pile downward and the secant stiffness decreases. For a given displacement, the load after a one minute hold is generally about eight to 12 percent lower than the peak load while the load after a five minute hold is about 10 to 14 percent lower than the peak load. The only exception is that the load after the one minute hold for the reaction pile is only about four percent lower than peak while the load after the five minute hold is about five percent lower than peak.

The resistance of a pile tends to decrease as the spacing between the pile and the wall decreases. However, the lateral resistance for the pile at 3.9D is only slightly higher than that for the pile at 3.1D as shown in Figure 5.5. For practical purposes, the two load-displacement curves could be assumed to be identical and suggests that piles located further away would yield similar results. Although piles were typically loaded to a pile head displacement of 3.0 inches, test had to be stopped for pile 2.8D at pile head displacement of 2.5 inches because there was visibly excessive wall panel deflection directly in front of the pile.

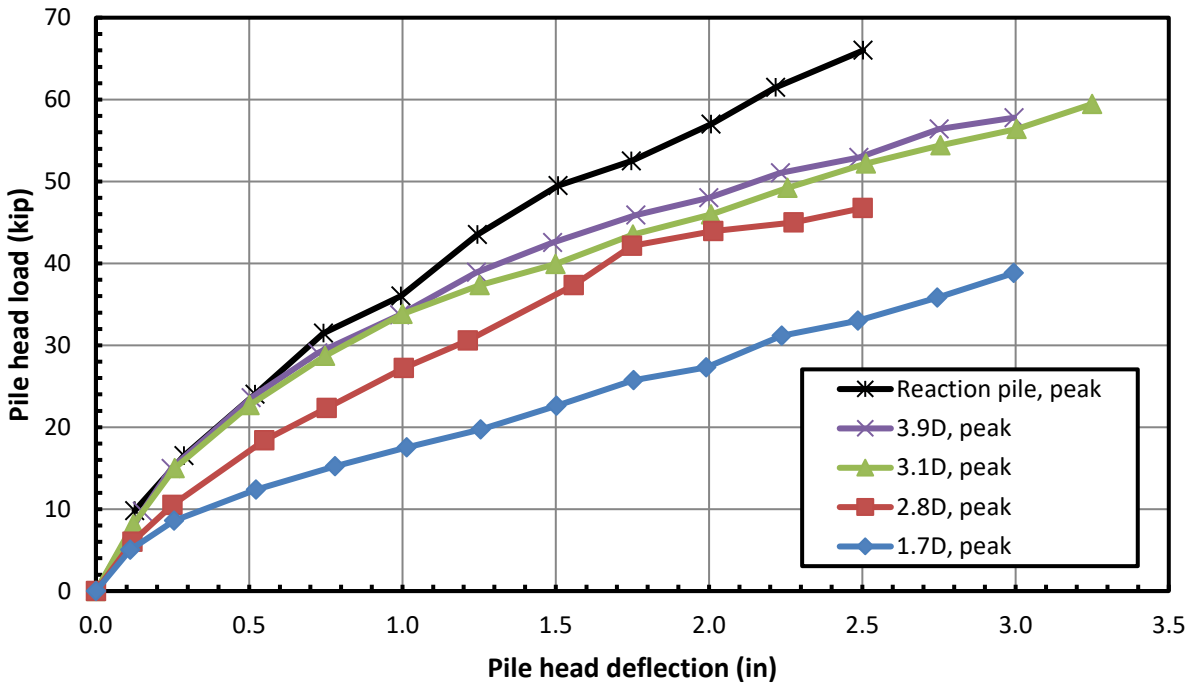

Figure 5.4: Comparison of load-displacement curves for the peak data points.

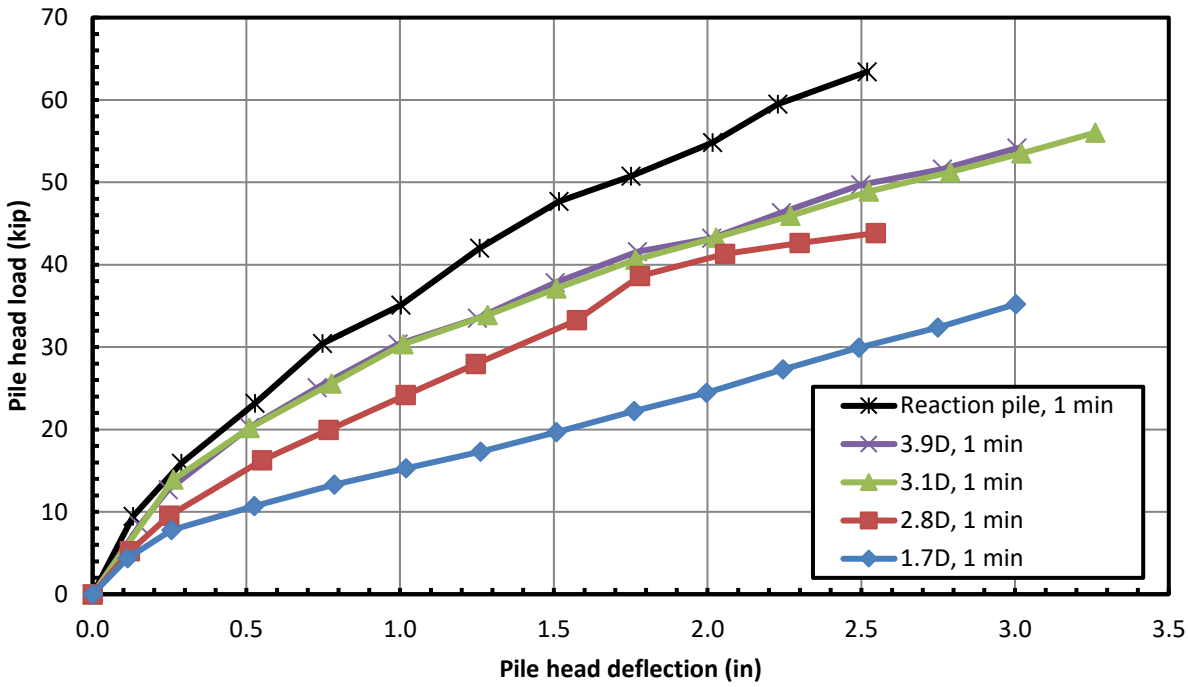

Figure 5.5: Comparison of load-displacement curves for the one minute hold data points.

Referring back to the soil density profile in Figure 3.12, the soil compaction between the wall and the tests piles were consistently less than 95 percent of the maximum density while the soil compaction around the reaction piles were generally at or above the specified 95 percent density requirement. The difference in compaction undoubtedly skewed the load-displacement curves higher in favor of the reaction piles and therefore data from the reaction piles were not used to compare directly with the other test piles. Relative to the piles at a distance of 3.1D and 3.9D from the wall, the piles 2.8D and 1.7D from the wall at 1 in. pile head deflection provided only about 80% and 50% of the lateral resistance, respectively. This decrease in resistance with decreasing distance from the wall is consistent with results from previous studies conducted by Pierson et al. (2009), Price (2012) and Nelson (2013).

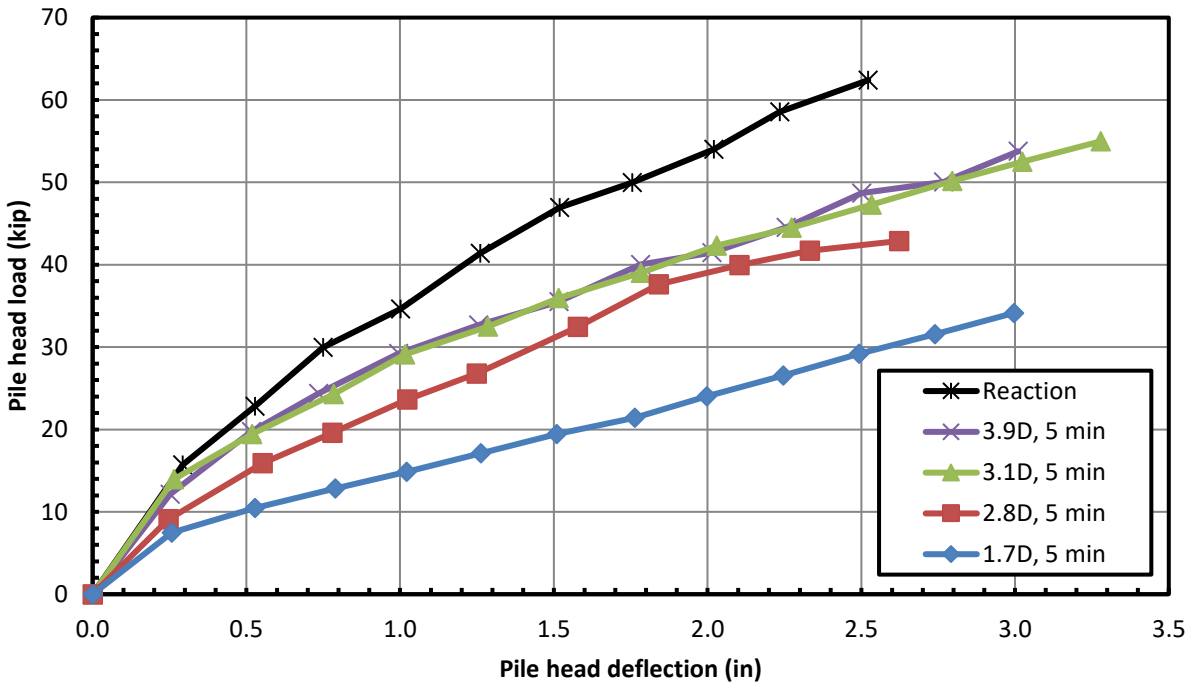

Figure 5.6: Comparison of load-displacement curves for the five minute hold data points.

Figure 5.7 shows the load-displacement curves for pile 1.7D (1.7 pile diameters from the wall). The curves for the one minute and five minutes data points are almost identical suggesting that there is very little change between one and five minutes of hold. Since all other pile tests showed similar trend, it was decided that all numerical and graphical data shown hereafter will be obtained from the one minute hold data analysis.

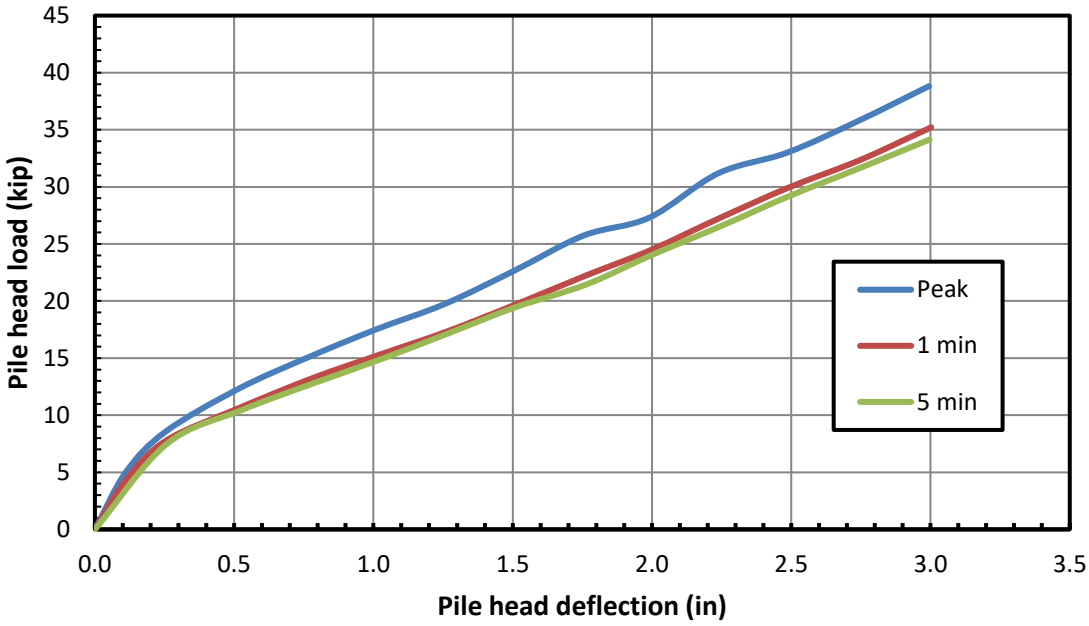

Figure 5.7: Load-displacement curve for pile 1.7D.

5.2 Soil Reinforcement Performance

The load on the steel strip reinforcement was calculated from the strain gauge data using Equation 5-1. The average value of the paired strain gauges was used when both gauges were functioning. If one of the paired gauges was found to be damaged during installation, only the data from the functioning gauge was used.

$$T_i = EA(\mu\varepsilon_i - \mu\varepsilon_o)(10^{-6}) \qquad (5\text{-}1)$$

where

T_i is the equivalent induced force in kips for the steel strip at the i^{th} data point.

E is the modulus of elasticity of the steel strip (29000 ksi),

A is the cross sectional area of the steel strip (0.31 in^2),

$\mu\varepsilon_i$ is the micro strain for the i^{th} data point, and

$\mu\varepsilon_o$ is the micro strain for the initial data point,

The tensile force in the reinforcing steel strips measured by the strain gauge is shown in Figure 5.8 through Figure 5.11. In general, the induced force in the reinforcement increases from the back face of the wall to the location of the pile and decreases toward the end of the reinforcement. It was also observed that the force in the reinforcement increases as the pile head load increases. The predicted pullout capacity using the FHWA method discussed in Berg et al. (2009) was calculated for comparison with the measured force in the reinforcement and is shown as the red dotted line in the plots.

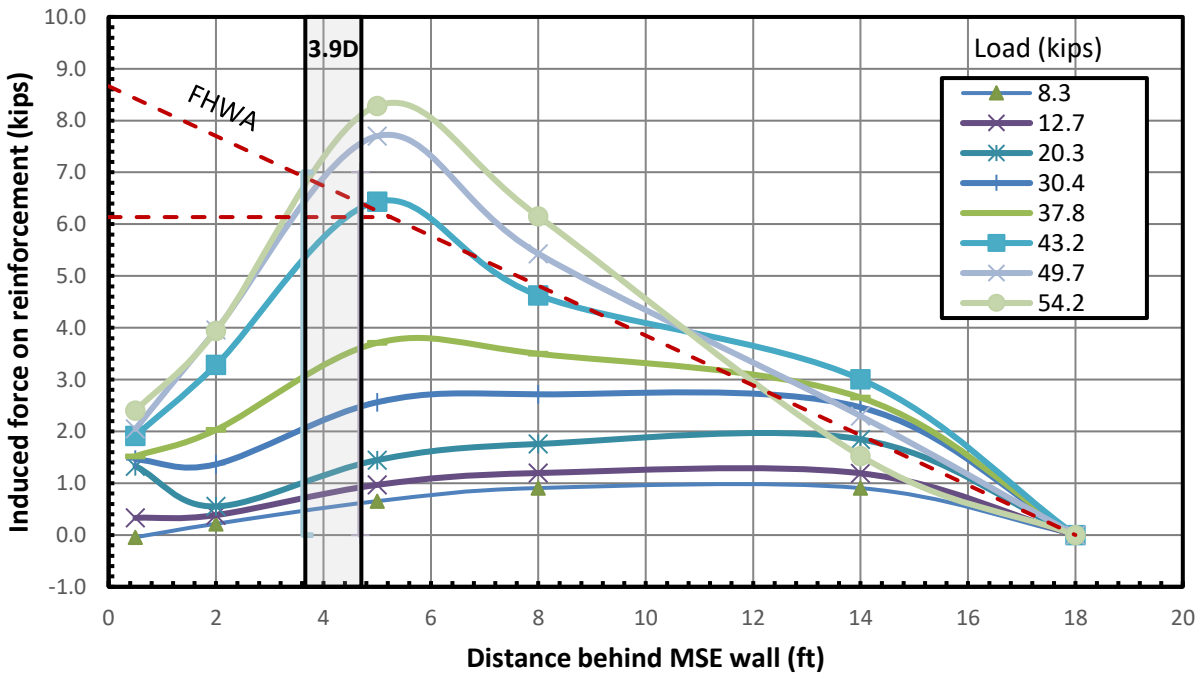

Figure 5.8: Induced force in the reinforcement for pile at 3.9D.

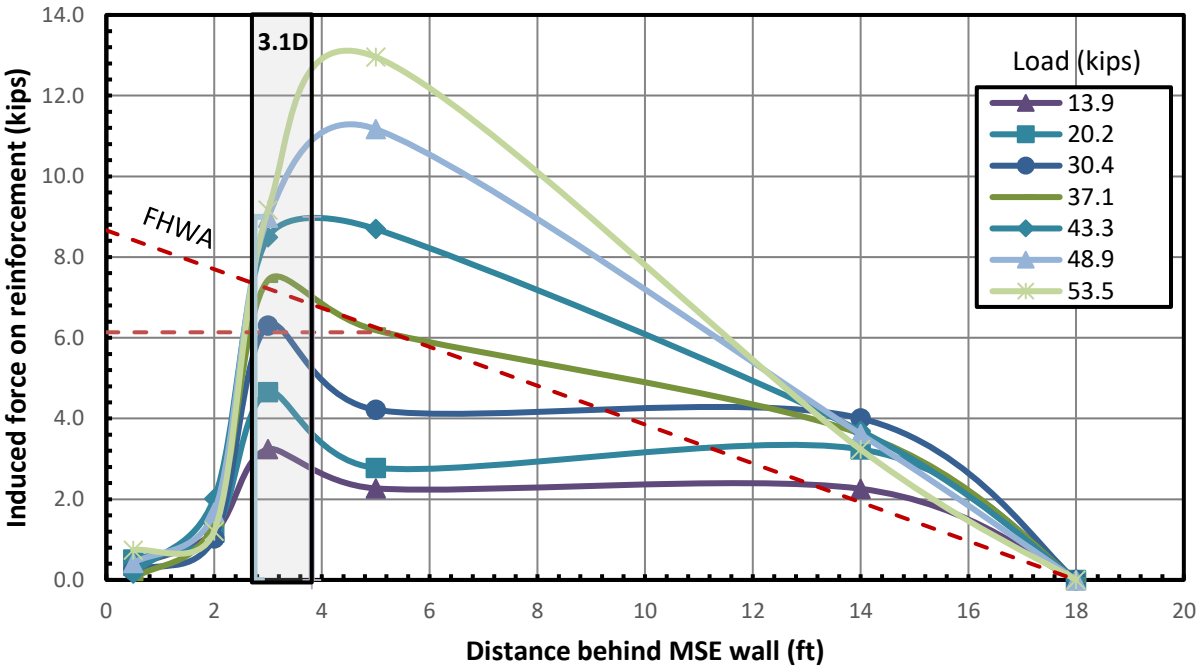

Figure 5.9: Induced force in the reinforcement for pile at 3.1D.

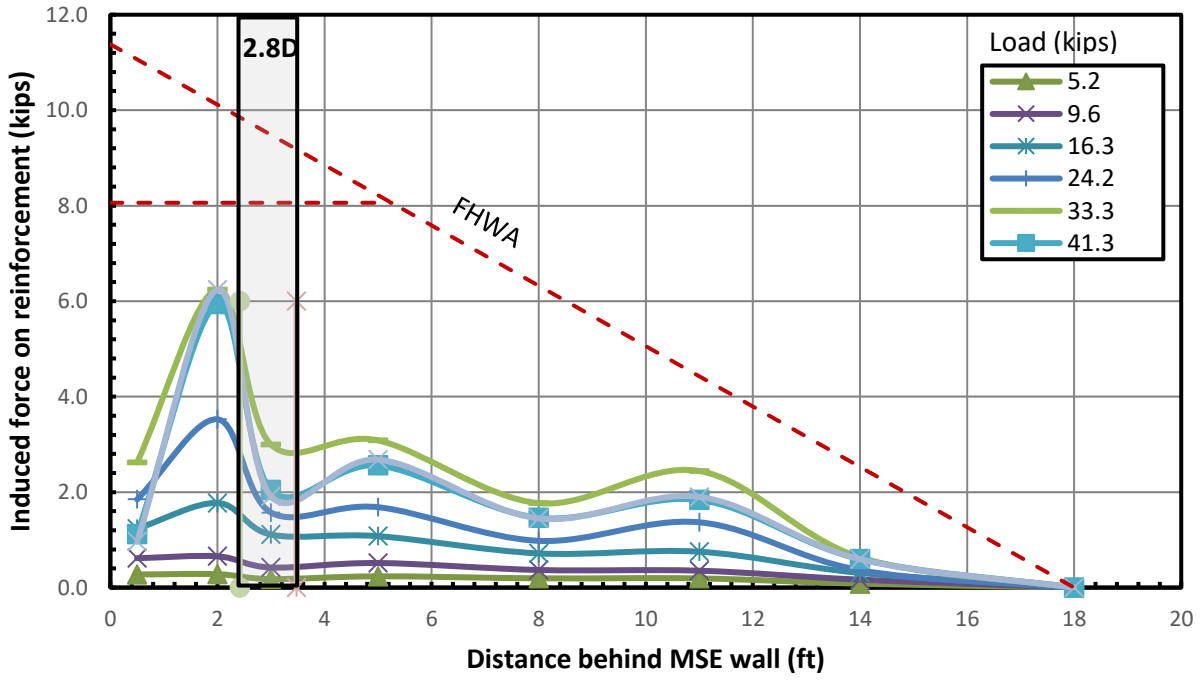

Figure 5.10: Induced force in the reinforcement for pile at 2.8D.

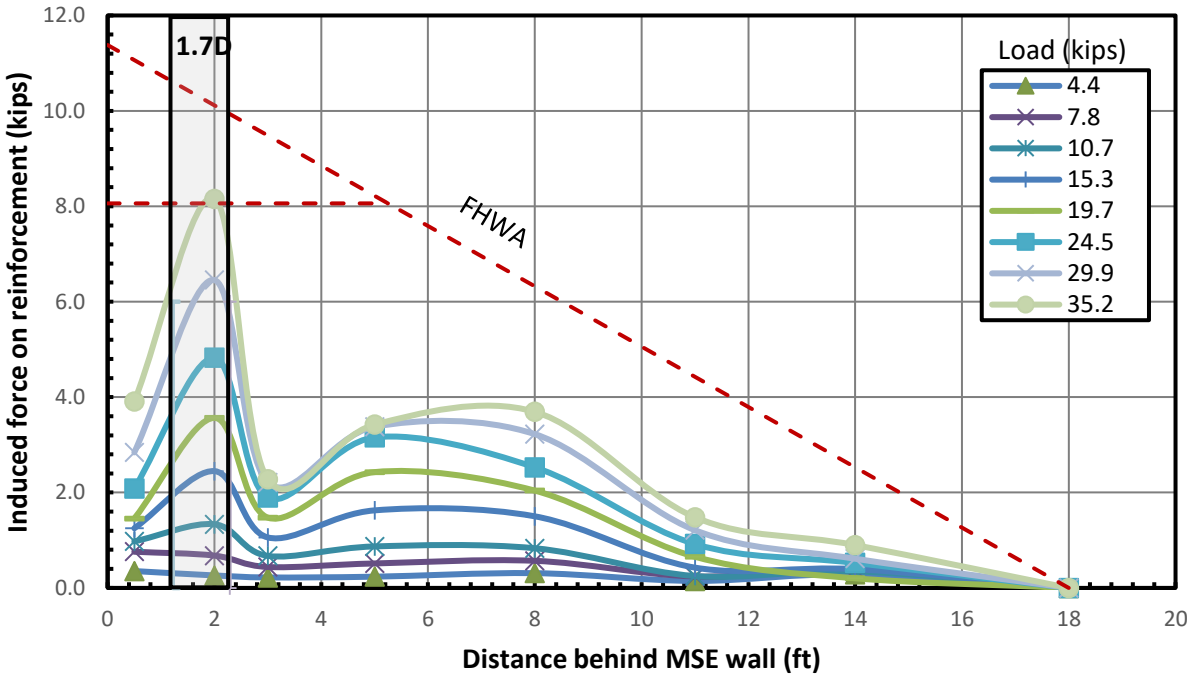

Figure 5.11: Induced force in the reinforcement for pile at 1.7D.

Since there were four steel strip reinforcements instrumented for each pile test, the induced force in the four reinforcements was simultaneously recorded and the plots are shown in Figure 5.12 through Figure 5.15. In general, it can be seen that the induced load in the reinforcement tends to increase when the reinforcement is placed closer to the pile and deeper in the soil profile. The induced force in the reinforcement also generally increases as the pile gets closer to the wall as seen in Figure 5.16.

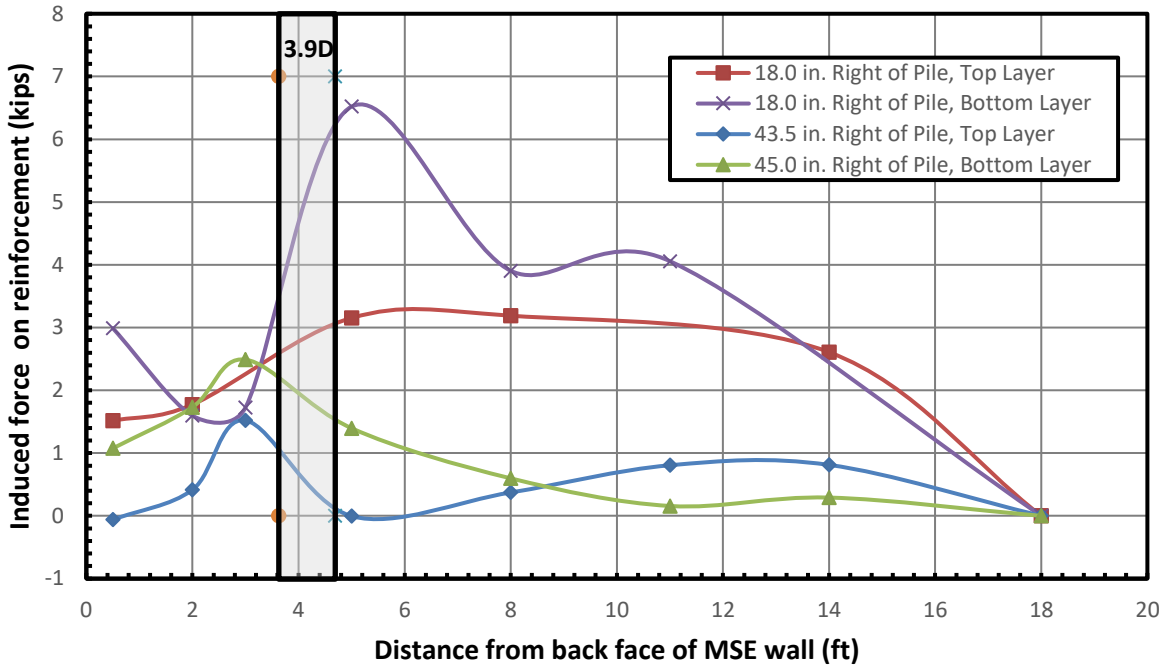

Figure 5.12: Induced force in the reinforcement for a pile head load of 33.5 kips at 3.9D.

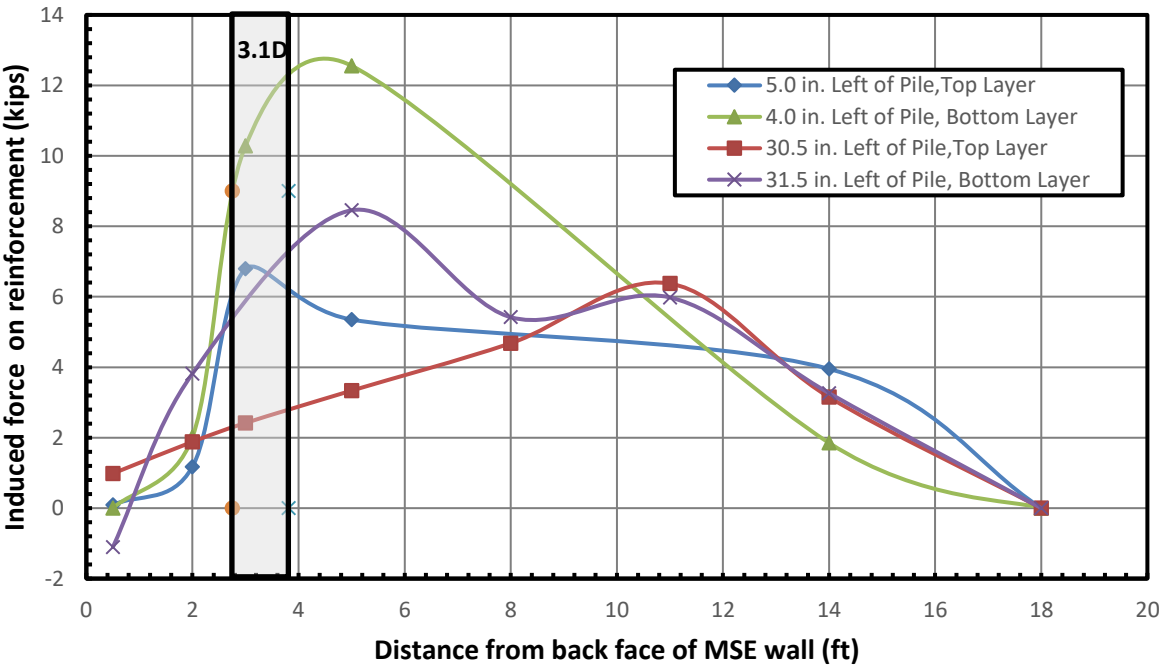

Figure 5.13: Induced force in the reinforcement for a pile head load of 33.9 kips at 3.1D.

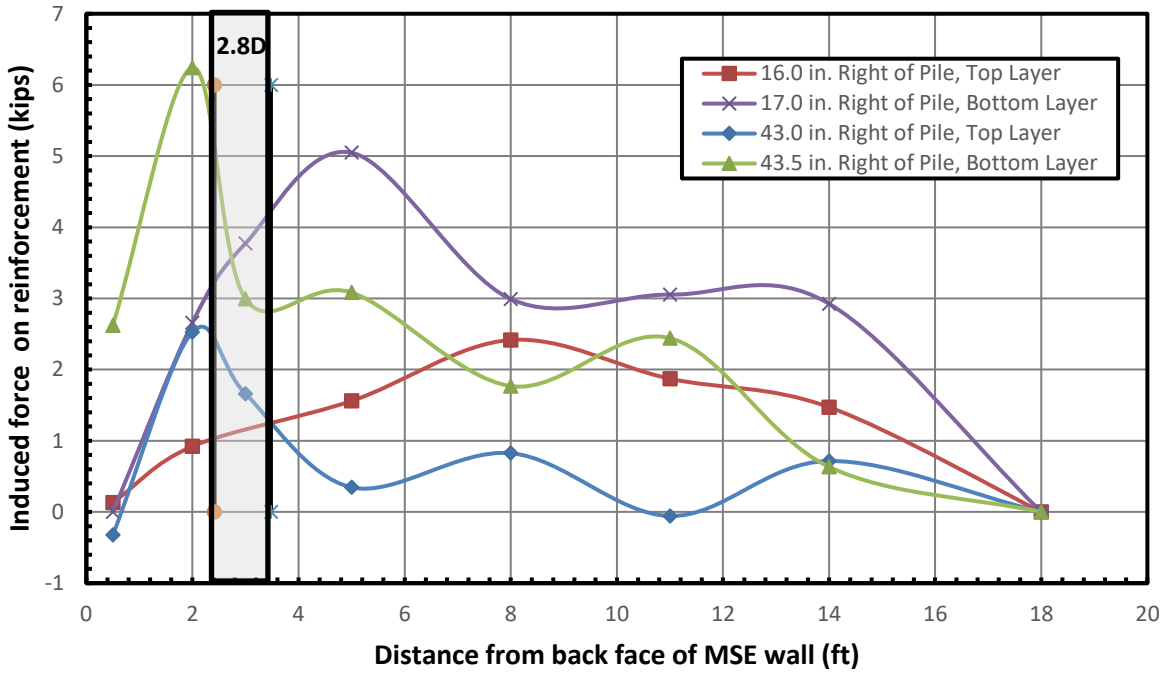

Figure 5.14: Induced force in the reinforcement for a pile head load of 33.3 kips at 2.8D.

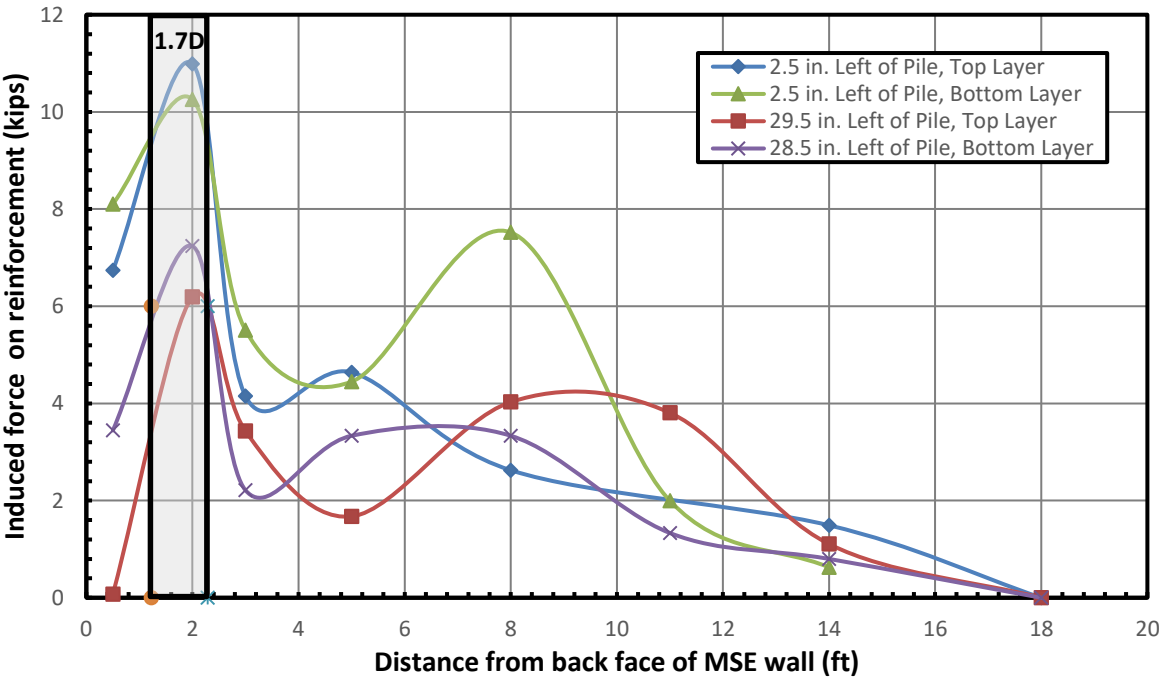

Figure 5.15: Induced force in the reinforcement for a pile head load of 32.4 kips at 1.7D.

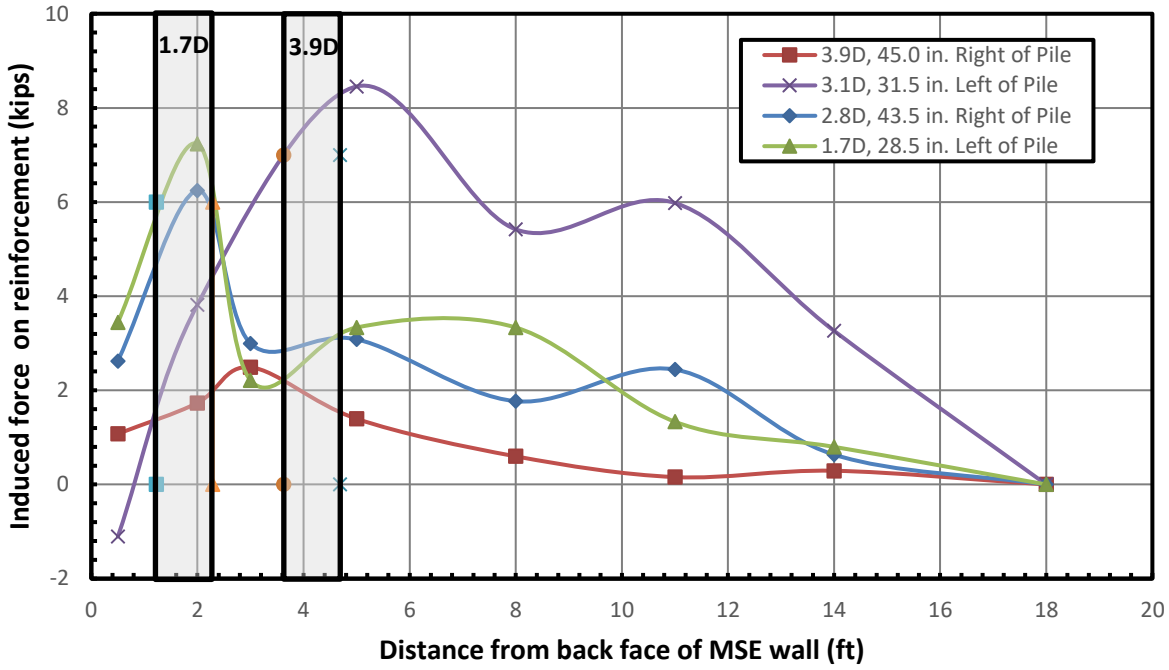

Figure 5.16: Induced force in the bottom layer reinforcement for all four pile tests (33 kips).

A conceptual framework for this observed performance is illustrated in Figure 5.17. The measured force distribution in the reinforcement suggests that soil in front of the pile is being pushed forward as the pile is loaded while the soil behind the pile is serving to anchor the steel strip. Behind the pile, the steel strip is moving towards the wall relative to the soil. This leads to a decrease in tension in the strip behind the pile as load is transferred to the surrounding soil by skin friction. In front of the pile, the soil is moving toward the wall relative to the steel strip. This leads to an increase in tension in the steel strip as load is transferred from the soil to the steel strip by skin friction. A positive tensile force in the reinforcement at the wall face is likely a result of the increased earth pressure on the wall from the pile loading.

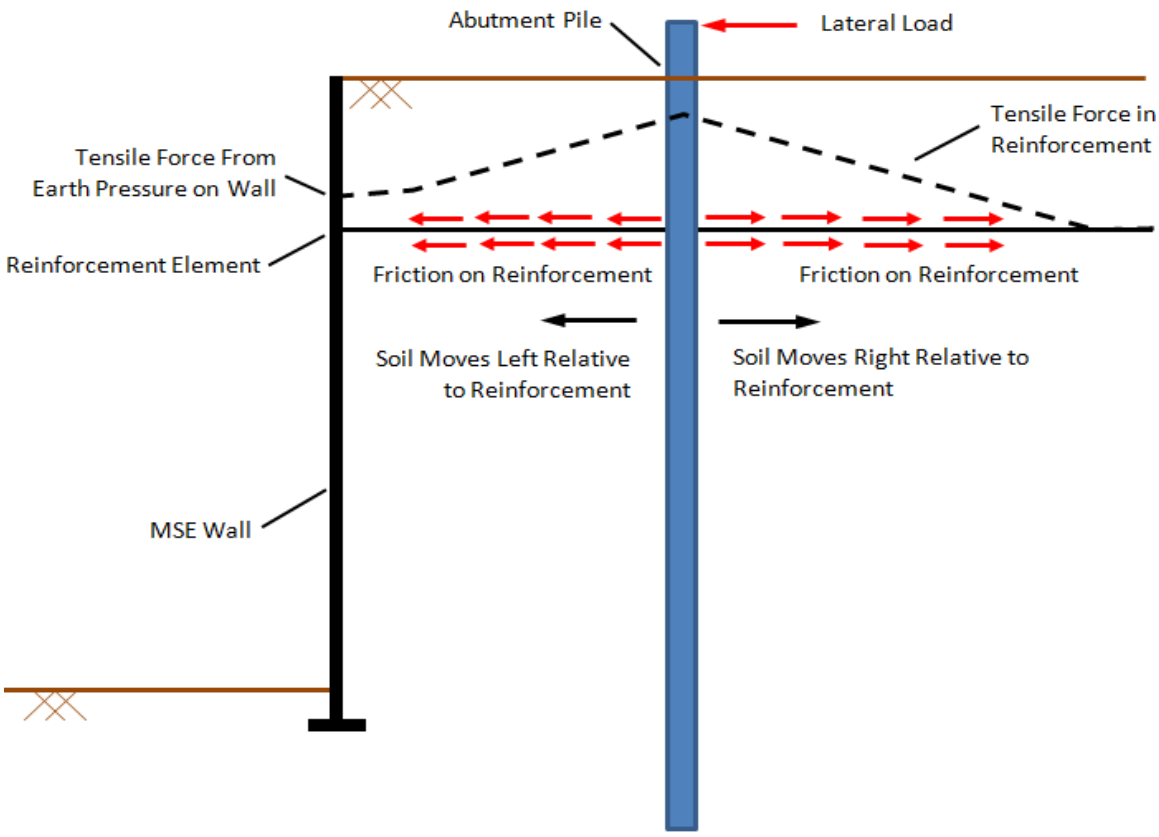

Figure 5.17: Interaction of soil and MSE wall reinforcement when pile is laterally loaded.

A plot of normalized induced load in the reinforcement versus normalized distance from the pile is shown in Figure 5.18. This plot is similar to those developed by Price (2012) and Nelson (2013). For comparison purposes, data from Nelson (2013) was included because ribbed steel strip reinforcements were also used in his tests. Most of the data from this study fall outside of the design envelope proposed by Nelson (2013). One of the main reasons for this discrepancy is attributed to how Nelson was generally getting significantly lower reinforcement induced forces in his tests. Because of this discrepancy, more data will be required from tests on the 20 ft. wall before deciding on whether a revision should be made to Nelson's proposed design envelope. Data from this study did provide useful information that shows how the reinforcements on the bottom layer generally have higher normalized induced load in the reinforcement.

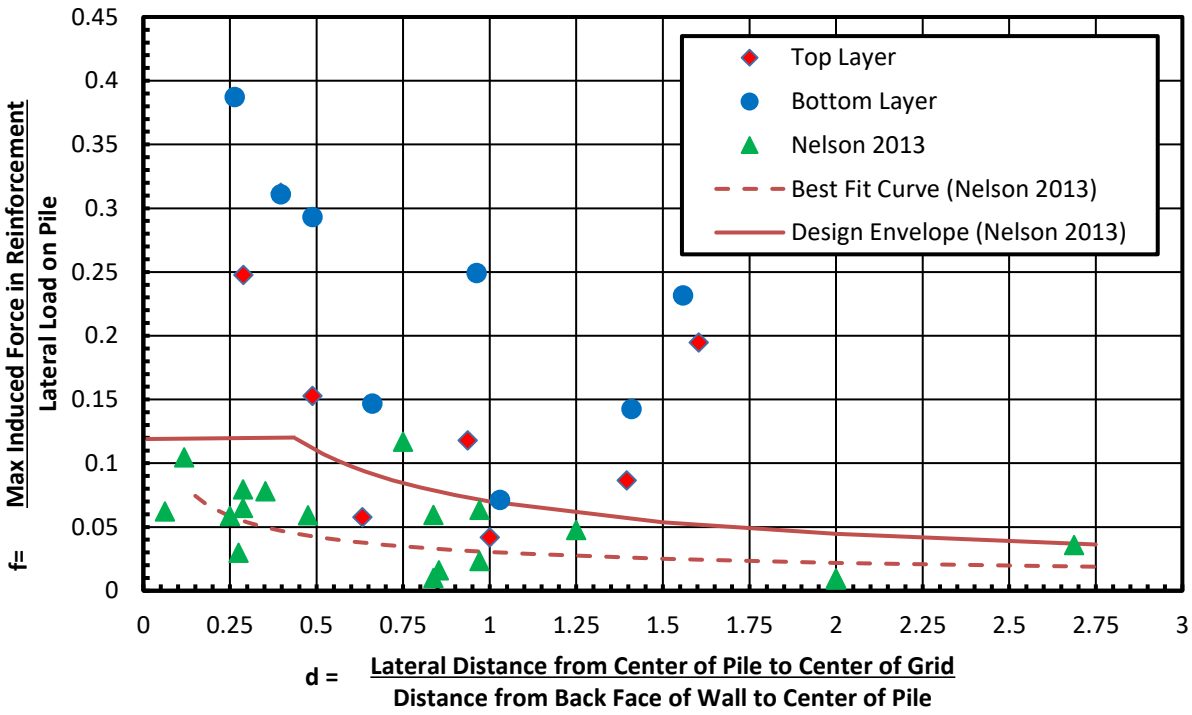

Figure 5.18: Normalized induced force in strip reinforcement vs. normalized distance from pile.

5.3 Displacement of Ground and Wall Panels

5.3.1 String Potentiometers

The displacement of the ground surface as a function of distance from the MSE wall for all four pipe pile lateral load tests at similar load level (approximately 33 kips) is shown in Figure 5.19. The pile closest to the wall (1.7D) produces the greatest ground displacement while the displacement typically decreases as piles are loaded further away from the wall. The displacements at the wall face are all relatively small with no cracking or permanent distress to the wall panels. However, it was observed that wall displacements are significantly higher for piles at 1.7D and 3.1D because both piles are located directly behind the joint between wall panels.

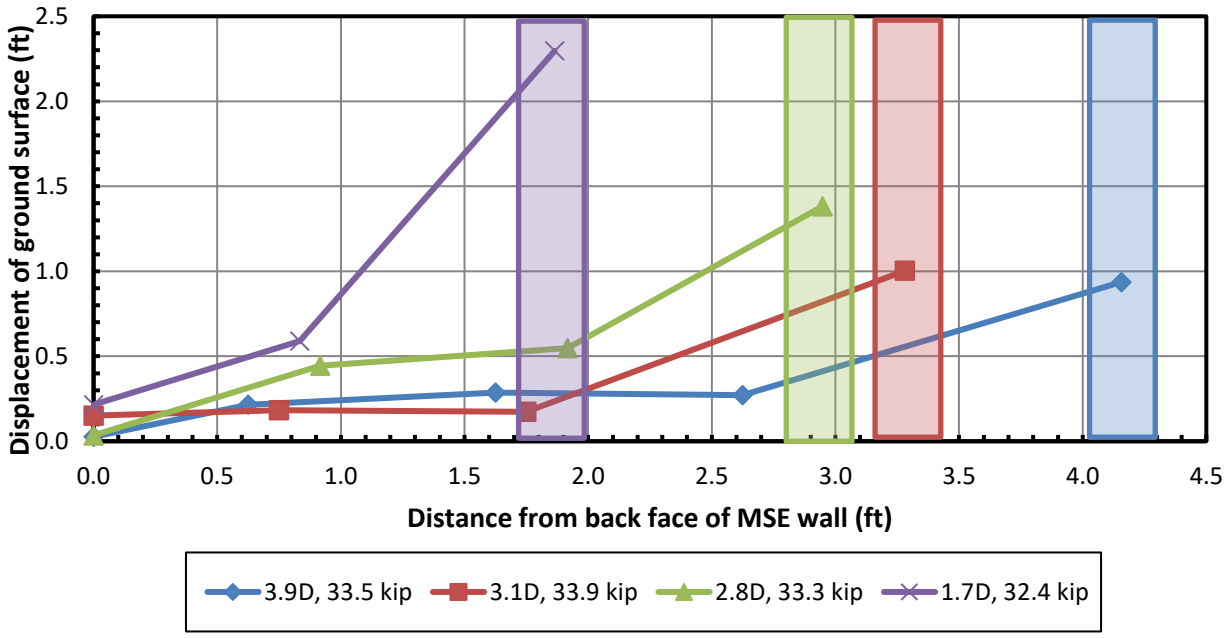

Figure 5.19: Horizontal displacement of the ground surface as a function of distance from the MSE wall at similar load level (approximately 33 kips).

The displacement of the ground surface as a function of distance from the MSE wall for the pile at 3.9D at several load levels is shown in Figure 5.20. Plots showing the ground surface displacement at different load levels for piles 1.7D, 2.8D and 3.1D are included in Appendix F. For all four pile tests, the soil displacement became relatively low at distances greater than about 1.5 pile diameters from the center of the piles and was typically less than 0.75 in. at maximum load exceeding 50 kips (see Figure 5.19 and Figure 5.20). To further explore the correlation between the ground movement and the distances from the wall for all piles, the ground displacement values were all divided by the maximum displacement at the pile for several load increments. Figures 5.21 through 5.24 show the normalized displacement curves for each test pile which were reasonably well correlated using this normalization procedure. In general, as the load increases the normalized displacements become more consistent for each load increment. The

normalized displacements are also more consistent for piles 1.7D and 3.1D which are both directly behind the wall joints.

Figure 5.25 provides a plot of the average normalized displacement for each pile as a function of normalized distance from the center of the pile. The ground displacement decreases significantly beyond 1.5 pile diameters for piles further away (3.1D and 3.9D) and one pile diameter for piles closer to the wall (1.7D and 2.8D) with a normalized displacement below 0.4 of the ground displacement at the pile.

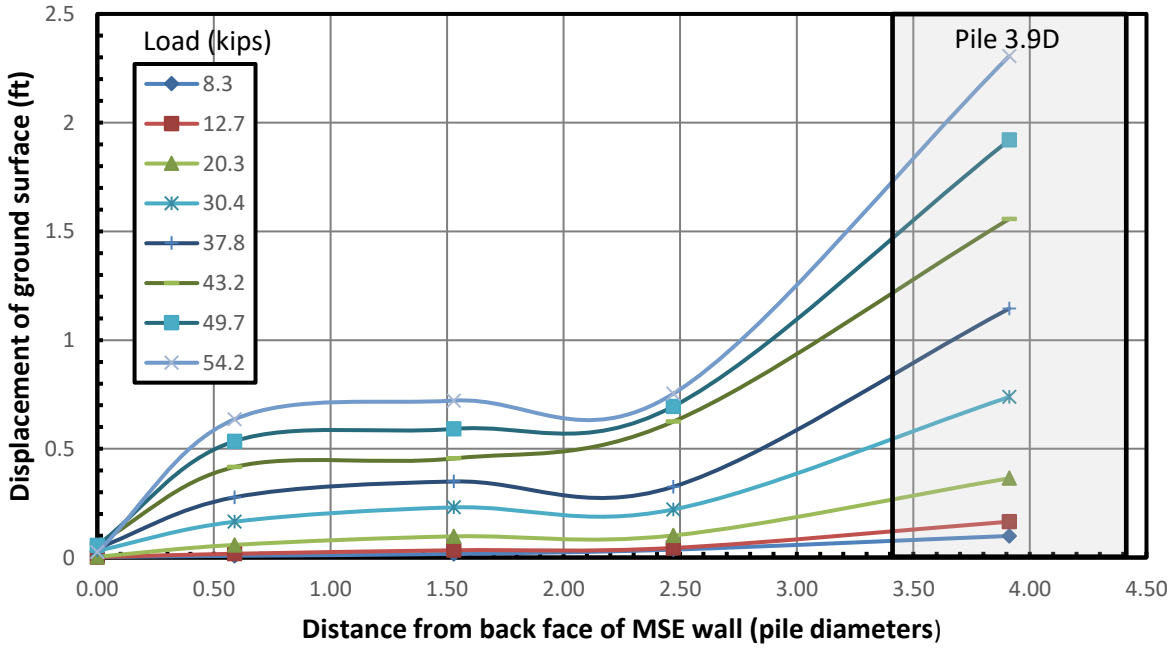

Figure 5.20: Horizontal displacements of the ground surface as a function of distance from the MSE wall at different load levels for pile 3.9D.

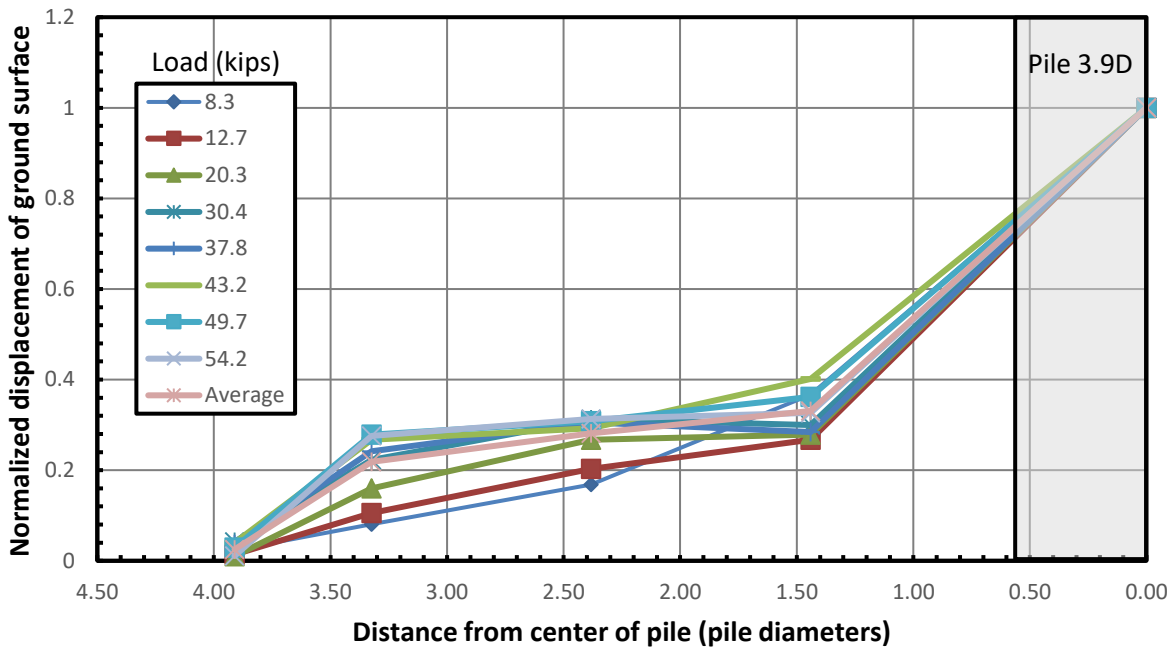

Figure 5.21: Normalized horizontal displacement of the ground surface as a function of distance from the center of the pile at 3.9D.

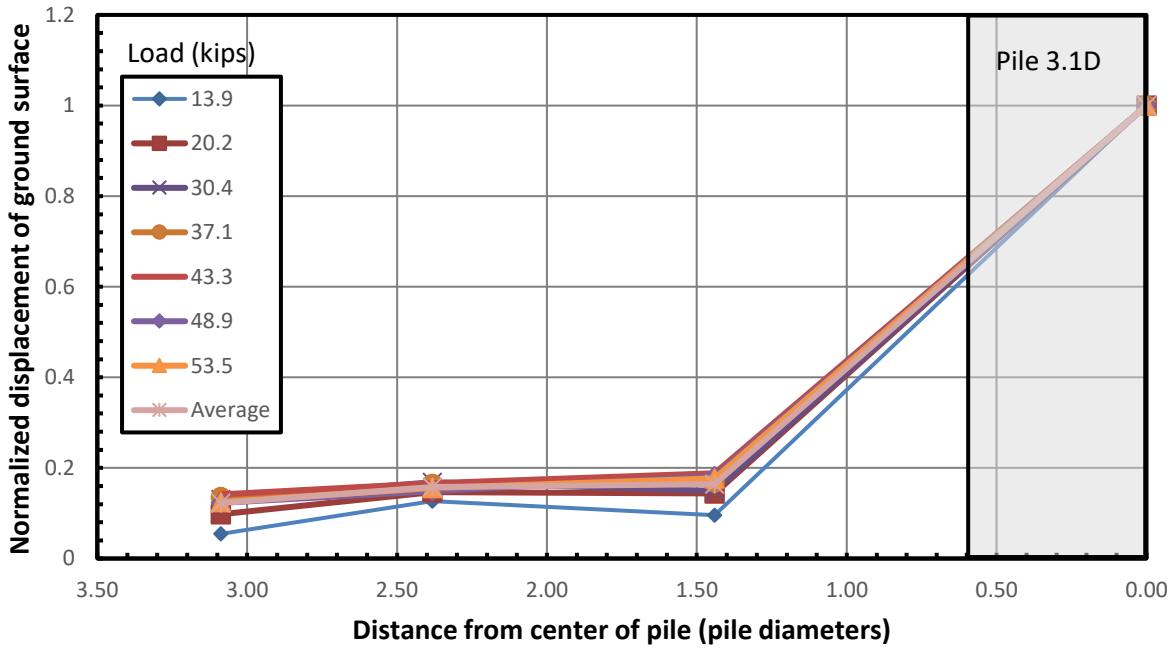

Figure 5.22: Normalized horizontal displacement of the ground surface as a function of distance from the center of the pile at 3.1D.

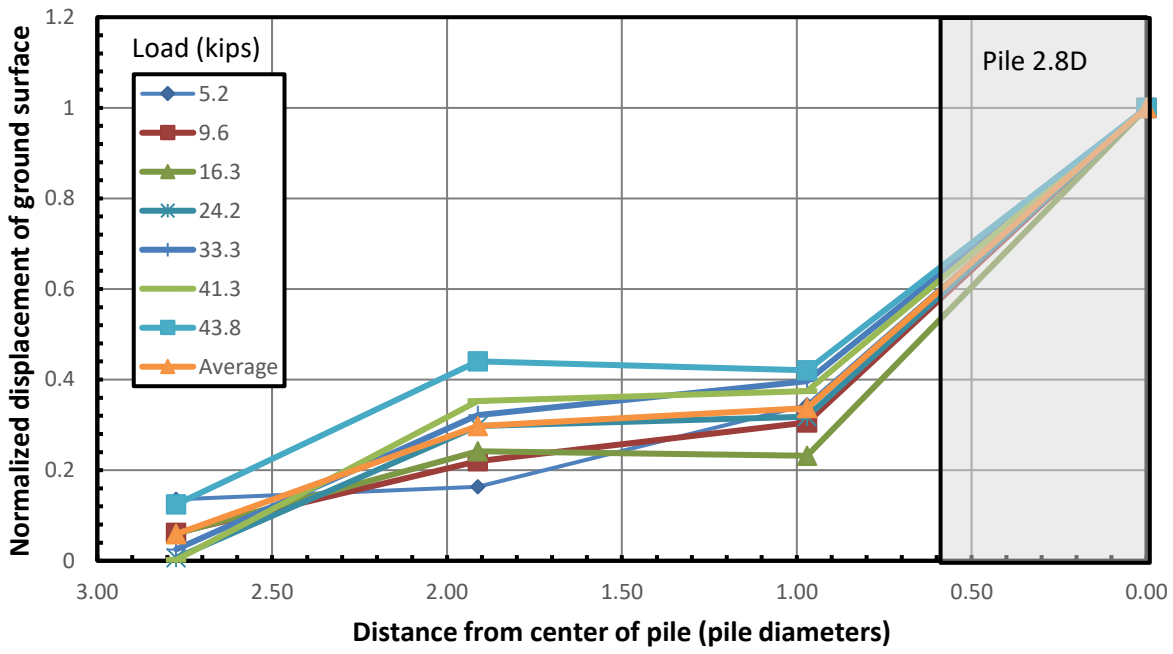

Figure 5.23: Normalized horizontal displacement of the ground surface as a function of distance from the center of the pile at 2.8D.

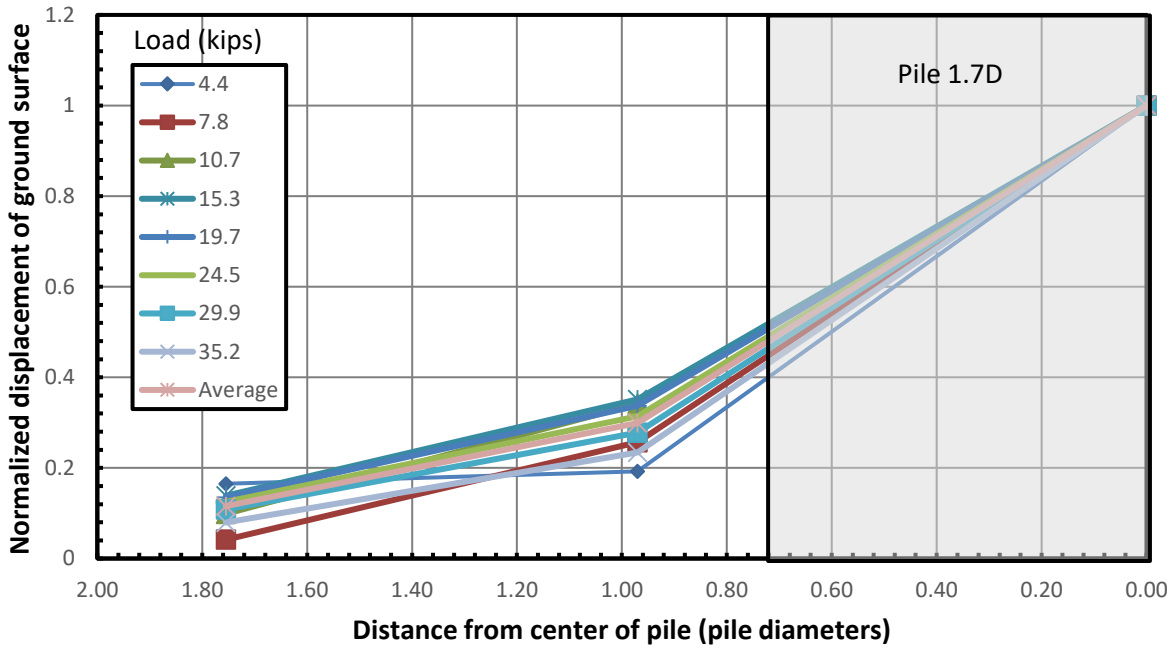

Figure 5.24: Normalized horizontal displacement of the ground surface as a function of distance from the center of the pile at 1.7D.

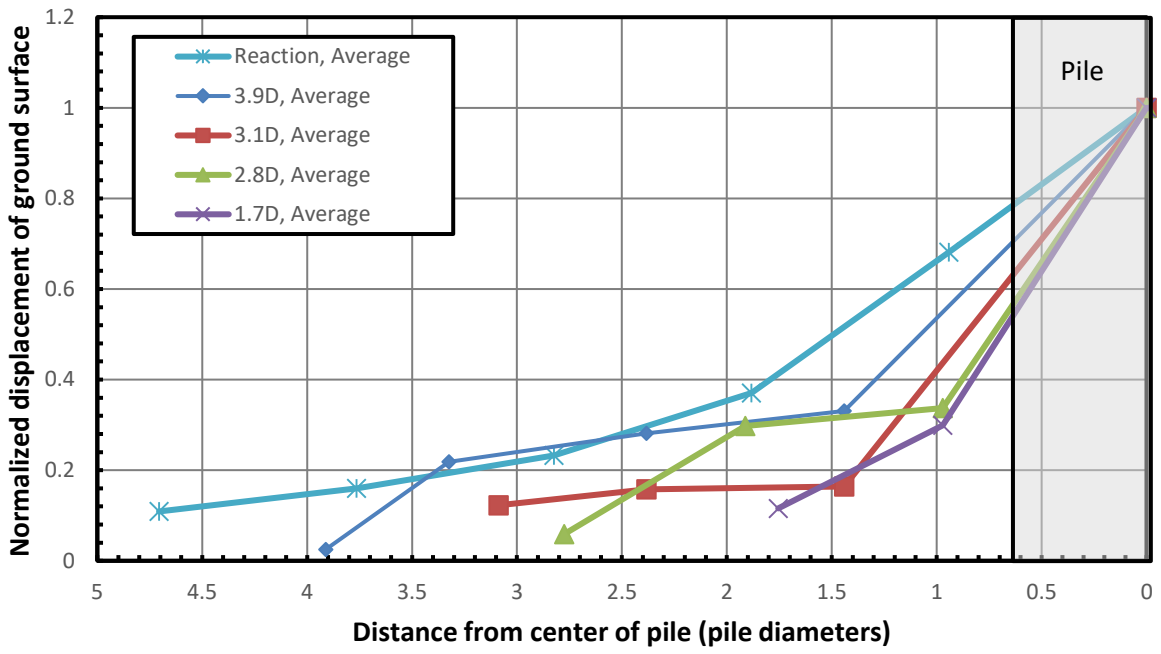

Figure 5.25: Average normalized horizontal displacement of the ground surface as a function of distance from the center of pile.

5.3.2 Photogrammetry

In addition to the use of string potentiometers, the wall panel displacement was also measured using DIC and shape arrays. The DIC provided accurate graphical and numerical data for this research purposes. Graphical representation for wall displacements directly in front of piles at 3.9D, 3.1D, 2.8D and 1.7D is shown in Figure 5.26. A series of wall displacement pictures at different pile head deflection is provided in Appendix H. The heat map shows area of concentrated displacement on the wall and has different shapes depending on whether the pile was loaded directly in front of a wall panel or on a joint between the wall panels. The different wall panel configuration makes it difficult to find a pattern between the four pile tests. However, it was observed that higher wall displacements are generally concentrated at the joints between the wall panels as seen in Figure 5.26.

With the DIC it was possible to determine the displacement of the wall panel at a point directly in front of the steel strip reinforcement. Plots were generated to compare the wall displacement in front of all the instrumented reinforcements for each test and are shown in Figure 5.27 to Figure 5.30. Typically, there is more displacement on the portion of the wall panel directly in front of the reinforcement closer to the pile. Although the curves show that the wall generally displaces outward with increasing pile head deflection, the shape is not linearly increasing with every pile head load. This may be due to wind disturbance on the DIC camera or a settings error on the DIC.

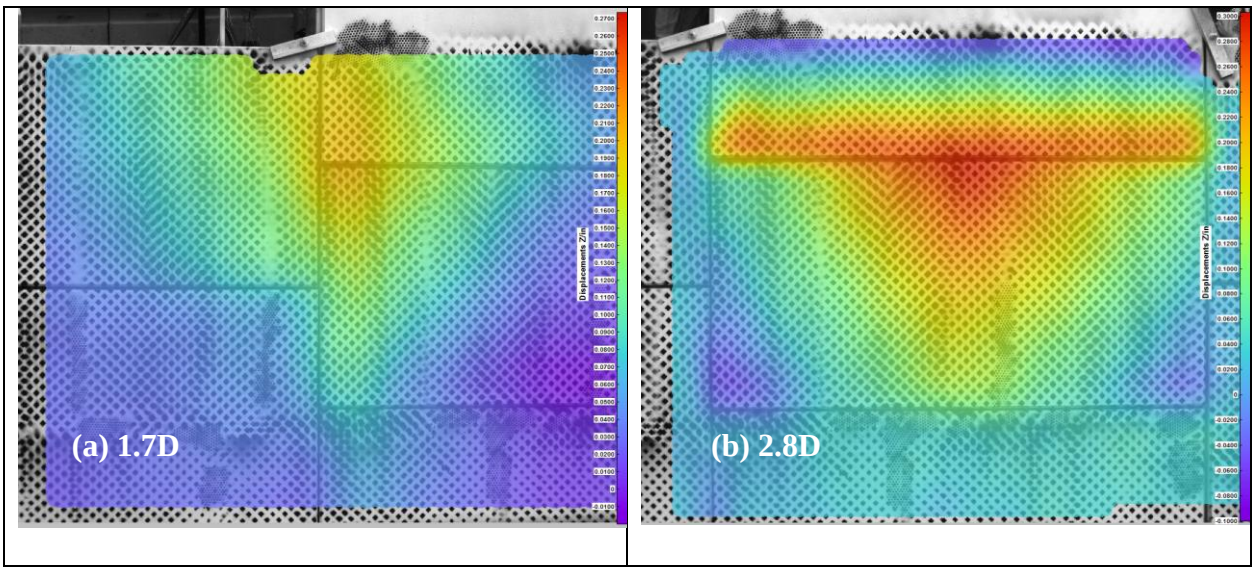

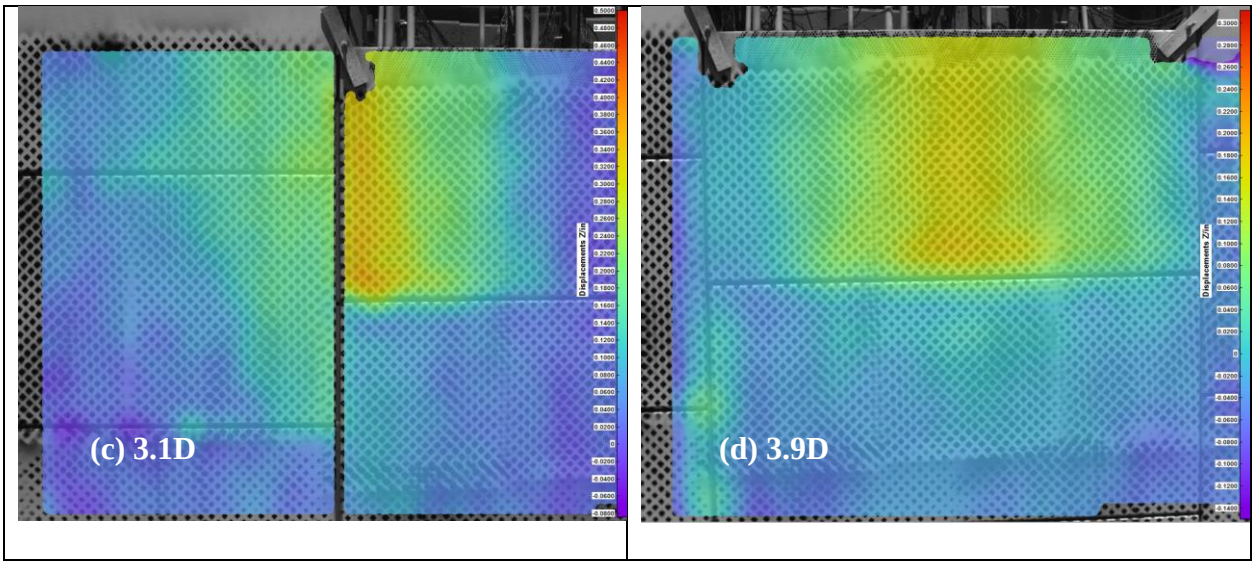

Figure 5.26: Wall displacement at 2.5 in. pile head deflection for pile at (a) 1.7D, (b) 2.8D, (c) 3.1D and (d) 3.9D.

Figure 5.26 shows that the wall panels for the test pile at 2.8D had significantly larger displacement at 2.5 in. pile head displacement when compared to the other test piles. With the help of Figure 5.29, it can be seen that the wall panel at the top was first rotating inward till about 25 kips of load before displacing outwards. This half panel setup of the top wall with only one layer of reinforcement (the second layer of reinforcement was located 45 in. below the ground surface on the bottom panel) was not sufficient to support the wall during the load test. Consequently, the load test had to be stopped at a pile head displacement of 2.5 in.

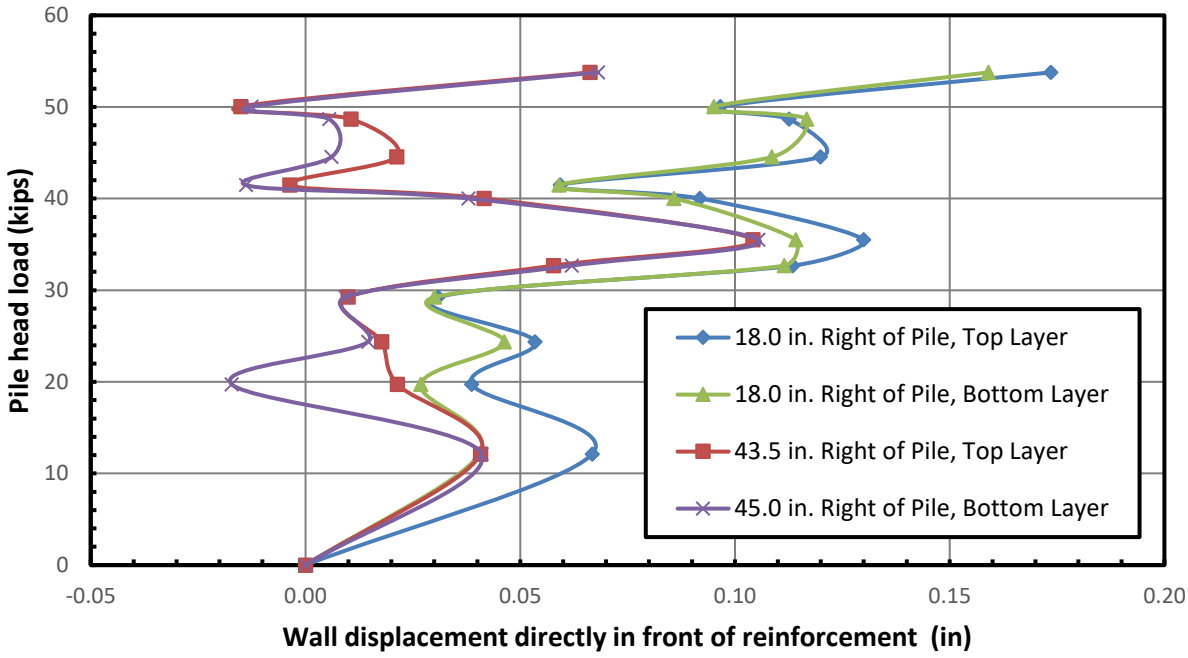

Figure 5.27: Pile head load vs. wall displacement at steel strip reinforcement for pile at 3.9D.

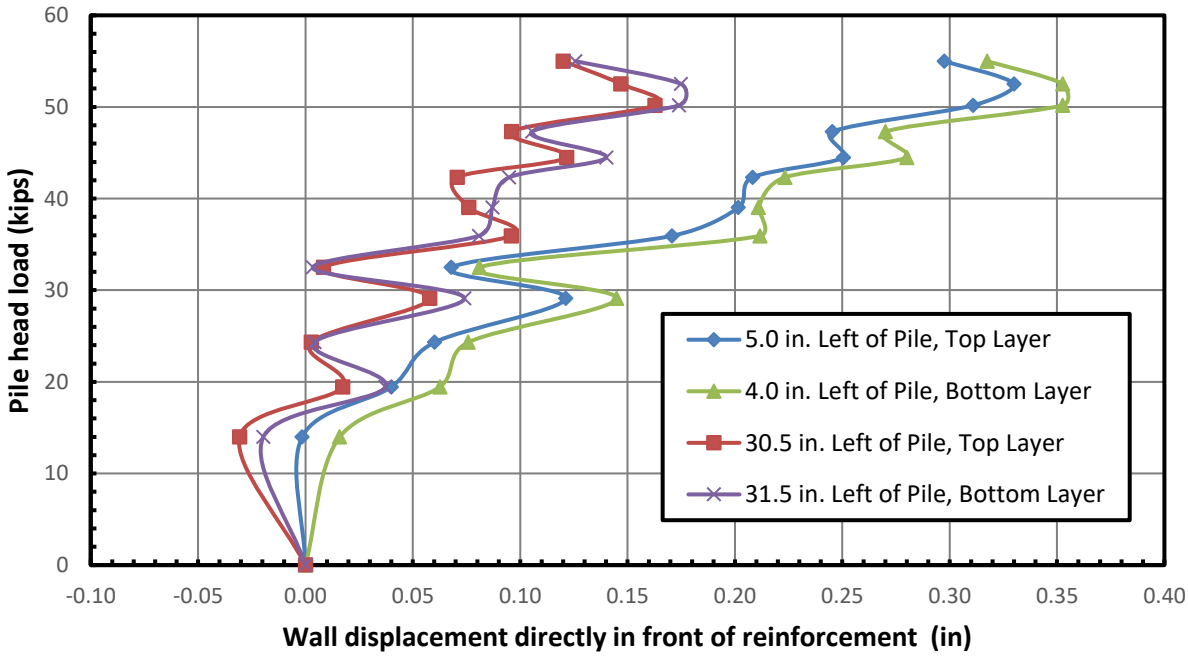

Figure 5.28: Pile head load vs. wall displacement at steel strip reinforcement for pile at 3.1D.

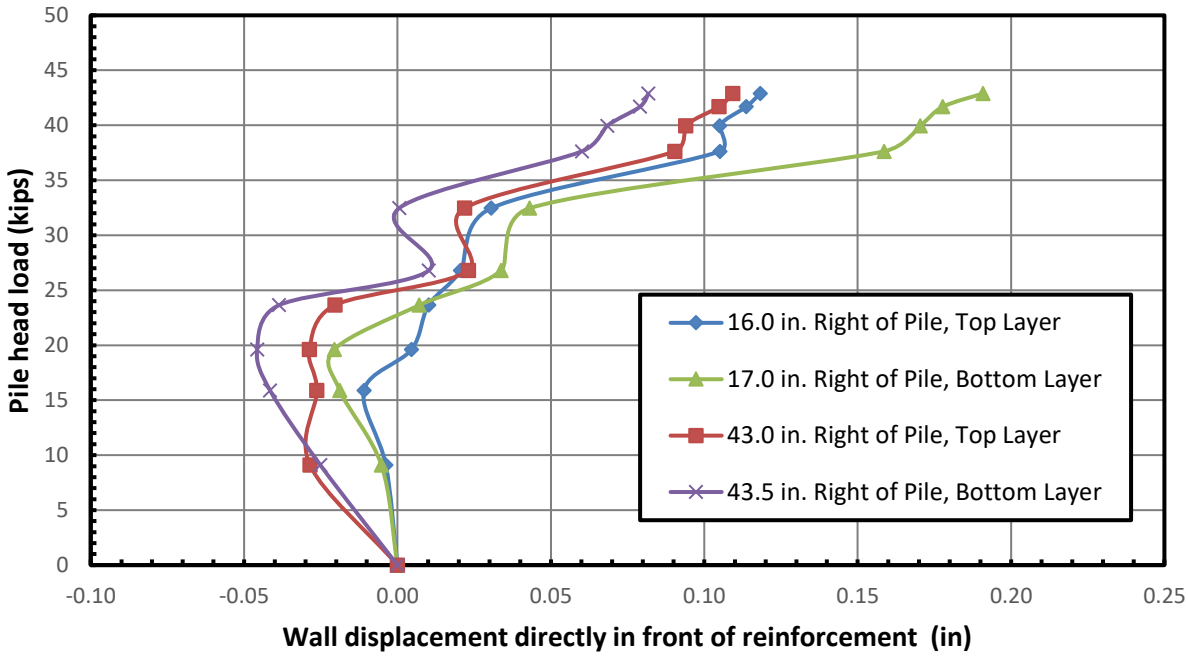

Figure 5.29: Pile head load vs. wall displacement at steel strip reinforcement for pile at 2.8D.

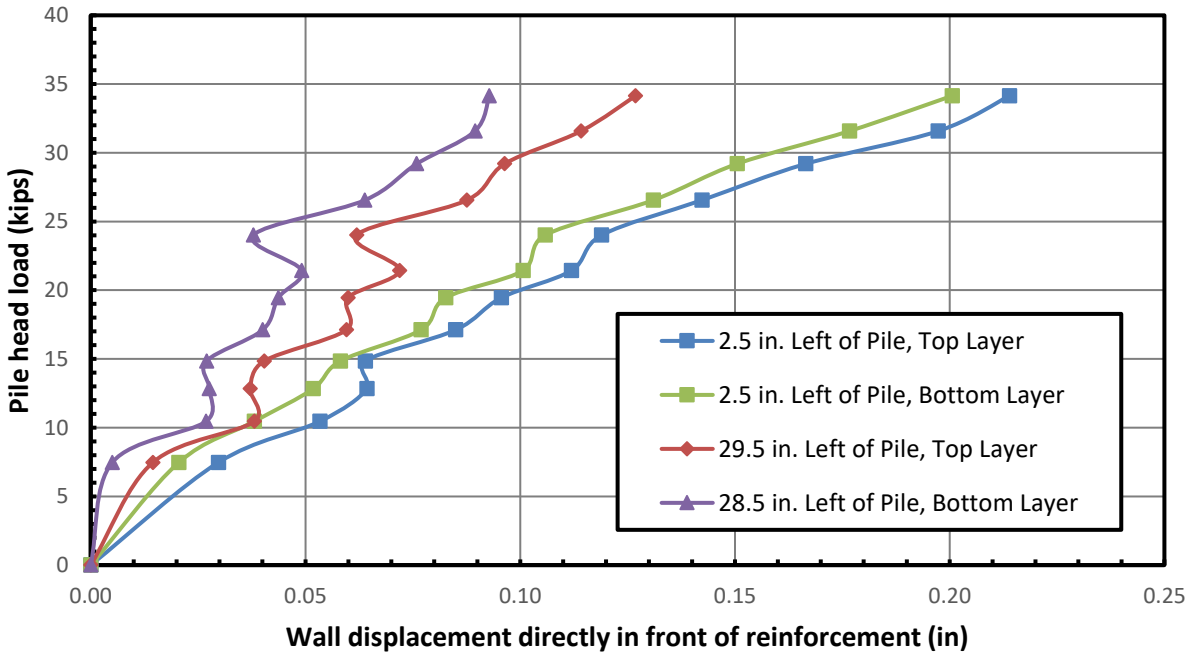

Figure 5.30: Pile head load vs. wall displacement at steel strip reinforcement for pile at 1.7D.

5.3.3 Shape Arrays

Since the DIC is a new technology recently adapted by the research team, data from the shape arrays were useful to verify the accuracy of the DIC. The wall displacement directly in front of the pile at 1.7D as measured by the shape arrays is shown in Figure 5.31. In comparison with the wall displacement as measured by the DIC (shown as black curve), the shape arrays show the correct wall displacement shape but exaggerate the displacement values significantly. The reason for this error is most probably due to the difficulty of getting good soil compaction close to the wall panels where the shape arrays were attached. Although the shape arrays did not provide accurate displacement values, they helped verify the accuracy of the wall displacement shape provided by the DIC.

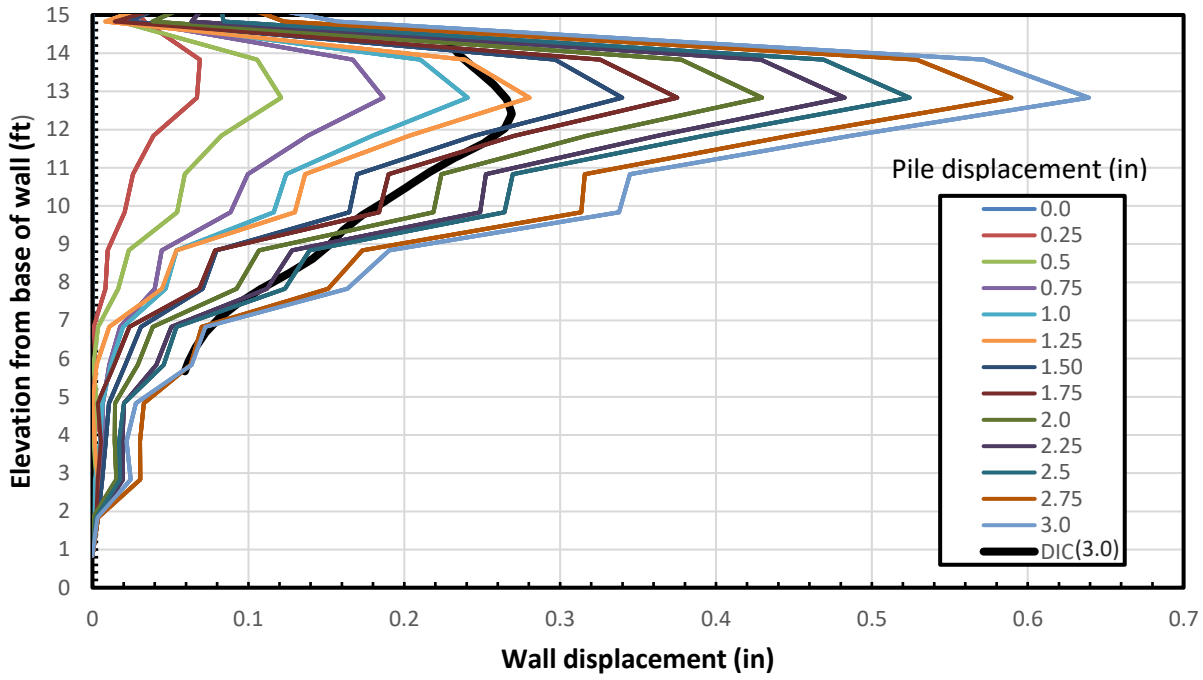

Figure 5.31: Displacement of wall directly in front of pile at 1.7D as measured by shape arrays.

5.3.4 Ground Elevation

Ground surface elevations in front of the pile were recorded with a level before and after each pile test. Significant cracking and heaving of the soil was observed as shown in Figure 5.32. The elevation of the ground surface as a function of distance from pile for piles 1.7D, 2.8D and 3.1D is shown in Figure 5.33. Unfortunately, ground surface elevation data points for pile 3.9D were unavailable. The maximum recorded soil heave was 2.64 in. immediately in front of both piles 3.1D and 2.8D and decreased to about half of this value at a distance of 1 ft. from the pile face.

Figure 5.32: Cracking and heaving of soil in front of pile 3.1D.

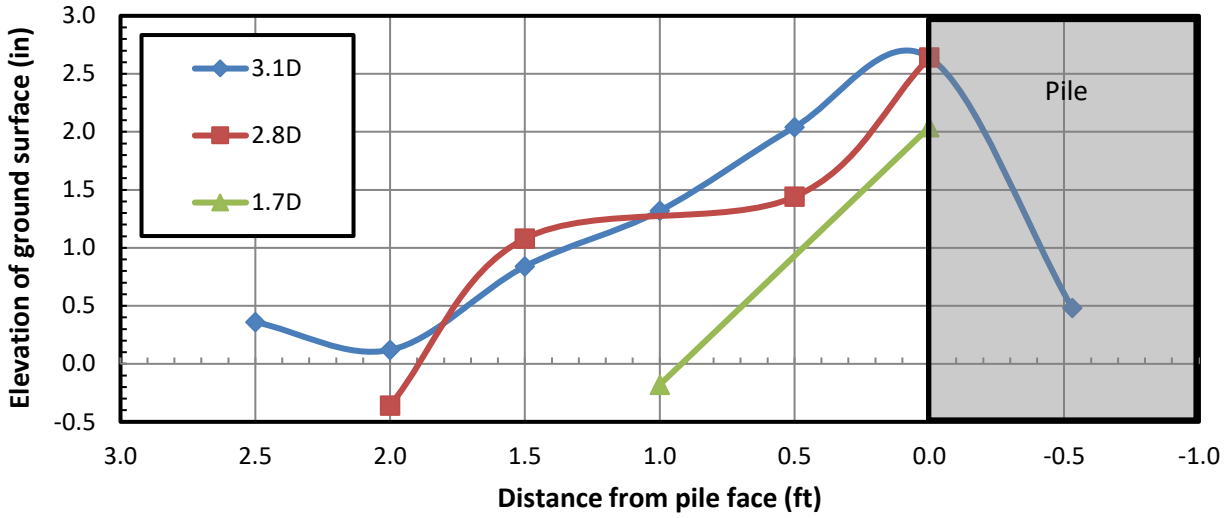

Figure 5.33: Elevation of ground surface as a function of distance from pile.

5.4 Pile Performance

The bending moment in the pile was calculated from the strain gauge data using Equation 5-2. The average value of the paired strain gauges was used when both gauges were functioning. If one of the paired gauges was found to be damaged during installation, only the data from the functioning gauge was used.

$$M_i = EI(\mu\varepsilon_t - \mu\varepsilon_c)(10^{-6})/(D_o) \quad (5\text{-}2)$$

where

M_i is the bending moment in inch-kips for the pile at the i^{th} data point.

E is the modulus of elasticity of the steel pile (29000 ksi),

I is the moment of inertia of the pile,

$\mu\varepsilon_t$ is the micro strain for the tension (+) side data point,

$\mu\varepsilon_c$ is the micro strain for the compression (-) side data point, and

D_o is the outside diameter of the pile.

Most of the strain gauges were well protected by the steel angles and expanding foam. Some of the gauges did get damaged either from pile driving or from the heat of the steel angle welding process. Nevertheless, that did not have much negative impact on data analysis because of the redundancy of the paired strain gauge setup. Some of the piles were rotated during pile driving which resulted in the strain gauges being out of alignment from the loading direction. To remediate this slight error, Equation 5-2 was modified to obtain the bending moment in a more accurate fashion as shown in Equation 5-3 below. The addition of the steel angles was also taken into account in the moment of inertia calculation of the piles.

$$M_i = EI(\mu\varepsilon_t - \mu\varepsilon_c)(10^{-6})/(2Y) \quad (5\text{-}3)$$

where

M_i is the bending moment in inch-kips for the pile at the i^{th} data point.

E is the modulus of elasticity of the steel pile (29000 ksi),

I is the moment of inertia of the pile (in^4),

$\mu\varepsilon_i$ is the micro strain for the tension side data point,

$\mu\varepsilon_o$ is the micro strain for the compression side data point, and

Y is the vertical distance to the strain gauge location as shown in Figure 5.34.

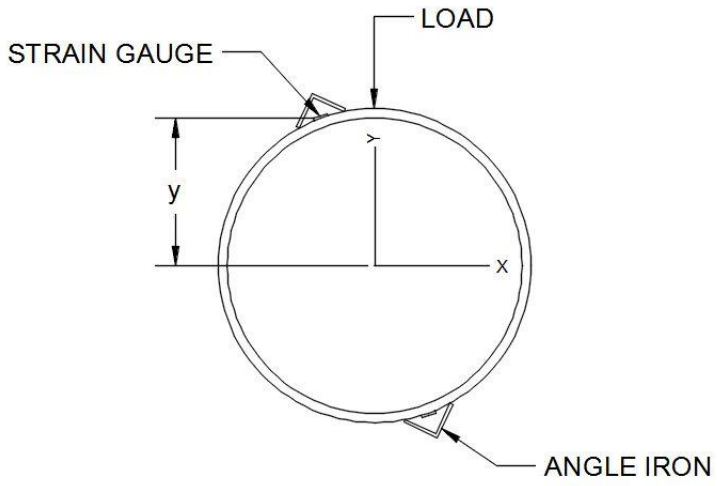

Figure 5.34: Correction for vertical distance to strain gauge location for bending calculations.

The measured bending moment for the pile at 3.9D is shown in Figure 5.35. The measured bending moment for the other pile tests are found in Appendix G. For the pile at 3.9D, the bending moment increases with increasing pile head load with a maximum value of 3310 in-kips at a depth of 7 ft. below the ground surface. The bending moment at a pile head load of 33 kips for all of the pile tests is shown in Figure 5.36. According to Figure 5.36, the bending moment for piles at 3.9D and 3.1D are relatively similar but the bending moment increases when the piles are located closer to the wall at 2.8D and 1.7D. It was also observed that the maximum bending moment occurs deeper in the soil profile for the pile at 1.7D. These observations show that there is less soil resistance as the piles are located closer to the wall.

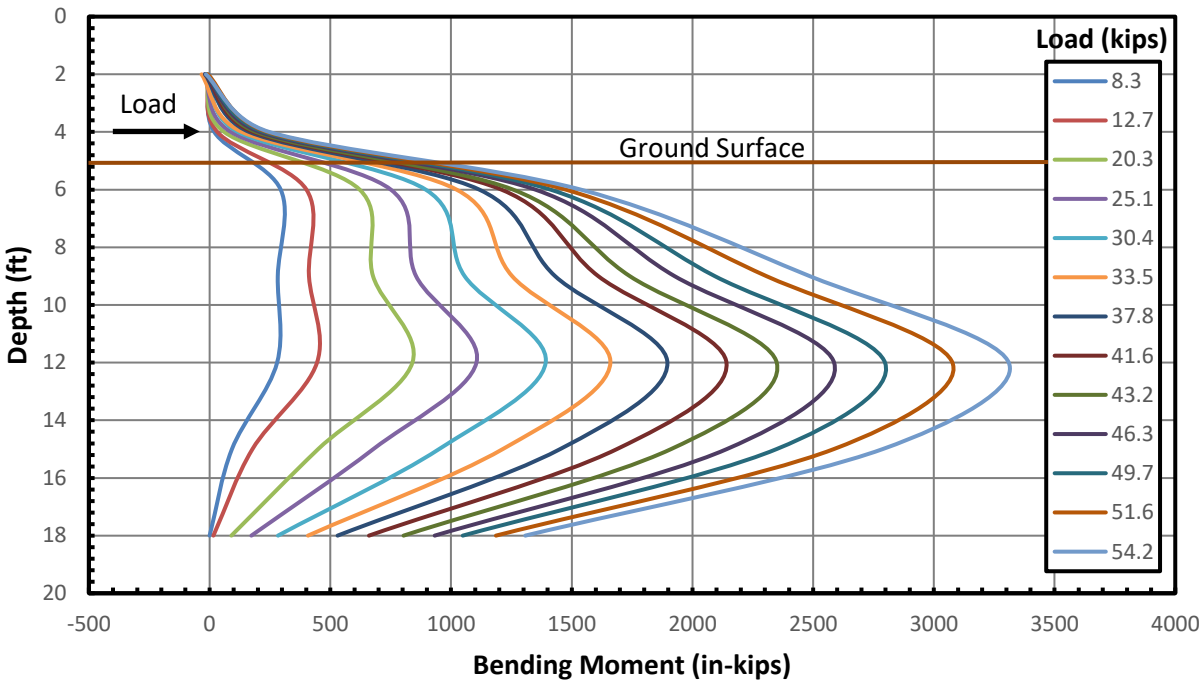

Figure 5.35: Bending moment vs. depth for pile at 3.9D.

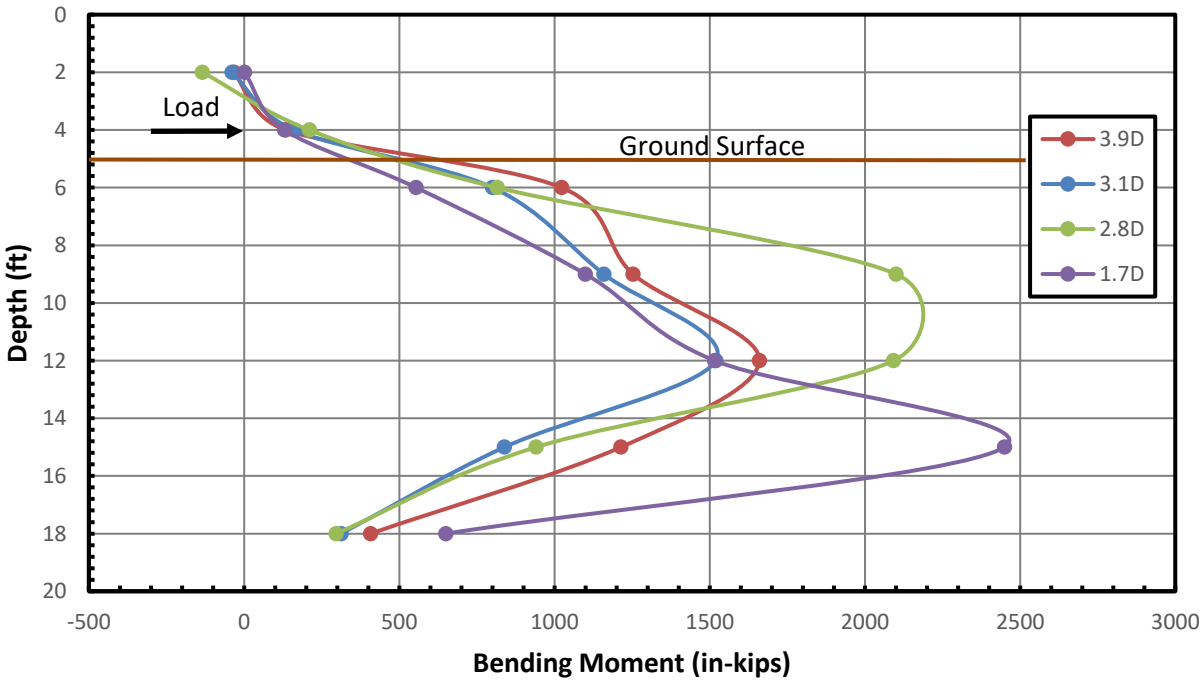

Figure 5.36: Bending moment vs. depth at pile head load of 33 kips.

6 LATERAL LOAD TESTING WITH STRIP REINFORCEMENT

Lateral load testing was performed between July 2, 2014 and July 17, 2014. A photo of the wall at the time of testing is shown in Figure 6.1. A profile view of the wall at the time of testing is shown in Figure 6.2. Testing was performed using the displacement control approach, where load was applied to reach displacement increments of 0.25 inches up to a total head deflection of 3 inches. Once the desired displacement was reached, the fluid flow into the jack was cut off so that jack displacement remained constant for 5 minutes. Pile head load and displacement readings were taken at the peak load, 1 minute hold, and 5 minute hold. It was seen that the load dropped off significantly from the peak load to the 1 minute hold, and slightly dropped off from the 1 minute hold to the 5 minute hold. The 1 minute hold represents equilibrium between the lateral pile load and resistance, and so it was decided to use the 1 minute hold as the final load. The peak load was only maintained for a few seconds before decreasing. Although the peak load might be appropriate for a rapidly applied load such as an earthquake it would overestimate the pile resistance for static loadings. The data for each test was collected using a Megadac data logger at a rate of 2 readings per second.

Figure 6.1 Photo of the wall at the time of testing.

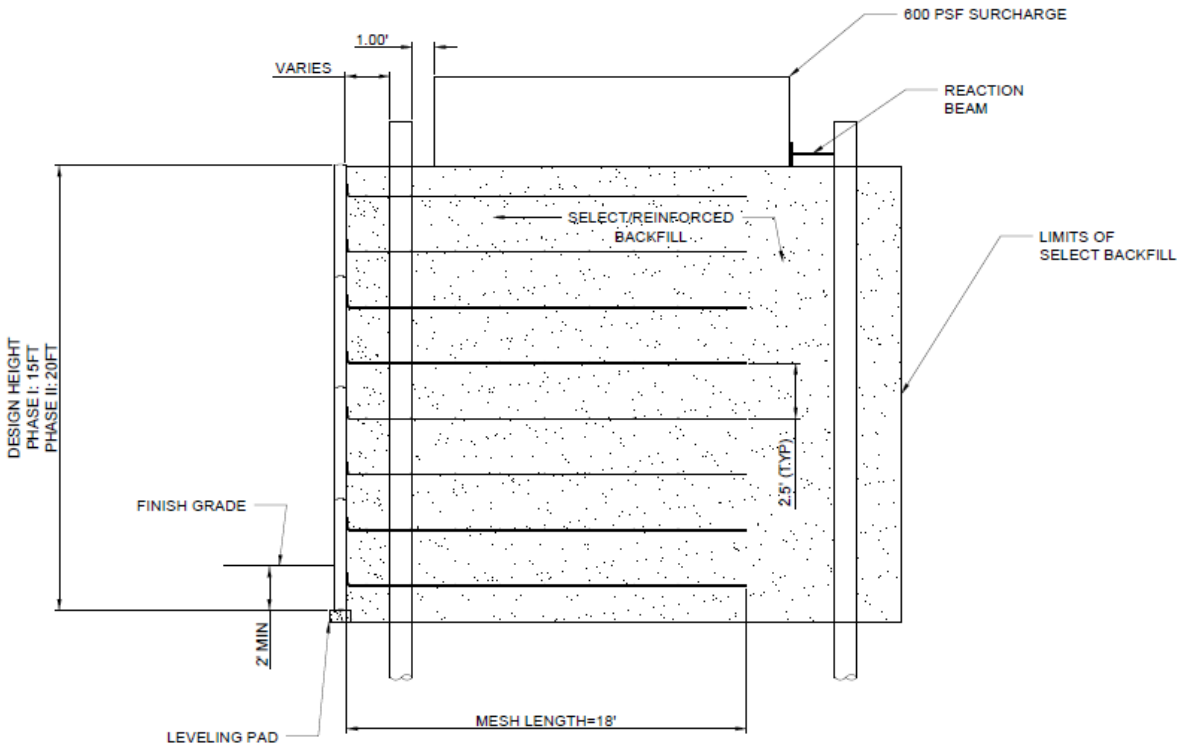

Figure 6.2 Profile view of the wall at the time of testing.

6.1 Load Displacement Curves

The load-displacement curves for each test for the peak loads are shown in **Figure 6.3**, and for the final loads are shown in **Figure 6.4**. In addition to the load-deflection curves for the four test piles near the MSE wall, a curve is also provided for a companion "reaction" pile that

was tested prior to the test on the piles near the wall. Because the "reaction" pile was loaded transverse to the wall against another reaction pile, at a distance of about 23 ft behind the wall, the pile resistance in this case is not affected by the presence of the wall. The reduction in load from the peak to final load is higher for piles that are closer to the wall and lower for piles that are farther away, although on average the reduction is about 9%.

In **Figure 6.3** and **Figure 6.4**, it can be seen that the lateral resistance of the pile decreases as the pile gets closer to the back face of the wall. However, the resistance of the 4.3D and 3.2D piles is very similar. This may be because the 4.3D pile was in front of a joint in the wall while the 3.2D pile was located in the center of a panel. This may have reduced the contribution of the reinforcement to the lateral resistance for the 4.3D pile and/or increased the resistance for the 3.2D pile, although the transverse reinforcement spacing was constant along the length of the wall. Alternatively, the curve for the 4.3D pile may be low because the soil was not adequately compacted in this vicinity relative to the 3.2D pile. Considering that hand compaction methods are used in the vicinity of an MSE wall and density control is often relaxed in this region, variations in relative compaction may be expected in occur in this region for MSE wall constructed in practice.

Interestingly, the 5.3D curve tracks the reaction pile curve until a deflection of 1.75 inches. This seems to indicate that a pile spacing of 5.3 diameters is far enough back from the face of the wall to not have any interaction. However, the 5.3D curve falls off after 1.75 inches of deflection. The decrease in pile resistance for the 5.3D pile relative to the reaction pile may be attributable to at least two factors. First, as indicated previously, the relative compaction of the soil densified by plate compactors in the vicinity of the piles near the wall is only about 88% to 92% . In contrast, the relative compaction of the soil behind the test piles was typically

between 95% and 97%. In addition, jumping jack compactors were used to compact soil around the reaction test piles. Although these differences in relative compaction may seem small, these differences lead to substantial differences in the relative density which strongly influences lateral pile resistance. Secondly, the reaction pile is located far enough back that its resistance would not likely be affected by the presence of the wall, but the pile at 5.3D spacing may have been affected by the presence of the wall. Based on previous full-scale tests, it seems likely that the presence of the wall does not affect the resistance of the 5.3D pile, but differences in compactive effort are the main source of the discrepancy.

The load-deflection curves for the 5.3D, 4.3D, and 3.2D piles exhibit a more hyperbolic shape that indicates progressive failure of the surrounding soil as the applied load increases. In contrast, the load-deflection curve for the 1.9D pile is relatively linear. This linear slope suggests that the resistance is primarily due to the pile stiffness and that the surrounding soil provides limited resistance. The reduced soil resistance is likely a combination of the close proximity of the pile to the wall and the difficulty of compacting the soil in the small space between the pile and the wall.

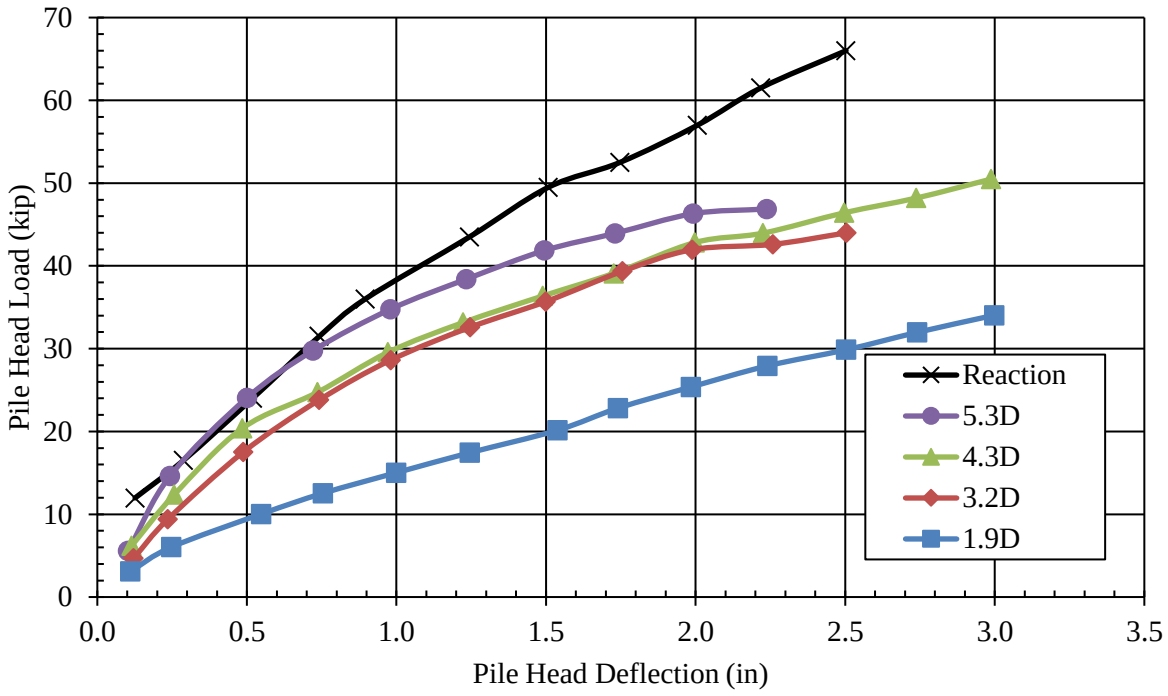

Figure 6.3 Pile head load vs deflection, peak load.

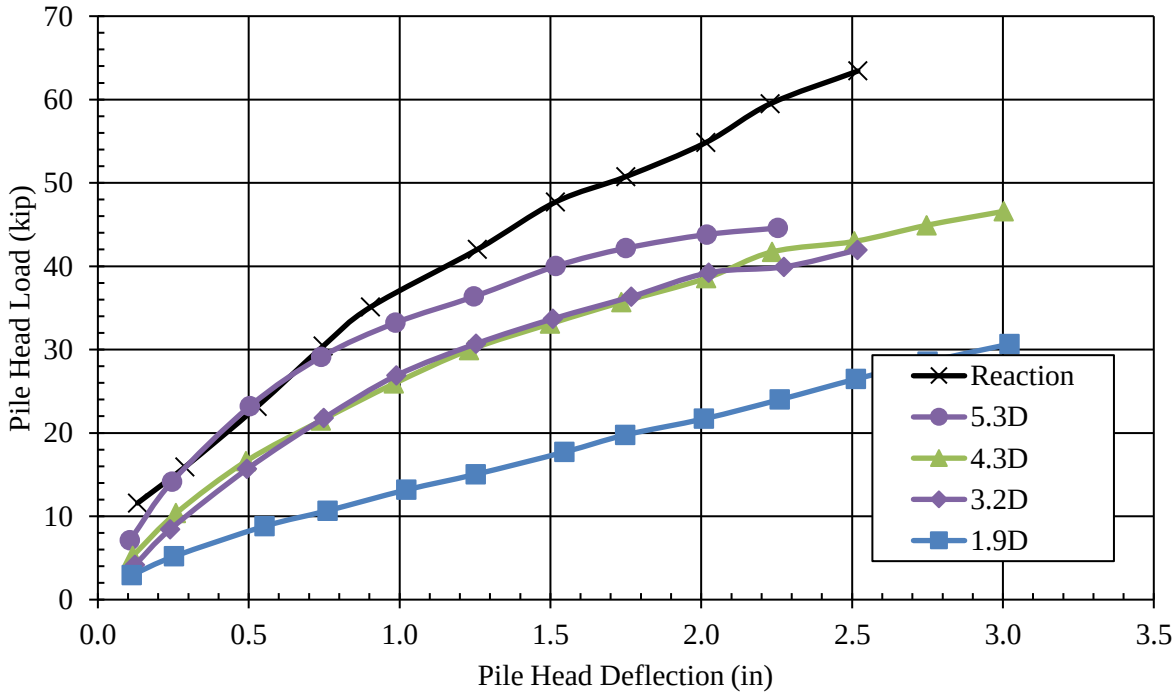

Figure 6.4 Pile head load vs deflection, final load.

6.2 Soil Reinforcement Performance

The load on the entire welded wire grid induced by the lateral pile load was calculated for instrumented grids using Equation 5-1. The average value of paired strain gauges was used when both strain gauges were working, otherwise, only the data from the functioning gauge was used.

$$\boldsymbol{T_i = EA(\mu\varepsilon_i - \mu\varepsilon_o)(10^{-6})B} \qquad (6\text{-}1)$$

where

T_i is the induced tension in kips for the wire grid at the i^{th} data point,
E is the modulus of elasticity of steel (29000 ksi),
A is the cross-sectional area of the wire instrumented (0.11 in^2),
$\mu\varepsilon_i$ is the average micro strain for the ith data point,
$\mu\varepsilon_o$ is the average initial micro strain, and
B is a location factor as equal to 5 for the welded wire grids in this study.

The induced force in the reinforcement for several pile head loads in each of the four tests piles is shown in **Figure 6.5** through **Figure 6.8**. As the pile head load increases, the peak load in the reinforcement also increases. In general, it can be seen that the induced force increases from the back face of the wall to the center of the pile, and then drops off toward the end of the reinforcement.

The induced force in the reinforcement for a certain pile head load for four different reinforcements for each test is shown in **Figure 6.9** through **Figure 6.12**. The plots show four welded wire grids for each test. There are two levels of reinforcement and a close and a far reinforcement. It can be seen in the plots that the induced load in the reinforcement tends to increase when the reinforcement is closer to the pile, and tends to increase when the reinforcement is deeper in the soil profile.

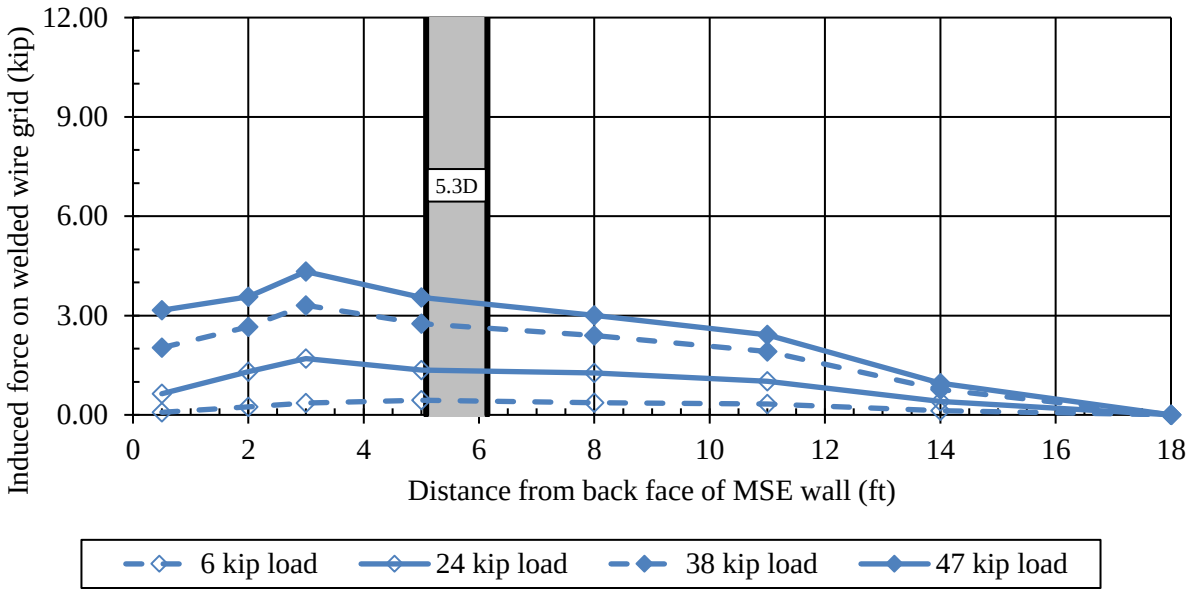

Figure 6.5 Induced force in the reinforcement for several pile head loads, 5.3D test.

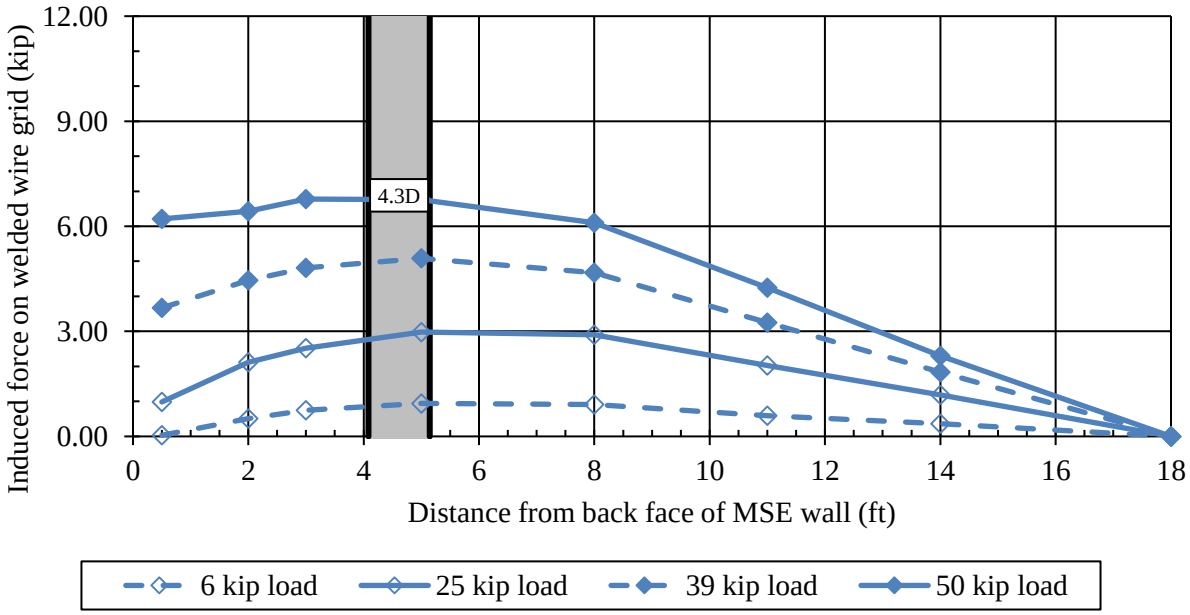

Figure 6.6 Induced force in the reinforcement for several pile head loads, 4.3D test.

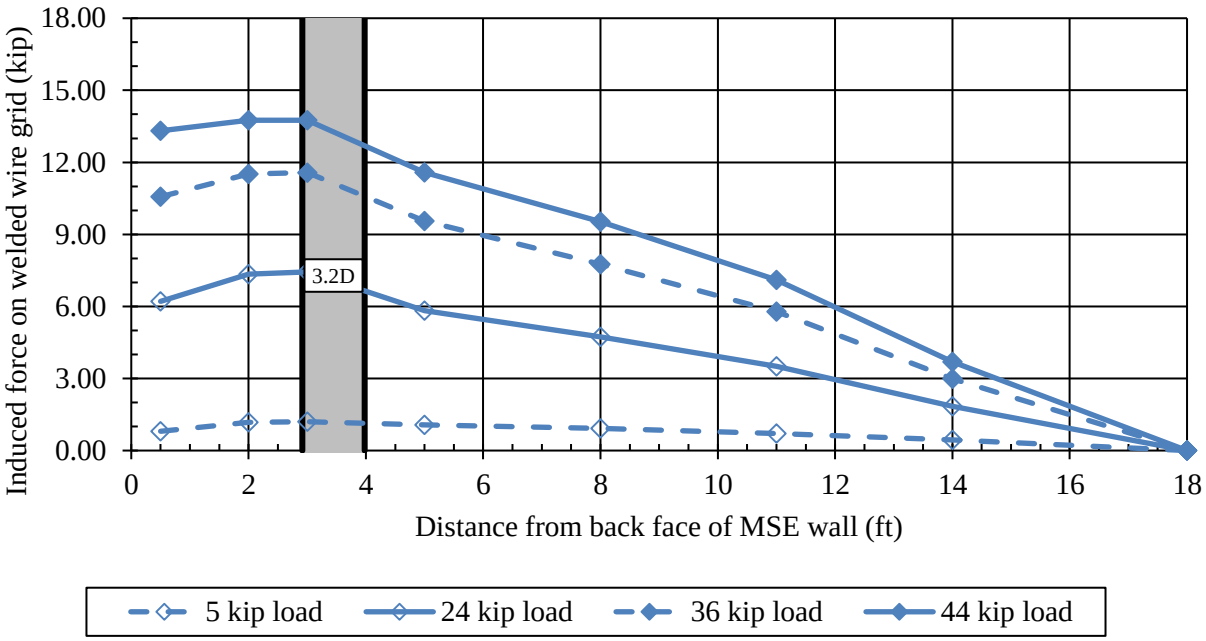

Figure 6.7 Induced force in the reinforcement for several pile head loads, 3.2D test.

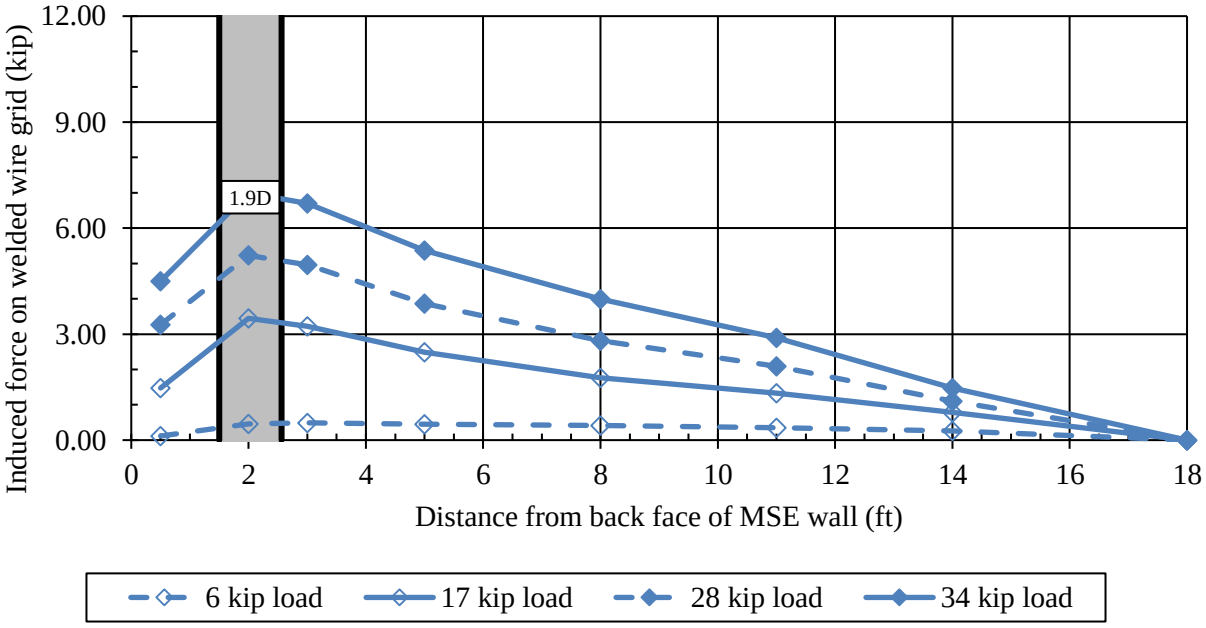

Figure 6.8 Induced force in the reinforcement for several pile head loads, 1.9D test.

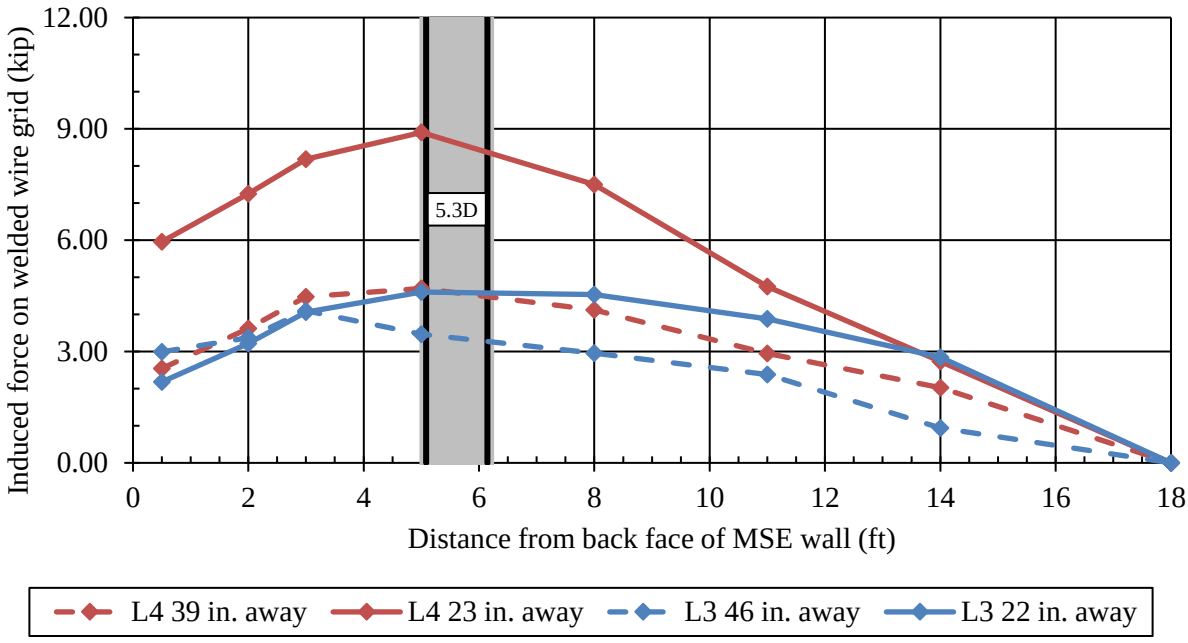

Figure 6.9 Induced force in the reinforcement for a 47 kip pile head load, 5.3D test.

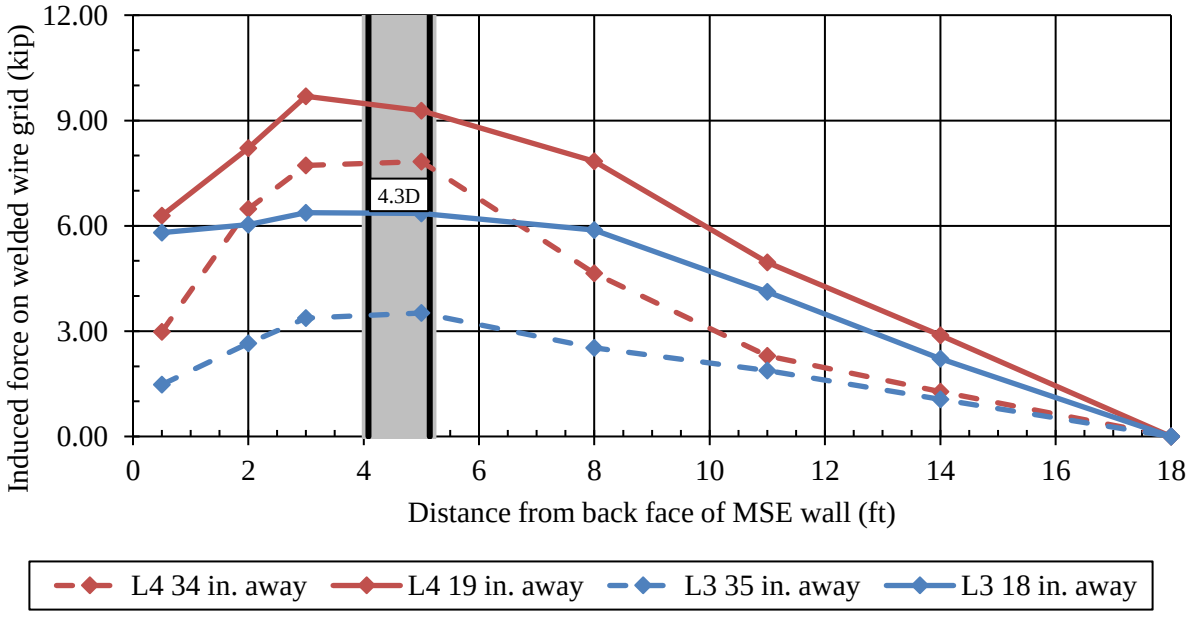

Figure 6.10 Induced force in the reinforcement for a 50 kip pile head load, 4.3D test.

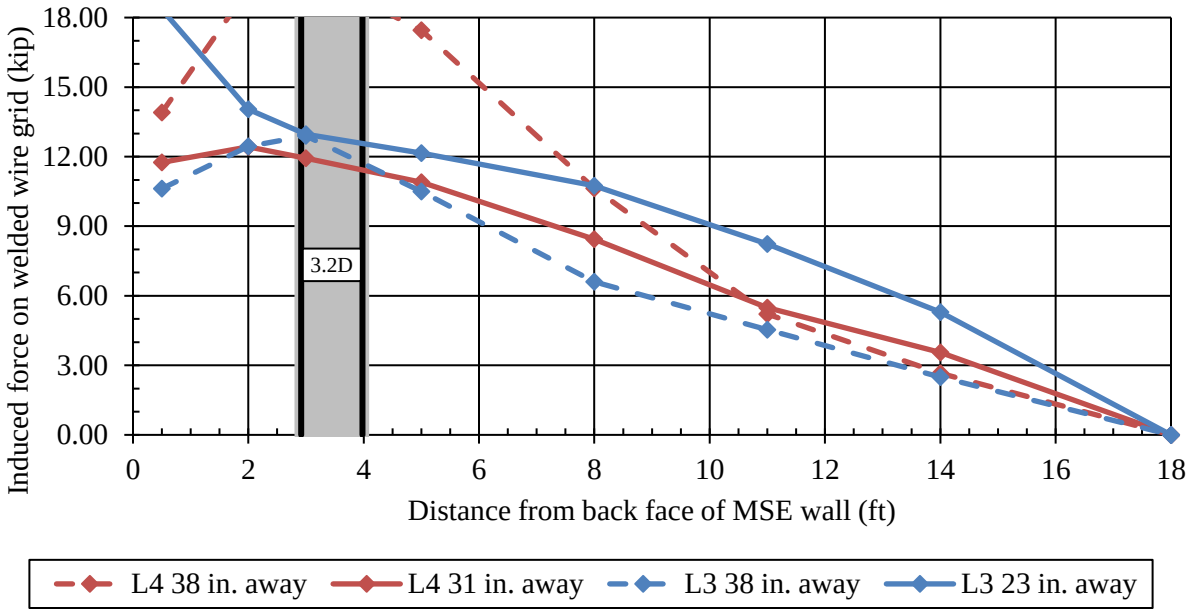

Figure 6.11 Induced force in the reinforcement for a 44 kip pile head load, 3.2D test.

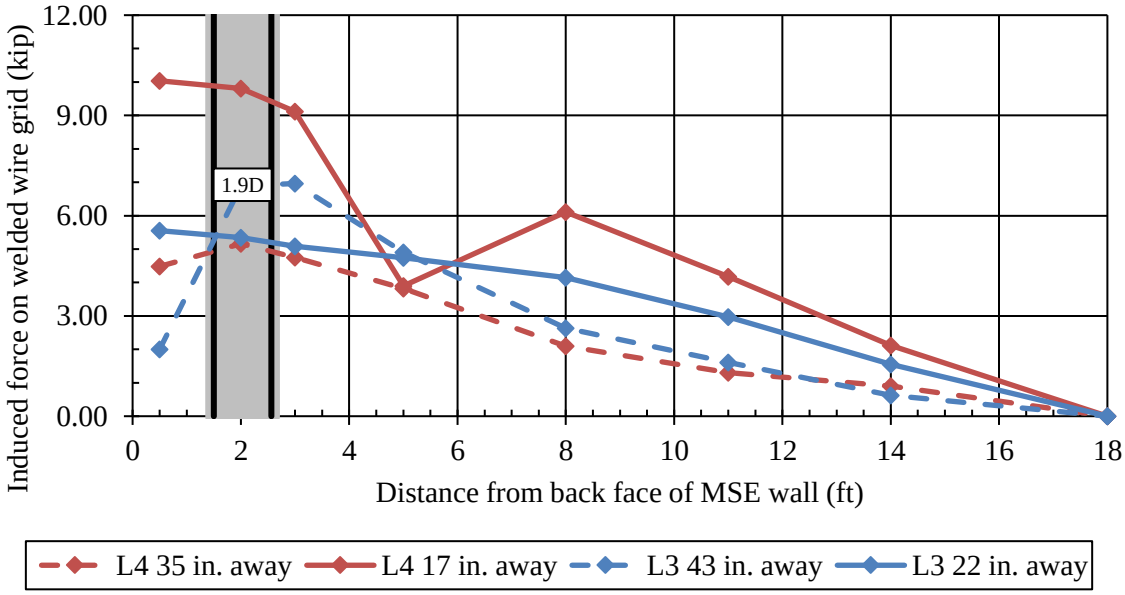

Figure 6.12 Induced force in the reinforcement for a 32 kip pile head load, 1.9D test.

Using the method discussed in Berg et al (2009), the predicted pullout capacity was calculated for each reinforcement level and compared to the measured load in the reinforcement.

This comparison is shown in **Figure 6.13**, for the L4 grid close to the pile. The measured curve seems to track the calculated curve quite well.

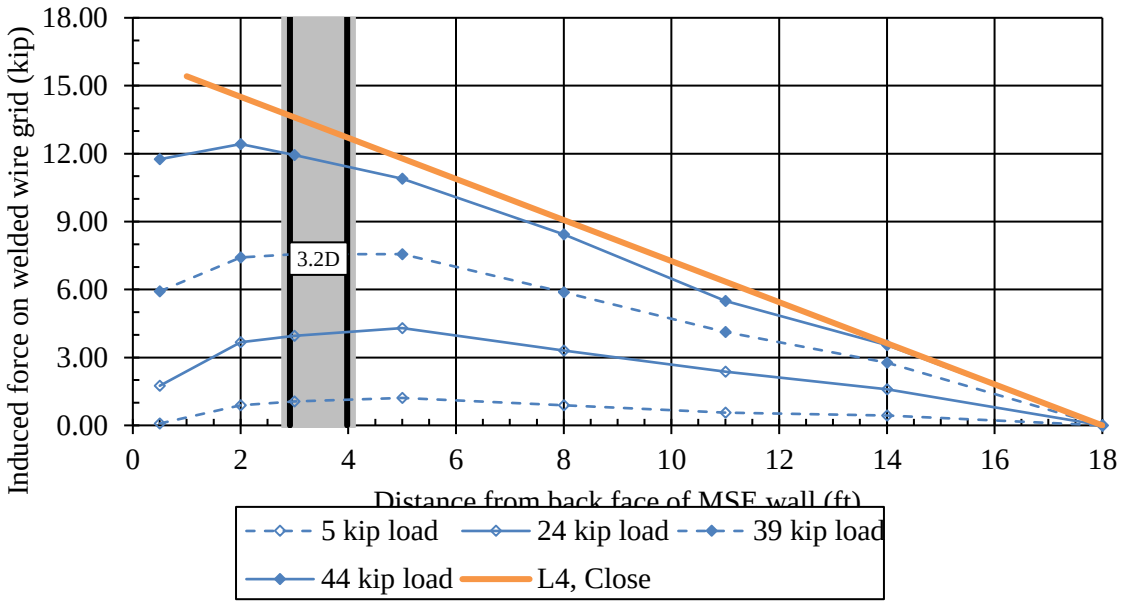

Figure 6.13 Comparison of measured load and calculated pullout capacity using Berg et al (2009).

A conceptual framework for this observed performance is illustrated in **Figure 6.14**. The measured force distribution in the grid suggests that soil in front of the pile is being pushed forward as the pile is loaded while soil behind the pile is serving to anchor the reinforcement grid. Behind the pile, the grid is moving towards the wall relative to the soil. This leads to a decrease in tension in the grid behind the pile as load is transferred to the surrounding soil by skin friction. In front of the pile, the soil is moving toward the wall relative to the grid. This leads to an increase in tension in the grid as load is transferred from the soil to the grid by skin friction. A positive tensile force in the reinforcement at the wall face is likely a result of the increased earth pressure on the wall from the pile loading.

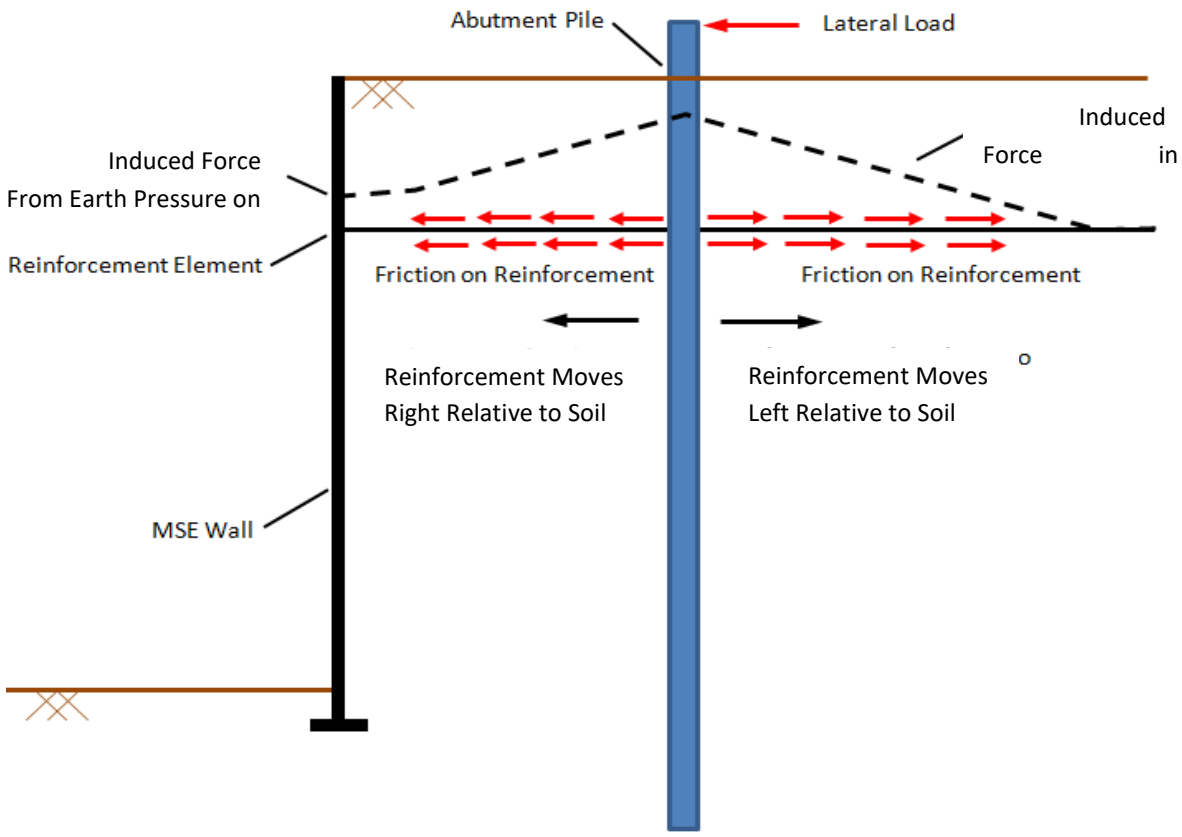

Figure 6.14 Interaction of soil and MSE wall reinforcement when pile is laterally loaded.

The induced force in the reinforcement generally increases as the pile gets closer to the wall. Based on the above framework, it seems that the 1.9D pile is too close to the wall to mobilize any resistance from the reinforcement. This relationship is shown more clearly in **Figure 6.15**, where the induced tensile force in the reinforcements for a constant load level of 34 kips is shown for all four tests. The induced load increases with decreasing pile spacing except for 1.9D, where the induced load is smaller.

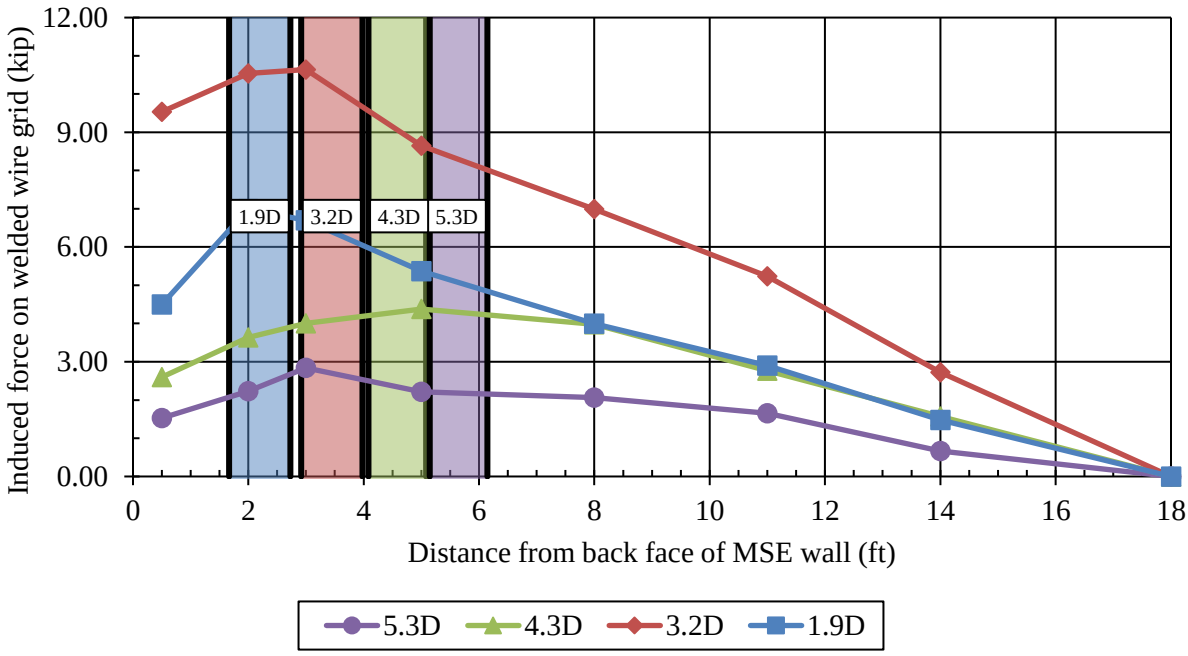

Figure 6.15 Induced force in the reinforcement farther from the pile and on the first level for a 34 kip pile head load for all four pile tests.

6.3 Induced Load in the Reinforcement

A plot of normalized induced load in the reinforcement vs normalized distance from the pile is shown in **Figure 6.16**. This plot is similar to those developed by Price (2012) and Nelson (2013), and includes data from Price, who tested welded wire grids. The best fit line and envelope from Price are also included. As can be seen, the data from this study fall outside of Price's envelope. Perhaps this is because the surcharge used in this study increased the factor of safety against pullout for the reinforcement.

It might be possible to revise the envelope proposed by Price to include the 5.3D and 4.3D test data from this study, but the data from the 3.2D and 1.9D tests do not fit into this framework. These results show that the plots from Price and Nelson are not adequate for design. Data from the other tests performed with this study will be used to develop more applicable design curves.

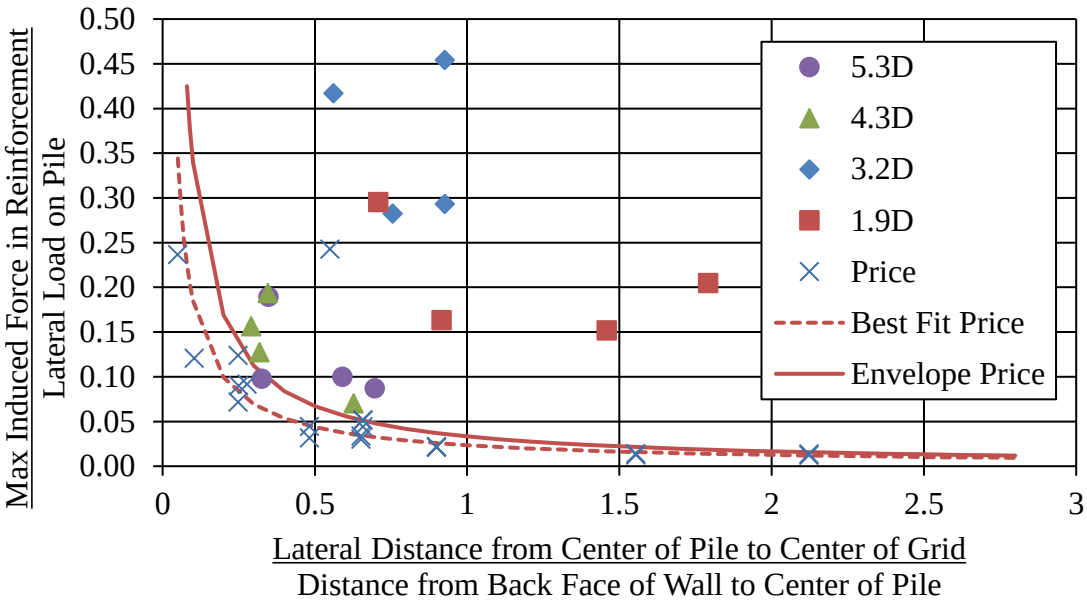

Figure 6.16 Normalized induced force in grid vs normalized distance from pile, including data from Price (2012).

6.4 Ground Displacement

During each test, the pile pushed the ground in front of it towards the wall. As the pile head displacement increased, the horizontal displacement of the ground also increased. This is shown for the 5.3D test in **Figure 6.17**. The horizontal displacement for all of the tests at a deflection level of 2.25 inches is shown in **Figure 6.18**. In each case, the ground moved toward the wall. It seems that wall displacement was greater when the pile spacing was greater, and decreased as pile spacing decreased. This is also supported by the plot in **Figure 6.19**, where the distance of the measurement in front of the pile is normalized by the distance of the pile behind the wall. The wall displacement may also be affected by the configuration of the wall panels. If the pile was behind a joint in the wall panels, the wall displacement increased. Also, wall panel rotation may have affected wall displacement. Each of the lines decreases with a similar shape toward the wall, and the wall displacement increases with increased pile spacing.

The ground was also pushed upward in front of the pile, as shown in **Figure 6.20**. This ground heave sometimes caused the stakes to which the string potentiometers were attached to rotate, resulting in more or less horizontal ground displacement. Vertical ground displacement is usually greatest directly in front of the pile, and decreases toward the wall.

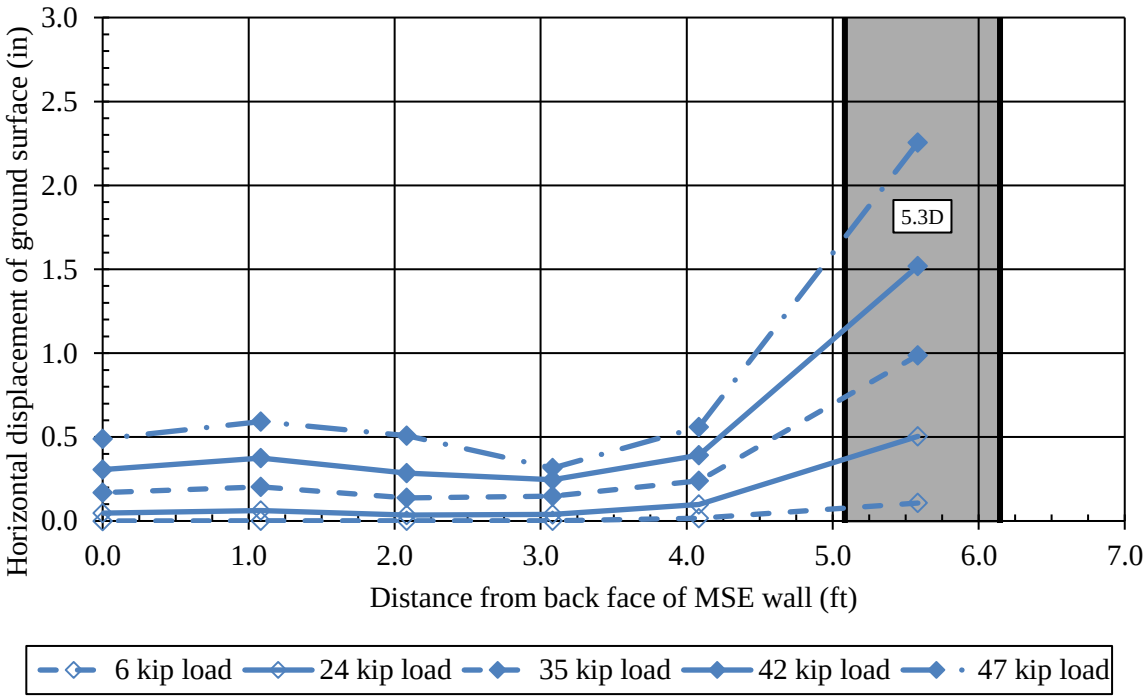

Figure 6.17 Increasing horizontal displacement of the ground surface with increasing pile head load for 5.3D test.

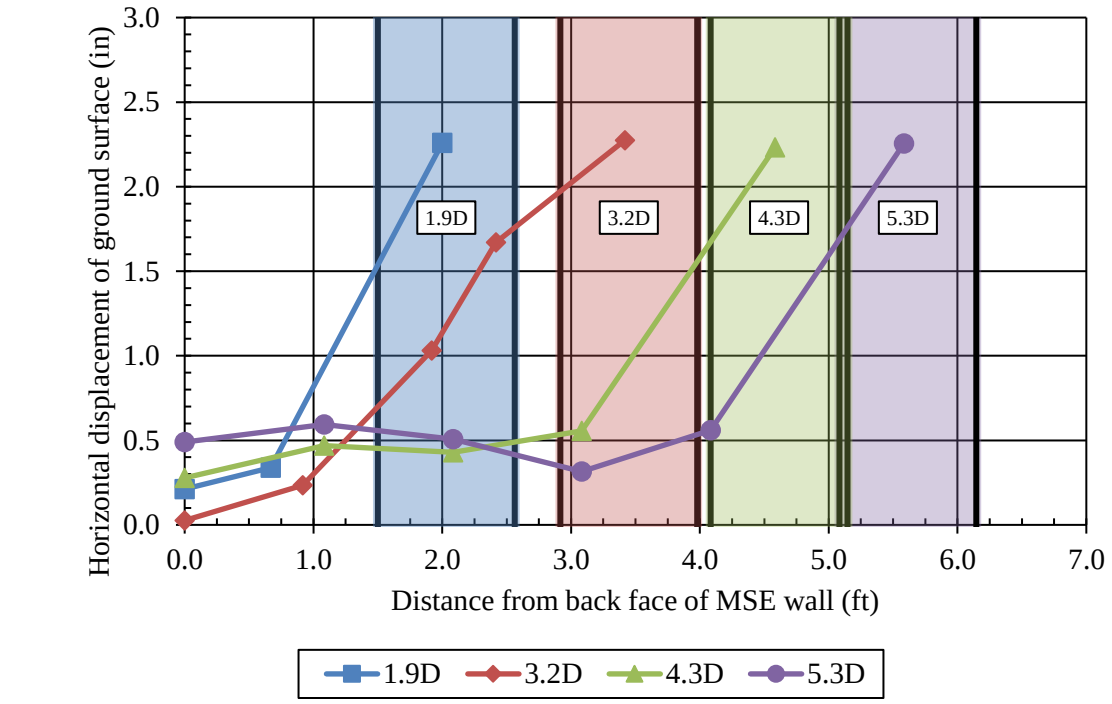

Figure 6.18 Horizontal ground displacement in front of each pile.

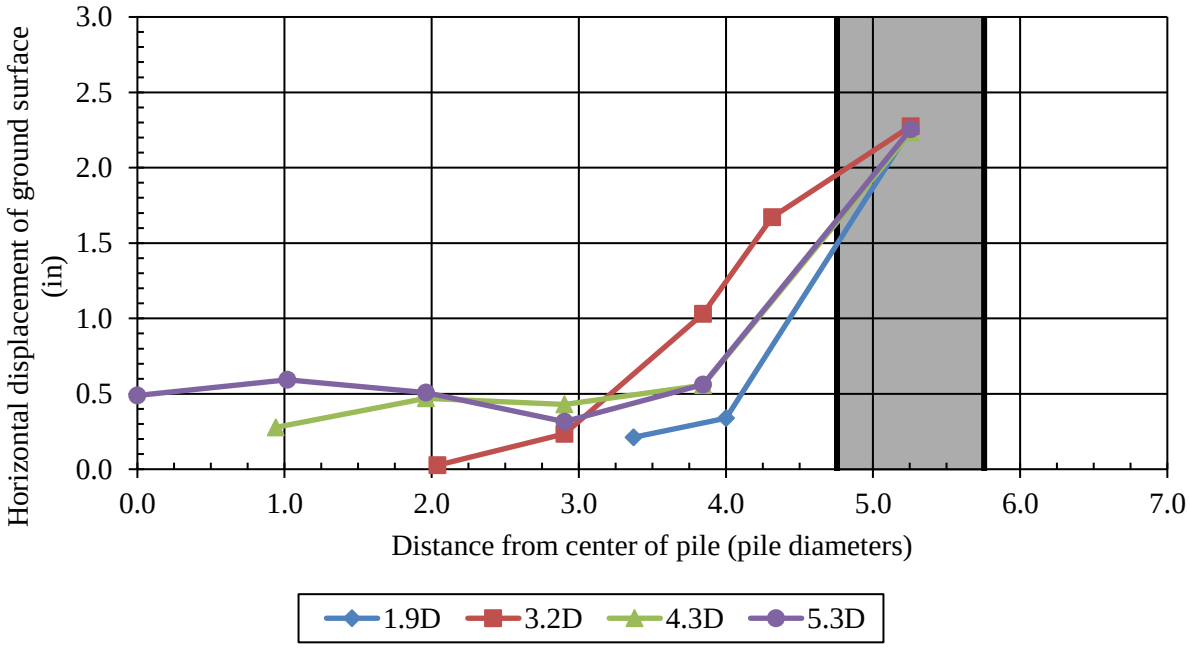

Figure 6.19 Horizontal ground displacement vs distance from center of pile in pile diameters.

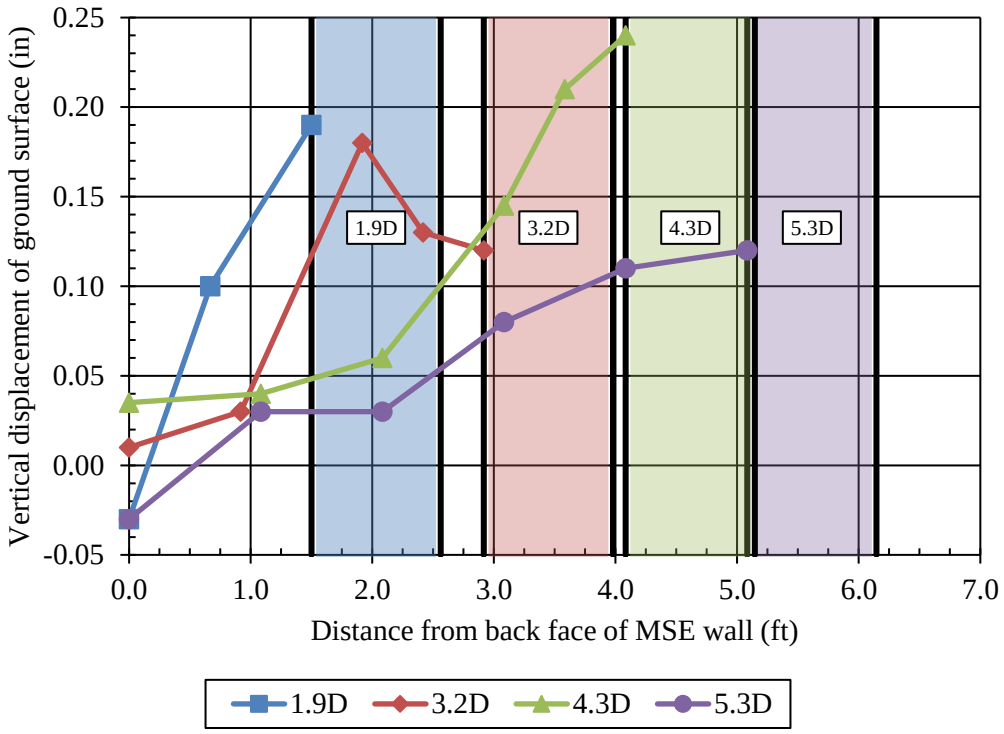

Figure 6.20 Vertical ground displacement in front of each pile.

Cracks usually developed in the soil during testing. A set of photos after each test is shown in **Figure 6.21**. In each photo, the angle iron indicates the direction to the wall face. Cracks in the ground are marked with orange curves. Cracks typically occurred to the sides of the piles and at 45 degree angles toward the wall.

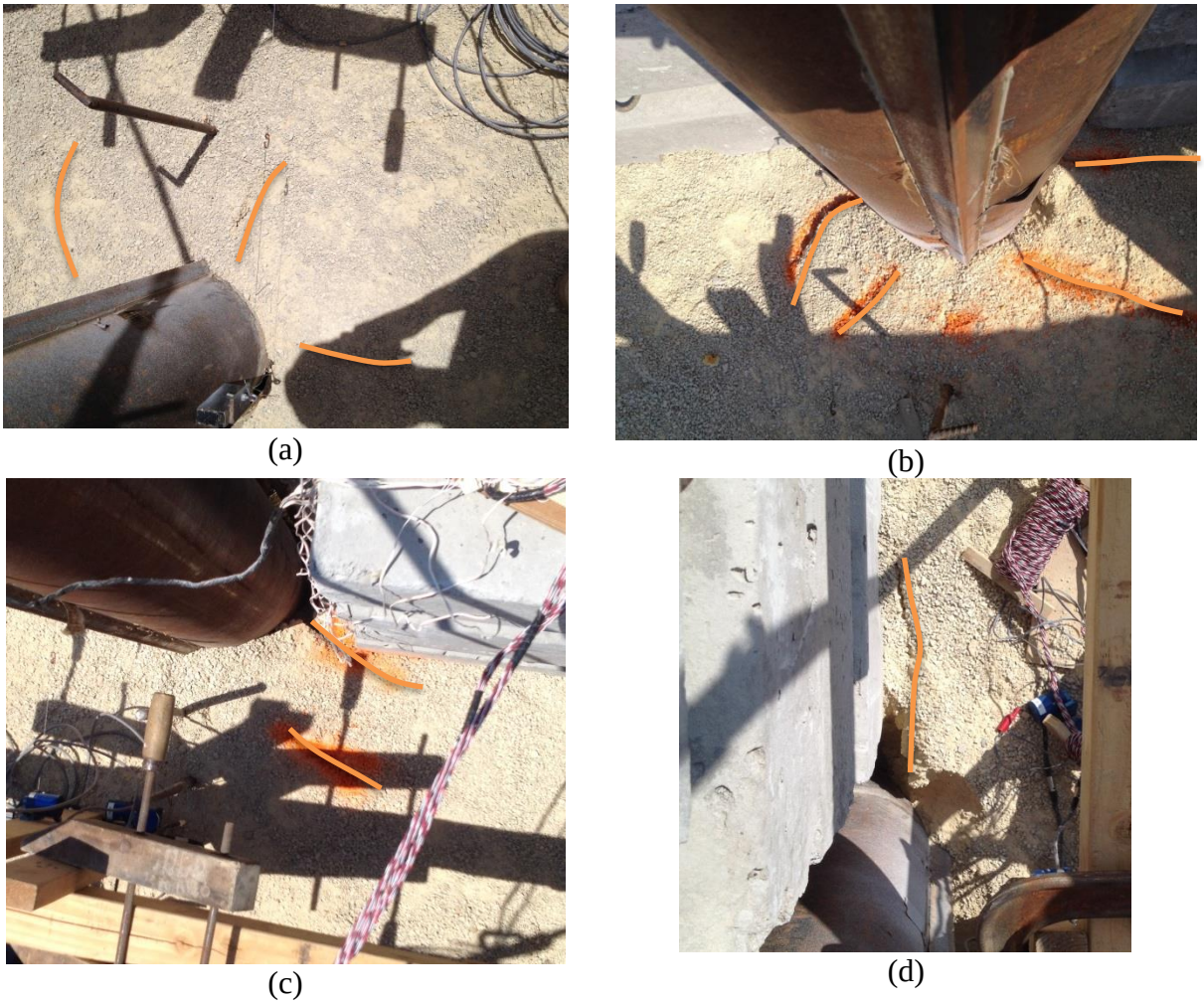

Figure 6.21 Cracks in the ground surface testing, (a) 5.3D (b) 4.3D (c) 3.2D (d) 1.9D.

6.5 Wall Panel Displacement

Wall panel displacement was measured with shape arrays and DIC. An example of a wall panel displacement profile from a shape array is shown in Figure 6.22. The wall generally displaces outward with increasing pile head deflection. A proposed position of each wall panel can be seen in the plot.

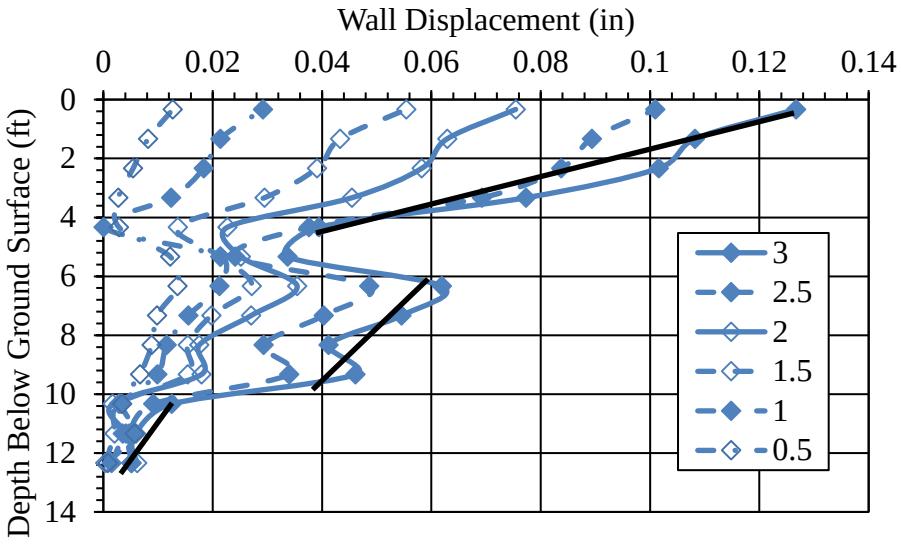

Figure 6.22 Wall panel displacement profile from a shape array for several pile head displacements, 4.3D test.

The shape array data was found to be difficult to deal with and somewhat inconsistent, due to issues with the measuring devices themselves. Because of this, shape array data was mostly used as a check for the measurements taken by the string potentiometers and DIC. A sample of a picture processed by the DIC system is shown in **Figure 6.23**. A series of pictures for each test is provided in Appendix H. The heat map shows the displacement of the wall panel over the entire area of interest. The maximum displacement at the top of the wall in the middle of the joint is about 0.46 inches, which is similar to what was measured by the string potentiometers, but does not agree with what was measured by the shape array. It is interesting that the displacement of the wall is focused at the joint between wall panels directly in front of the pile. Also, it seems that the wall displacement is limited to one wall panel on either side of the pile, and one to 1.5 wall panels down.

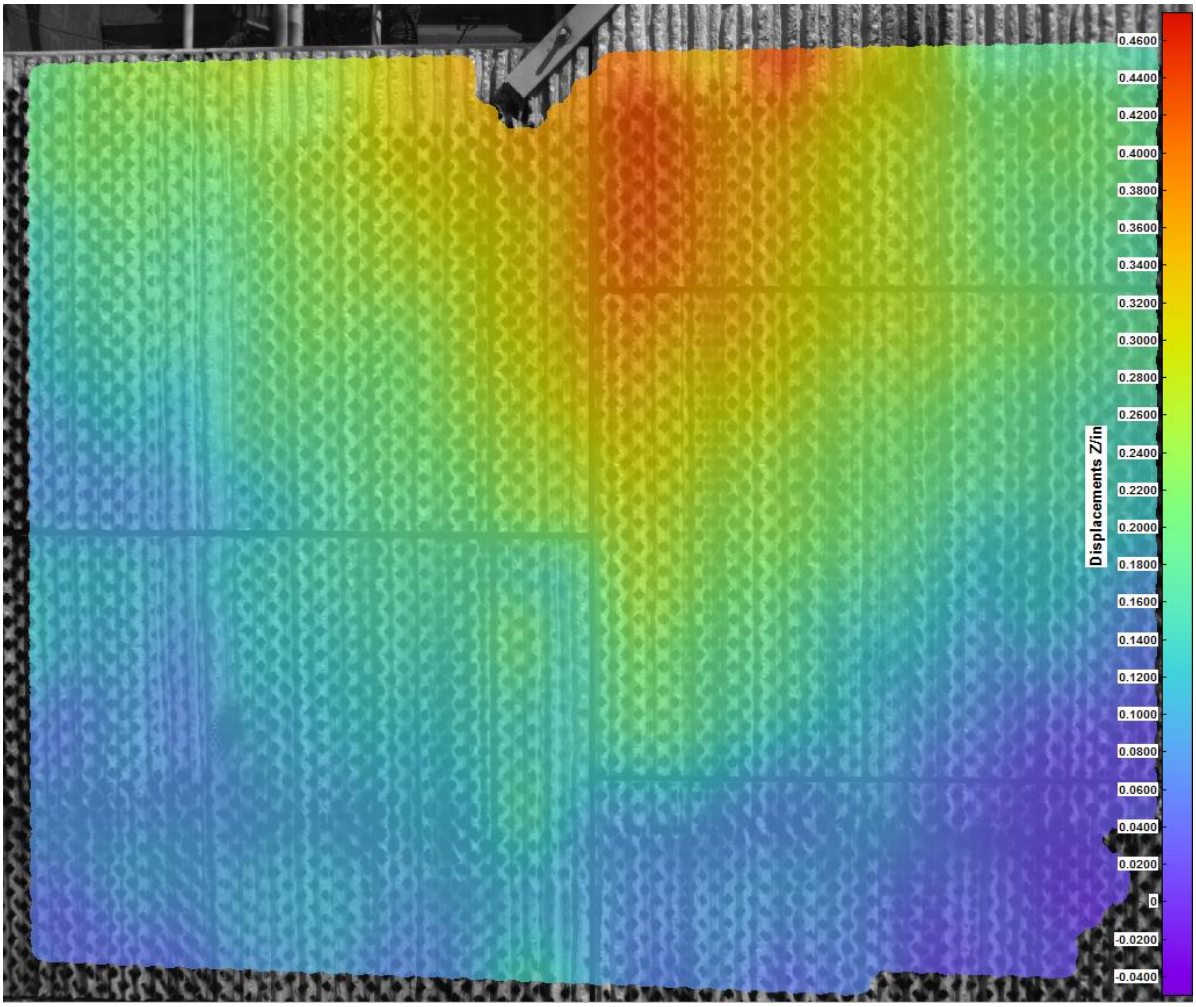

Figure 6.23 Sample processed photo of the wall from DIC, 3 inch pile head displacement, 4.3D test.

Using the DIC results, it was possible to find the deflection of the wall panel at the level of the grid reinforcement for each pile head load. The results for each test are shown in **Figure 6.24** through **Figure 6.27**. In these plots, it can be seen that the relationship between pile head load and grid deflection is mostly linear. As the pile gets closer to the wall, the deflection of the grid increases for the same loads. These results show that as the pile gets closer to the wall, the response of the system is softening.

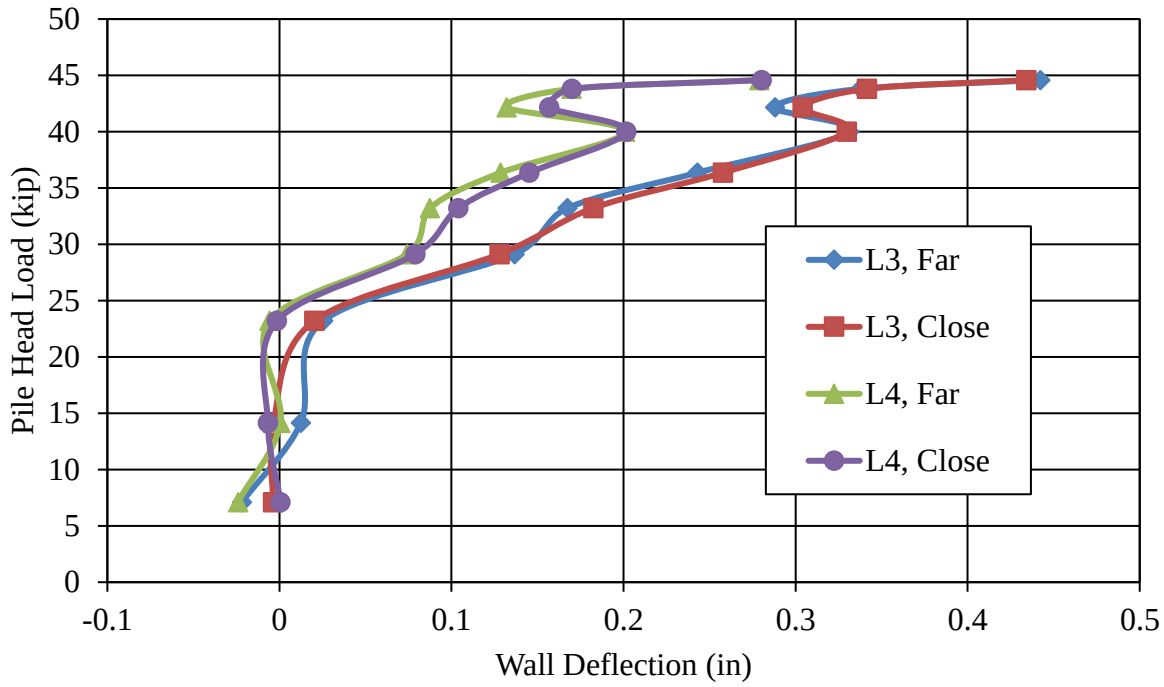

Figure 6.24 Grid deflection vs pile head load, 5.3D test.

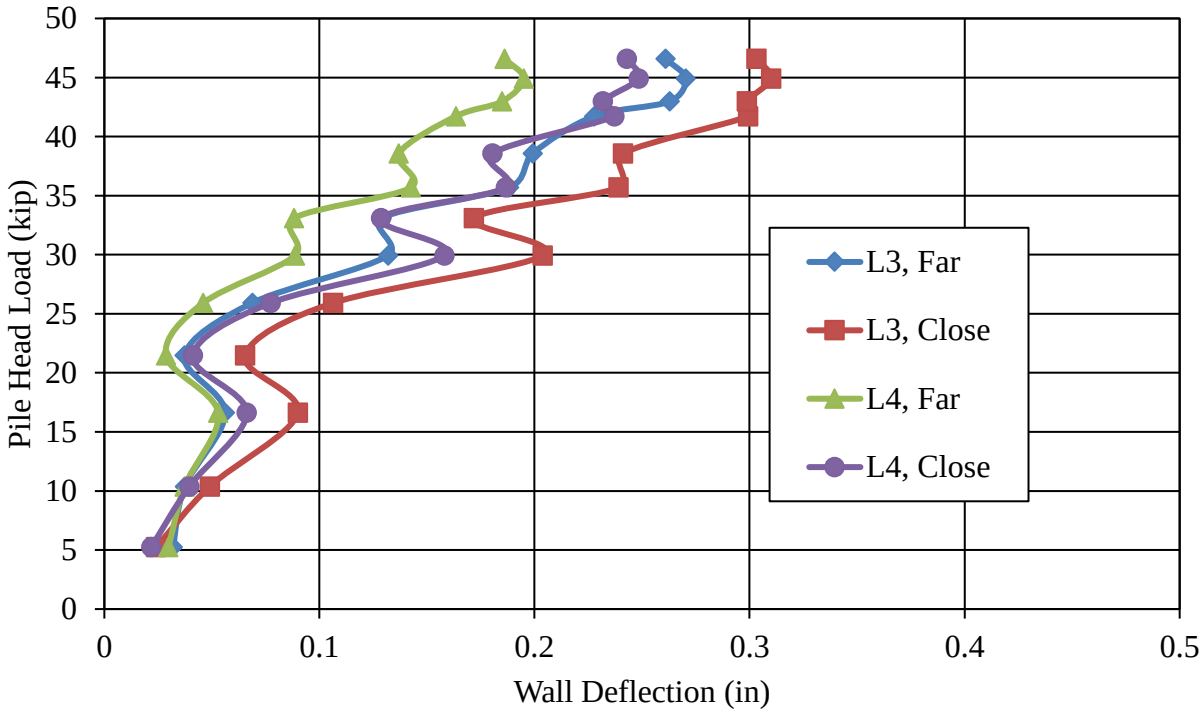

Figure 6.25 Grid deflection vs pile head load, 4.3D test.

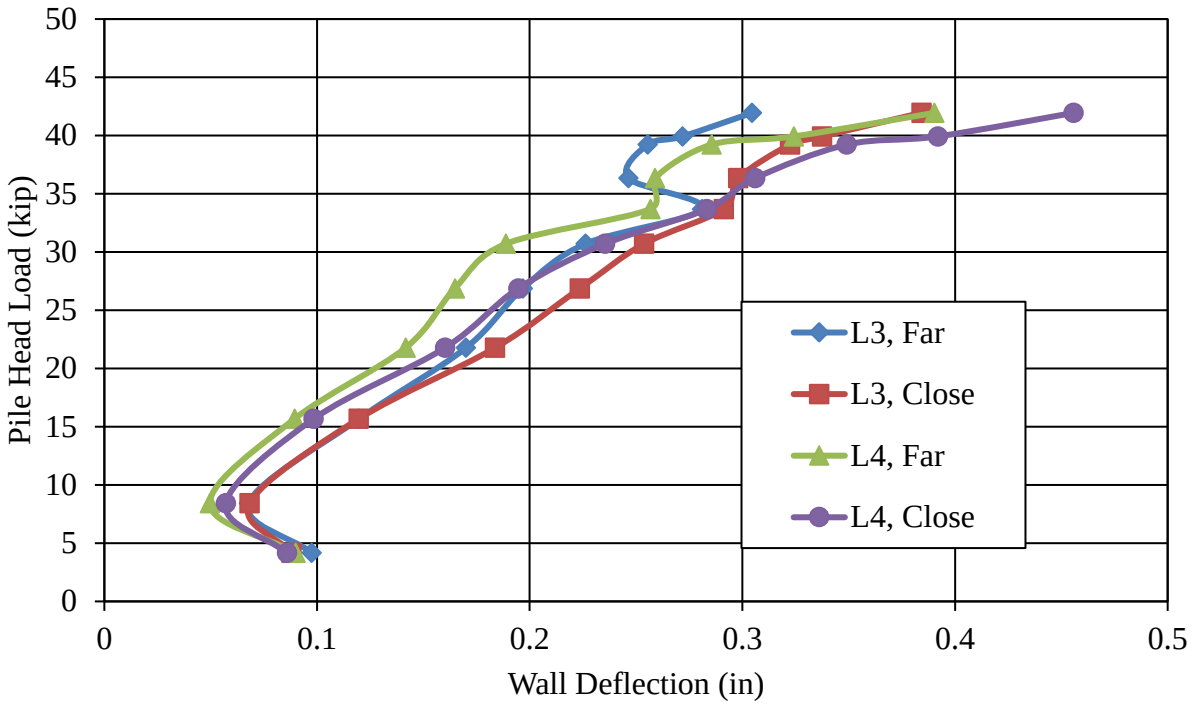

Figure 6.26 Grid deflection vs pile head load, 3.2D test.

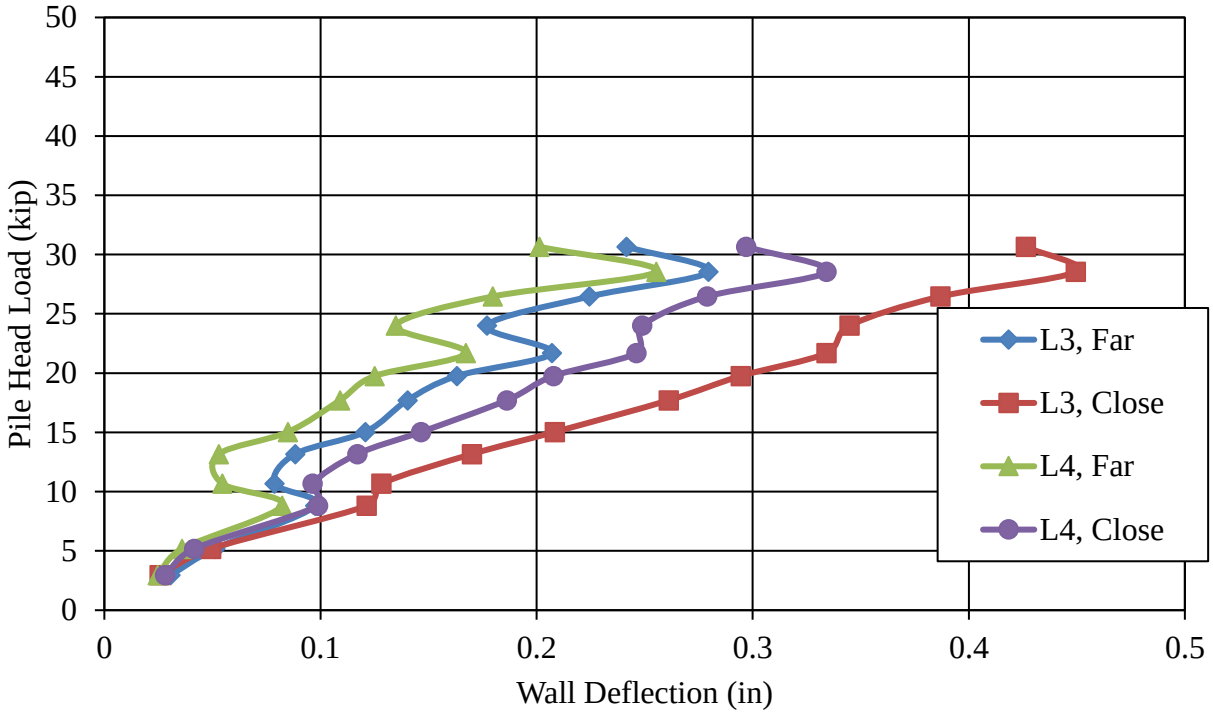

Figure 6.27 Grid deflection vs pile head load, 1.9D test.

6.6 Pile Performance

The bending moment in the pile is calculated from the strain gauge data using Equation 5-2. The values from paired strain gauges were averaged when both strain gauges were working. When only one strain gauge was working, only data from that gauge was used.

$$\boldsymbol{M_i = \frac{EI}{D_o}[(\mu\varepsilon_{ti} - \mu\varepsilon_{to}) - (\mu\varepsilon_{ci} - \mu\varepsilon_{co})](10^{-6})} \qquad (5\text{-}2)$$

where

M_i is the bending moment in inch-kips for the pile at the i^{th} data point,
E is the modulus of elasticity of steel (29000 ksi),
I is the moment of inertia of the pile in in^4,
$\mu\varepsilon_{ti}$ is the micro strain for the i^{th} data point on the tension (+) side of the pile,
$\mu\varepsilon_{to}$ is the micro strain for the initial data point on the tension side of the pile,
$\mu\varepsilon_{ci}$ is the micro strain for the i^{th} data point on the compression (-) side of the pile,
$\mu\varepsilon_{co}$ is the micro strain for the initial data point on the compression side of the (-) pile, and
D_o is the outside diameter of the pile in inches.

The bending moment in the pile increased with increasing pile head load. This trend is shown in **Figure 6.28**, where the bending moment in the pile for several pile head load levels is shown for the 5.3D test. The bending moment in the pile at a constant load level for each pile test is shown in **Figure 6.29**. In general, it can be observed that the maximum bending moment in the pile occurs deeper below the ground surface as the pile gets closer to the wall. One explanation of this is that there is less soil resistance to the load for closer piles.

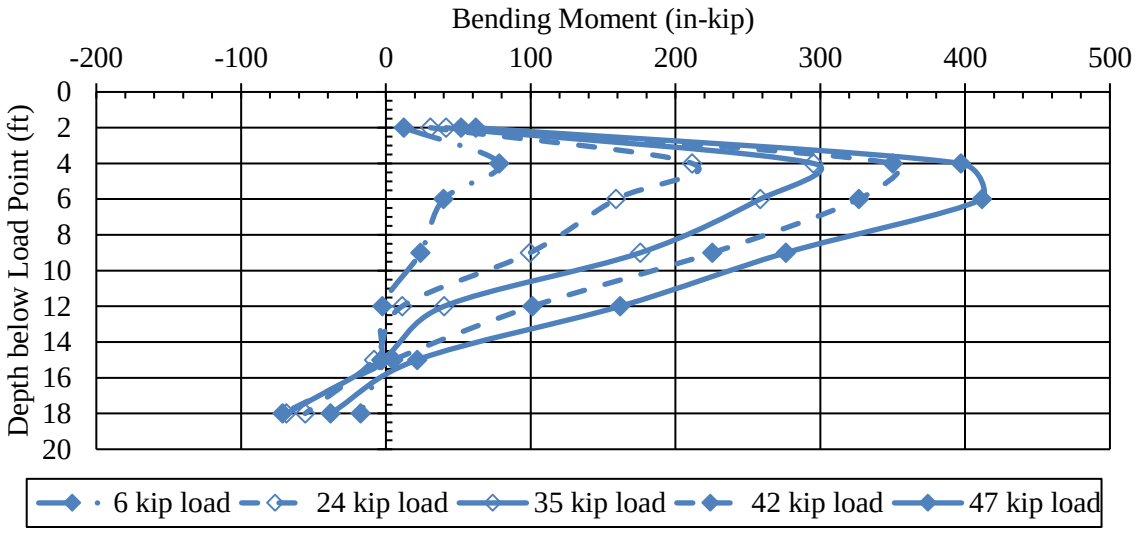

Figure 6.28 Bending moment vs depth for several pile head loads for the 5.3D test.

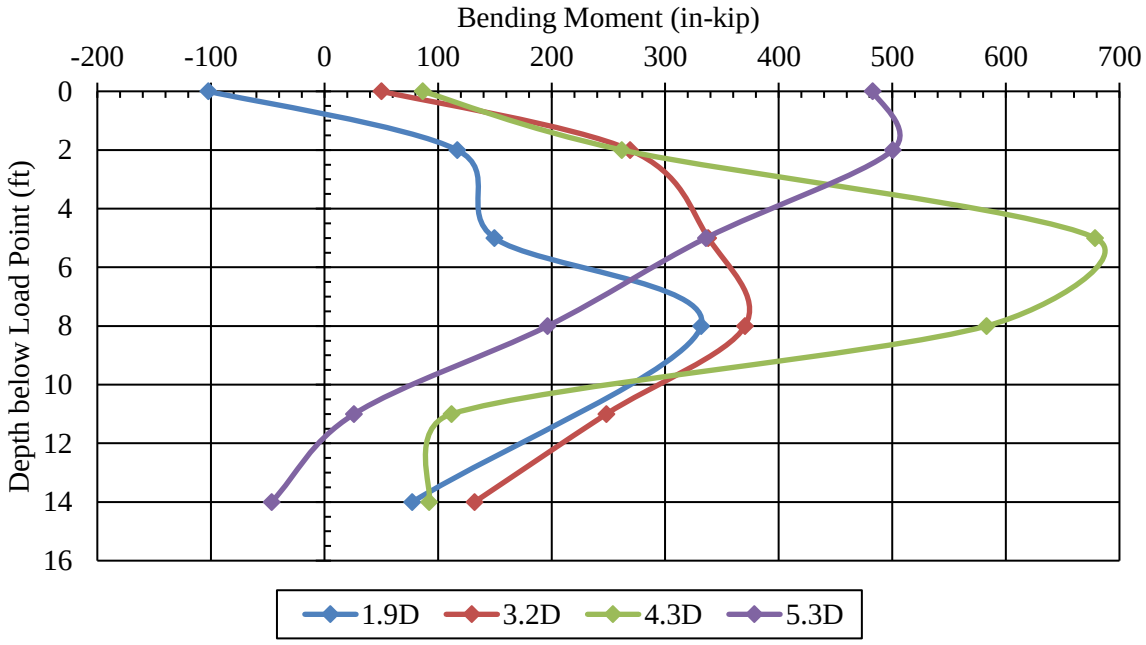

Figure 6.29 Bending moment vs depth for a displacement of 2.25 inches. test.

7 LATERAL PILE LOAD ANALYSIS

The lateral pile load analyses were performed using the computer program LPILE (Reese et al. 2004). LPILE uses a finite difference method in which a pile is modeled as a beam and the soil is modeled as a series of discrete non-linear p-y springs where p represents the horizontal soil resistance per length of pile and y is the horizontal displacement. The method uses an iterative approach to obtain compatible force and displacement along the length of the pile.

Considering that the yield strengths of the piles were reasonably high at 57 ksi, the non-yielding elastic section was selected for the LPILE section type to simplify the analysis. The inputs required include the modulus of elasticity of steel and the moment of inertia of the steel section.

Relatively few lateral load tests have been performed on piles in dense gravelly sands similar to the compacted fill behind the MSE walls (Macklin and Chou, 1988 and Smith et al. 2000). As a result, stiffness and strength parameters for laterally loaded piles in gravelly soils are not well defined in LPILE. Therefore, some back-calculations were required to obtain relevant soil parameters for analyses in LPILE. With the appropriate back-calculations, the p-y curve shape was able to be modeled within the framework of the API (1982) sand p-y curve. The moist unit weight was well known based on density testing but the friction angle (ϕ) and stiffness (k) values had to be refined based on back-calculation procedures. Figure 7.1 shows the curves used for the API method which was used as a reference to determine a reasonable ϕ and k value. While these two parameters both have effect on the entire computed load-displacement curve, the friction angle has the greatest effect at large displacements where the soil strength becomes fully developed. In contrast, the stiffness parameter has the greatest influence on the shape of the load-displacement curve at smaller displacements. Guided by this understanding, the load-displacement curves were

computed for each test pile with a curve fitting approach by modifying the friction angle and stiffness to find the best match to the test data plots for the one minute hold time.

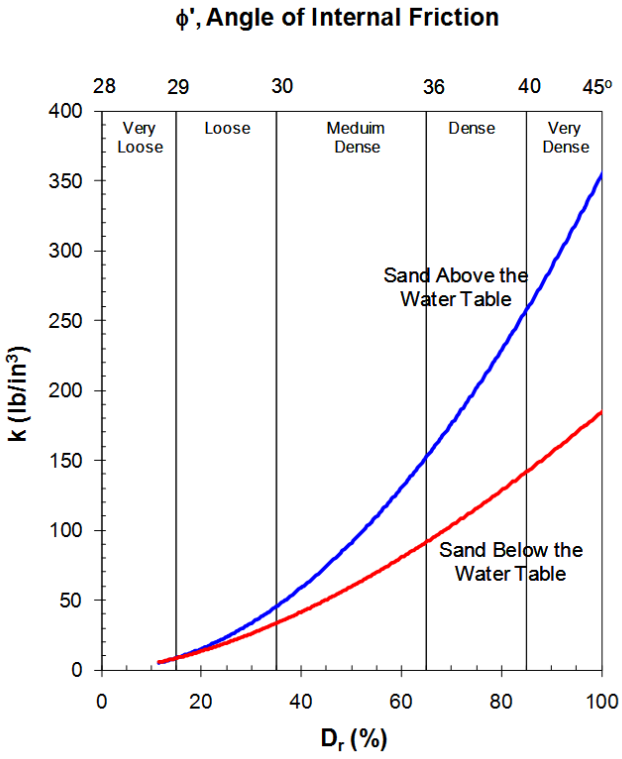

Figure 7.1: Modulus of subgrade reaction, k used for API sand criteria in p-y analysis (API 1982).

A pinned-head condition was used for the boundary condition for each LPILE analysis by applying a shear force to the top of the pile and setting the applied moment to zero. Loads were typically applied similar to the loads needed to push the pile at specific displacements during the tests.

The soil profile for the LPILE analysis consists of two generalized layers. The top layer of soil is the reinforced fill with a thickness equal to the wall height. The second layer is the underlying native soil extending to the end of the pile. Parametric analyses indicate that the properties of the deeper layers of the native soil had relatively little impact on the computed load-

deflection and bending moment-depth curves. Table 6.1 shows the pile properties input for the LPILE analysis. Table 6.2 shows the soil layering and properties used in the analysis including the friction angle (ϕ) and stiffness (k) values for the reinforced fill that provided the best agreement with the measured data.

Table 7.1: Pile properties for LPILE analysis at MSE wall reinforced with steel strips.

Pile Shape	Total length (ft)	Number of increments	Distance from pile top to top of ground surface (in)	Outside diameter (in)	Wall thickness (in)	Moment of inertia (in^4)	Area (in^2)	Modulus of elasticity (ksi)	Yield stress (psi)
Circular Pipe	35	200	12	12.75	0.375	314	13.6	29000	Elastic

Table 7.2: Soil properties for LPILE analysis at MSE wall reinforced with steel strips.

Depth (ft)	Description	Soil type (p-y model)	Eff. Unit weight (pcf)	Friction angle (deg)	p-y modulus, k (pci)
1 - 16	Reinforced Fill	API Sand (O'Neil)	129	39	225
16 - 35	Underlying native soil	API Sand (O'Neil)	125	34	100

.

7.1 Load Displacement Curves

The back-calculated friction angle of 39º and stiffness of 225 lb/in^3 used in the analysis appear to be reasonable for dense compacted gravel as shown in Figure 7.1. The computed load deflection curve from the LPILE analysis is shown in Figure 7.2.

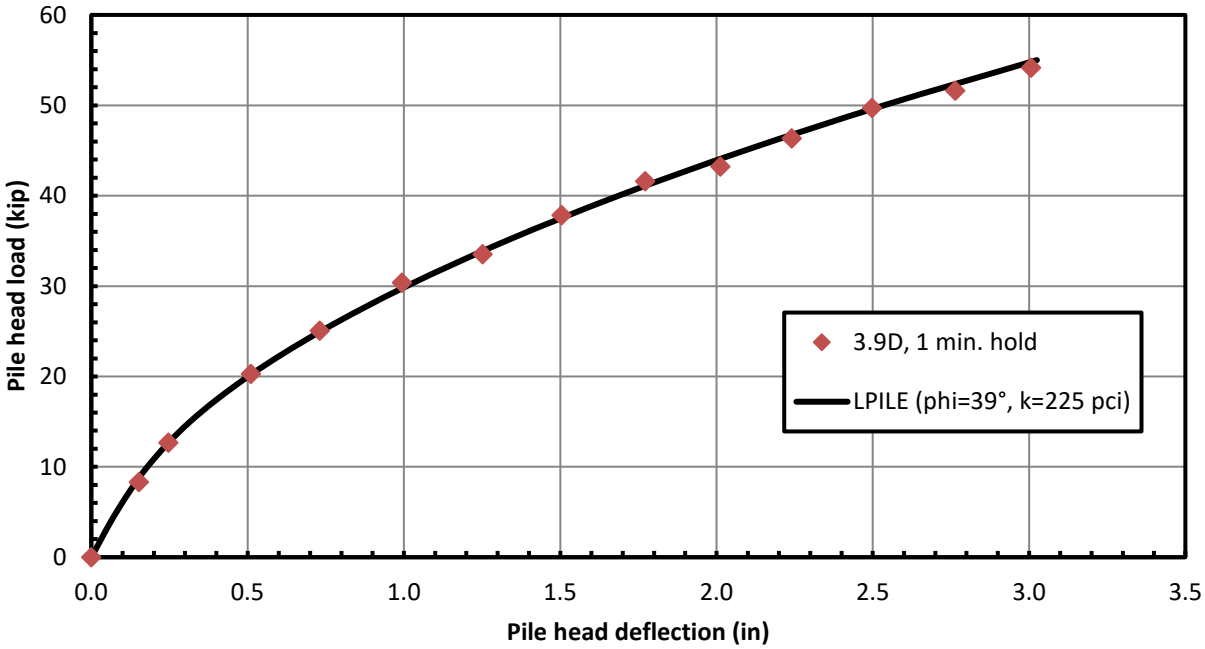

Figure 7.2: Comparison of computed and measured load-displacement curves for pile 3.9D

Using the same soil model developed for the pile furthest from the wall (3.9D), p-multipliers were obtained by back-analysis to match the measured load-deflection curves for the piles at closer spacing. These p-multipliers were used to simulate the reduction in soil strength as piles are placed closer to the wall. Back calculated p-multipliers to account for the reduced soil capacity of piles 3.1D (3.1 pile diameters behind wall), 2.8D (2.8 pile diameters behind the wall) and 1.7D (1.7 pile diameters behind wall) were 0.95, 0.7 and 0.33, respectively. The computed pile head load versus displacement curves using these p-multipliers are shown in Figure 7.3 relative to the measured curves. A summary of the p-multipliers used to match the load-deflection curves is shown in Table 7.3.

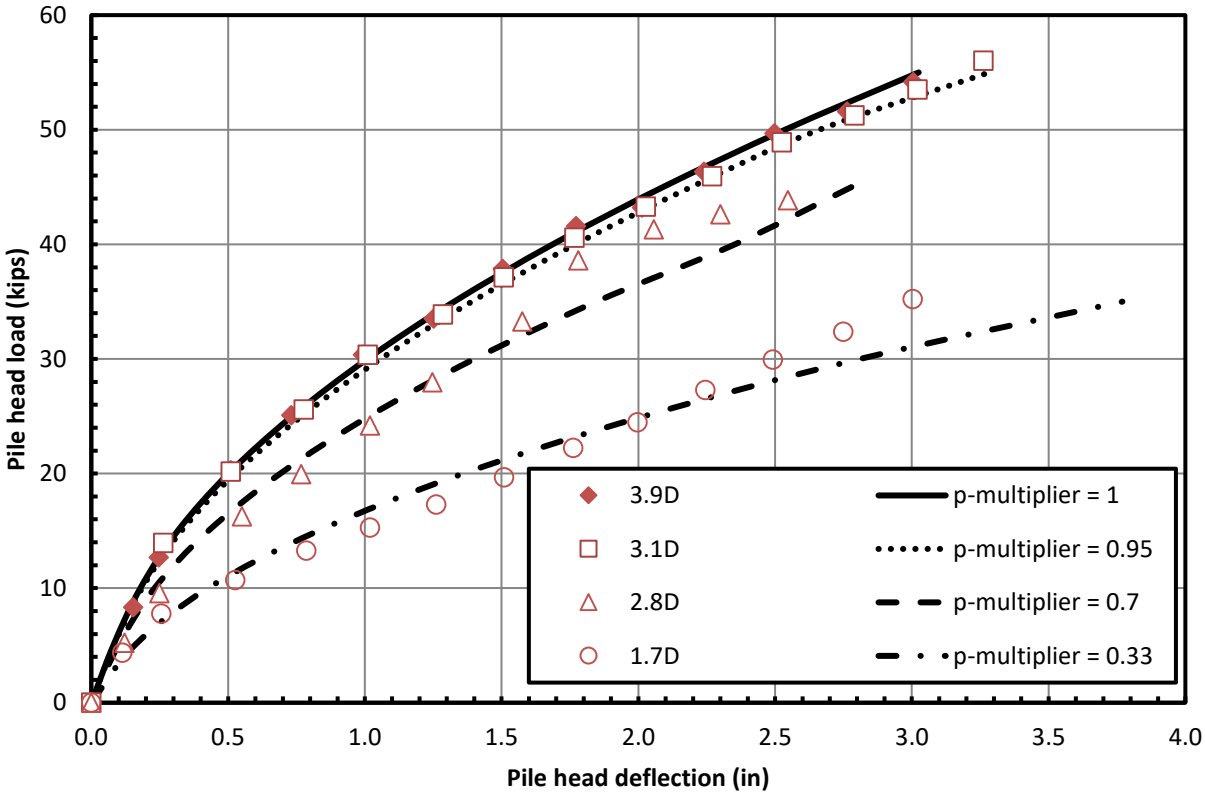

Figure 7.3: Comparison of computed and measured load-displacement curves for piles with ribbed strip reinforcements

Table 7.3: P-multipliers for pipe piles reinforced with ribbed steel strips.

Pile	P-multiplier
3.9D	1.0
3.1D	0.95
2.8D	0.70
1.7D	0.33

The measured load-deflection curves match the computed curves reasonably well using the back calculated p-multipliers especially at smaller pile deflections. The measured pile head load is

visibly larger than the computed pile head load at higher deflection for piles at 2.8D and 1.7D, suggesting that the soil still provides reasonable stiffness than expected when the piles are placed closer to the wall.

7.2 Bending Moment Curves for piles with ribbed strip reinforcements

The computed bending moment versus depth curves based on ϕ=39º and k=225pci for the different p-multiplier analyses is plotted with the measured bending moment versus depth curves for the maximum applied lateral load in Figures 7.4 to 7.7. As seen in the bending moment curves, there is good agreement on the shape and values of the computed and measured bending moment curves. The value of the maximum measured bending moment is within 20 percent of the maximum computed bending moment while the depth of the maximum measured bending moment is located within two feet of the computed bending moment.

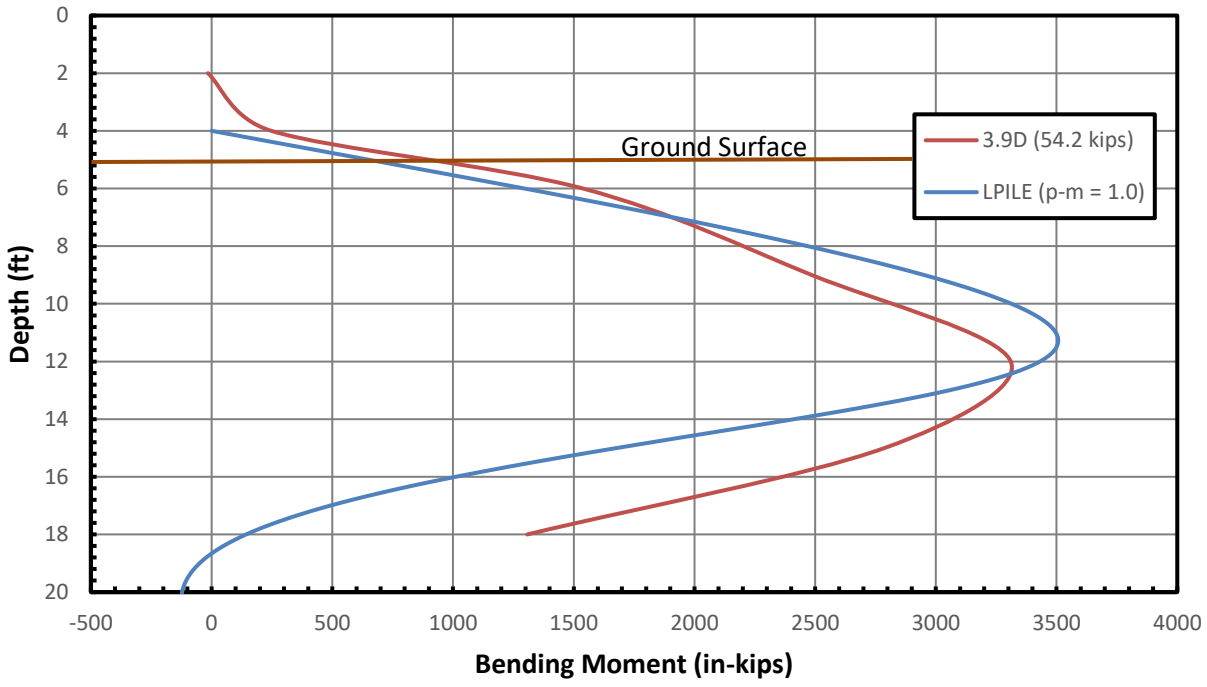

Figure 7.4: Comparison of measured and computed bending moment for pile at 3.9D with a 54.2 kip load.

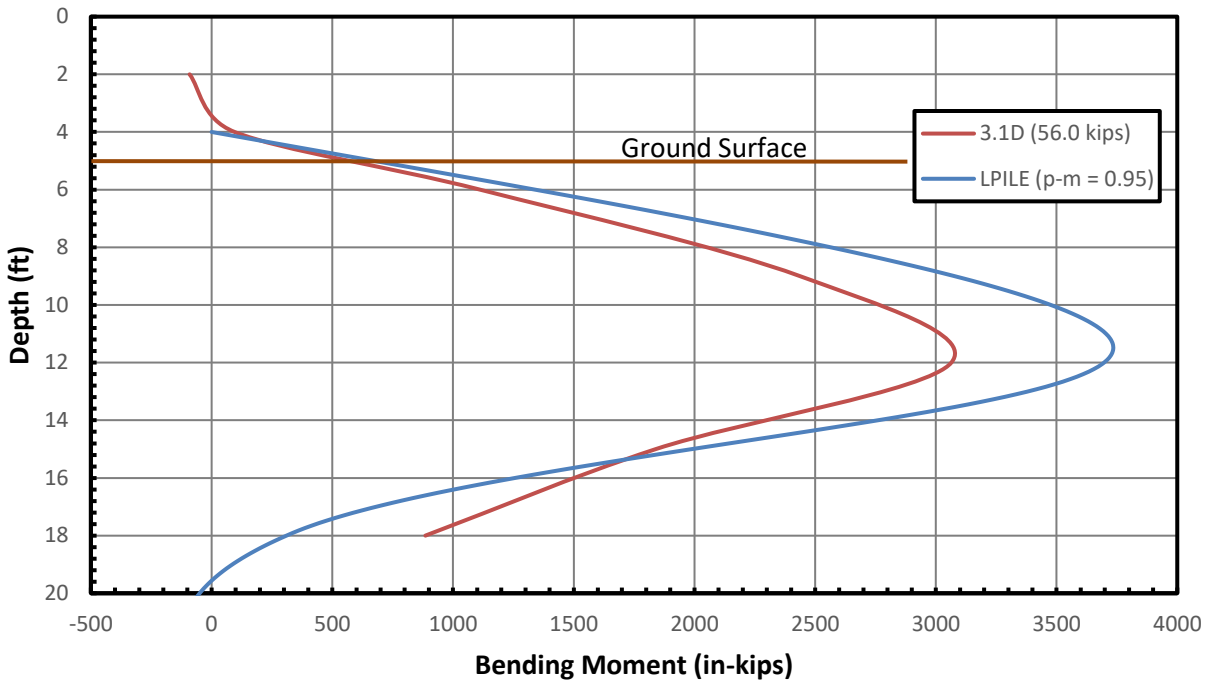

Figure 7.5: Comparison of measured and computed bending moment for pile at 3.1D with a 56.0 kip load.

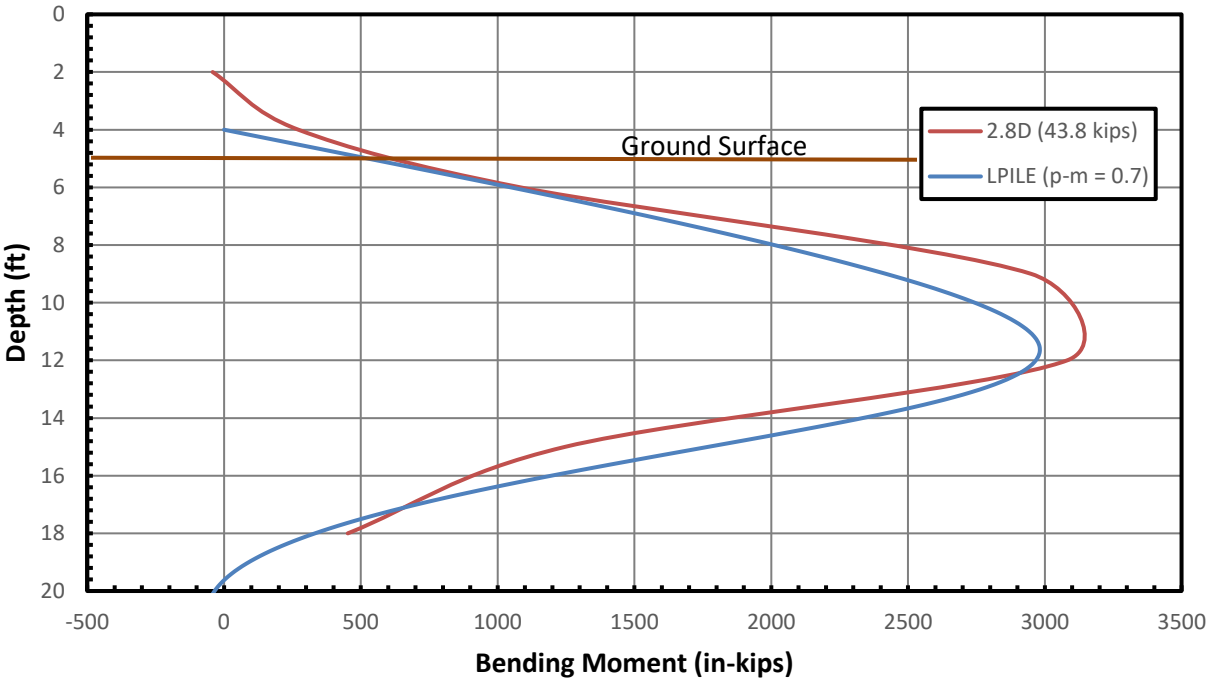

Figure 7.6: Comparison of measured and computed bending moment for pile at 2.8D with a 43.8 kip load.

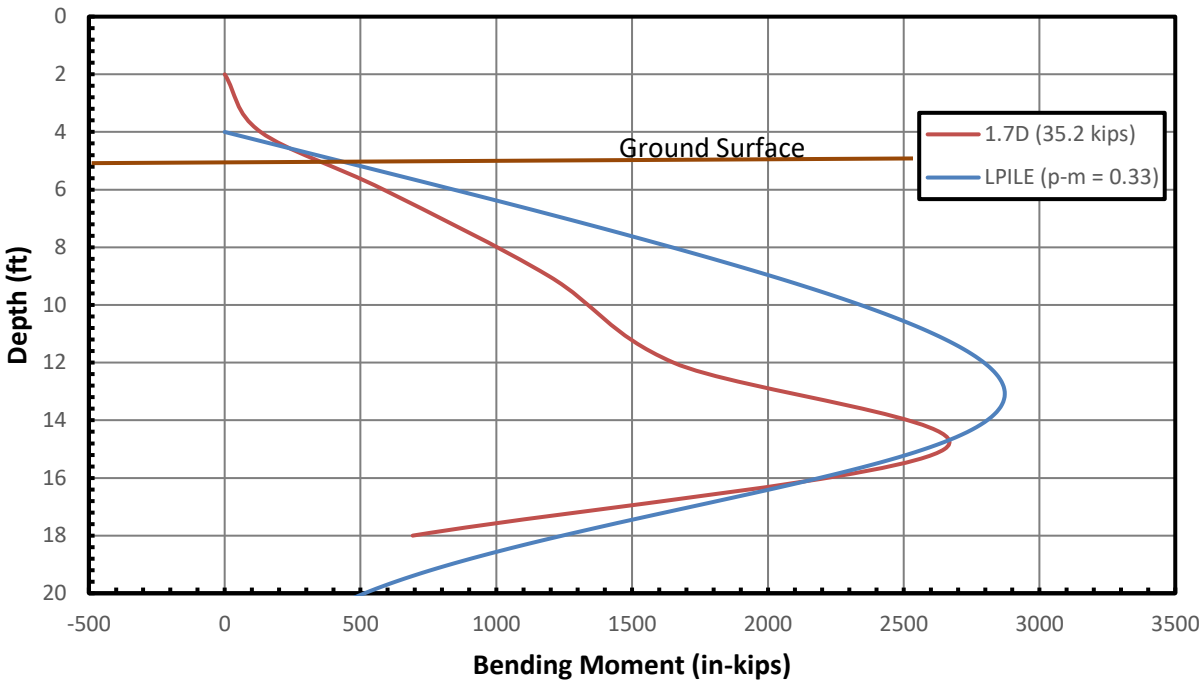

Figure 7.7: Comparison of measured and computed bending moment for pile at 1.7D with a 35.2 kip load.

7.3 P-Multiplier Analysis for piles in soil reinforced with ribbed steel strips

The results from the lateral load analyses discussed in Section 6.1 are summarized in Figure 7.8. This figure plots the p-multiplier versus the normalized distance from the wall, taken as the distance from the back face of the wall to the center of the pile (S) divided by the diameter of the pile (D). One of the curves is labeled "RECo Pipe (L/H = 0.90)" consisting of the four test piles (1.7D, 2.8D, 3.1D and 3.9D). The label L/H refers to the ratio of the length of the reinforcement to the height of the MSE wall at the time of testing. A p-multiplier of 1 indicates that there is no influence of the wall on the lateral resistance of the pile whereas a p-multiplier less than 1 indicates that the presence of the wall is causing a reduction in the lateral resistance provided by the reinforced soil. This curve is plotted in comparison to another curve labeled as "Nelson (2013)" consisting of three tests on the three Provo Center Street test pile with steel strip reinforcements

previously done by Nelson (2013) and a curve labeled as "Price (2012)" consisting of five tests previously done by Price (2012).

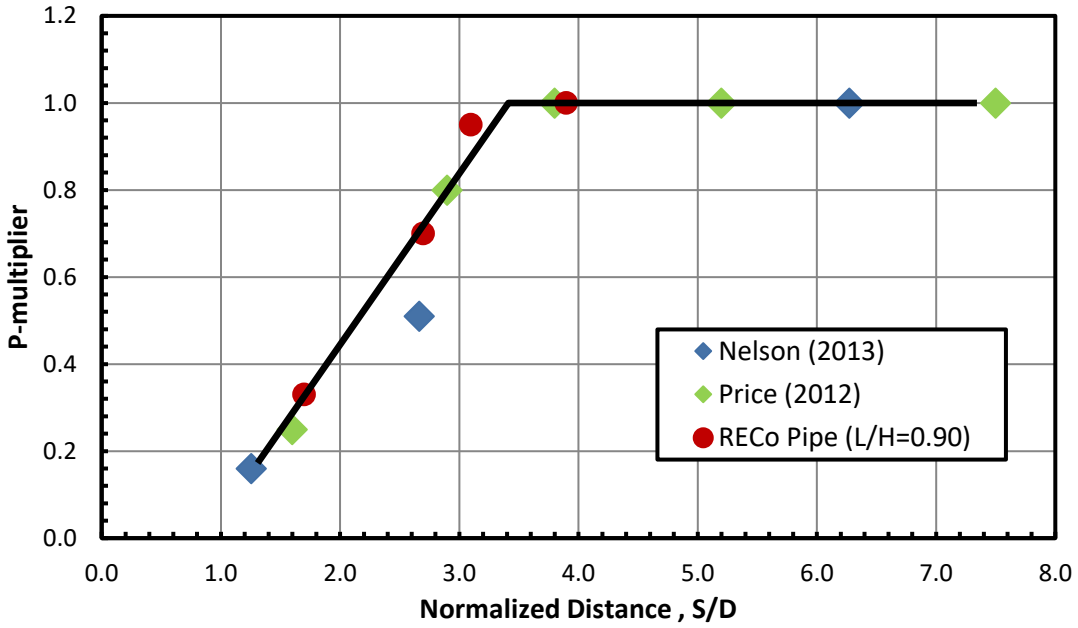

Figure 7.8: P-multiplier curves.

The original curves from Price (2012) and Nelson (2013) have reinforcement length to wall height (L/H) ratio between 1.1 and 1.6 but these ratios did not include the height of the surcharge present at the test locations. By including the height of the surcharge, the ratios fall between 1.05 and 1.2 and are comparable to data from this study which has an L/H ratio of 0.9 after adding 5 ft. of surcharge height to the test wall height of 15 ft.

A regression line was developed for the data with p-multiplier less than 1 and is shown in Equation 7-1 for piles with ribbed strip reinforcements. The results from these tests are in good agreement with results from Price (2012) and Nelson (2013) showing that as a pile is placed closer to the back face of the wall the lateral resistance is reduced.

$$P_m = 0.36S/D - 0.33 \qquad (7\text{-}1)$$

Where P_m is the p-multiplier, and S/D is the spacing, S, from the center of the pile to the back of the MSE wall divided by the pile diameter, D.

7.4 Results of LPILE Analysis on piles in soil reinforced with welded wire grid

The LPILE model was first calibrated by matching the load-deflection curve to the test data for the 5.3D pile. This assumed that the load-deflection curve for this pile was not affected by proximity to the wall, as discussed above. Given the experience from previous full-scale tests, this assumption appears to be reasonable. The reduction in resistance for pile located 5.3D behind the wall relative to the reaction pile is likely a result of compaction differences. S/D is the distance of the pile behind the back face of the wall in pile diameters.

Table 7.4 shows the soil properties for the two layer profile used in the analyses. The friction angle and soil stiffness shown are the values back-calculated in LPILE that produce the best agreement with the test data. The back calculated friction angle and subgrade modulus for the reinforced fill is reasonable for dense sand, but is higher than that used for the pile in the sand reinforced with the ribbed steel strips.

Table 7.4 Soil Profile Properties used in LPILE Analysis

Depth (ft)	Description	Soil Type (p-y model)	Effective Unit Weight, σ' (psf)	Friction Angle, ϕ (degrees)	p-y Modulus, k (pci)
1 to 14	Reinforced Fill	API Sand (O'Neill)	129	43	300
14 to 40	Natural Soil	API Sand (O'Neill)	125	34	100

For piles closer to the wall, the soil resistance was reduced by using a constant p-multiplier to match the computed load-deflection curve to the measured curve. The p-multipliers used to match these load-deflection curves are shown in **Table 7.5**. The computed load-

deflection curves for each of the three piles are shown in **Figure 7.9**, along with the load-deflection curves from the test data for comparison.

Table 7.5 P-multipliers for circular pipe piles in sand reinforced with welded wire grid.

Pile	P-multiplier
5.3D	1.0
4.3D	0.57
3.2D	0.57
1.9D	0.20

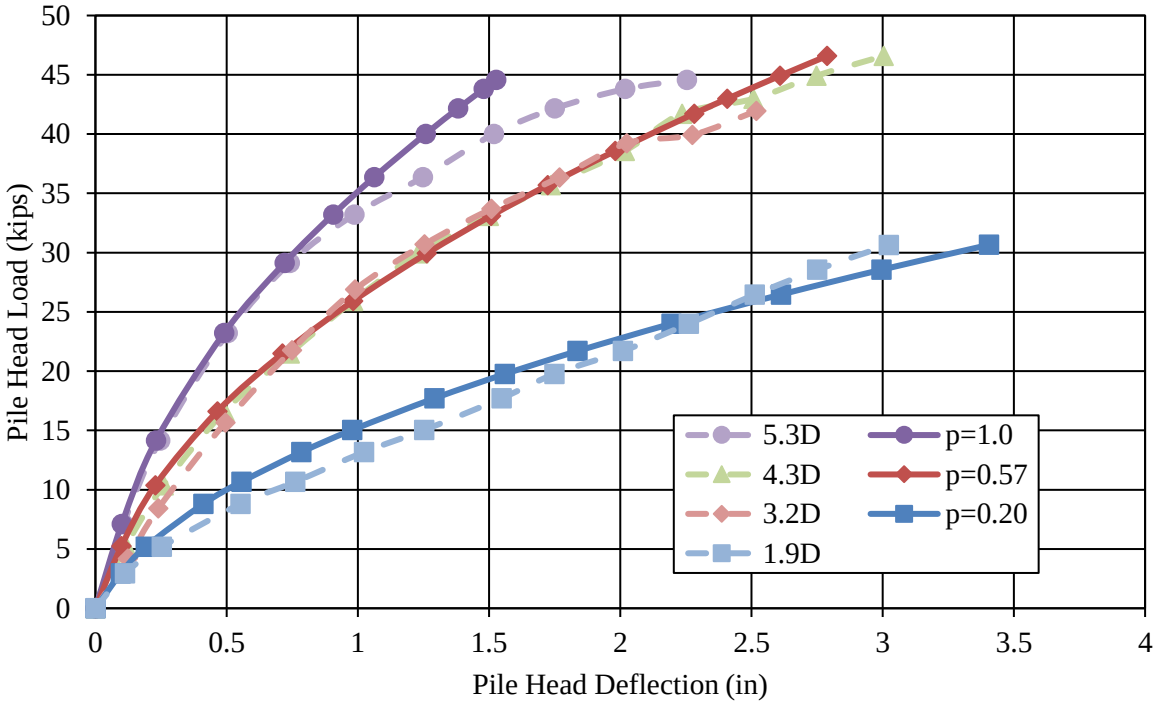

Figure 7.9 Computed pile head load vs deflection, with load deflection curves for comparison.

Although the agreement is relatively good, it should be noted that the computed curves do not exactly match the test data. Every effort was made to produce a well-calibrated model in LPILE, however, the curves seem to be shaped somewhat differently, leading to differences between the curves within certain deflection ranges. The differences are most obvious at the beginning and end of the curves. There is good agreement through the middle part of the curves,

indicating that inconsistencies may have occurred at the beginning and ending of each test, while overall the test data is reasonable. Or, perhaps, the model used in LPILE does not adequately reflect what is happening at large displacement where yielding could be occurring at larger loads.

The computed bending moment vs depth curves for each of the LPILE models are shown in **Figure 7.10** through **Figure 7.13**, along with the bending moment vs depth curves from the test data. The shape of the curves are similar, however, the computed curves are much larger than the measured curves, generally about seven times larger. It was found through subsequent investigation that the strain gauges had been installed with the incorrect surface attached to the pile. Testing in the lab showed that the correction factor for these gauges was between 3 and 5. Therefore, the following plots show the bending moment measured by the strain gauges, corrected by the indicated factor, and computed in LPILE. This comparison shows that the corrected values of bending moment come much closer to those predicted by LPILE.

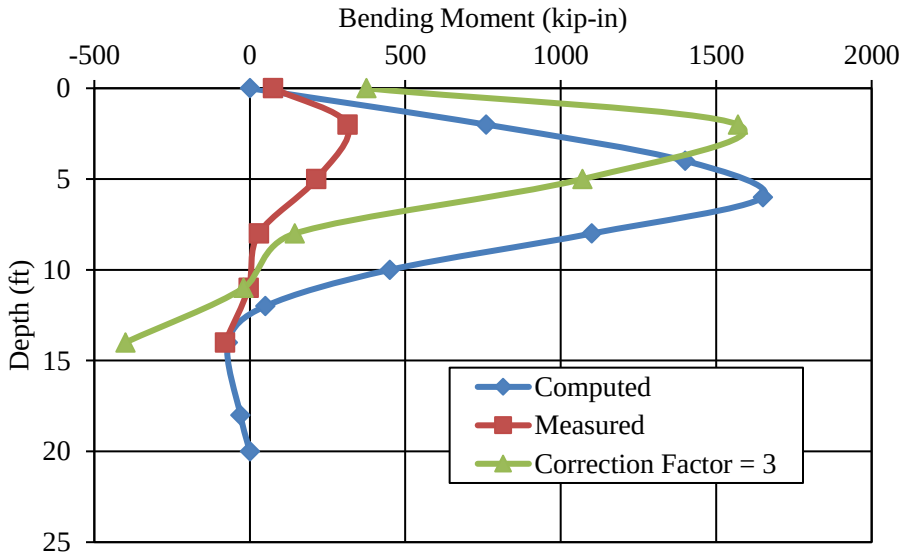

Figure 7.10 Bending moment vs depth for 5.3D pile, 35 kip pile head load, computed, measured and corrected.

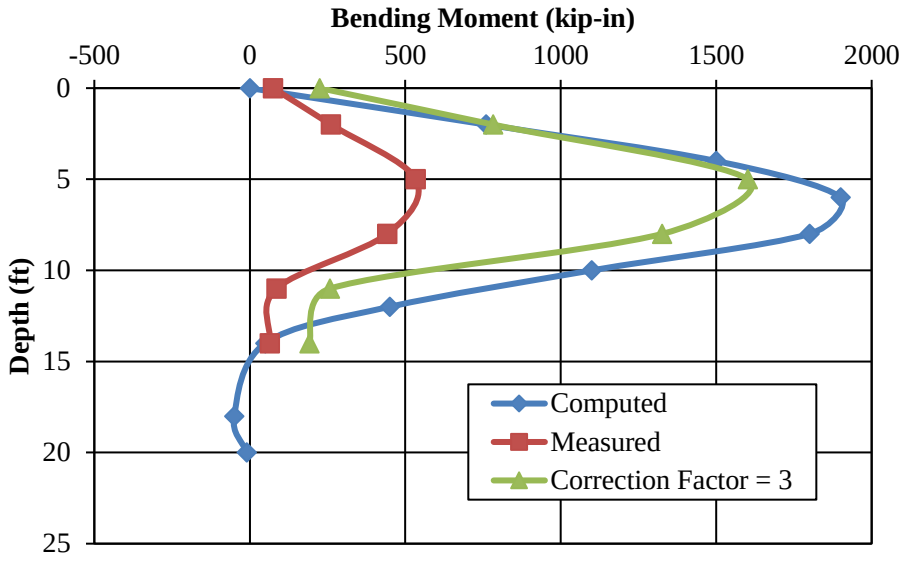

Figure 7.11 Bending moment vs depth for 4.3D pile, 36 kip pile head load, computed, measured and corrected.

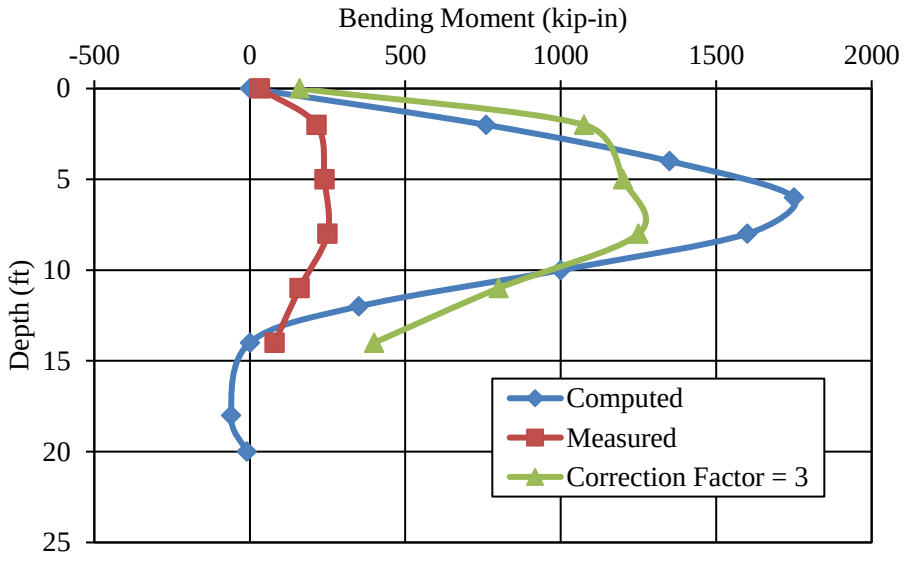

Figure 7.12 Bending moment vs depth for 3.2D pile, 33 kip pile head load, computed, measured and corrected.

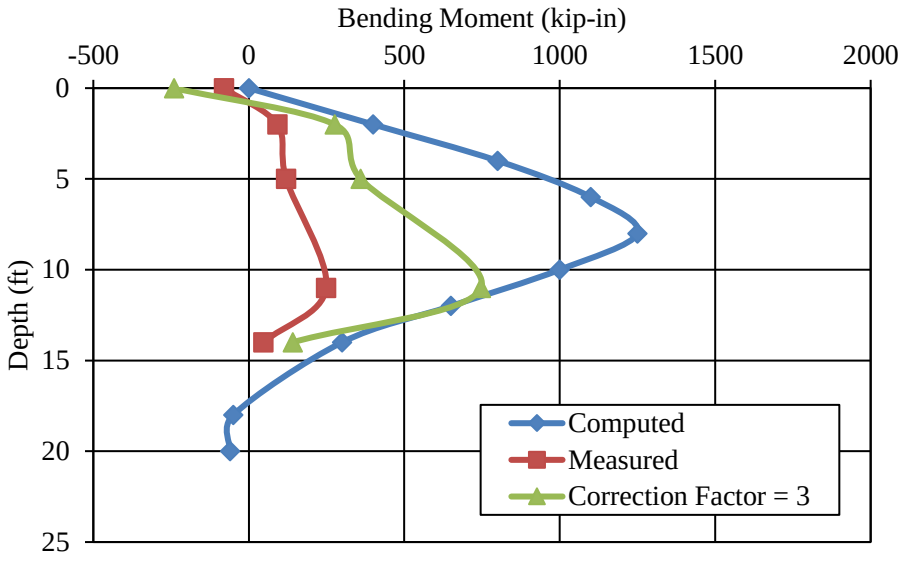

Figure 7.13 Bending moment vs depth for 1.9D pile, 20 kip pile head load, computed, measured and corrected.

7.5 P-Multiplier vs Pile Spacing Curves for Piles in Sand with Welded Wire Grid

The back-calculated p-multipliers for each pile load were plotted against the normalized spacing in each case as shown in **Figure 7.14**. The normalized spacing is the distance from the center of the pile to the back face of the wall divided by the pile diameter. **Figure 7.14** also includes data from Price (2012) and Nelson (2013), who produced similar curves. A p-multiplier of 1.0 indicates that there is no influence of the wall on the load-deflection curve, while a p-multiplier less than 1.0 indicates that the presence of the wall reduces the lateral resistance of the pile.

The original curves found in Price (2012) and Nelson (2013) show trends for length of reinforcement to wall height (L/H) ratios for 1.1 and 1.6. However, these ratios did not take into account the surcharge that was present at each test location. Taking this into account, the L/H ratio was found in each case to be between 1.05 and 1.2, and so the differences were neglected

and the points were plotted on the same line. In this study, the L/H ratio for the series of tests was found to be 0.9, including the surcharge. This ratio is obtained by dividing the reinforcing length of 18 ft by the effective wall height. In these tests, the effective wall height is 15 ft plus the surcharge of 600 psf divided by the unit weight of the backfill material (129 pcf) which yields a value of 19.7 ft.

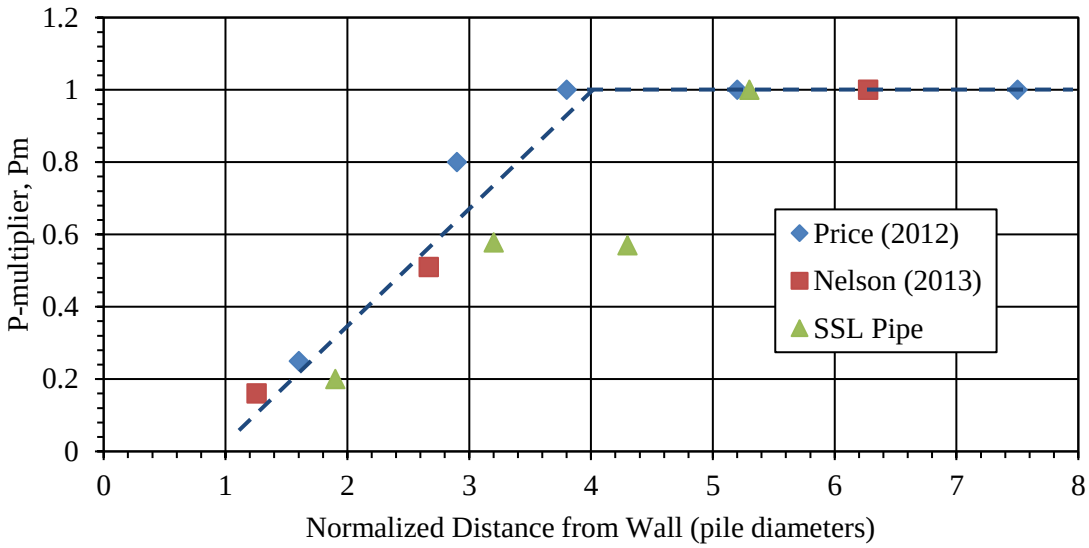

Figure 7.14 P-multiplier curves vs. normalized spacing for welded wire reinforcement.

The lower part of the curve shown in **Figure 7.14** is from regression analysis of the data with p-multipliers less than 1. The data point corresponding to the 4.3D test was treated as an outlier and was not included in the regression analysis. The equation for the regression line is shown in Equation 7-2.

$$P_m = 0.32(S/D) - 0.304 \qquad (7\text{-}2)$$

where P_m is the p-multiplier, and S/D is the distance of the pile behind the back face of the wall, in pile diameters.

The SSL pipe data is from this study and agrees with the data from Price (2012) and Nelson (2013). Overall, as a pile is placed closer to the back face of the wall, the lateral resistance is reduced.

7.6 P-Multiplier vs Pile Spacing Curves for Piles in Sand with Welded Wire Grid

The back calculated p-multipliers from the eight lateral pile load tests conducted with the MSE wall at 15 ft are plotted together with the results from tests conducted by Price (2012) and Nelson (2013) in **Figure 7.15**. In general, the agreement between the results from this study and previous studies is relatively good, especially considering the variations in reinforcement type, reinforcement length to height ratios and backfill types and densities represented by the various tests. The variation of the p-multiplier, P_m , as a function of normalized spacing (S/D) based on all the test data is given by the equation

$$P_m = 0.34(S/D) - 0.28 \quad \text{for (S/D)} < 3.8 \tag{7-3a}$$

$$P_m = 1.0 \quad \text{for (S/D)} > 3.8 \tag{7-3b}$$

As noted previously, these results indicate that the lateral pile resistance of piles with diameters less than about 16 inches is unaffected by the presence of the wall (P_m = 1.0) when they placed more the 3.8 pile diameters from back of the wall. For piles spaced closer than 3.8 pile diameters from the wall, the lateral resistance of the soil near the pile decreases approximately linearly as the spacing decreases.

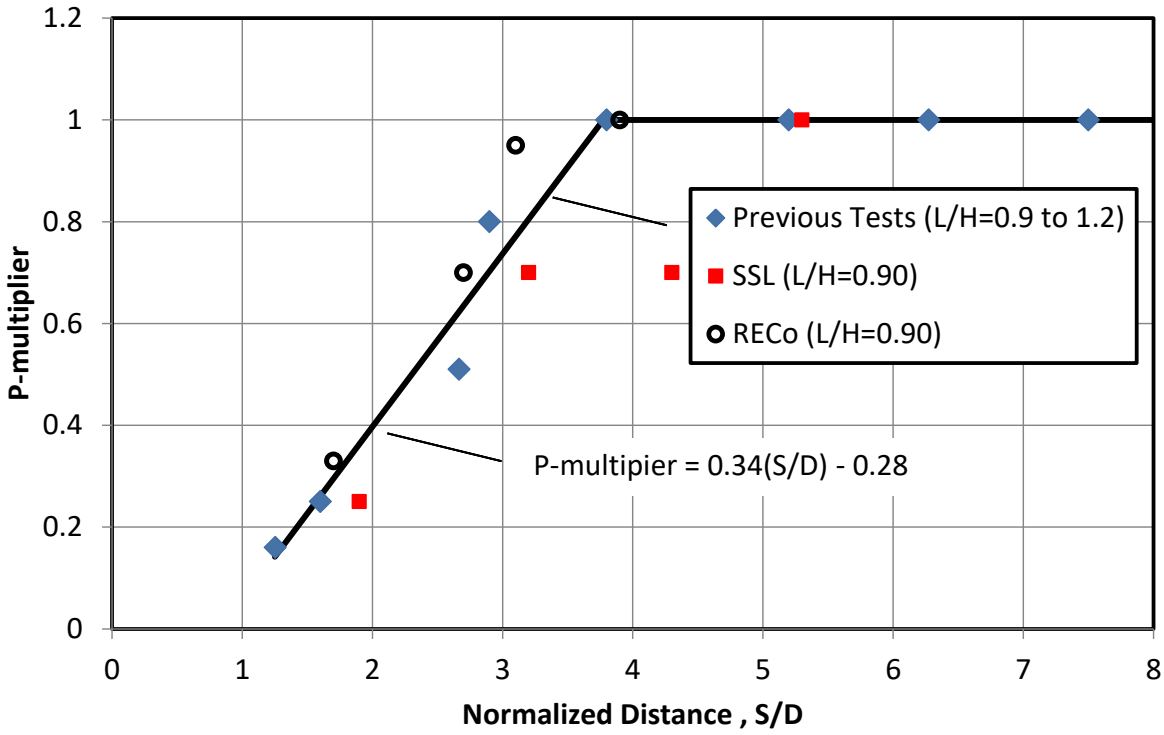

Figure 7.15 P-multiplier curves normalized by factor of safety against pullout for the top two layers of reinforcement.

8 PRELIMINARY CONCLUSIONS

1. The results from two series of lateral pile load tests near the 15-ft high MSE wall face indicate that the lateral pile resistance decreases as the distance behind the MSE wall decreases. These results are in agreement with previous full-scale tests.
2. The decrease in lateral pile resistance can be successfully modeled using a p-multiplier concept to reduce the lateral soil resistance as the pile spacing behind the wall decreases.
3. A curve has been developed to define the relationship between p-multipliers and the normalized spacing (S/D) of the pile behind the back face of the MSE wall. The curve includes data from this study and from previous studies performed by Price (2012) and Nelson (2013). The curve suggests that when a pile is placed at a distance greater than about four pile diameters (D) behind the back face of the wall, the lateral resistance of the pile is not affected by the presence of the wall and therefore a p-multiplier of 1 can be used for the pile. When a pile is placed less than four pile diameters behind the back face of the wall, the lateral soil resistance on the pile is reduced linearly as shown in Figure 7.15.
4. Although there is clearly scatter in the data points about the best-fit p-multiplier curve, the results suggest that the curve is not strongly influenced by the difference in reinforcement type (ribbed strips vs. welded wire grid) or the reinforcement length to height ratio (0.9 to 1.2) for the pile diameters tested (12 to 16 inch).
5. The induced tensile force in the reinforcement:
    - increases as the lateral load on the pile increases,
    - generally decreases as the transverse spacing from the pile increases, and

- is generally higher for the second layer of reinforcement than for the top layer.

6. The induced force in the reinforcement typically increases along the length of the reinforcement from the back face of the wall to the center of the pile, and then decreases from the center of the pile to the end of the reinforcement. This load distribution develops because the soil between the pile and the wall is moving towards the wall relative to the reinforcement and induces load in the reinforcement through skin friction. Behind the pile, the reinforcement is moving toward the wall relative to the soil and load is transferred from the reinforcement to the surrounding soil through skin friction.
7. Because the tensile force in the reinforcement is influenced by a number of factors, a multiple linear regression model will need to be developed to predict the induced tensile force resulting from lateral pile loading. Results from these tests will be combined with results from additional tests with different wall heights prior to performing these regression analyses.

REFERENCES

American Petroleum Institute (API) (1982). "API recommended practice for planning, designing and constructing fixed offshore platforms" API RP 2A, 13th Edition.

Berg, R.R., Christopher, B.R., and Samtani, N.C. (2009). "Design of Mechanically Stabilized Earth Walls and Reinforced Soil Slopes" FHWA, Washington, D.C., Report No. FHWA-NHI-10-024, 306 p.

Dunker, K. F., and Liu, D. (2007). "Foundation for Integral Abutments" *Practice Periodical on Structural Design and Construction,* 12(1), 22-30.

Elias, V., and Christopher, B.R. (1997). "Mechanically Stabilized Earth Walls and Reinforced Soil Slopes, Design and Construction Guidelines" FHWA, Washington, D.C., Report No. FHWA-SA-96-071, 371 p.

Khodair, Y. A., and Hassiotis, S. (2005). "Analysis of Soil-Pile Interaction in Integral Abutment" *Computers and Geotechnics,* 32, 201-209.

Kim, W., and Laman, J. A. (2010). "Integral Abutment Bridge Response Under Thermal Loading" Engineering Structures 32, 1495-1508.

Koseki, J. (2012). "Use of Geosynthetics to Improve Seismic Performance of Earth Structures" *Geotextiles and Geomembranes,* 34, 51-68.

Lawson, W.D., Jayawickrama, P.W., Wood, T.A., and Surles, J.G. (2012). "Pullout Resistance Factors for Inextensible MSE Reinforcements Embedded in Sandy Backfill" Paper 13-2684, *Transportation Research Record, Journal of the Transportation Research Board,* Washington DC.

Macklin, P.R. and Chou, N.N.S. (1988). "A lateral load test on seven-foot diameter caissons" Procs. Symposium on Lateral Load Capacity of Caissons and Piles, Denver Colorado. p. 330-338.

Maruri, R. F., and Pedro, S. H. (2005). "Integral Abutment and jointless bridges (IAJB) 2004 survey summary." Proc., 2005 FHWA *Conf. on Integral-Abutment and Jointless Bridges,* Federal Highway Administration, Washington, D.C., 12-29, <http://www.cemr.wvu.edu/cfc/conference/Proceeding.pdf>.

Nelson, K.R. (2013). "Lateral Resistance of Piles Near Vertical MSE Abutment Walls at Provo Center Street" MS Thesis, Department of Civil and Environmental Engineering, Brigham Young University, Provo, UT.

Pierson, M., Parsons, R.L., Han, J., Brown, D.A. and Thompson, W.R. (2009). "Capacity of Laterally Loaded Shafts Constructed Behind the Face of a Mechanically Stabilized Earth Block Wall" Kansas Department of Transportation, K-TRAN: KU-07-6.

Pierson, M. (2007). "Behavior of Laterally Loaded Shafts Constructed Behind the Face of a Mechanically Stabilized Earth Block Wall" MS Thesis, Civil Engineering, University of Kansa, Kansas City, KS.

Price, J.S. (2012). "Lateral Resistance of Piles Near Vertical MSE Abutment Walls" MS Thesis, Department of Civil and Environmental Engineering, Brigham Young University, Provo, UT.

Reese, L.C., Wang, S.T., Isenhower, W.M., and Arrellaga, J.A. (2004). "LPILE Plus v5.0 for Windows: A program for the analysis of piles and drilled shafts under lateral loads" Technical Manual, Ensoft, Inc., Austin, TX.

Rollins, K.M., Price, J.S., and Nelson, K.R. (2013). "Lateral Resistance of Piles Near Vertical MSE Abutment Walls" Utah Department of Transportation, Report No. UT-13.04.

Smith, T.D.; Park, R., Hannan, R. (2000). "Lateral load prediction and testing of 3.05 m dia. shafts" Geotechnical Special Publication, n 94, ASCE, p 184-197.

APPENDIX A. FACTOR OF SAFETY AGAINST PULLOUT CALCULATIONS

Curve definitions for steel grids

Depth below top of wall, Z (ft)	K_r/K_a	
0	1.7	20
20	1.2	10

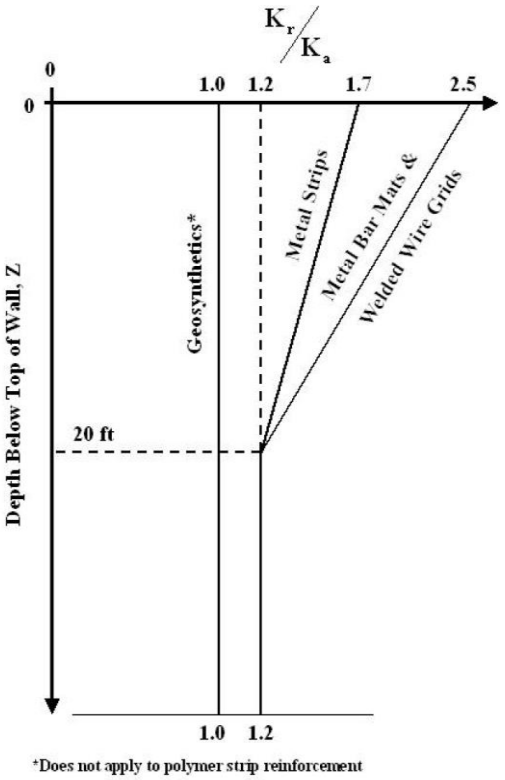

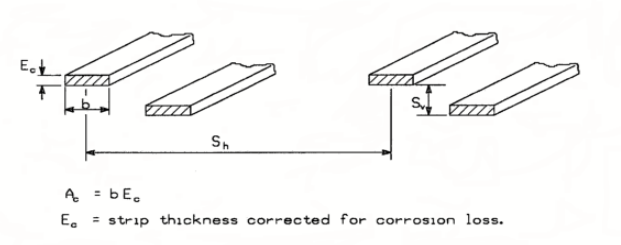

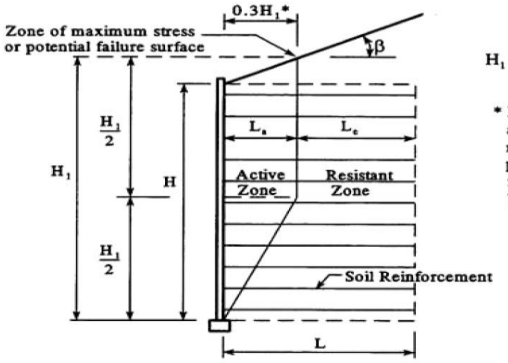

$$H_1 = H + \frac{\tan\beta \times 0.3H}{1 - 0.3\tan\beta}$$

* If wall face is battered, an offset of $0.3H_1$ is still required, and the upper portion of the zone of maximum stress should be parallel to the wall face

Description:		**3.9D**																	
Given:		MSE wall with inextensible reinforcement consisting of steel strips. No live load present. Deadload present at some test locations.																	
Determine:		Factor of safety against pullout for the load condtions just prior to lateral load testing.																	
Known:																			
	Wall Properties																		
	Wall Height at time of Test		H	15	ft														
	Angle of sloping backfill		β	0	º														
				0	rad														
			H_1	17.5	ft	$H+H_q/2$													
	Soil Properties																		
	Moist unit weight		γ_r	129	pcf														
	Friction angle		ϕ_r'	39	º														
				0.68	rad														
	Active Earth Pressure Coefficient		K_a	0.23		$\tan^2(45-\phi_r'/2)$													
	$C_u =$	D_{60}/D_{10}		60		D_{60}	3	mm											
	$1.2+\log C_u \le 2.0$			2		D_{10}	0.05	mm											
		$\tan\phi_r'$		0.80978															
	Reinforcement Properties (steel grids)						Z (ft)		Le		La (ft)								
	Vertical spacing		S_v	2.5	ft			0	12.75	$L_t-0.3H_1$									
	Horizontal spacing		S_h	2.25	ft		$H_1/2$	8.75	12.75	$L_t-0.3H_1$									
	Length of reinforcement		L_t	18	ft		H	15	18	L_t	5.25								
	Surcharge																		
	Unit weight of surcharge		γ_q	120	pcf														
	Height of surcharge		H_q	5	ft														
	Surcharge		q	600	psf														
	Surcharge distance from Wall		d	5.156	ft				Average Factor of Safety against pullout										**2.7**

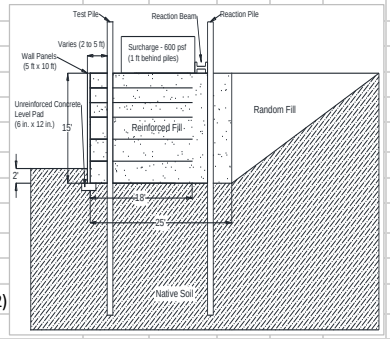

Reinforcement Level	Depth to Layer, Z (ft)	K_r/K_a	K_r	$\sigma_v=\gamma_r(Z)$ (psf)	$\sigma_H=K_r(\sigma_v)$ (psf)	$T_{max}=\sigma_H(S_v)$ (lbs/ft)	b (ft)	$R_c=b/S_h$	F*	L_e (ft)	Pullout Capacity, P_{C1}=	$FS_{PO}=P_{C1}/T_{max}$
1	1.25	1.7	0.38	1028	390	975	0.16	0.07	1.926	12.75	2727	2.8
2	3.75	1.6	0.37	1463	535	1337	0.16	0.07	1.777	12.75	3583	2.7
3	6.25	1.5	0.35	1898	667	1667	0.16	0.07	1.628	12.75	4260	2.6
4	8.75	1.5	0.34	2334	786	1966	0.16	0.07	1.479	12.75	4758	2.4
5	11.25	1.4	0.32	2769	894	2235	0.16	0.07	1.331	14.85	5914	2.6
6	13.75	1.4	0.31	3205	989	2472	0.16	0.07	1.182	16.95	6938	2.8

APPENDIX B. GENEVA ROCK LABORATORY TEST REPORT

GENEVA ROCK PRODUCTS, INC.
1565 West 400 North • P.O. Box 538 • Orem, UT 84059 • (801) 765-7800 • Fax (801) 765-7830 • www.genevarock.com

AGGREGATE SUBMITTAL

Report of Physical Properties

GRP Material Description: Fill - 3/8" HARDPAC
GRP Material Code: FINE
Source Location/Code: North Hansen / 527
Report Date: April 15, 2014
Reviewed by: Victor Johnson
Report No. 527FINE00114

TEST RESULTS

Standard	PHYSICAL PROPERTIES		Result	Test Source
ASTM C 29 AASHTO T19	Unit Weight	Unit Weight, lbs./cu.ft. =	112.0	
		Voids, % =	30	
		☐ Jigged ☐ Loose ☑ Rodded		
ASTM D1557 AASHTO T180	Modified Proctor	Max. density, lbs./cu.ft. =	133.0	
		Optimum Moisture, % =	7	
ASTM D698 AASHTO T99	Standard Proctor	Max. density, lbs./cu.ft. =	128.0	
		Optimum Moisture, % =	7.8	
ASTM D4318 AASHTO T89/90	Liquid Limit	Liquid Limit=	0	
	Plastic Limit	Plastic Limit=	0	
	Plasticity Index	Plasticity Index=	NP	
ASTM C131 AASHTO T96	L.A. Abrasion	Small Coarse Loss, % =		
		Grading/Revolutions, =		
ASTM C535	L.A. Abrasion	Large Coarse Loss, % =		
		Grading/Revolutions, =		
ASTM C 128 AASHTO T84	Fine Specific Gravity & Absorption	Bulk Specific Gravity (dry) =	2.581	
		Bulk Specific Gravity, SSD =	2.599	
		Apparent Specific Gravity =	2.628	
		Absorption, % =	0.7	
ASTM C 127 AASHTO T85	Coarse Specific Gravity & Absorption	Bulk Specific Gravity (dry) =		
		Bulk Specific Gravity, SSD =		
		Apparent Specific Gravity =		
		Absorption, % =		
ASTM D2419 AASHTO T176	Sand Equivalent	Sand Equivalent, % =	34	
ASTM C 88 AASHTO T104	Soundness	Coarse Soundness Loss, % =		
		Magnesium No. of Cycles =		
	Soundness	Fine Soundness Loss, % =	1.0	
		Sodium Sulfate No. of Cycles =		
ASTM C 1252 AASHTO T304	Fine Aggregate Angularity	Uncompacted Voids, % =	48.3	
		Method C (as received material)		
ASTM C40 AASHTO T21	Organic Impurities	Coarse Aggregate, % =	Lighter Plate # 1	
		Fine Aggregate, % =		
ASTM C142 AASHTO T112	Clay / Friable Particles	Coarse Aggregate, % =		
		Fine Aggregate, % =	0.0	
ASTM C123 AASHTO T113	Lightweight Pieces	Coarse Aggregate, % =		
		Fine Aggregate, % =		
ASTM D1883 AASHTO T193	CBR	Surcharge = 10 lbs CBR @ 0.1"=	50	
		Swell% = 0.0% CBR @ 0.2"=	99	
ASTM D5821	Fractured Face	1 or 2 Faces =		
		Fractured Face, % =		
ASTM D2487	Soil Classification	Group Symbol =	GW-GM	
		Group Name =	Well-graded gravel with silt and sand	
ASTM D2488	Soil Description & Identification	Group Symbol =	Cu=66.7 Cc=1.8	
		Group Name =		

SIEVE ANALYSIS

ASTM C136 AASHTO T27

Sieve Size	% Passing	Spec.
450 mm (18")		
375 mm (15")		
300 mm (12")		
250 mm (10")		
225 mm (9")		
200 mm (8")		
150 mm (6")		
125 mm (5")		
100 mm (4")		
75.0 mm (3")		
63.0 mm (2-1/2")		
50.0 mm (2")		
37.5 mm (1-1/2")		
25.0 mm (1")		
19.0 mm (3/4")		
12.5 mm (1/2")	100	
9.5 mm (3/8")	100	
6.3 mm (1/4")		
4.75 mm (No.4)	77	
2.36 mm (No.8)	52	
2.00 mm (No.10)		
1.18 mm (No.16)	37	
0.600 mm (No.30)	30	
0.425 mm (No.40)		
0.300 mm (No.50)	25	
0.180 mm (No.80)		
0.150 mm (No.100)	20	
0.075 mm (No.200)	14	

ASTM D422 Hydrometer =		
ASTM C566 AASHTO T255 Moisture Content, % =		
ASTM C136 AASHTO T27 Fineness Modulus (FM) =		
AASHTO M145 Classification of Soils =	A1B	
ASTM D4791 Ratio = Flat & Elongated =		

GRP Materials | Aggregate Physical Properties Report | Version 02.11.08

APPENDIX C. EXACT LOCATION OF STRAIN GAUGES

Label	Pile Test	Layer	Distance Behind Back Face of MSE Wall (ft)						
			0.5	2.0	3.0	5.0	8.0	11.0	14.0
1A	1.7D/2.8D	Top	0.500	2.000	3.000	5.000	8.000	11.000	14.000
1B	1.7D/2.8D	Top	0.500	1.958	3.000	4.958	7.979	11.063	14.063
2A	1.7D/2.8D	Top	0.500	2.000	3.042	5.000	8.000	11.000	14.000
2B	1.7D/2.8D	Top	0.500	2.042	2.958	5.042	8.083	11.083	14.083
5A	3.1D/3.9D	Top	0.583	2.000	3.000	5.000	8.000	11.000	14.000
5B	3.1D/3.9D	Top	0.458	2.000	3.000	5.000	8.000	11.000	14.000
6A	3.1D/3.9D	Top	0.458	2.000	3.000	5.000	8.000	11.000	14.000
6B	3.1D/3.9D	Top	0.500	2.000	3.083	5.000	8.000	11.000	14.000
9A	1.7D/2.8D	Bottom	0.500	2.000	3.042	5.000	8.042	11.042	14.042
9B	1.7D/2.8D	Bottom	0.458	2.000	3.000	5.000	8.000	11.000	14.000
10A	1.7D/2.8D	Bottom	0.500	2.083	2.917	5.083	7.938	10.958	13.958
10B	1.7D/2.8D	Bottom	0.500	2.000	2.917	5.000	8.083	11.083	14.083
12A	3.1D/3.9D	Bottom	0.583	2.000	3.000	5.000	8.000	11.000	14.000
12B	3.1D/3.9D	Bottom	0.500	2.000	3.083	5.000	8.000	11.000	14.000
13A	3.1D/3.9D	Bottom	0.500	2.000	3.000	5.000	8.042	11.042	14.042
13B	3.1D/3.9D	Bottom	0.500	1.917	3.000	4.917	7.917	10.917	13.917

APPENDIX D. LOAD DISPLACEMENT CURVES

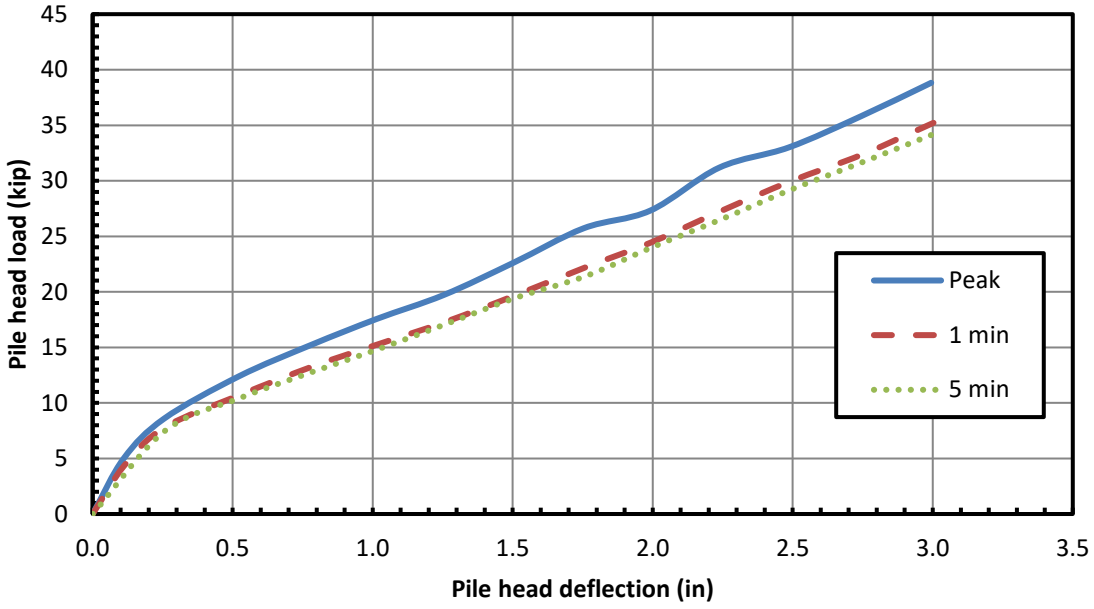

Figure D 1: Load-displacement curve for 1.7D test.

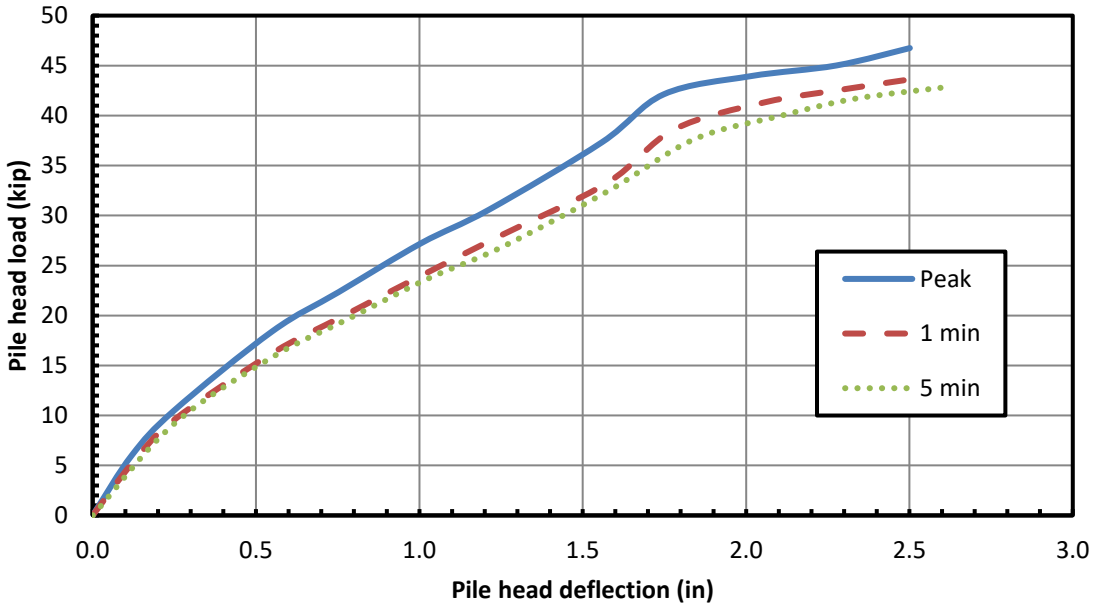

Figure D 2: Load-displacement curve for 2.8D test.

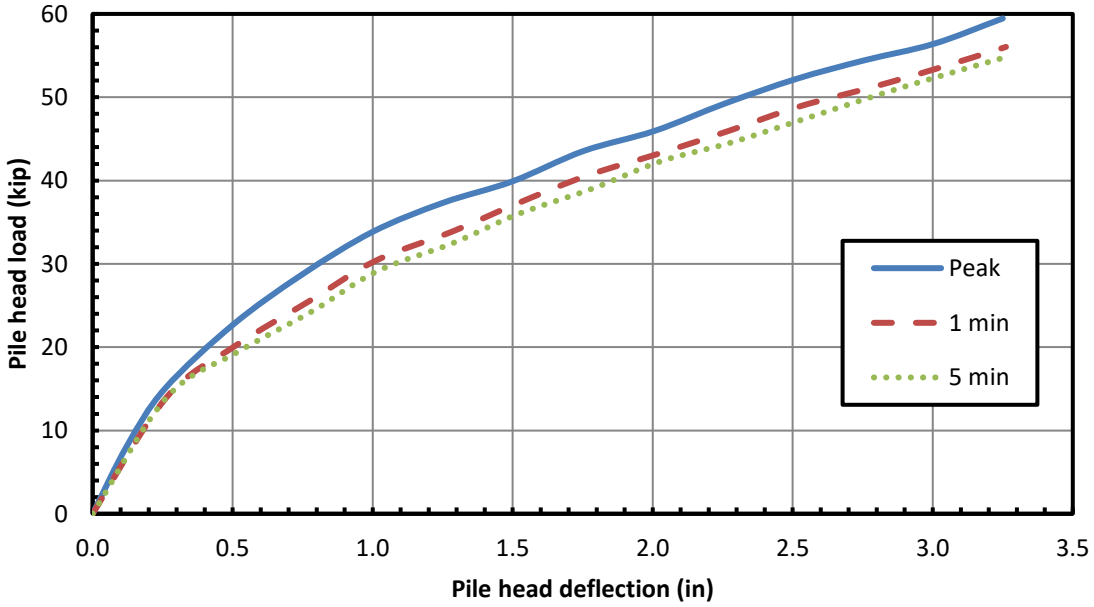

Figure D 3: Load-displacement curve for 3.1D test.

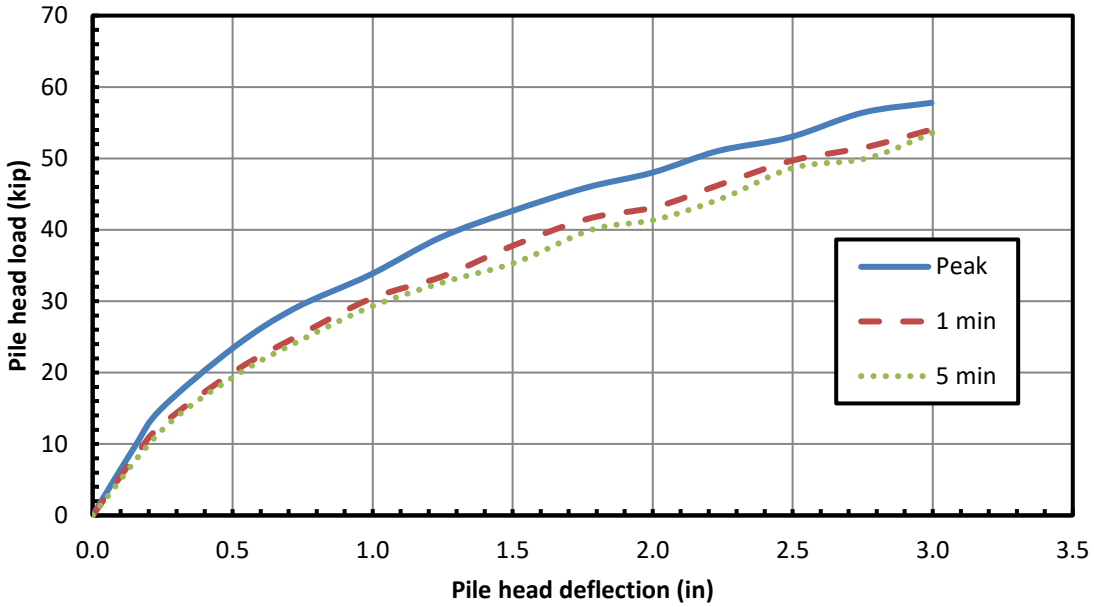

Figure D 4: Load-displacement curve for 3.9D test.

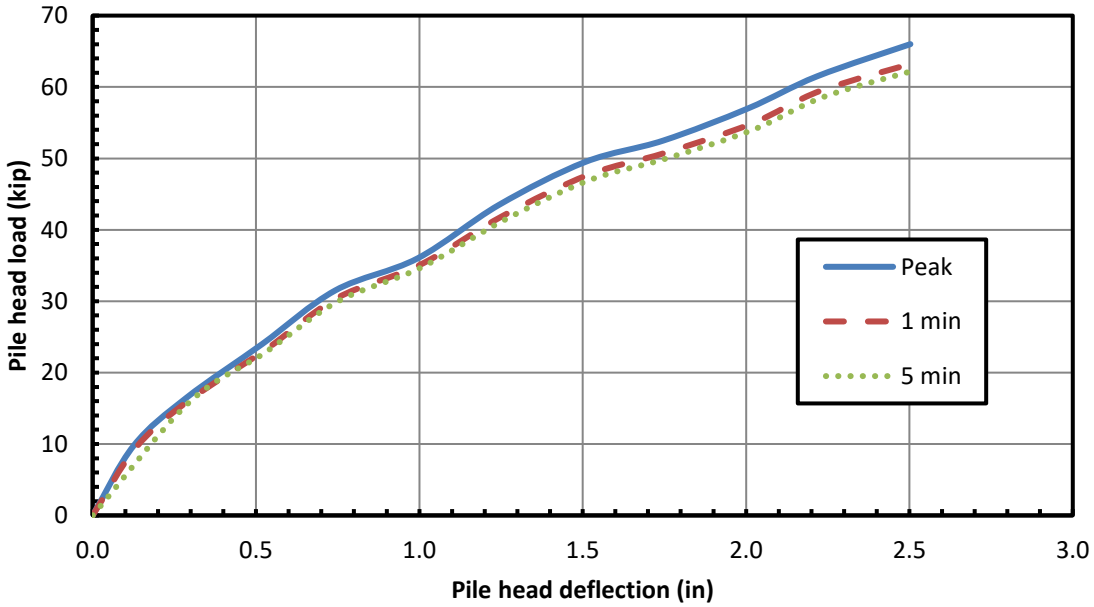

Figure D 5: Load-displacement curve for reaction pile test.

APPENDIX E. INDUCED FORCE IN THE REINFORCEMENT CURVES

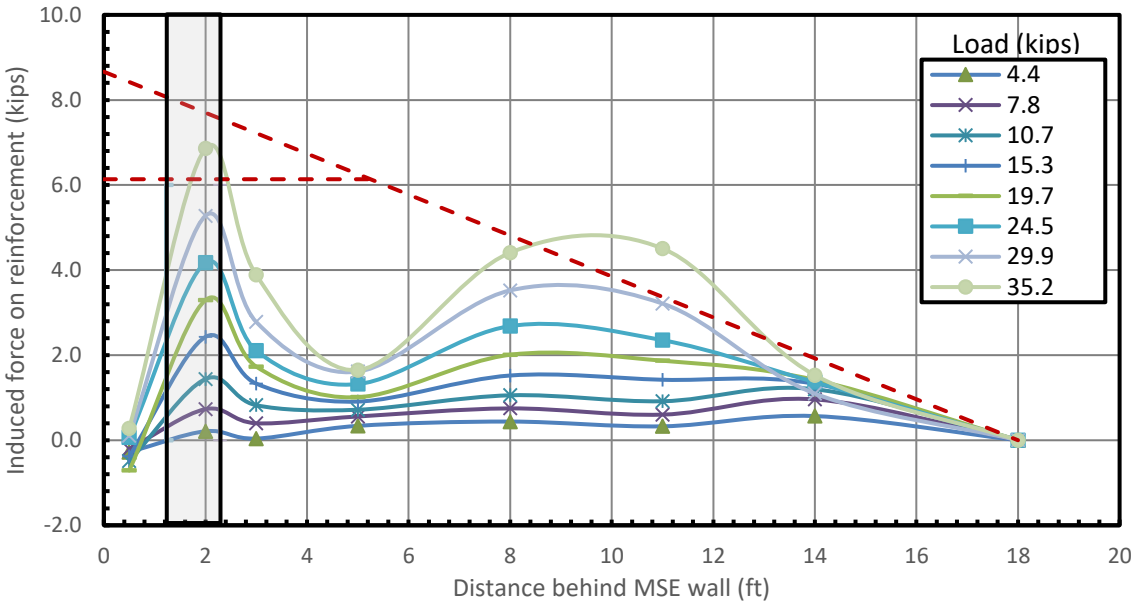

Figure E 1: Induced force in steel strip vs. distance from back face of wall, 1.7D test, top layer, 29.5 in. away.

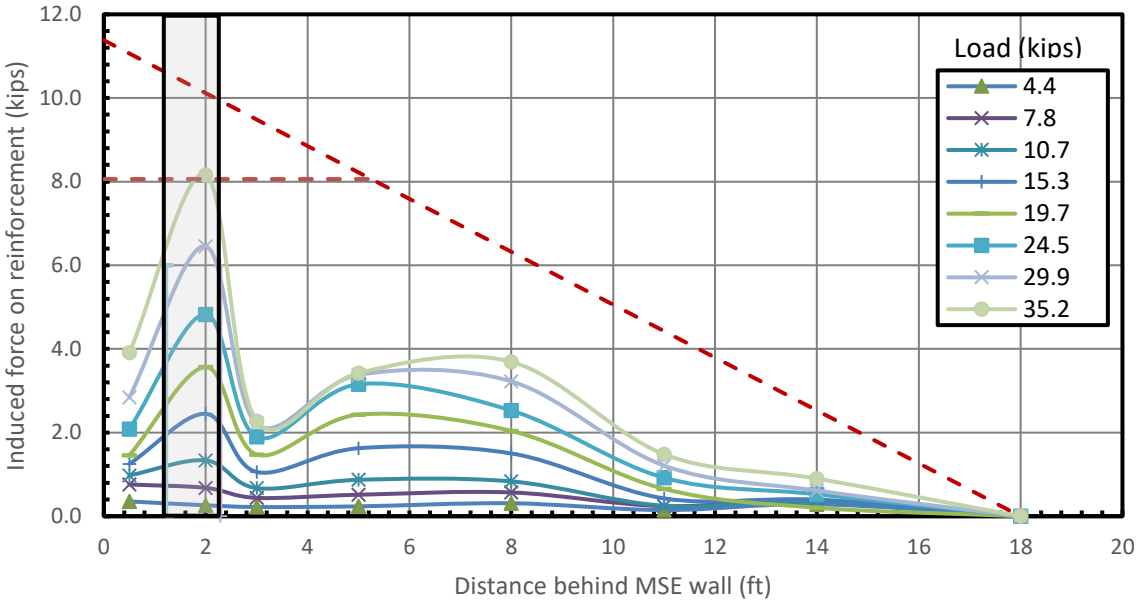

Figure E 2: Induced force in steel strip vs. distance from back face of wall, 1.7D test, bottom layer, 28.5 in. away.

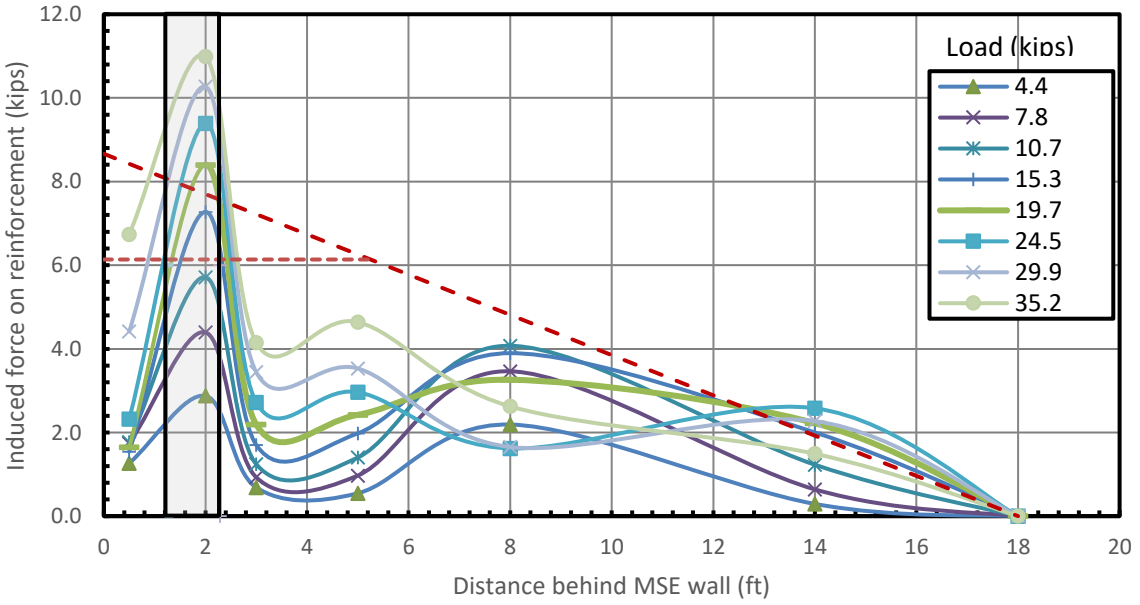

Figure E 3: Induced force in steel strip vs. distance from back face of wall, 1.7D test, top layer, 2.5 in. away.

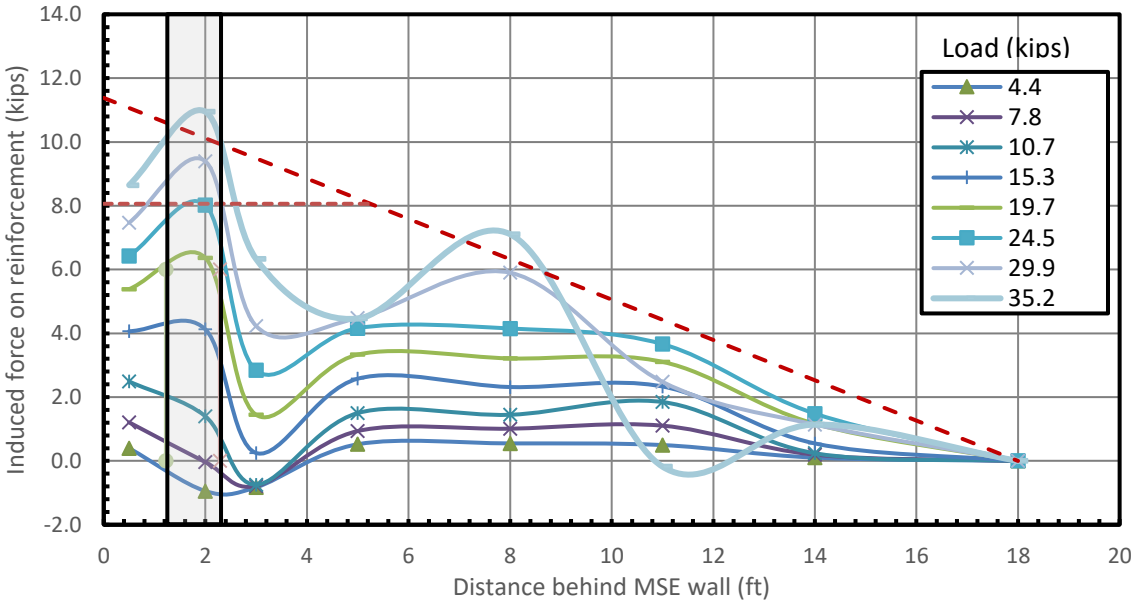

Figure E 4: Induced force in steel strip vs. distance from back face of wall, 1.7D test, bottom layer, 2.5 in. away.

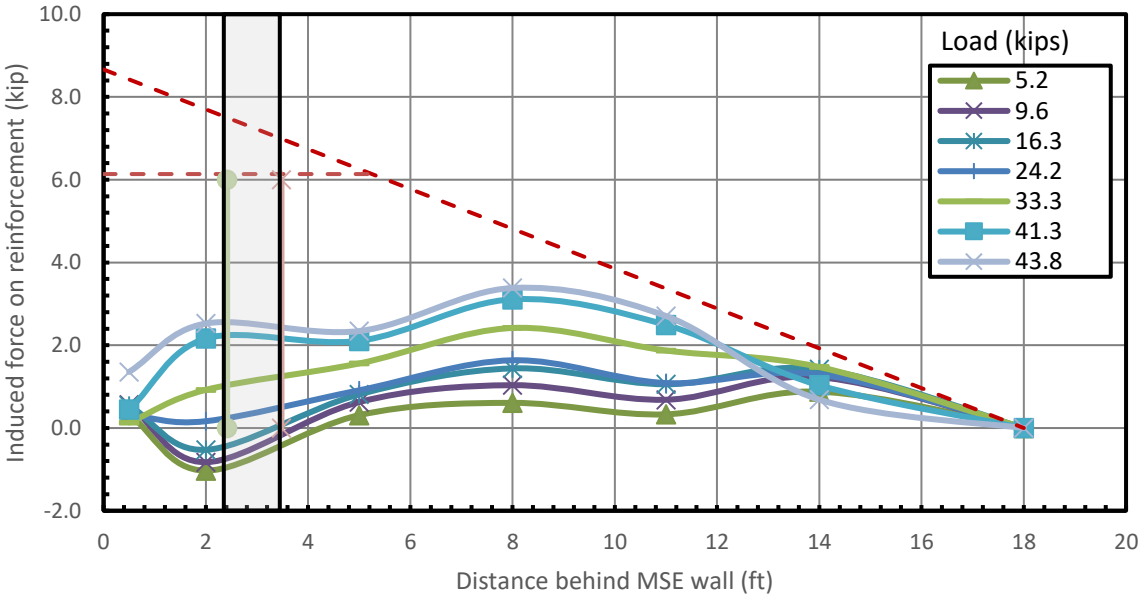

Figure E 5: Induced force in steel strip vs. distance from back face of wall, 2.8D test, top layer, 16 in. away.

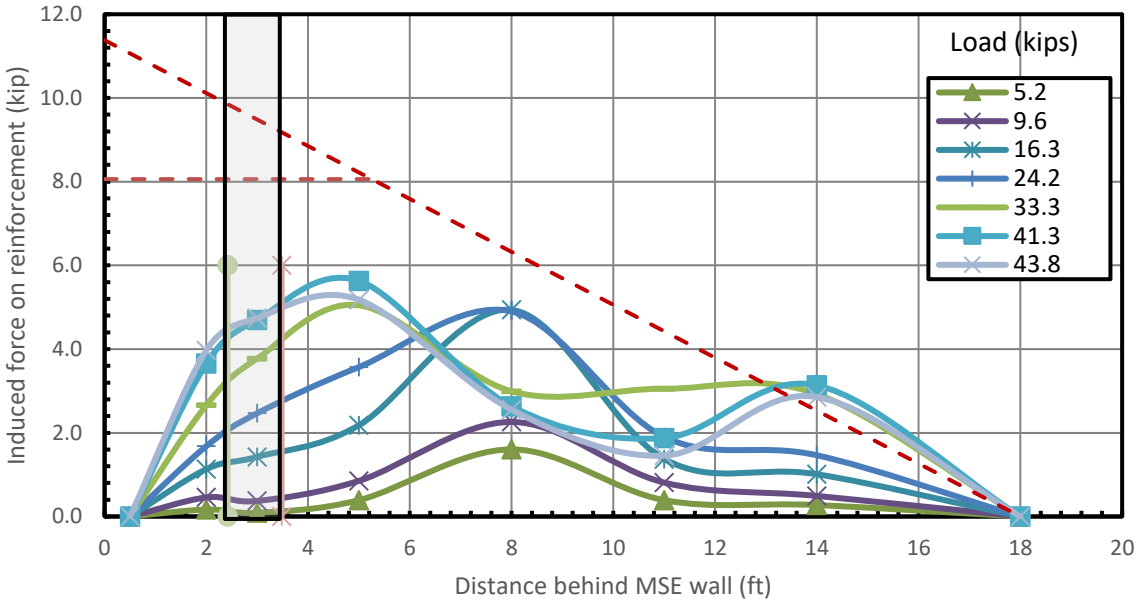

Figure E 6: Induced force in steel strip vs. distance from back face of wall, 2.8D test, bottom layer, 17 in. away.

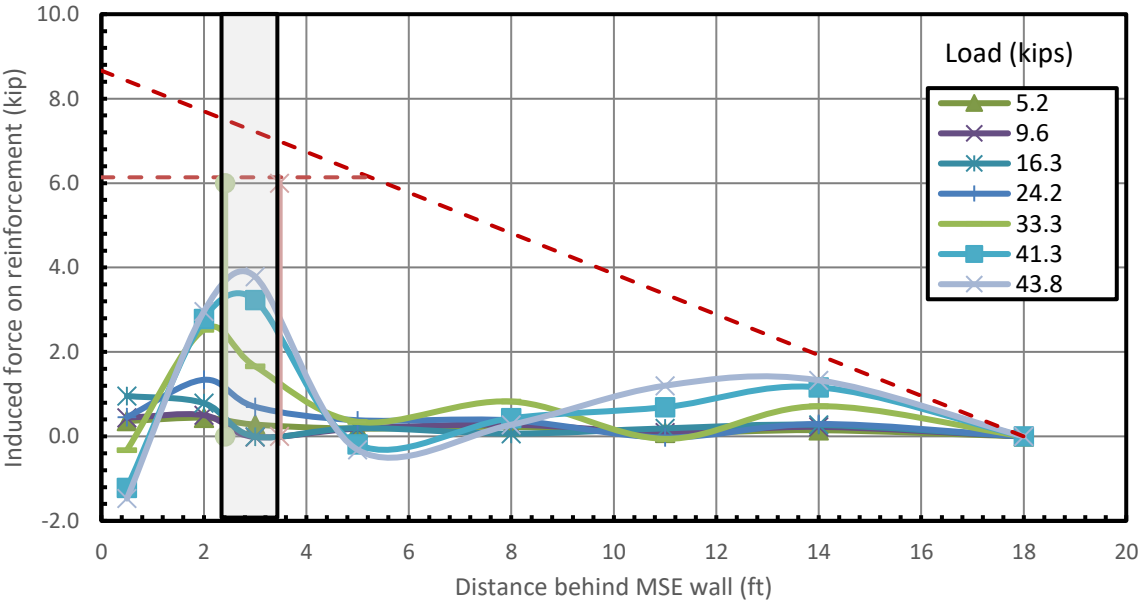

Figure E 7: Induced force in steel strip vs. distance from back face of wall, 2.8D test, top layer, 43 in. away.

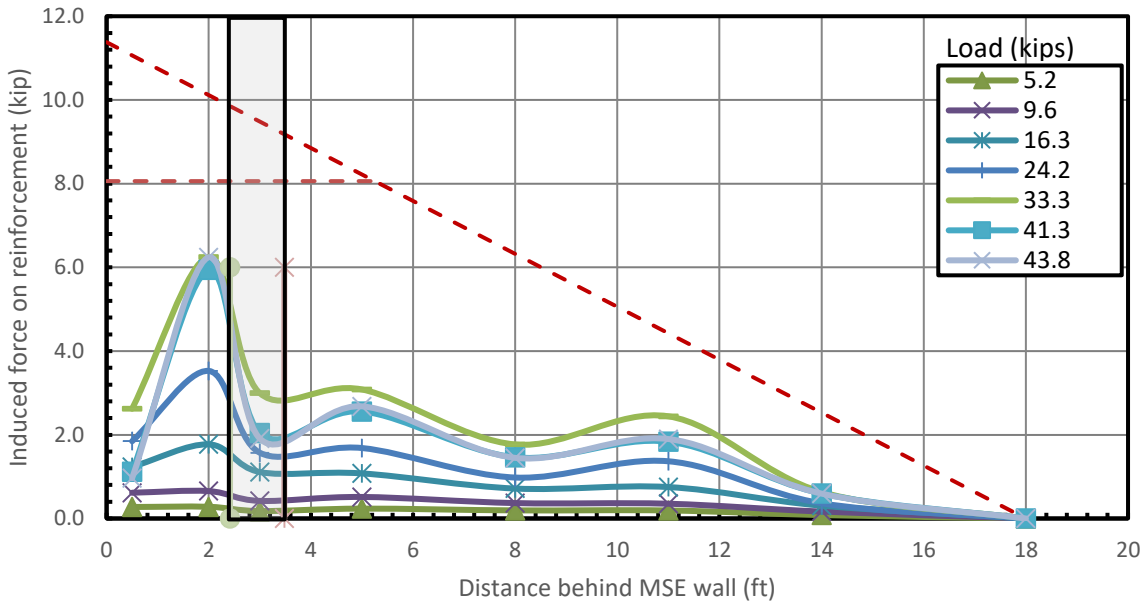

Figure E 8: Induced force in steel strip vs. distance from back face of wall, 2.8D test, bottom layer, 43.5 in. away.

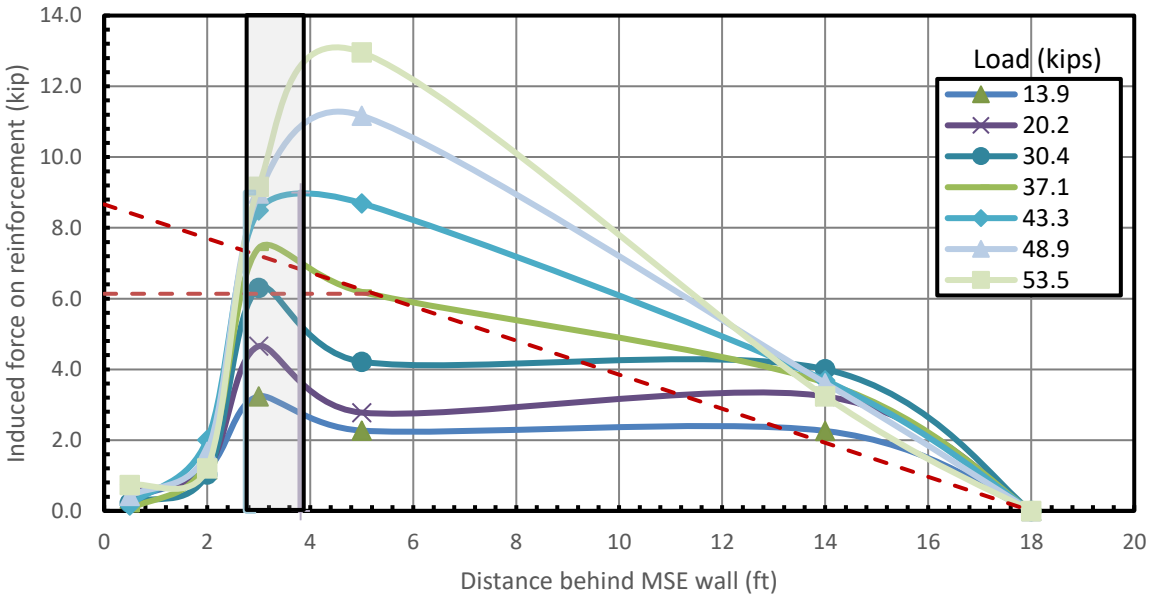

Figure E 9: Induced force in steel strip vs. distance from back face of wall, 3.1D test, top layer, 5 in. away.

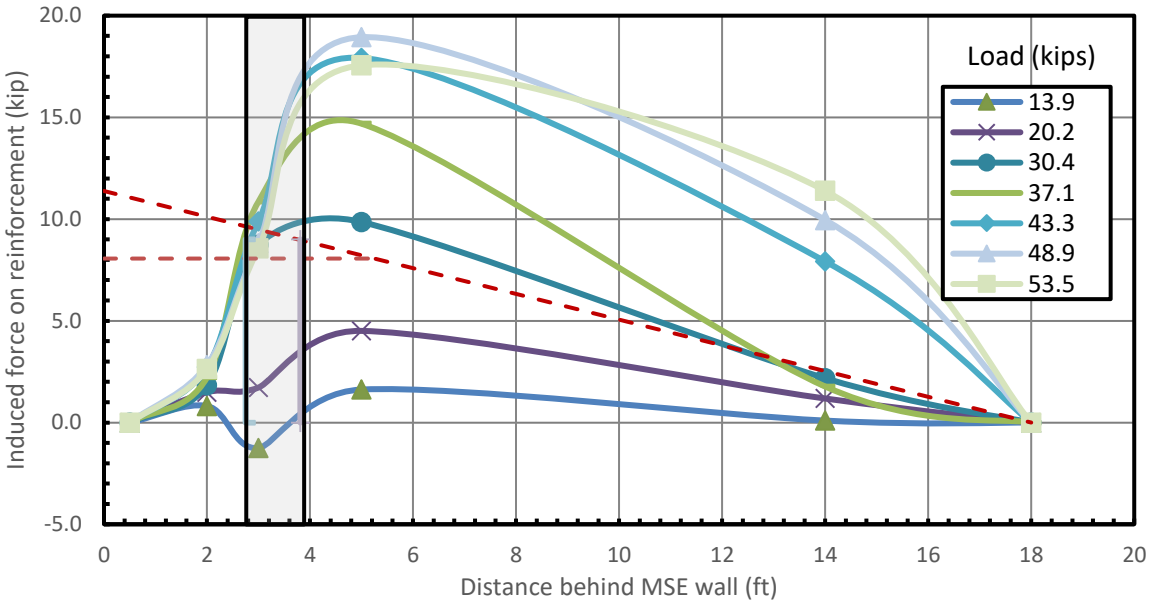

Figure E 10: Induced force in steel strip vs. distance from back face of wall, 3.1D test, bottom layer, 4 in. away.

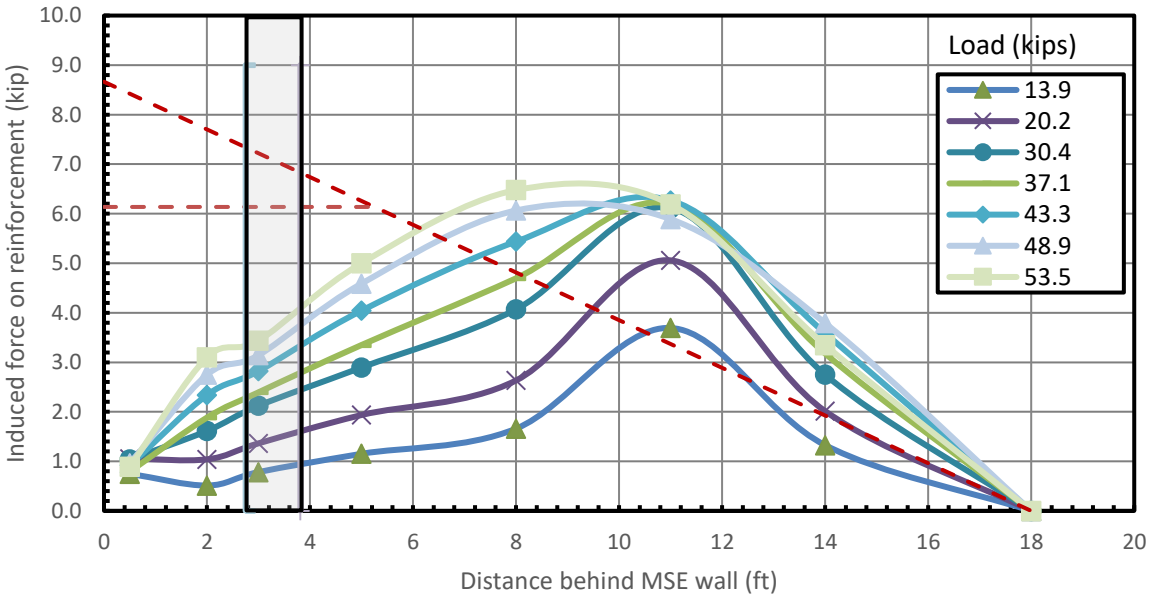

Figure E 11: Induced force in steel strip vs. distance from back face of wall, 3.1D test, top layer, 30.5 in. away.

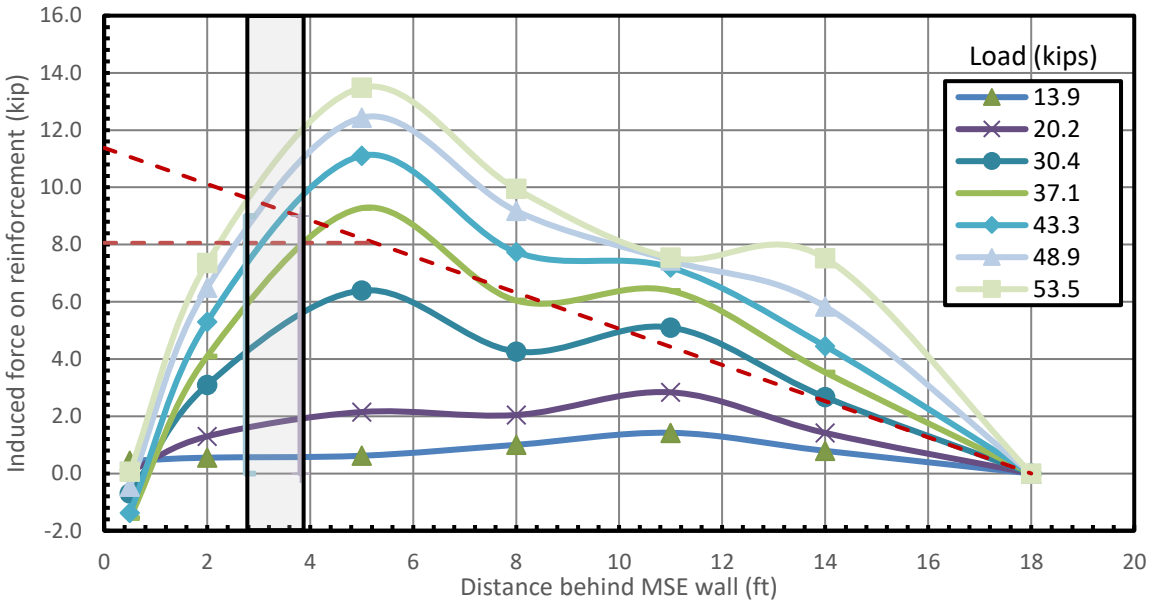

Figure E 12: Induced force in steel strip vs. distance from back face of wall, 3.1D test, bottom layer, 31.5 in. away.

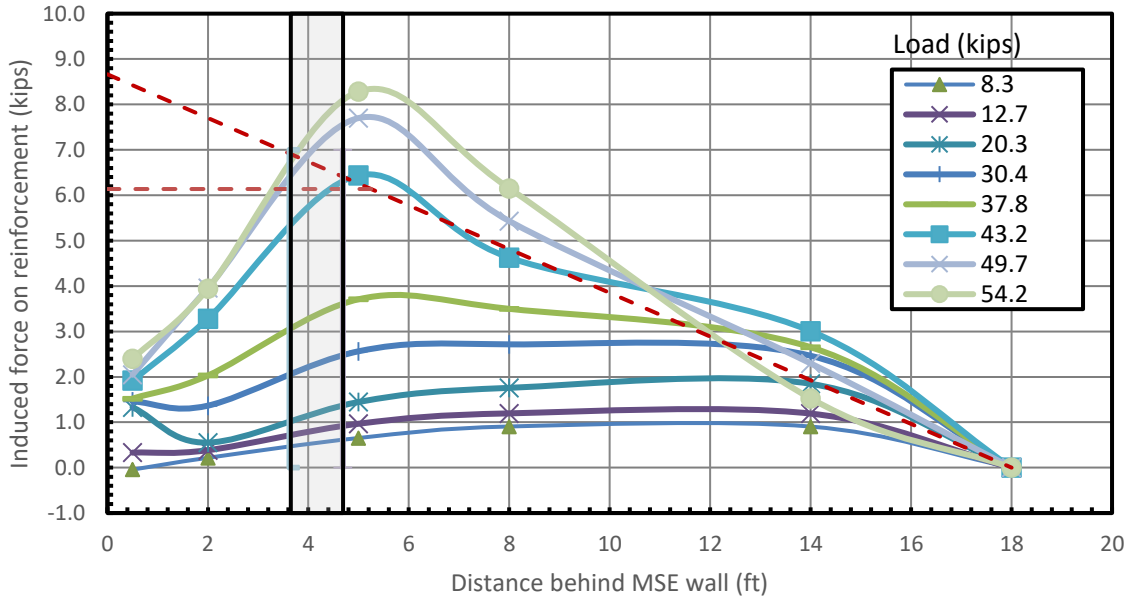

Figure E 13: Induced force in steel strip vs. distance from back face of wall, 3.9D test, top layer, 18 in. away.

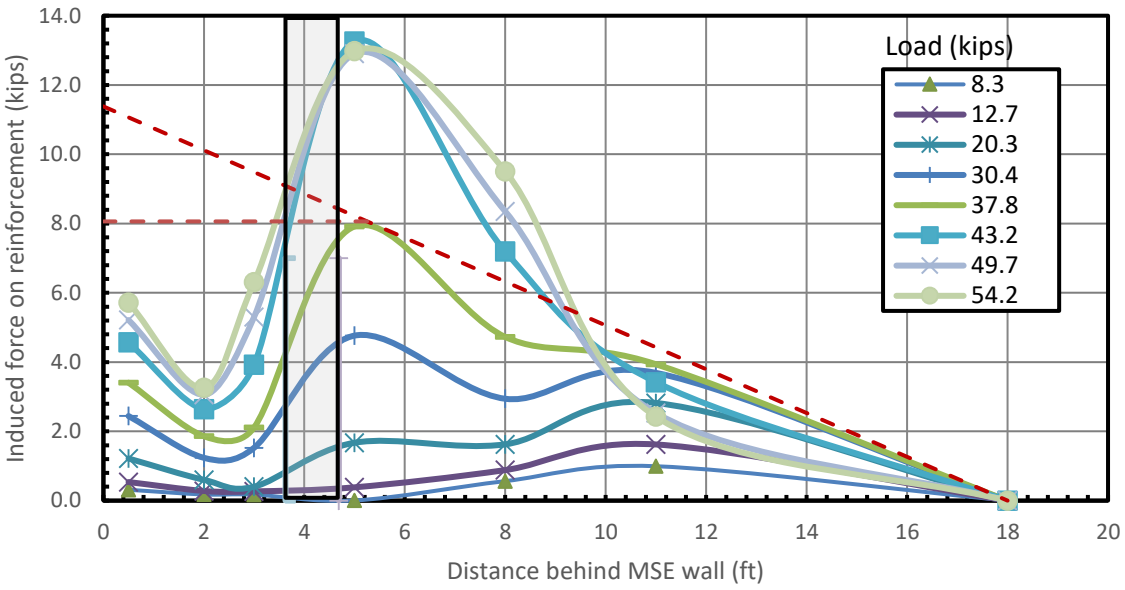

Figure E 14: Induced force in steel strip vs. distance from back face of wall, 3.9D test, bottom layer, 18 in. away.

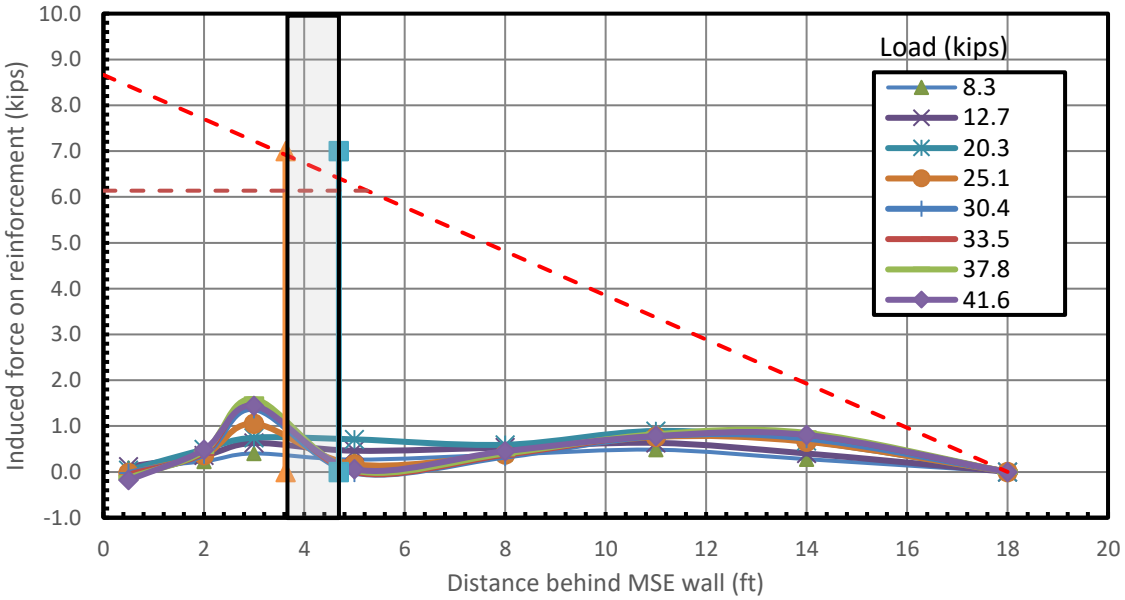

Figure E 15: Induced force in steel strip vs. distance from back face of wall, 3.9D test, top layer, 43.5 in. away.

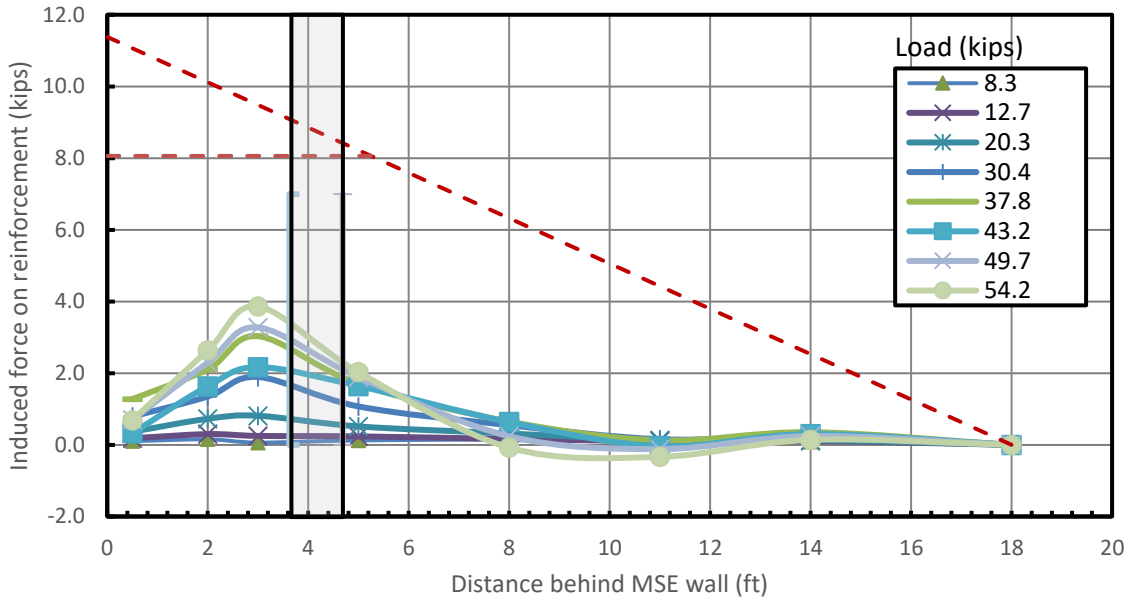

Figure E 16: Induced force in steel strip vs. distance from back face of wall, 3.9D test, bottom layer, 45 in. away.

APPENDIX F. GROUND DISPLACEMENT CURVES

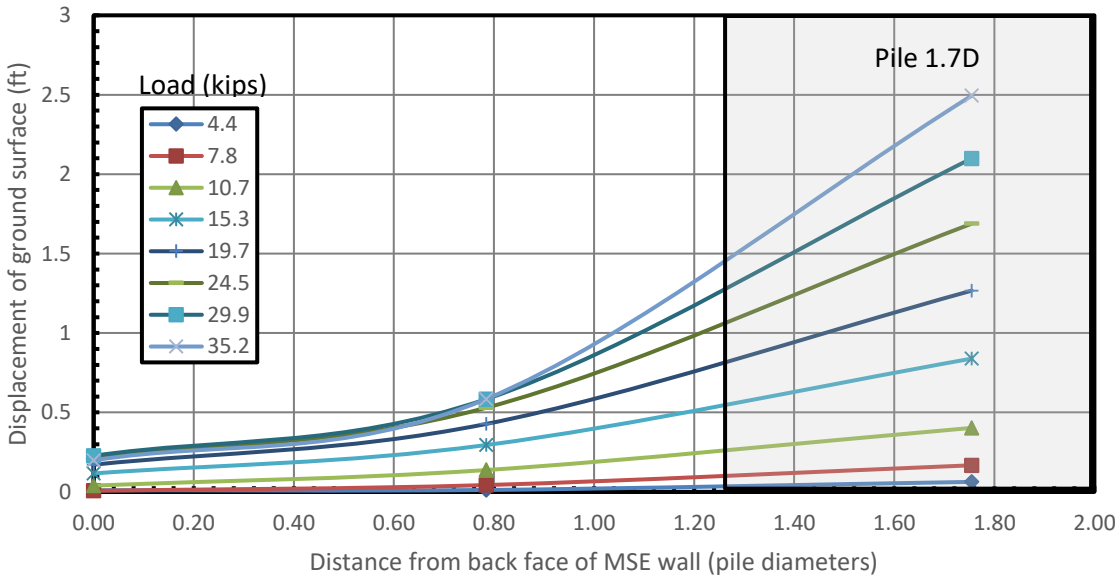

Figure F 1: Horizontal displacement of ground surface vs. distance from the back face of MSE wall, 1.7D test.

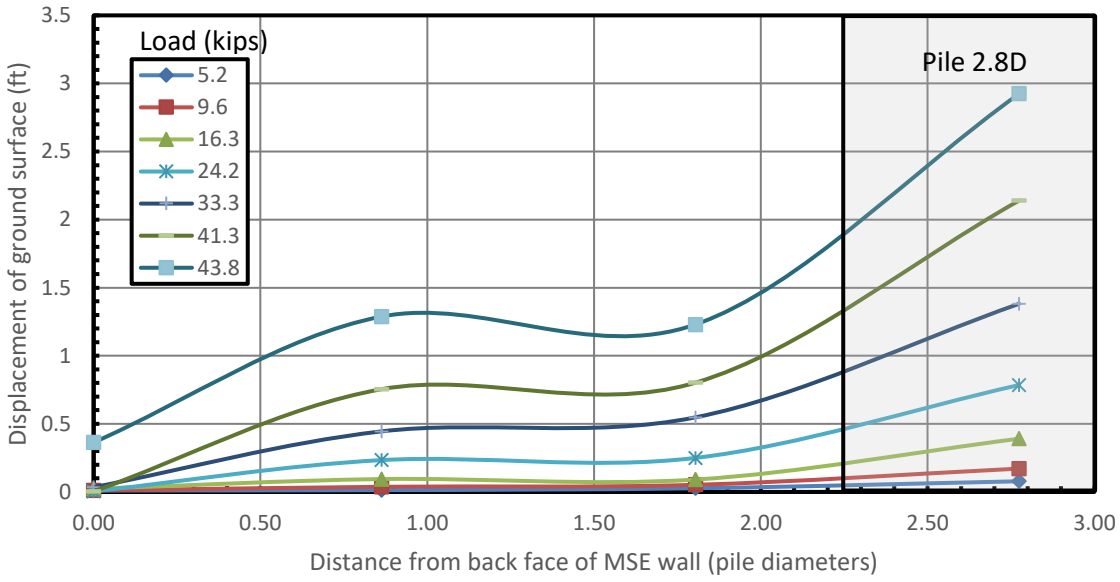

Figure F 2: Horizontal displacement of ground surface vs. distance from the back face of MSE wall, 2.8D test.

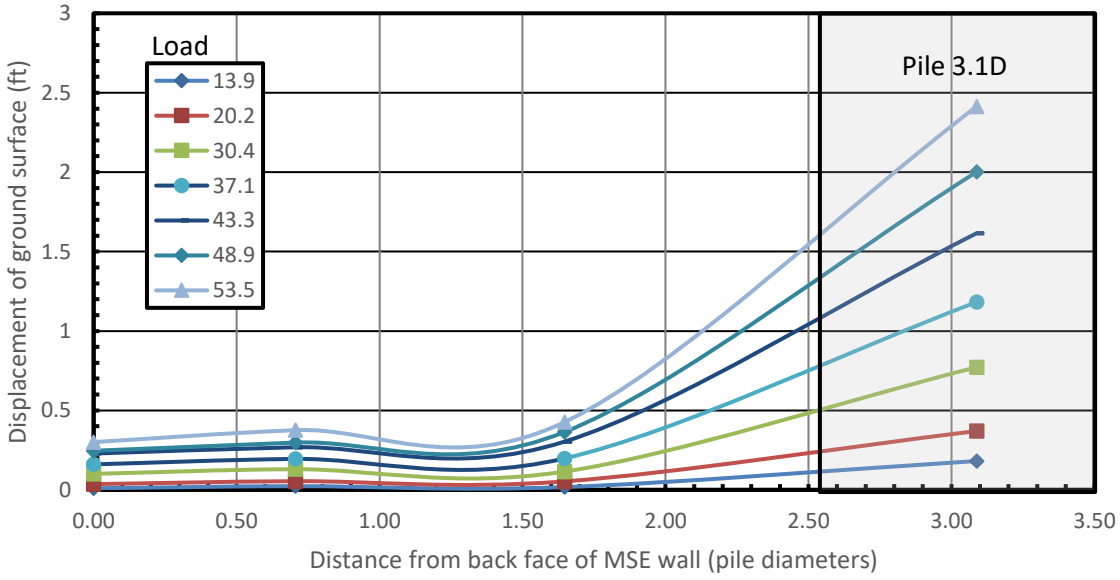

Figure F 3: Horizontal displacement of ground surface vs. distance from the back face of MSE wall, 3.1D test.

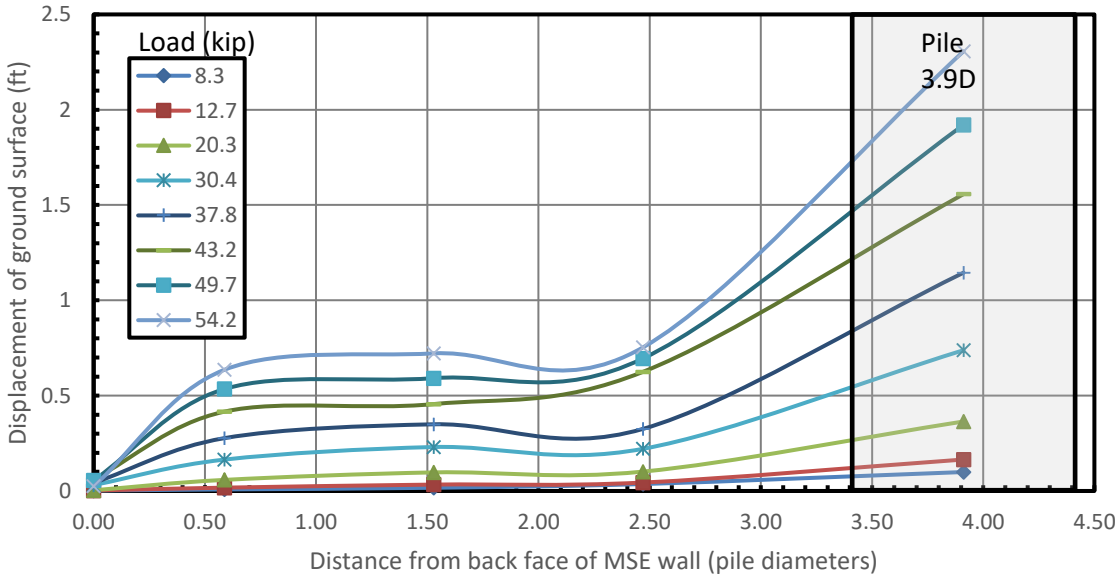

Figure F 4: Horizontal displacement of ground surface vs. distance from the back face of MSE wall, 3.9D test.

APPENDIX G. BENDING MOMENT CURVES

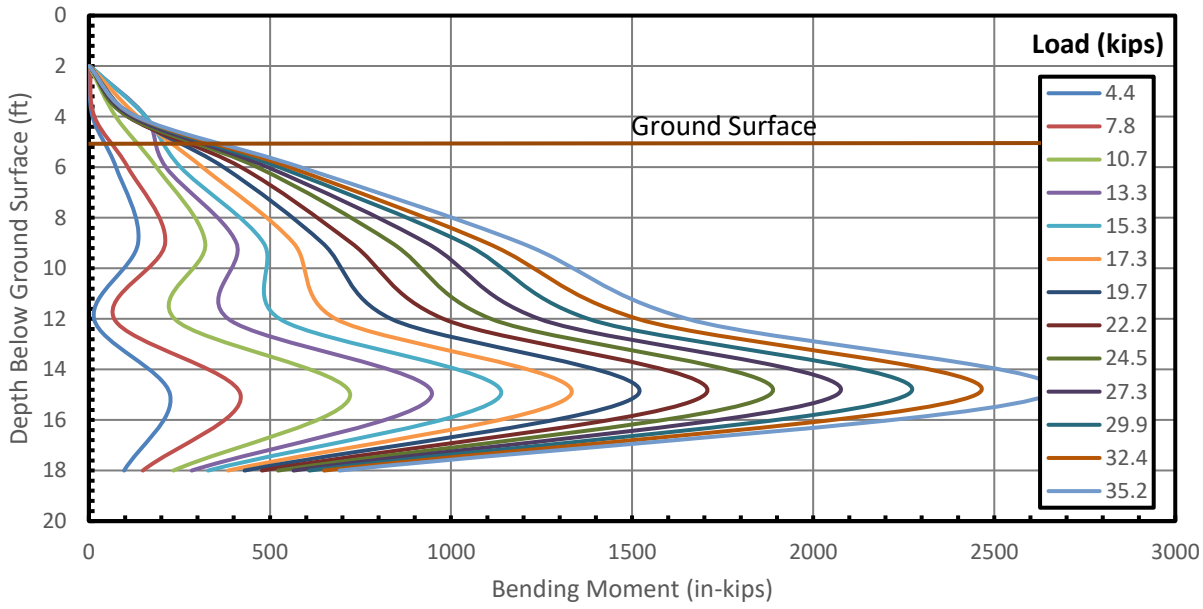

Figure G 1: Bending moment vs. depth, 1.7D test.

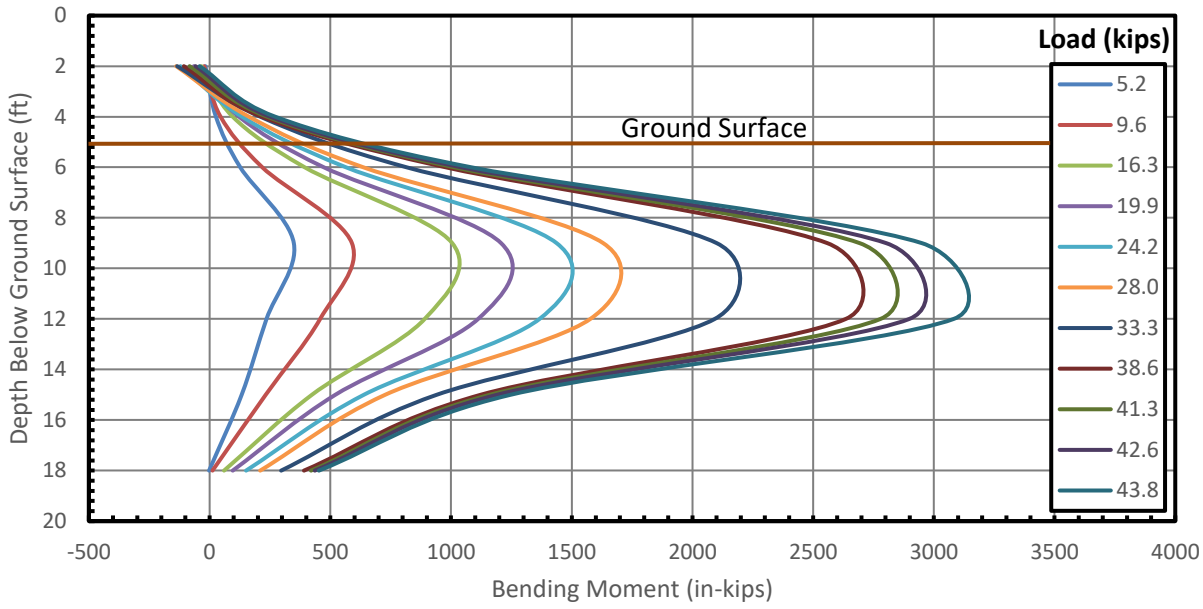

Figure G 2: Bending moment vs. depth, 2.8D test.

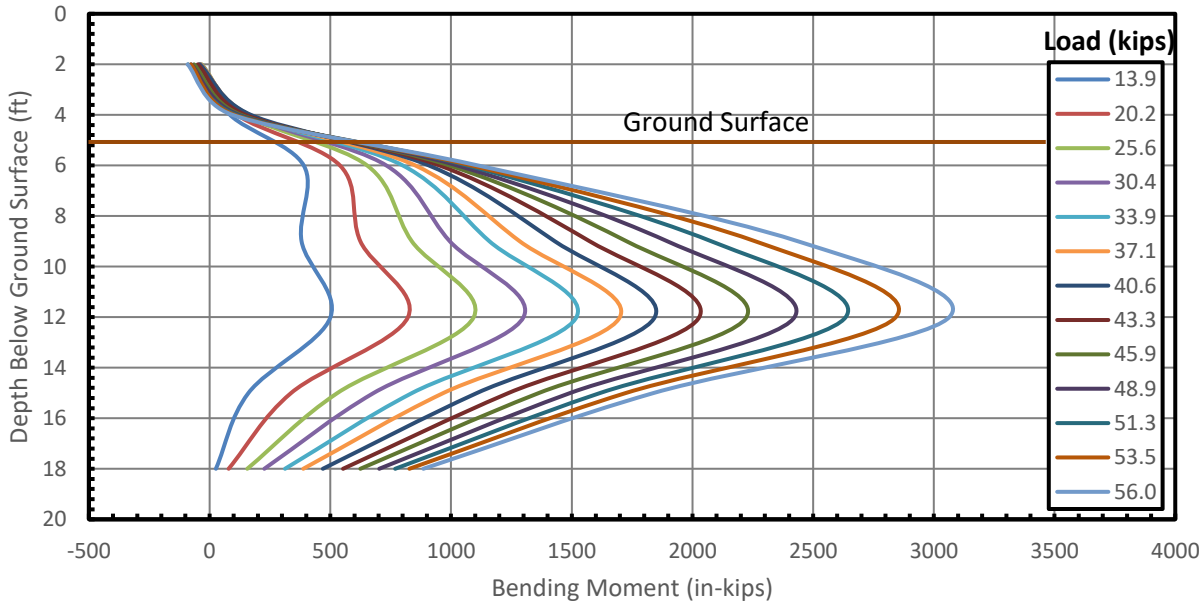

Figure G 3: Bending moment vs. depth, 3.1D test.

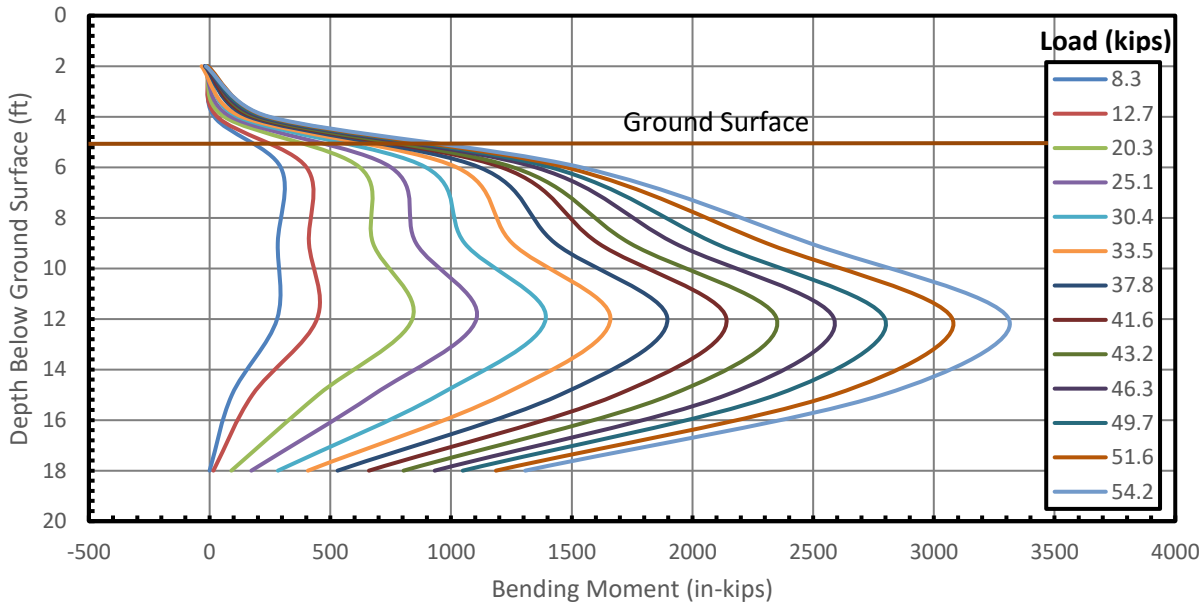

Figure G 4: Bending moment vs. depth, 3.9D test.

APPENDIX H. DIC PICTURES

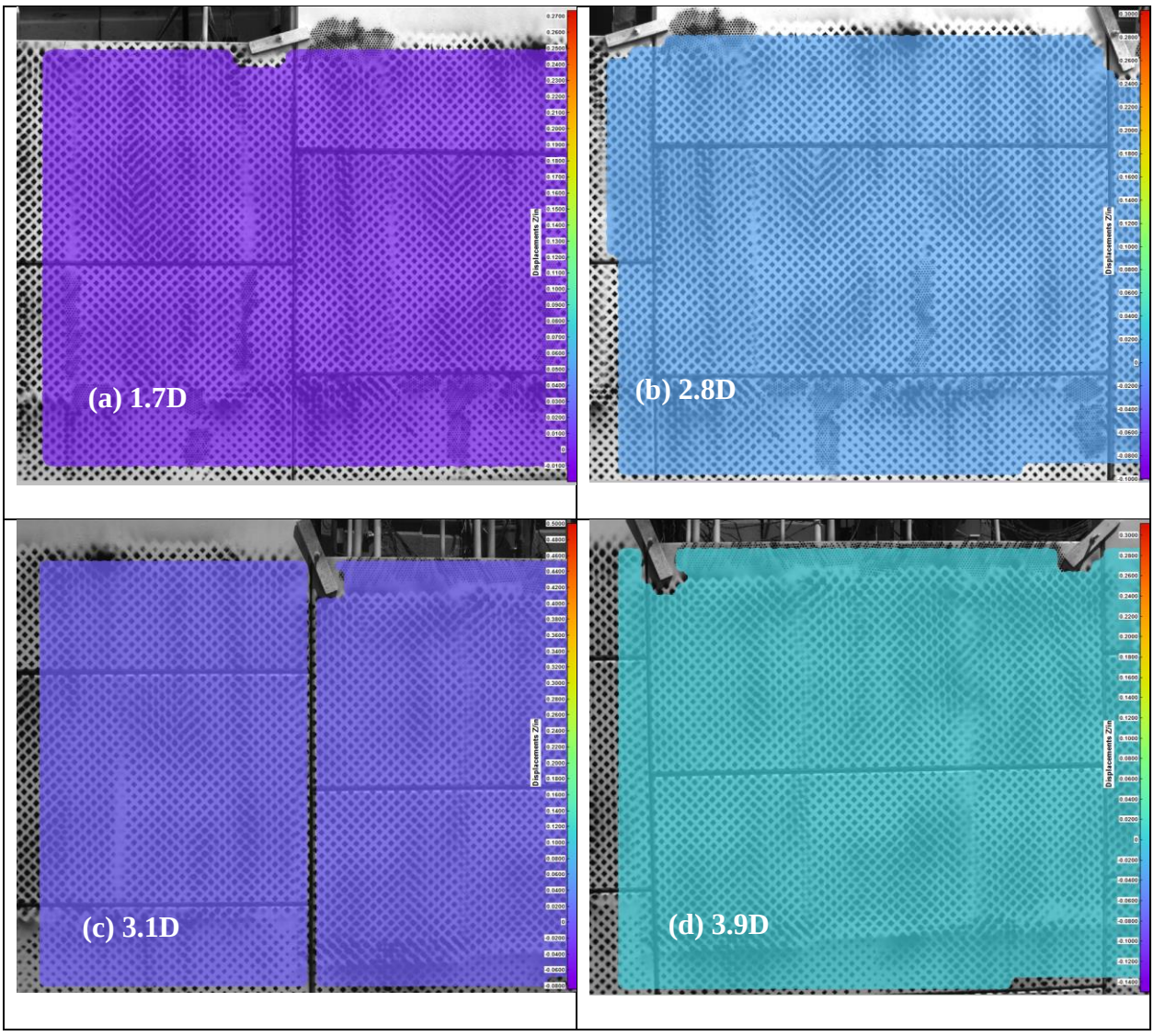

Figure H 1: Wall displacement at 0 in. pile head deflection for pile at (a) 1.7D, (b) 2.8D, (c) 3.1D and (d) 3.9D.

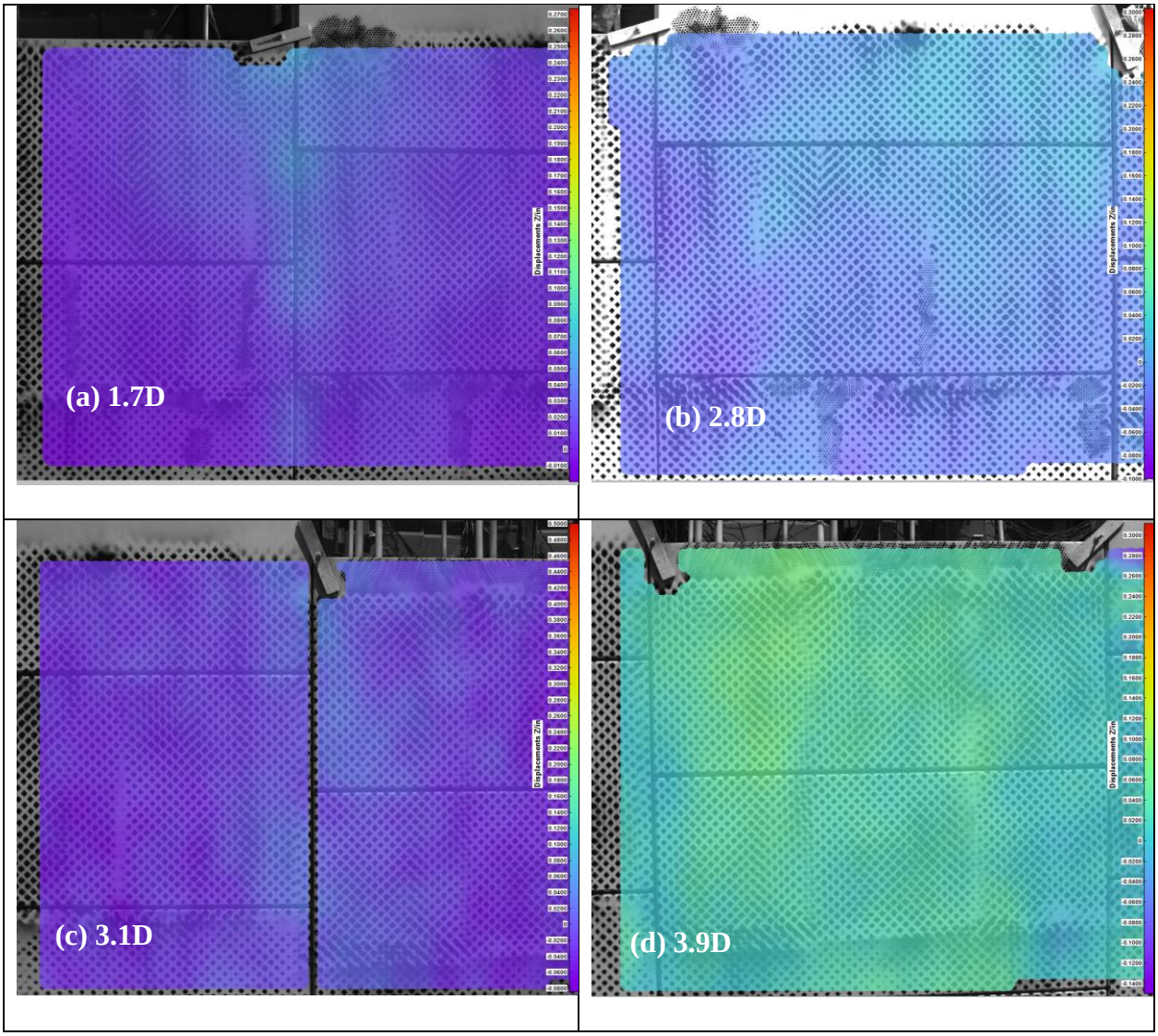

Figure H 2: Wall displacement at 0.25 in. pile head deflection for pile at (a) 1.7D, (b) 2.8D, (c) 3.1D and (d) 3.9D.

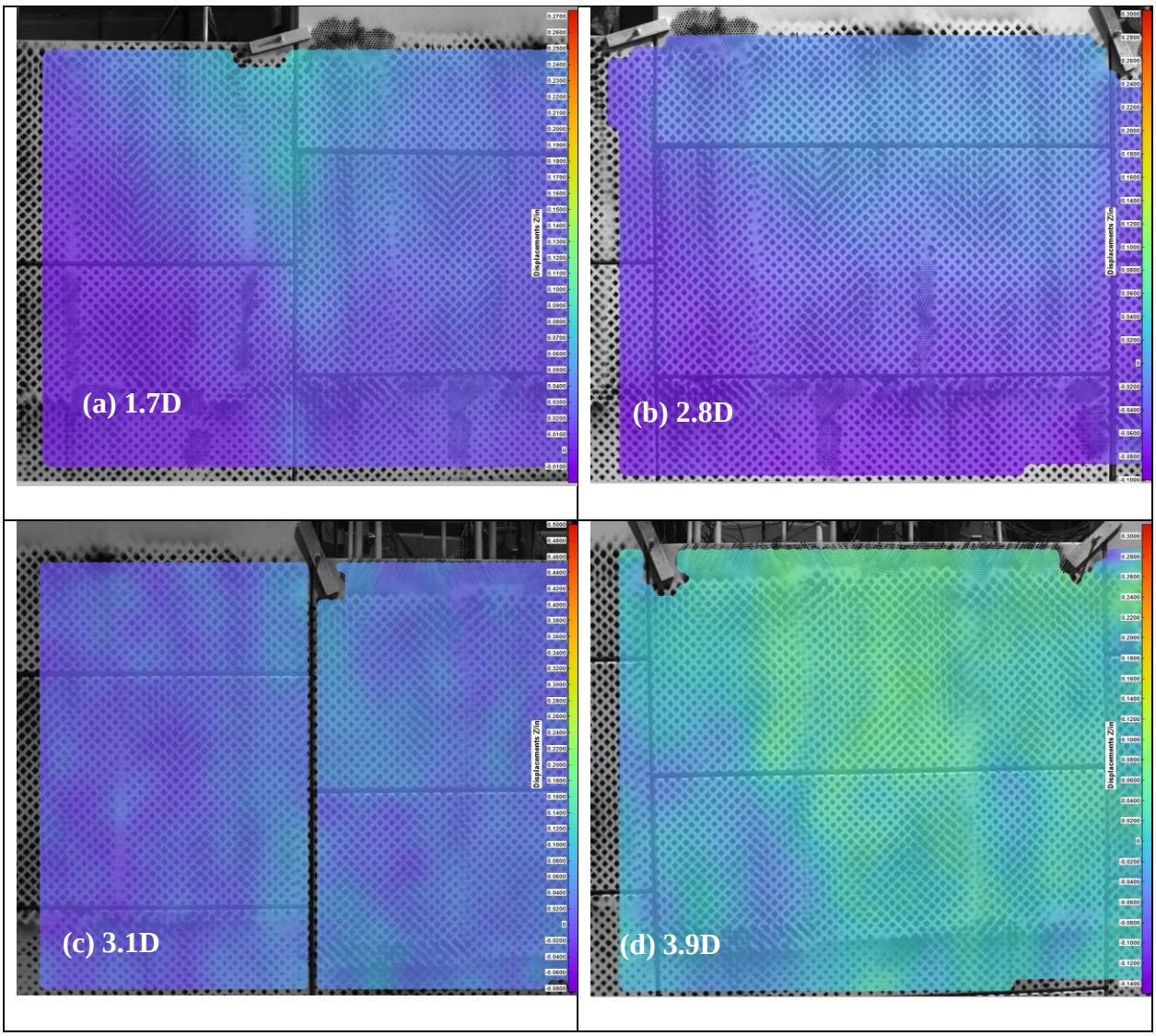

Figure H 3: Wall displacement at 0.5 in. pile head deflection for pile at (a) 1.7D, (b) 2.8D, (c) 3.1D and (d) 3.9D.

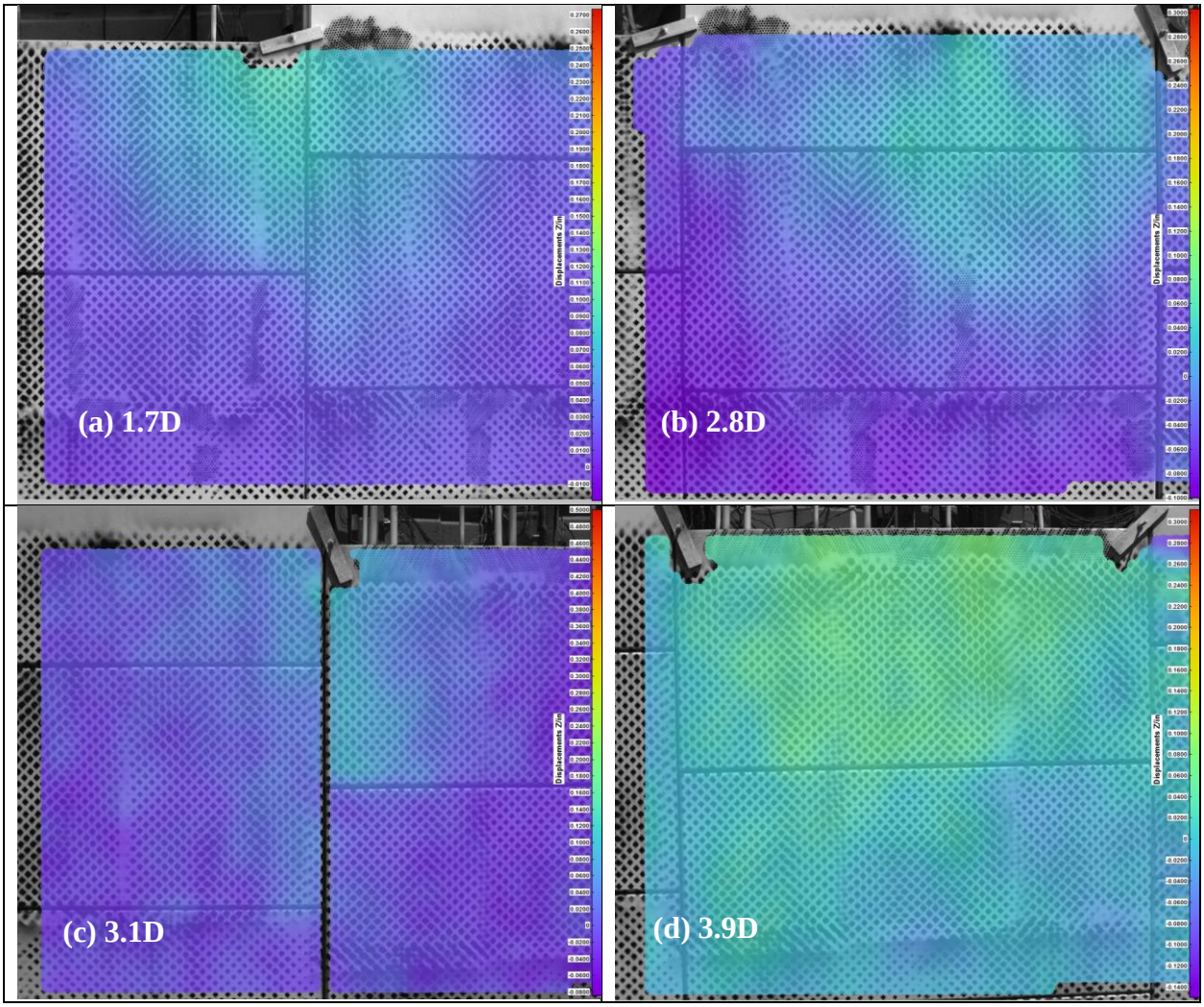

Figure H 4: Wall displacement at 0.75 in. pile head deflection for pile at 1.7D, (b) 2.8D, (c) 3.1D and (d) 3.9D.

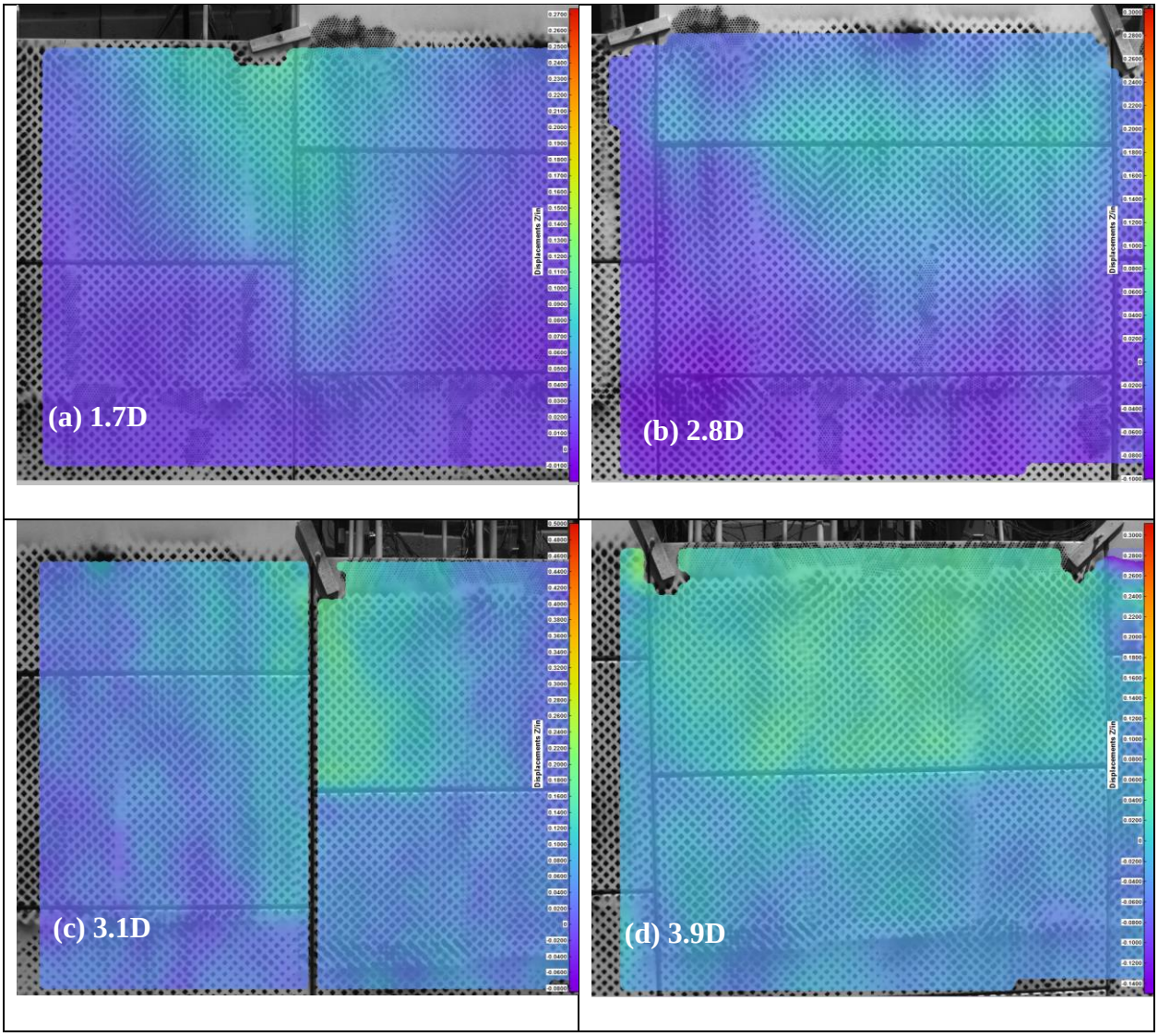

Figure H 5: Wall displacement at 1.0 in. pile head deflection for pile at (a) 1.7D, (b) 2.8D, (c) 3.1D and (d) 3.9D.

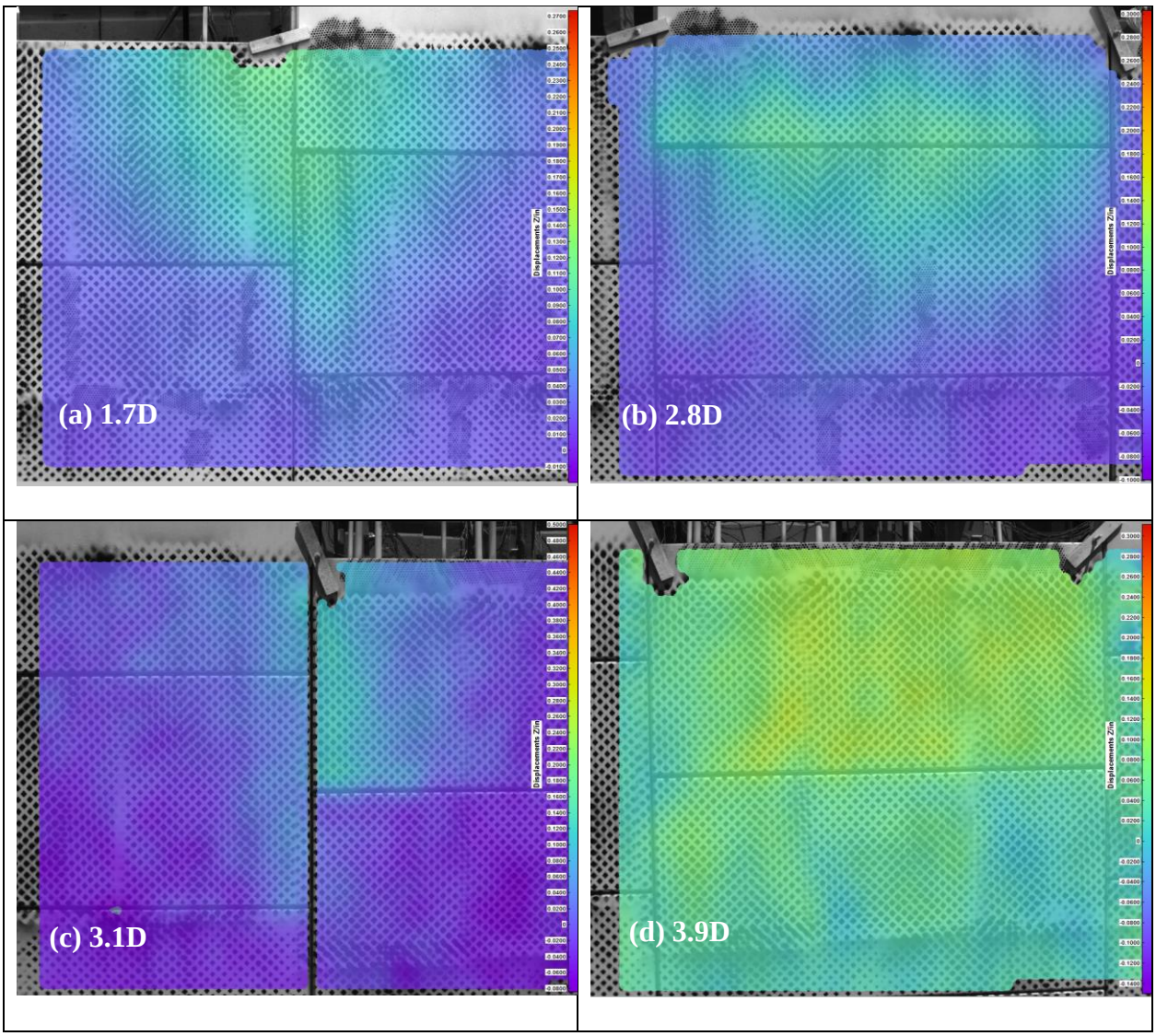

Figure H 6: Wall displacement at 1.25 in. pile head deflection for pile at (a) 1.7D, (b) 2.8D, (c) 3.1D and (d) 3.9D.

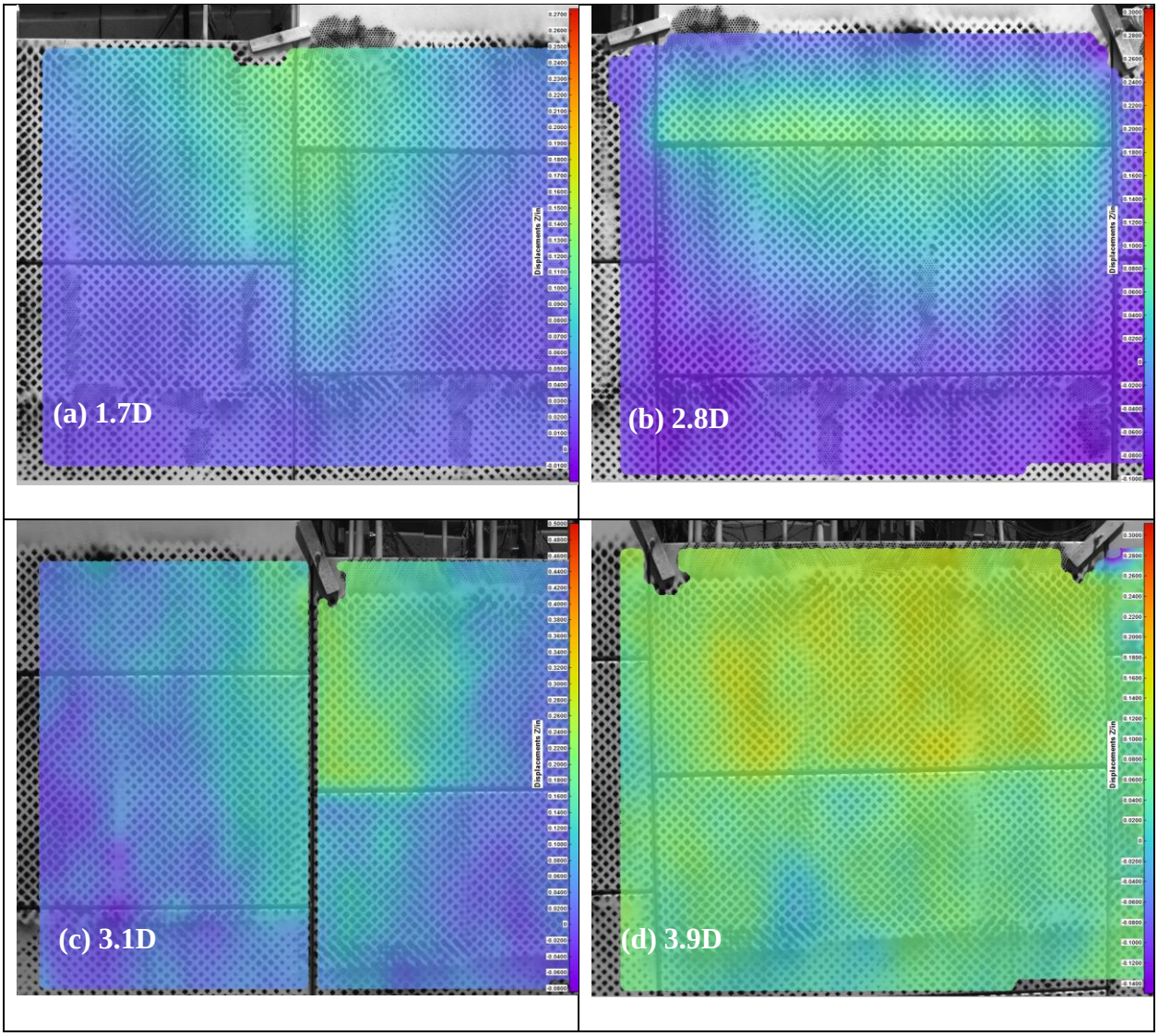

Figure H 7: Wall displacement at 1.5 in. pile head deflection for pile at (a) 1.7D, (b) 2.8D, (c) 3.1D and (d) 3.9D.

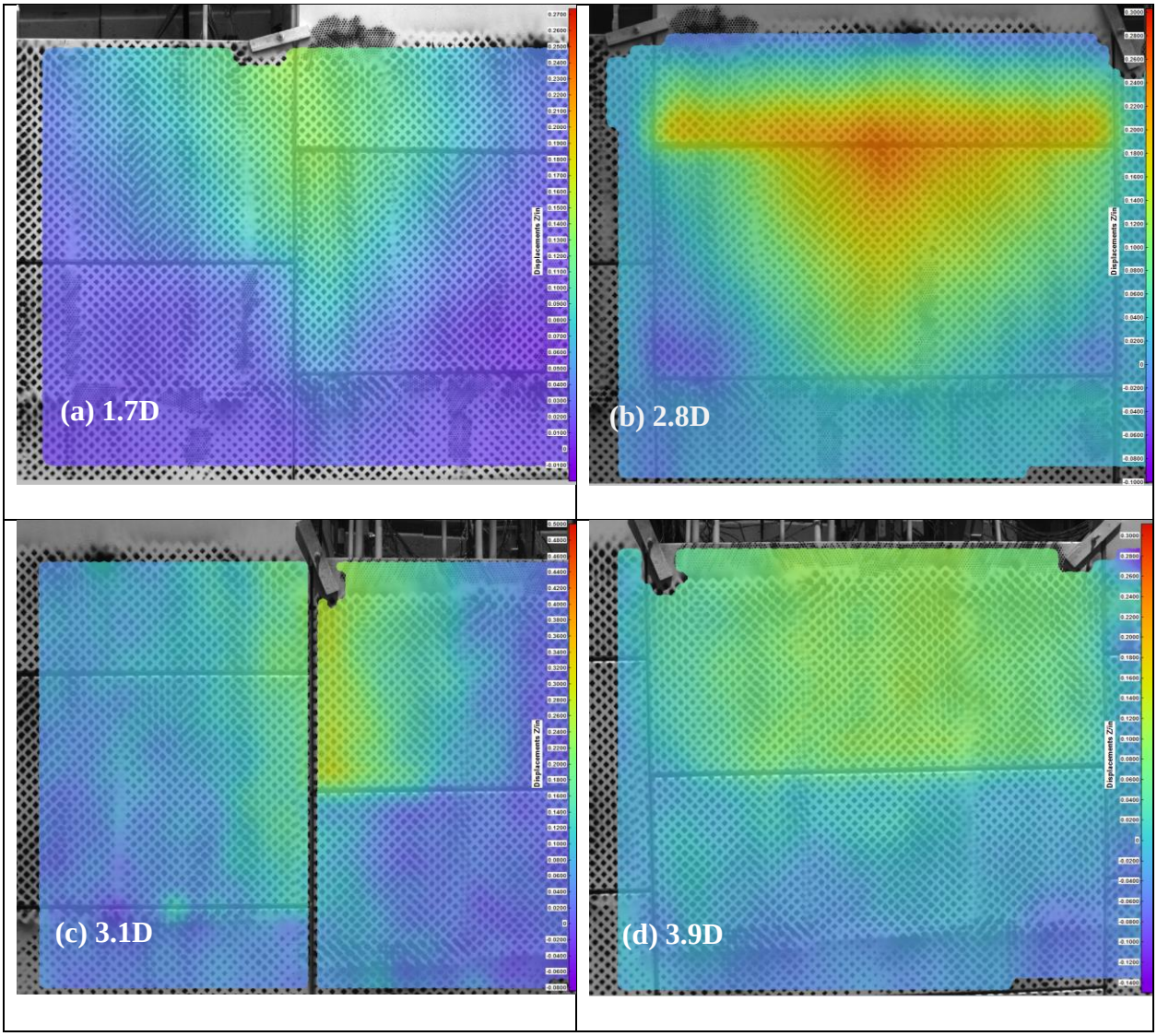

Figure H 8: Wall displacement at 1.75 in. pile head deflection for pile at (a) 1.7D, (b) 2.8D, (c) 3.1D and (d) 3.9D.

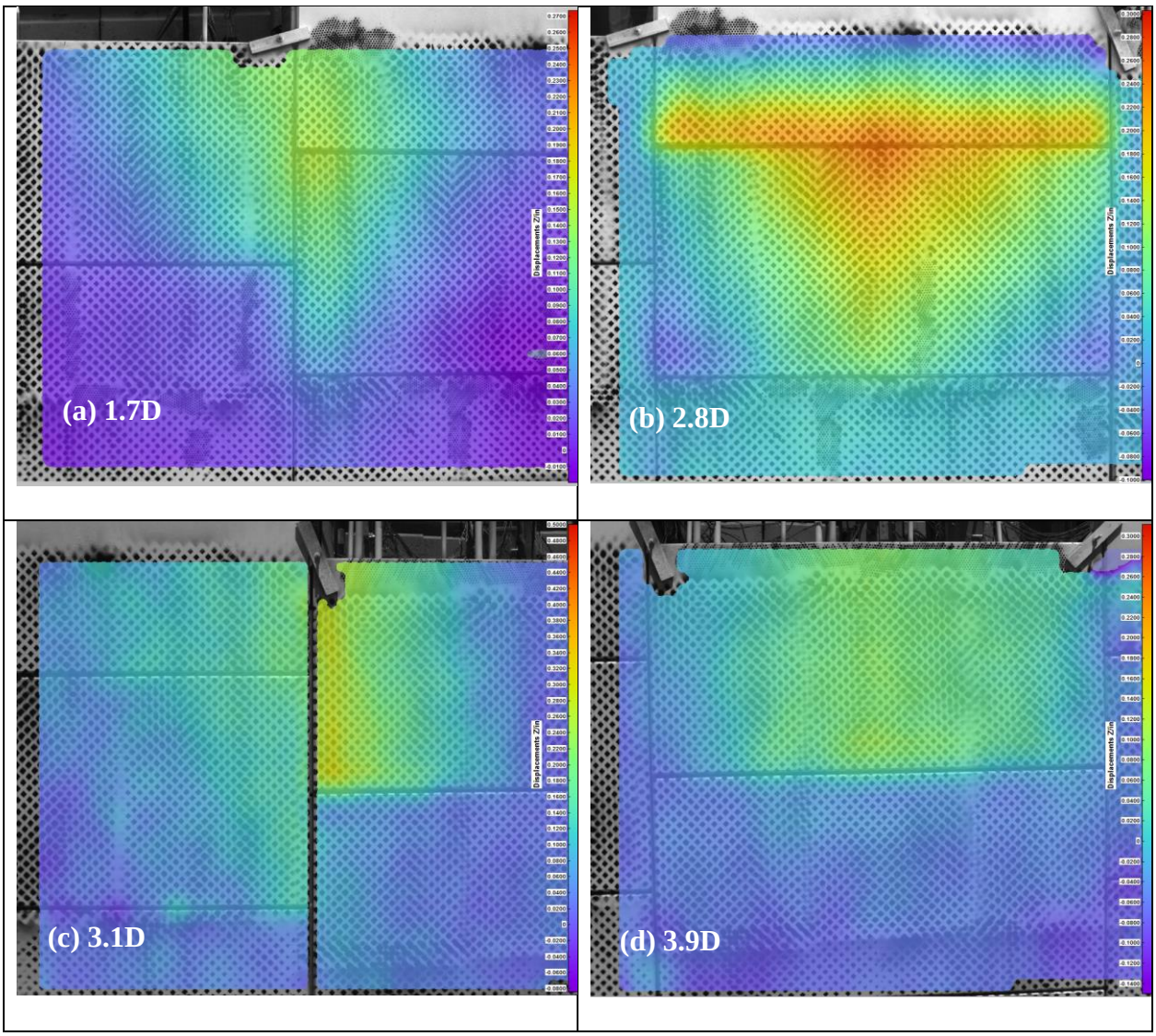

Figure H 9: Wall displacement at 2 in. pile head deflection for pile at (a) 1.7D, (b) 2.8D, (c) 3.1D and (d) 3.9D.

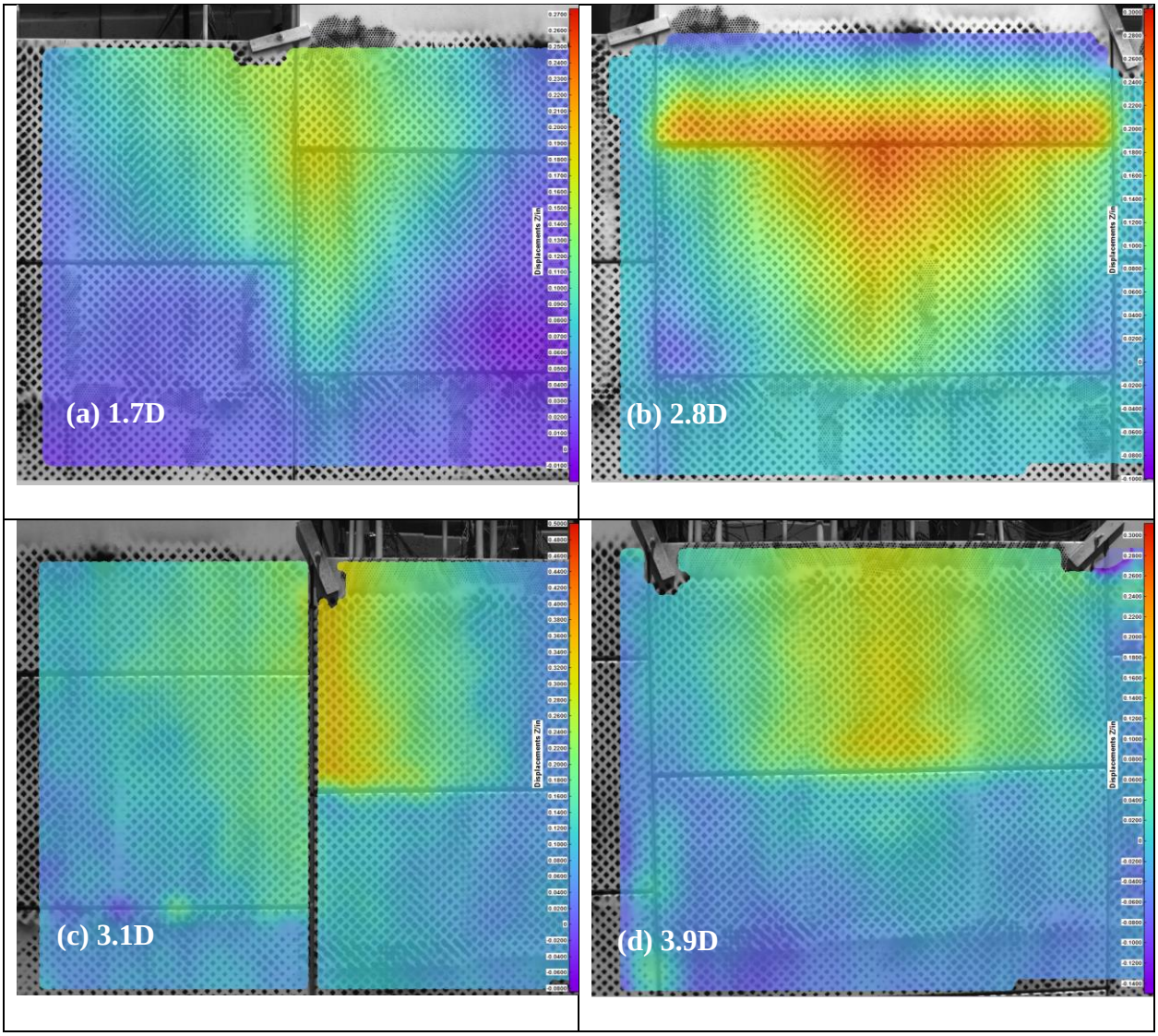

Figure H 10: Wall displacement at 2.25 in. pile head deflection for pile at (a) 1.7D, (b) 2.8D, (c) 3.1D and (d) 3.9D.

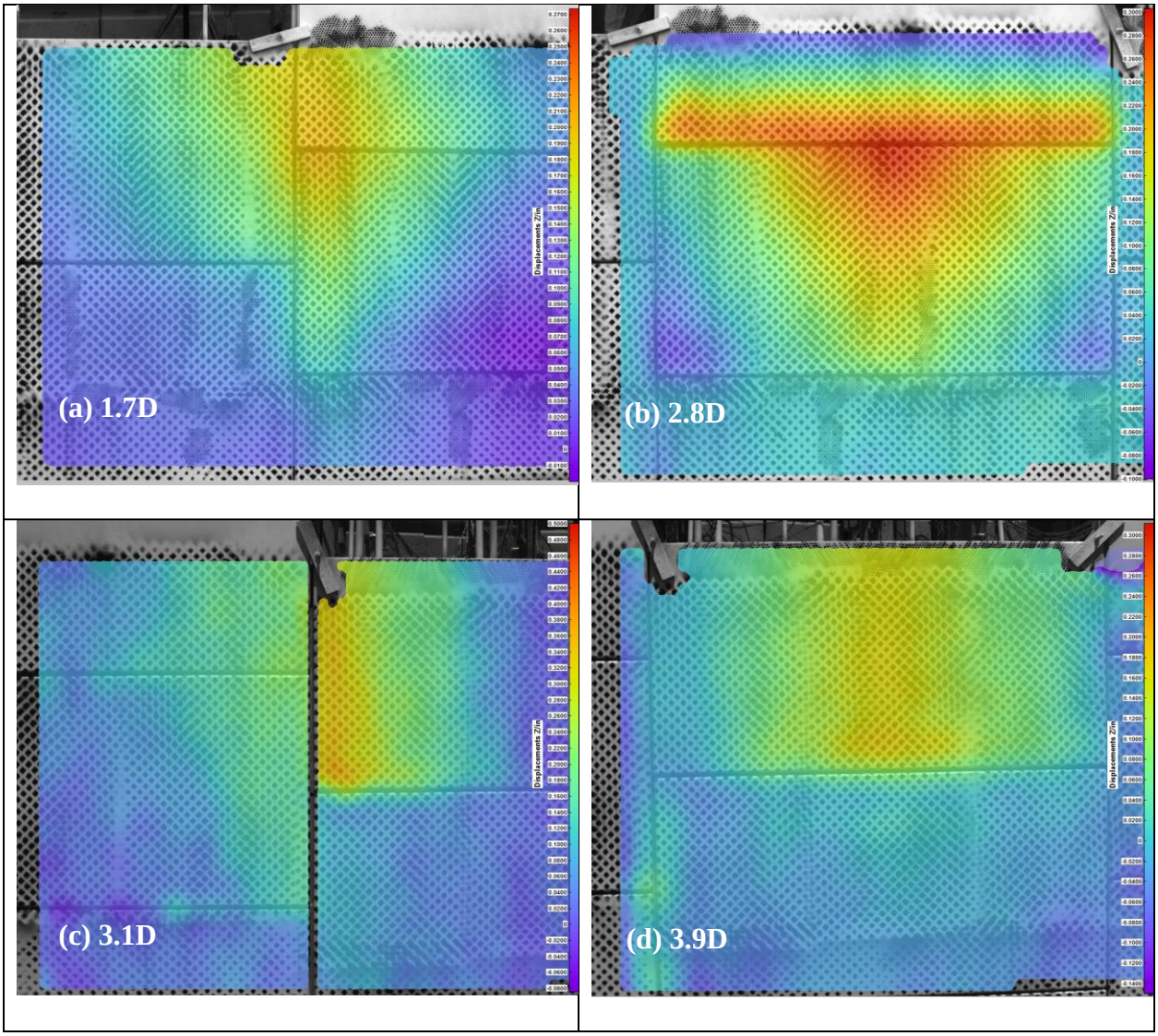

Figure H 11: Wall displacement at 2.5 in. pile head deflection for pile at (a) 1.7D, (b) 2.8D, (c) 3.1D and (d) 3.9D.

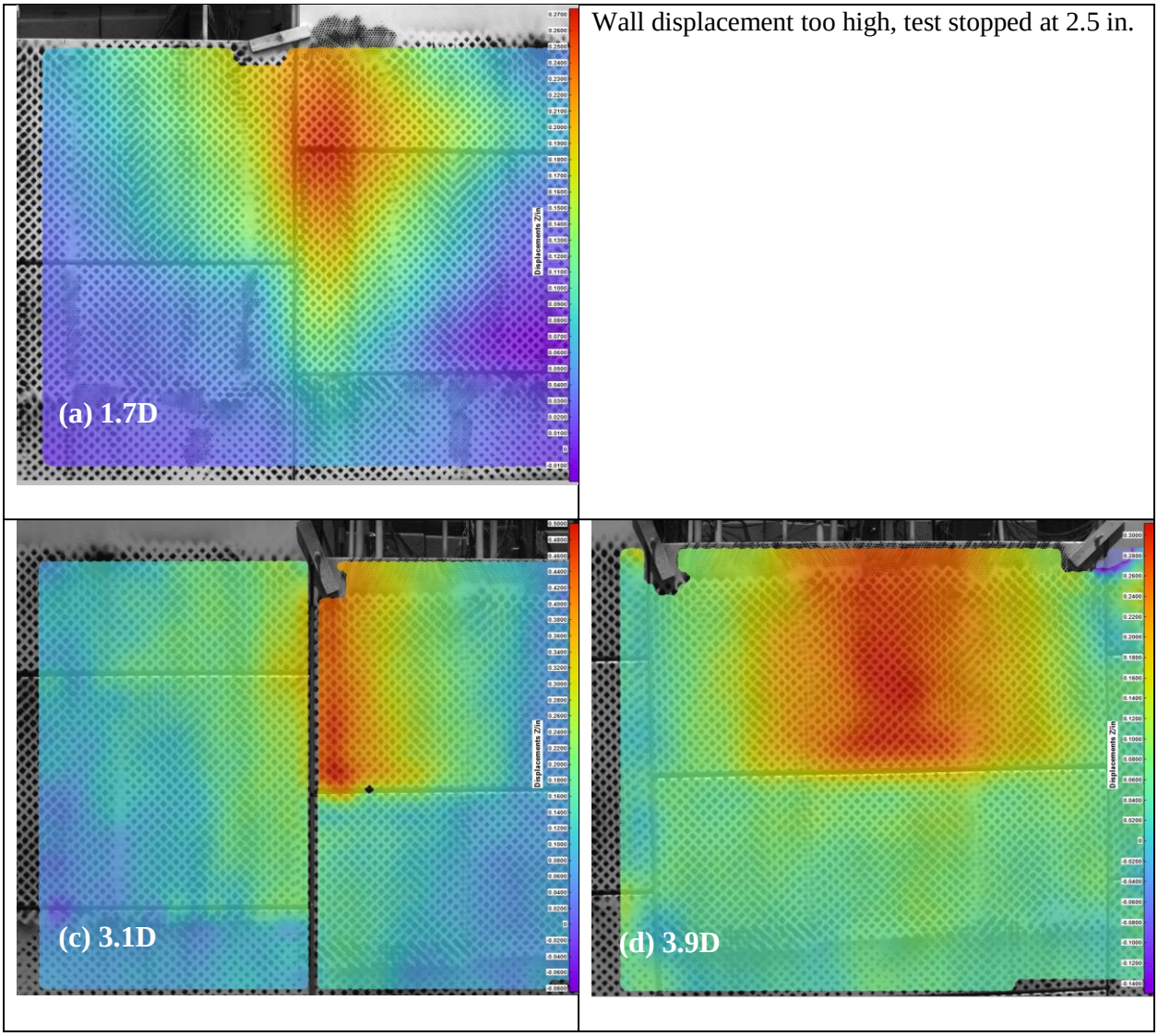

Figure H 12: Wall displacement at 3 in. pile head deflection for pile at (a) 1.7D, (b) 2.8D, (c) 3.1D and (d) 3.9D.